

Adaptive-Radiation Therapy Using
Functional Magnetic-Resonance Imaging
In Head and Neck Cancers

Dr Amit Gupta

The Institute of Cancer Research
The Royal Marsden Hospital

Thesis submitted for the degree of Doctor of
Medicine to University of London
March 2020 – July 2022

DECLARATION

The work and data presented in this thesis are my personal work performed in the role of a Clinical Research fellow working for the head and neck oncology team at The Royal Marsden Hospital/The Institute of Cancer Research between March 2020 and July 2022. Any collaborations or assistance from other individuals are acknowledged in the texts.

TABLE OF CONTENTS

DECLARATION.....	2
LIST OF FIGURES.....	6
LIST OF TABLES.....	7
ABBREVIATIONS.....	8
ACKNOWLEDGEMENTS.....	10
ABSTRACT.....	11
1 INTRODUCTION	12
1.1 BACKGROUND.....	12
1.1.1 <i>Risk Factors</i>	12
1.1.2 <i>Incidence</i>	13
1.2 MANAGEMENT STRATEGIES FOR HEAD AND NECK CANCERS	14
1.2.1 <i>Radiotherapy</i>	14
1.2.2 <i>Organ-at-Risk Sparing</i>	15
1.2.3 <i>Chemotherapy</i>	17
1.3 PROGNOSIS	17
1.3.1 <i>Recurrence Patterns</i>	18
1.4 RISK-STRATIFICATION FOR HEAD AND NECK CANCERS AND TREATMENT ADAPTATION	19
1.4.1 <i>Risk Stratification</i>	19
1.4.2 <i>Treatment De-escalation</i>	20
1.4.3 <i>Treatment Intensification</i>	24
1.5 ADAPTIVE RADIOTHERAPY	27
1.5.1 <i>Anatomical-Adaptive Radiotherapy</i>	28
1.5.2 <i>Biological-Adaptive Radiotherapy</i>	29
1.6 MRI-GUIDED ADAPTIVE RADIOTHERAPY	32
1.6.1 <i>MRI-Guided Anatomical ART</i>	33
1.6.2 <i>MRI-guided Biological ART</i>	34
1.7 ADAPTIVE RADIOTHERAPY FOR EARLY-STAGE GLOTTIC CANCERS	40
1.7.1 <i>Background</i>	40
1.7.2 <i>Dose-Volume Effects to Organs at Risk</i>	41
1.7.3 <i>Laryngeal Motion</i>	43
1.7.4 <i>Evolution of Radiotherapy for Early-Stage Glottic Cancers</i>	44
1.8 OUTLINE OF THESIS	46
1.9 REFERENCES	47
2 CHAPTER 2: FUNCTIONAL MRI-GUIDED ADAPTIVE RADIOTHERAPY FOR HEAD AND NECK CANCERS	65
2.1 INTRODUCTION	65
2.2 AIMS AND HYPOTHESES.....	67
2.3 MATERIALS AND METHODS	68
2.3.1 <i>Patient Criteria</i>	68
2.3.2 <i>INSIGHT II Study Design</i>	68
2.3.3 <i>CT and MRI Scan Protocols</i>	70
2.3.4 <i>DWI/ ADC Analysis</i>	71
2.3.5 <i>Target Delineation, Radiotherapy Planning and Replanning</i>	72
2.3.6 <i>Statistical Analyses</i>	73
2.4 RESULTS	74
2.4.1 <i>Patient Demographics</i>	74
2.4.2 <i>ADC Data</i>	77
2.4.3 <i>DWI-MRI Sequence Agreements</i>	80

2.4.4	MRI-Guided Adaptive Planning	84
2.5	DISCUSSION.....	88
2.5.1	Diagnostic-MR and MR-Linac DWI/ADC.....	88
2.5.2	Adaptive Radiotherapy Planning.....	92
2.6	FURTHER WORK.....	98
2.7	REFERENCES	99
3	CHAPTER 3: NOVEL FUNCTIONAL MRI-BASED BIOMARKERS FOR HEAD AND NECK CANCER .	102
3.1	INTRODUCTION	102
3.2	AIMS AND HYPOTHESES.....	104
3.3	MATERIALS AND METHODS.....	105
3.3.1	Patient Criteria	105
3.3.2	Scan Protocols	105
3.3.3	Image Post-Processing	105
3.3.4	Image Analyses	107
3.3.5	Statistical Analyses.....	108
3.4	RESULTS	110
3.4.1	Patient Demographics.....	110
3.4.2	IVIM on the Diagnostic-MR Scanner	110
3.4.3	IVIM on the MR-Linac.....	113
3.4.4	Hypoxic-MRI on the MR-Linac	117
3.4.5	MR-Linac Perfusion Fraction vs. Hypoxia	122
3.4.6	Spatial Correlation between Perfusion and Hypoxic MRI.....	124
3.5	DISCUSSION.....	125
3.5.1	Intravoxel Incoherent Motion.....	125
3.5.2	Imaging Hypoxia on the MR-Linac	127
3.5.3	Biomarker Development.....	130
3.5.4	Conclusions.....	131
3.6	FURTHER WORK	133
3.7	REFERENCES	134
4	CHAPTER 4: ANATOMICAL-ADAPTIVE RADIOTHERAPY FOR EARLY-STAGE SQUAMOUS CELL	
	CANCERS OF THE GLOTTIS.....	138
4.1	INTRODUCTION	138
4.2	AIMS AND HYPOTHESES.....	139
4.3	METHODS.....	140
4.3.1	Patient Selection.....	140
4.3.2	PHASE 1: Image Acquisition and Analyses	140
4.3.3	PHASE 2: Radiotherapy Planning Studies	144
4.3.4	Statistical Analysis.....	147
4.4	RESULTS	148
4.4.1	Patient Demographics and Previous Dosimetry	148
4.4.2	PHASE 1: Laryngeal Motion.....	150
4.4.3	PHASE 2: Adaptive-Radiotherapy Planning	152
4.4.4	Impact of Swallowing on Dose Delivery	156
4.5	DISCUSSION.....	157
4.5.1	Phase 1 – Motion and Toxicity Analyses	157
4.5.2	Phase 2 – Planning Studies.....	160
4.6	FURTHER WORK	163
4.7	REFERENCES	164
5	SUMMARY OF CHAPTERS.....	166
5.1	CHAPTER 2 – DWI AND ADC	166
5.2	CHAPTER 3 – IVIM AND HYPOXIC IMAGING	167
5.3	CHAPTER 4 - ADAPTIVE RADIOTHERAPY FOR EARLY-STAGE GLOTTIC CANCERS	168
5.4	CONCLUSIONS	169

6	APPENDICES	170
6.1	APPENDIX A	170
6.1.1	<i>MRI Scan Parameters – INSIGHT II Study</i>	<i>170</i>
6.1.2	<i>MRI Scan Parameters - MR-Linac.....</i>	<i>170</i>
6.2	APPENDIX B.....	171
6.2.1	<i>Dose constraints for baseline clinical radiotherapy plans</i>	<i>171</i>
6.3	APPENDIX C.....	172
6.3.1	<i>INSIGHT II (Diagnostic MR) ADC Data – Primary Tumour</i>	<i>172</i>
6.3.2	<i>INSIGHT II (Diagnostic MR) ADC Data – Lymph Node</i>	<i>173</i>
6.4	APPENDIX D	174
6.4.1	<i>MR-Linac ADC Data – Primary Tumour</i>	<i>174</i>
6.4.2	<i>MR-Linac ADC Data – Lymph Node</i>	<i>175</i>
6.5	APPENDIX E.....	176
6.5.1	<i>Structure Doses for INSIGHT II NON-ADAPTED Radiotherapy Plans.....</i>	<i>176</i>
6.5.2	<i>Structure Doses for INSIGHT II ADAPTED Radiotherapy Plans.....</i>	<i>177</i>
6.6	APPENDIX F	178
6.6.1	<i>Structure Doses for INSIGHT II Standard and Dose-Escalated Plans</i>	<i>178</i>
6.7	APPENDIX G	179
6.7.1	<i>Perfusion fractions for Primary Tumour (Diagnostic-MRI).....</i>	<i>179</i>
6.7.2	<i>Perfusion fractions for Lymph Node (Diagnostic-MRI).....</i>	<i>179</i>
6.8	APPENDIX H	180
6.8.1	<i>Perfusion Fractions – Primary Tumour</i>	<i>180</i>
6.8.2	<i>Perfusion Fraction – Lymph Node.....</i>	<i>181</i>
6.9	APPENDIX I.....	182
6.9.1	<i>Perfusion below 15% - Primary Tumour</i>	<i>182</i>
6.9.2	<i>Perfusion Fraction below 15% - Lymph Node</i>	<i>183</i>
6.10	APPENDIX J	184
6.10.1	<i>Hypoxic Fraction – Primary Tumour</i>	<i>184</i>
6.10.2	<i>Hypoxic Fraction – Lymph Node</i>	<i>185</i>
6.11	APPENDIX K.....	186
6.11.1	<i>Mean doses for all radiotherapy plans.....</i>	<i>186</i>

LIST OF FIGURES

Figure 1-1, Head and neck anatomical compartments.....	13
Figure 1-2, Schematic of the MR-Linear Accelerator.	33
Figure 1-3, Single-Shot Spin-Echo Diffusion-Weighted MRI.	35
Figure 1-4, Apparent Diffusion Coefficient and Intra-Voxel Incoherent Motion. ..	36
Figure 1-5, 3D-CRT Plan for Early-Stage Glottic Cancers.	41
Figure 2-1, INSIGHT II trial workflow.	69
Figure 2-2, Diagnostic DW-MRI sequences.....	71
Figure 2-3, Percentage ADC changes for Primary and Lymph Node disease.....	79
Figure 2-4, ssEPI vs. RESOLVE ADCs for Primary and Lymph Node disease.	81
Figure 2-5, Bland-Altman Plots for Primary and Lymph Node Tumours.....	82
Figure 2-6, Correlation Analyses for Double-Baseline DW-MRIs on MR-Linac...	83
Figure 2-7, Bland-Altman Plot for MR-Linac ADC Repeatability ($\times 10^{-3} \text{ mm}^2\text{s}^{-1}$).	83
Figure 2-8, Percentage Dose Difference between Adapted and Non-Adapted Radiotherapy Plans.	85
Figure 2-9, Correlation Between Depth Change (mm) and Weight Loss (%).	86
Figure 2-10, Percentage Dose Difference between Standard and Dose-Escalated Radiotherapy Plans.	87
Figure 3-1, Example of perfusion and R2* maps.	106
Figure 3-2, IVIM plot of b-value against natural logarithm of signal intensity.....	107
Figure 3-3, Percentage Changes of Perfusion Fractions for Primary and Lymph Node Disease.	111
Figure 3-4, Correlations of Percentage Changes Between Perfusion Fraction and ADC.	112
Figure 3-5, Bland Altman Plot For Primary Tumour ADC vs. Perfusion Fraction Percentage Changes at Week 2.	113
Figure 3-6, Percentage Changes of Perfusion Fractions for Primary and Lymph Node Disease.	114
Figure 3-7, Correlations between Perfusion Fraction and ADC.....	116
Figure 3-8, Double-baseline comparisons for Perfusion Fractions.....	117
Figure 3-9, Example R2* Map.....	118
Figure 3-10, Percentage Changes of Hypoxic Fraction for Primary and Lymph Node Diseases.....	119
Figure 3-11, Correlations between Hypoxic Fraction and ADC.	121
Figure 3-12, Correlations between Double-Baseline Hypoxic Fraction Images. ..	122
Figure 3-13, Perfusion against Hypoxic Fractions.....	123
Figure 3-14, Spatial Correlations Between Perfusion fraction and R2*.....	124
Figure 4-1, Patient setup on the Elekta Unity MR-Linear Accelerator.	141
Figure 4-2, Cine-MR imaging protocol.	141
Figure 4-3, Motion analysis of laryngeal structures.	143
Figure 4-4, Definition of motion measurements.	144
Figure 4-5, Swallow-Related Motion Data.	152
Figure 4-6, Motion Breakdown into Anterior and Superior Components.	152
Figure 4-7, Mean doses for Organ at Risks.	155

LIST OF TABLES

Table 1-1, 5-year overall survival for head and neck cancers.	18
Table 1-2, Summary of studies using induction chemotherapy to guide radiotherapy dosing strategy.	22
Table 1-3, Summary of studies investigating de-escalation of adjuvant therapy after primary surgery.	23
Table 1-4, Summary of current or recent phase-3 studies evaluating immunotherapy-based treatment intensification.	26
Table 2-1, Patient Risk Stratification.	69
Table 2-2, Patient Characteristics and Treatment Outcomes.	76
Table 2-3, Pearson’s Correlation Coefficients for ssEPI vs RESOLVE ADC.	81
Table 2-4, Bland-Altman data.	82
Table 2-5, Mean Percentage Differences and Corresponding Standard Deviations.	86
Table 4-1, Radiotherapy planning target definitions.	146
Table 4-2, Patient demographics and radiation dosimetry.	149
Table 4-3, Laryngeal Motion (mm), Duration and Frequency Data.	151
Table 4-4, Dose Statistics for Patients Separated by T-Stage.	153
Table 6-1, MRI scan parameters for INSIGHT II study.	170
Table 6-2, MRI scan parameters for MR-Linac.	170
Table 6-3, Radical head and neck radiotherapy dose constraints.	171
Table 6-4, ADC data for Primary tumours.	172
Table 6-5, ADC data for Involved Lymph Nodes.	173
Table 6-6, ADC Data for Primary Tumours.	174
Table 6-7, ADC Data for Lymph Nodes.	175
Table 6-8, Raw Dosimetry Data for Non-Adapted Radiotherapy Plans.	176
Table 6-9, Raw Dosimetry Data for Adapted Radiotherapy Plans.	177
Table 6-10, Raw Dose Data for Standard and Dose-Escalated Plans for INSIGHT II Non-Responding Patients.	178
Table 6-11, Perfusion Fraction Data for Primary and Lymph Node Diseases.	179
Table 6-12, Perfusion Fraction data for Primary Tumour.	180
Table 6-13, Perfusion Fraction data for Lymph Nodes.	181
Table 6-14, Mean doses for Structures.	186

ABBREVIATIONS

(A/B)-ART	(Anatomical/Biological)-Adaptive Radiotherapy
3D-CRT	3-Dimensional Conformal Radiotherapy
ADC	Apparent Diffusion Coefficient
AJCC	American Joint Committee on Cancer
ANACONDA	ANAtomically-CONstrained Deformation image-registration Algorithm
BOLD	Blood-Oxygen Level Dependent
BW	Bandwidth
CI	Confidence Interval
CRT	Concurrent Chemoradiotherapy
CT	Computed Tomography
CTV	Clinical Target Volume
DCE-MRI	Dynamic Contrast Enhanced-MRI
DFS	Disease-Free Survival
DWI	Diffusion Weighted Image
EBV	Epstein-Barr Virus
EQD2	Equivalent dose in 2 Gy per fraction
ESGC	Early-Stage Glottic Squamous Cell Carcinoma
FA	Flip Angle
FDG	Fluoro-deoxyglucose
fMRI	Functional-MRI
GTV	Gross Tumour Volume
HNC	Head and Neck Cancer
HPV	Human Papilloma Virus
IGRT	Image-Guided Radiotherapy
IMPT	Intensity-Modulated Proton Therapy
IMRT	Intensity-Modulated Radiotherapy (photons)
IPCM	Inferior Pharyngeal Constrictor Muscle
ITV	Internal Target Volume
IVIM	Intravoxel Incoherent Motion
LRC	Locoregional Control
LVI	Lympho-Vascular Invasion
MR-Linac	MR-Linear Accelerator
MRgRT	MR-Guided Radiotherapy
MRI	Magnetic Resonance Imaging
MTV	Metabolic Tumour Volume
NSA	Number of Signal Averages
NTCP	Normal Tissue Complication Probability
OAR	Organ at Risk
OE-MRI	Oxygen-Enhanced MRI
OR	Odds Ratio
OS	Overall Survival
PD-L1	Programme Death-Ligand 1
PET	Positron Emission Tomography
PNI	Peri-Neural Invasion
PRV	Planning Risk Volume
PTV	Planning Target Volume
RESOLVE	REadout Segmentation Of Long Variable Echo-trains
SCC	Squamous Cell Carcinoma

SPAIR	SPECTral Attenuated Inversion Recovery
ssEPI	Single-Shot Echo-Planar Image
SUV _(mean/max)	Standardised Uptake Value (mean/max)
TBR	Tumour Background Ratio
TCP	Tumour Control Probability
TE/TR	Echo Time/Repetition Time
TLG	Total Lesion Glycolysis
TLM	Trans-Oral Laser Microsurgery
TNM	Tumour Node Metastasis
TORS	Trans-Oral Robotic Surgery
TPF	Docetaxel, Platinum and 5-fluorouracil
TPS	Treatment Planning System
VMAT	Volumetric-Modulated Arc Therapy
d-Hb	Deoxy-Haemoglobin
SVCI	Single Vocal-Cord Irradiation

ACKNOWLEDGEMENTS

I would like to thank my supervisors Kee Wong and Kevin Harrington and the entire head and neck oncology department at The Royal Marsden Hospital for offering me the opportunity to work amongst their team and providing me with such a fantastic educational experience. Their supervision and guidance have allowed me to attain a set of skills and knowledge that will put me in good stead for the remainder of my career.

This work would not have been possible without the expertise and support of Alex Dunlop, Dualta Mcquaid, Andreas Wetscherek and Wajiha Bano, who have all gone above and beyond to assist me with the work described in this thesis and I am indebted to them for their efforts.

Additionally, I would like to extend my thanks to all the members of the head and neck research team, who provided assistance with coordination of scans and management of patients on trials. This includes the MR-Linac and diagnostic-MRI radiographer teams who, very kindly, accommodated all the patients I referred for scans and treatments. Thank you in particular to Helen Barnes and Georgina Hopkinson for organising scanning slots and accommodating all of the patients who were referred for research scans.

This work would not be possible without the patients who kindly gave up their time to take part in the various studies and I thank them for their support during such a difficult period in their lives.

Lastly, I would like to thank my research-fellow friends and colleagues in Orchard House who provided me with entertainment, endless nourishment and were always available to lend ears to discuss and troubleshoot research-related issues. Their support kept me motivated to keep going during the most difficult periods during this post.

ABSTRACT

Treatment strategies for locally-advanced head and neck cancers have evolved with a strong emphasis on treatment adaptation based on disease risk or intra-treatment response. Magnetic resonance imaging offers an ideal platform to perform adaptive radiotherapy as it is non-invasive, adds no additional radiation risk and allows superior soft-tissue definition to conventional CT-based methods. This thesis explored the role of functional-MRI for delivering adaptive radiotherapy for head and neck cancers.

This thesis analysed the treatment-related changes of two diffusion-weighted image sequences (ssEPI and RESOLVE) and demonstrated good concordance between the two sequences when assessing for disease response in the second week of radiotherapy. As part of the INSIGHT II trial, ssEPI was used to help dose-escalate for non-responding patients (change in ADC <15% in week 2 of chemo-radiotherapy) without compromising the dose to organs at risk such as parotid glands. There was a modest dose-sparing effect for low-risk and responding tumours.

However, there were no patients with residual disease in this study to validate the findings from the original INSIGHT study, as to whether an Apparent Diffusion Coefficient threshold of 15% (for ssEPI and RESOLVE) is able to stratify between responders and non-responders. Exploratory imaging biomarkers such as intra-voxel incoherent motion and T2* did not show any significant trends to stratify patients into risk groups or determination of treatment response.

The final chapter explores laryngeal motion and shows that laryngeal motion is most prominent in the cranio-caudal directions. However, this motion is not deemed significant as the duration and frequency of swallow are limited. Individualised treatment target volumes, based on respiratory-related laryngeal motion, were created for radiotherapy-planning studies using intensity-modulated based methods. This approach significantly spared organs at risk such as carotid arteries. Analysis of intra-fraction swallow-related motion demonstrated no compromise in dose to the treatment target when treating smaller targets.

1 INTRODUCTION

1.1 Background

Head and neck cancer (HNC) accounts for roughly 12000 new cancer diagnoses per year and it is the eight most common cancer in the United Kingdom (U.K.) (1). Over the past three decades, the global incidence of all HNC has increased by 37% (2). HNC account for 2% of all cancer-related deaths, 36% of which occur in people aged 75 years and over.

The head and neck region is divided into anatomical compartments, where the aetiologies, treatment strategies and prognoses of HNCs may differ (Figure 1-1). HNC most frequently occurs in the epithelial cells of the mucosa that line the head and neck surface (3). Squamous cell carcinoma (SCC) represents the most frequently occurring (>90%) histopathological subtype within the head and neck region (4). Less common pathologies such as adenocarcinoma, sarcomas and benign tumours may also develop, with salivary gland tumours occurring in roughly 300 patients per year in England and Wales (5). In the U.K., oropharyngeal and hypopharyngeal cancers are the commonest sites affected (collective annual incidence of 34%), followed by oral cavity (26%), larynx (22%), paranasal sinuses/nasal cavity (4%) and nasopharynx (2%) (1). For all HNCs, males are roughly 2.7-times more frequently affected and have a roughly 2.8-times higher risk of death compared to women (6).

1.1.1 Risk Factors

Traditionally, tobacco consumption has remained the strongest and well-established risk factor for all HNC (7). To determine the individual contribution of smoking or alcohol consumption on carcinogenesis and to quantify the magnitudes of risk, Hashibe et al analysed individual-level data from the INHANCE collaboration's 25000 subject database (8). Without alcohol consumption as a confounding factor, the odds ratio (OR) for risk of developing HNC amongst smokers with less than ten pack-years (versus never smokers) is 2.13 (95% confidence interval (CI) 1.52-2.98). Berthiller et al demonstrate

the strong relationship between dose intensity of smoking tobacco and risk of developing HNC when patients have a greater than ten pack-year smoking history (9). Alcohol consumption in never smokers is independently associated with an increased risk (OR 2.04, 95% CI 1.29-3.21) of developing oropharyngeal, hypopharyngeal and laryngeal cancers, with clear dose-response relationships for both tobacco and alcohol use (8,10).

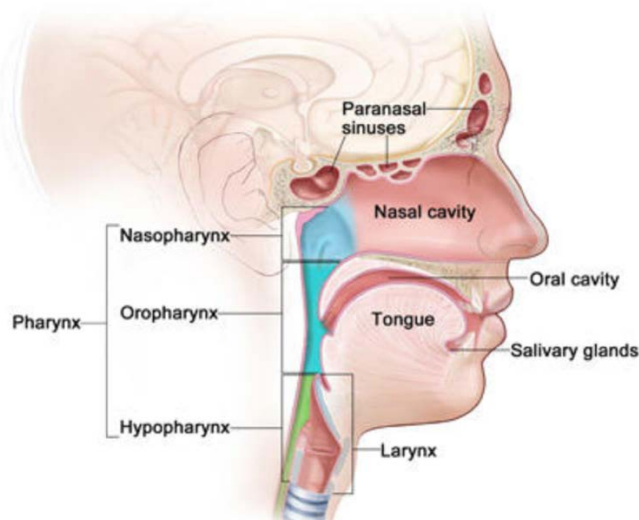


Figure 1-1, Head and neck anatomical compartments.

The oropharynx, hypopharynx, larynx, nasopharynx, oral cavity and nasal cavity/paranasal sinuses account for the majority of sites where HNC may occur. The most common aetiologies may differ between compartments [Figure from National Cancer Institute, (11)].

The role of human papilloma virus (HPV) in the pathogenesis of a subset of HNC was described over twenty years ago (12). HPV-driven HNC most commonly occurs in the oropharynx with a particular predilection for the tonsils (13). It has been described that the persistence of biofilms and the overexpression of programme death-ligand 1 (PD-L1) within invaginated tonsillar crypts provides the ideal environment for HPV to evade the immune system and be present long enough to induce oncogenic transformation of infected cells (14).

1.1.2 Incidence

The incidence of oropharyngeal cancers has continued to rise by roughly 2.9% per year over the past ten years (15). This is largely driven by an increased rate of diagnosis of HPV-associated HNC, with HPV now the most common cause of oropharyngeal cancers in developed countries (16). Over a similar time period, the incidence of HNC

associated with more traditional risk factors, such as smoking and alcohol, have decreased by up to 3% per year due to the reduced exposure to tobacco (17).

It is hoped that offering an HPV vaccine to both boys and girls aged 12-13 years since 2019 will reduce the rate and duration of infections from the known highly-oncogenic subtypes of HPV, (Gardasil 9 protects against HPV 6, 11, 16, 18, 31, 33, 45, 52 and 58) (18). The vaccination uptake rates in the U.K. are slowly improving each year, with 61% of eligible girls and 54.7% of boys having completed the two-dose schedule in 2021 (19). The impact of the vaccination programme on the incidence of HPV-driven HNC may not be seen for at least 10-20 years due to the latency period between HPV infection and clinically apparent cancer (20).

Incidence of the subtypes of HNC vary across the world, depending on local practices and exposure to the carcinogenic factors described, as well as other contributors such as betel nut chewing and Epstein-Barr Virus (EBV) infection (21). Globally, over 50% of oral cavity cancers occur in South-Central Asia, which is likely related to the synergistic effect of tobacco smoking and betel nut chewing (22). Nasopharyngeal carcinoma most frequently occurs in East-Asian countries, where EBV has a crucial pathogenic role in the more frequent non-keratinising WHO type 2 and 3 forms (23). Oropharyngeal cancers most frequently occur in Western Europe (24).

1.2 Management Strategies for Head and Neck Cancers

1.2.1 Radiotherapy

Radiotherapy involves the use of ionising radiation, in the form of electromagnetic waves or particulate matter, to achieve cellular kill as a consequence of direct or indirect damage to deoxyribonucleic acid (DNA) (25). Technological advances in radiological imaging with the development of multi-leaf collimation have allowed the implementation of progressively more conformal radiotherapy techniques, resulting in improved dose distributions within target tissues, whilst reducing dose to normal structures (26).

The four Rs of radiotherapy describes why radiation treatments are conventionally fractionated to take advantage of the differential responses between normal and tumour

tissues (repair and repopulation) and to optimise tumour-stem cell kill (by reoxygenation and cell-cycle redistribution) (27). Conventional fractionation regimens for radiotherapy use 1.8-2 Gy per fraction, in order to spare late-reacting normal tissues in head and neck cancer (28). Altered fractionation regimens with a higher or lower dose per fraction (hypofractionation or hyperfractionation, respectively) or greater than five fractions per week (acceleration) have previously been explored and these strategies are now utilised in tumour types such as CHART for lung (29), hypofractionation for prostate (30) and hypofractionation for breast (31) cancers.

The importance of altered fractionation for head and neck SCCs has been demonstrated in the DAHANCA 6 & 7 study in 2003 (32). In an attempt to achieve improved local tumour control by circumventing the effects of accelerated tumour repopulation, this study compared accelerated radiotherapy (six fractions per week) against standard fractionation (five fractions per week), for HNC. This resulted in a statistically significant 10% improvement in loco-regional control (LRC) at five years, where the effect was most apparent in the primary lesion, as opposed to involved regional lymph nodes. The updated MARCH meta-analysis data show that hyperfractionation is the most superior mode of altered fractionation for HNC, where the greatest benefit was also noted for the primary tumour and patients aged below 50 years (33). In the U.K., hypofractionation is commonly utilised for a five fraction per-week regimen, with no known compromise in LRC (34,35).

1.2.2 Organ-at-Risk Sparing

As dose-intensification with acceleration or hypofractionation has become the standard of care for managing some HNCs, the main factor limiting further dose-intensification strategies for high-risk tumours has been toxicity, the need for organ-at-risk (OAR) sparing and maintenance of function and quality of life (36).

In patients receiving radical-dose radiotherapy for HNC, grade 2 and 3 xerostomia is reported in almost 50% and 5%, respectively (37). Chronic impairment of salivary gland function is known to have adverse effects on taste, mastication and difficulty with speech

and swallow (38). The phase 3 PARSPORT trial definitively demonstrated that parotid-sparing intensity-modulated radiotherapy (IMRT), with a contralateral-parotid constraint of <24 Gy, resulted in reduced rates of xerostomia without an adverse impact on LRC or overall survival (OS) (39). Saarilahti et al show in their relatively small phase 2 study that restriction of the contralateral submandibular gland to a similar maximum dose of 25 Gy results in an objective improvement in unstimulated salivary gland function (40). This finding has since been replicated in other non-randomised studies (41,42).

Swallow is a complex function that involves the use of over thirty groups of muscles and nerves (43). Dysphagia of grade ≥ 1 is described in up to 70% of patients during radiotherapy, causing both acute and potentially chronic adverse effects on speech and nutrition (44). A systematic review by Duprez et al shows that the mean dose to the pharyngeal constrictor muscles (PCM) serves as a strong predictor of chronic dysphagia (45). The phase 3 DARS trial aimed to investigate the impact of sparing the PCM and resultant impact on long-term swallowing outcomes (46). The results demonstrated significant improvements in MD Anderson Dysphagia Inventory (MDADI) scores at one year post-radiotherapy when PCM dose was constrained to <50 Gy (47).

Platinum chemotherapy, which can be given concomitantly with radiotherapy, is a known risk factor for sensorineural hearing loss, likely as a result of direct accumulation within the cochlea (48). The cochlea is an additional OAR in close vicinity to the parotid gland, sinuses and nasopharynx. Cochlea-sparing IMRT was investigated in the COSTAR phase 3 randomised study, which recruited patients with primary parotid cancers that required adjuvant radiotherapy, (without concomitant chemotherapy) (49). A mean-dose constraint of <39 Gy was accepted to the ipsilateral cochlea but this did not result in any objective improvement in preventing hearing loss.

Future strategies aim to further reduce radiation dose to OARs and improve acute and late toxicities as well as overall quality of life. TORPEdO is a currently recruiting multi-centre phase 3 study, which compares intensity-modulated proton therapy (IMPT)

against intensity-modulated photon therapy for oropharyngeal cancers (50). PRESERVE is a currently open phase 2 randomised study aiming to assess the recurrence and survival rates after omitting adjuvant radiotherapy to dissected neck regions with no pathological nodal disease in oral cavity SCCs (51).

1.2.3 Chemotherapy

Steel G and Peckham M initially postulated four main interactions between concomitant chemotherapy and radiotherapy (52). One of the interactions described is that of radiosensitisation and to enhance the cytotoxic effects of radiotherapy (53). The definitive meta-analysis by Pignon et al demonstrated an absolute OS benefit in favour of CRT of 4.5% at five years, with a smaller magnitude of benefit noted for patients aged >70 years (54). CRT with platinum monotherapy has since become the standard-of-care treatment strategy in patients up to 70 years of age and a glomerular filtration rate of 45 ml/min or above.

1.3 Prognosis

An improved understanding and appreciation of the risk factors for HNC has resulted in an update of the AJCC Tumour Node Metastasis (TNM) classification system to the eighth edition, which has been in use since 2018. HPV-positive oropharyngeal, HPV-negative oropharyngeal or hypopharyngeal or laryngeal and nasopharyngeal cancers are now separated into different staging systems to reflect the differences in underlying disease biology and prognoses. The inclusion of extra-nodal extension was also a new feature in the eighth edition as its presence denotes an adverse effect on prognosis and it is described as one of the strongest predictors of distant metastasis (55,56).

Patients with HPV-associated oropharyngeal SCC more frequently present with larger volume and cystic lymph-node disease compared to their HPV-negative counterparts (57). HPV-associated lymph-node disease has been observed to regress at a faster pace and shows better radio-sensitivity and LRC (58). However, despite the more rapid regression, complete resolution of HPV-associated lymph-node disease has been noted to be slower (59).

Patients with HPV-associated oropharyngeal cancer who have a significant smoking history have a worse prognosis than those who have never smoked (60). Distant metastasis rates are similar between HPV-associated and -negative HNC (61). For this reason, despite the better LRC for HPV-associated HNC, longer-term surveillance and further risk-stratification strategies and biomarkers are required.

Table 1-1 displays the TNM stage-dependent five-year OS rates for local/locally-advanced pharyngeal and laryngeal SCCs. Although the table suggests all stage III oropharyngeal cancers have similar OS rates, stage III HPV-associated SCC includes T3-4 N2 disease, compared to a less-extensive stage III HPV-negative SCC, which includes T3 N0 or T1-3 N1. Stage IV HPV-associated SCC includes any tumour or nodal stage but with distant metastasis (62).

Stage	5-year Overall Survival (%)				
	Nasopharynx	OPC (HPV pos)	OPC (HPV neg)	Hypopharynx	Larynx
1	90	90	75	65	70
2	85	78	65	59	45
3	80	55	55	40	40
4	70	-	40	30	33

Table 1-1, 5-year overall survival for head and neck cancers.

Stage IV cancer in this table denotes non-metastatic (M0) disease only (1). Stages based on AJCC TNM 8th Edition.

1.3.1 Recurrence Patterns

There is a continuously growing body of evidence that suggests treatment failure and sites of recurrence are most common within the high-dose Clinical Target Volume (CTV) after a course of radical radiotherapy (63). This suggests a need for improved patient stratification algorithms that identify those that require treatment escalation.

Bollen et al retrospectively analysed their disease recurrence patterns in a cohort of 385 patients treated for all HNCs over a ten-year period (64). They stressed the importance of accurate and consistent target delineation as they noticed no marginal and very limited out-of-field recurrences in the local region of disease. They also highlight the need to understand and identify biological characteristics of tumours on an individual basis, to overcome radio-resistant tumour regions. Radio-resistant features of tumours, including hypovascularity, hypoxia or increased number of cancer stem cells may require

treatment intensification with radiation dose escalation or tailoring of systemic therapy (65).

Nevens et al investigated the recurrence patterns after a reduction in the microscopic radiation dose (40 Gy in 2 Gy per fraction, as opposed to the standard 50-56 Gy) to elective nodal regions and noted that both loco-regional and distant metastasis rates were similar to that described in the literature (66). Based on such data, there has been suggestion that development of distant metastasis largely depends on the presence of pre-existing microscopic disease, the prevalence of which may not be affected by effective loco-regional disease clearance with radiotherapy (67,68).

1.4 Risk-stratification for Head and Neck Cancers and Treatment Adaptation

1.4.1 Risk Stratification

The current standard of care of radiotherapy does not take patients' HPV status into account, despite the well described impact of HPV on radiosensitivity. Therefore, recent studies have focused on stratifying patients into risk groups to deliver dose de-escalated or escalated radiotherapy, particularly for pharyngeal and laryngeal cancers (69).

RTOG 0129 was a phase 3 randomised trial comparing accelerated CRT against standard fractionation for locally-advanced HNC (70). Ang et al analysed the median five-year outcome data from RTOG 0129 to establish the effects of HPV status on survival (71). Sixty percent of the patient cohort had oropharyngeal cancers and roughly 50% of all patients had HPV-associated HNC, with the remainder being either HPV-negative (roughly 27%) or unknown HPV status (roughly 24%).

They demonstrated that HPV and smoking statuses are the major independent determinants of OS, followed by the tumour and nodal stage. They outlined three risk groups (low, intermediate and high), where HPV-associated tumours with less than ten pack-year smoking history and nodal stage $<N2b$ are deemed at low risk of local or distant-recurrence. A smoking history greater than ten pack-year, nodal disease $\geq N2b$ or any HPV-negative tumour renders the disease as intermediate or high risk. In addition to

this conclusion, O’Sullivan et al further demonstrated that the three-year risk of distant metastases in HPV-associated HNC (less than ten pack-year smoking and stage N0-2b) are similar when treated with CRT or radiotherapy alone (93%) (72). However, the risk of distant-disease control was lower when N2c disease was treated with radiotherapy alone (73%) compared to CRT (92%). Despite this stratification having been performed with the older AJCC seventh edition, this risk stratification for pharyngeal and laryngeal HNC still continues to serve as a framework for conducting adaptive-treatment studies.

The differences in outcomes between the risk groups have warranted adjustments of management strategies, where low-risk HNCs require dose de-escalation and intermediate/high-risk HNCs require dose escalation (73). However, the heterogeneity in tumour response and outcomes in the intermediate/high-risk groups suggests that further biomarkers are needed to differentiate between those HNCs that would most benefit from dose-adaptation (74).

1.4.2 Treatment De-escalation

Ang et al described the hazard ratio for OS as 0.41 (95% CI 0.29-0.57, $p < 0.001$) for HPV-associated tumours and 1.01 (95% CI 1-1.01, $p < 0.002$) for every pack-year of smoking, which rose by 1% for every additional pack-year (71). The favourable prognosis for low-risk HPV-associated HNC has generated studies looking to improve functional and toxicity outcomes by de-escalating treatment, without compromising survival outcomes. Some of the potential methods that have been employed include de-escalation of adjuvant radiotherapy, omission or exchanging of the concurrent platinum-therapy component of CRT, or induction systemic therapy with reduced dose radiotherapy or surgery (72). The focus of discussion will be surrounding radiotherapy-based strategies. However, Tables 1-2 and 1-3 summarise the studies that investigated systemic therapy and surgical strategies to de-escalate the intensity of treatment.

1.4.2.1 Radiation Dose De-escalation

The MACH-NC meta-analysis did not analyse outcomes with stratification for HPV status (54). However, there are limited studies from around the time of this meta-analysis that aimed to explore de-escalation to radiotherapy only for HPV-associated HNC.

O'Sullivan et al retrospectively compared survival outcomes between patients with all-stage HPV-associated oropharyngeal SCCs that were managed with radiotherapy alone or CRT (75). A range of radiation doses were used, with the majority of patients receiving altered fractionations of radiotherapy with or without concurrent platinum, (60 Gy in 25 fractions over 5 weeks, 64 Gy in 40 fractions over 4 weeks (twice daily fractions) or 70 Gy in 35 fractions over 6-7 weeks). There were many confounding factors, including a large proportion of the radiotherapy-only cohort were above the age of 70 years, who are thought not to benefit from concurrent chemotherapy. They concluded that radiotherapy-alone shows poorer survival for stage IV disease, but they do not differentiate between fractionation schedules.

Chen et al attempted a similar retrospective analysis in a smaller cohort of patients with HPV-associated HNC (76). Their analyses suggest comparable OS (83%), LRC (90%) and distant metastasis-free survival (88%) rates to those reported in the literature at the time.

More recently, the phase 2 INFIELD study has investigated a radiation dose-reduction strategy to elective nodal regions in 72 patients with all-stage oropharyngeal or laryngeal (except T1-2 N0) SCCs (77). Clinically involved and suspicious lymph nodes were treated to a dose of 70 Gy and 64 Gy in 30 fractions over 5 weeks, respectively. Elective nodal regions were treated to a reduced dose of 40 Gy in 20 fractions over 4 weeks. 90% of patients received concurrent platinum. Five out of seven nodal recurrences occurred in the high-dose field. Two nodal recurrences occurred in the elective field. Median survival data has not yet been reported.

EVADER is a phase 2 study in low-risk HPV-associated all-stage oropharyngeal SCCs, evaluating omission of radiotherapy alone or CRT to conventionally targeted elective nodal regions (78). Recruitment has completed and results are awaited.

<u>Trial</u>	<u># Patients</u>	<u>Phase</u>	<u>Eligibility Criteria</u>	<u>Induction Chemo Regimen</u>	<u>Radiation doses</u>	<u>Outcomes</u>
RAVD, (2016) (79)	89	1/2	-Stage IVb HNC	2 cycles (3 weekly) Cisplatin (75 mg/m ²) Paclitaxel (175 mg/m ²) Cetuximab (250 mg/m ²) Everolimus discontinued after interim analysis	If ≥50% reduction in total tumour diameter, 75 Gy/50 f (BD) to gross disease only If <50% reduction in total tumour diameter, adjacent nodal station at risk additionally treated to 45 Gy/30 f (BD) Concurrent chemotherapy: paclitaxel (100mg/m ²), 5-FU (600mg/m ² /day for 5d) and hydroxyurea (500mg PO, BD for 5d) every 14d, (TFHX)	2-year PFS/OS: responders 86%/83.5% non-responders 68.7%/85.4% (p-value > 0.05)
Chen A et al (2017) (80)	44	2	-Stage III-IVb, p16+, oropharyngeal SCC	2 cycles (3 weekly) Carboplatin (AUC 6) Paclitaxel (175 mg/m ²)	Based on RECIST V1.1 criteria If partial or complete response, 57 Gy/27 f to gross disease and 43 Gy to uninvolved nodes If less than partial response, 60 Gy/30 f to gross disease and 48 Gy to uninvolved nodes Concurrent chemotherapy with weekly paclitaxel (30mg/m ²)	2-year PFS 92% (95% CI 77-97%) 2-year LRC 95% (95% CI 80-99%)
ECOG 1308 (2017) (81)	80	2	-Stage III-IVb, p16+, oropharyngeal SCC	3 cycles (3 weekly) Cisplatin (75 mg/m ²) Paclitaxel (90 mg/m ²) Cetuximab (250 mg/m ²)	Complete responders: 54 Gy/27 f over 5.5 weeks All other patients: 69.3 Gy/33 f over 6 weeks All patients received elective nodal irradiation to 51.3 Gy/27 fractions Concurrent weekly Cetuximab (250 mg/m ²)	2-year PFS/OS for all patients 78%/91% 2-year PFS/OS for complete responders 80%/94%
OPTIMA (2018) (82)	62	2	-p16+ oropharyngeal SCC -Low-risk: ≤T3, ≤N2b, ≤10 pack-year smoking -High-risk: T4, ≥N2c, >10 pack-year smoking	3 cycles (3 weekly) Carboplatin (AUC 6) Weekly paclitaxel (100 mg/m ²)	Low-risk disease with ≥50% response: 50 Gy/25 f alone over 5 weeks Low-risk with 30-50% / high-risk with ≥50% responses: 45 Gy/30 f (BD) with concurrent chemotherapy: paclitaxel (100mg/m ²), 5-FU (600mg/m ² /day for 5d) and hydroxyurea (500mg PO, BD for 5d) every 14d Low-risk <30% / high-risk <50% responses: 75 Gy/50 f (BD) with above chemotherapy	2-year PFS/OS: Low-risk 95%/100% High-risk 94%/97%
OPTIMA 2 (2021) (83)	73	2	-Oropharyngeal SCC -High-risk: T4 N2c-3/ >20 pack-year smoking/non-HPV -All other disease deemed low-risk	3 cycles (3 weekly) Nivolumab (360 mg) (+ 6 months adjuvant) Weekly nab-paclitaxel (100 mg/m ²)	Arm A: Low-risk ≥50% response: 50 Gy/25 f over 5 weeks alone OR TORS Arm B: High-risk ≥50% or low-risk <50% responses: 50 Gy/25 f + cisplatin OR 45 Gy/30f (BD) over 6 weeks + TFHX Arm C: High-risk <50% or low-risk <30% responses: 70 Gy/35 f over 7 weeks + cisplatin OR 75 Gy/50 f (BD) over 10 weeks + TFHX	2-year PFS/OS: all patients 90.4%/93.3% Arm A: 96.3%/96% Arm B: 85.8%/91.9% Arm C: 100%/100%
Quarterback (2019) (84)	22	1	-Stage III-IVb HNC ≤20 pack-year smoking	3 cycles (3 weekly) Docetaxel (75 mg/m ²) Cisplatin (100 mg/m ²) 5-Fluorouracil (750 mg/m ² over 4d)	p16+ and partial/ complete responses: randomised between standard of care 70 Gy/35 f over 7 weeks OR reduced dose (Rd) 56 Gy/28 f over 5.5 weeks Concurrent chemotherapy was weekly carboplatin (AUC 1.5)	<i>Trial ended early due to lack of financial support</i> Three-year PFS/OS: Std 87.5% Rd 83.3% (p-value >0.05)

Table 1-2, Summary of studies using induction chemotherapy to guide radiotherapy dosing strategy.

All staging as per AJCC TNM 7th Edition. AUC (area under the curve); BD (twice daily); CI (confidence interval); HNC (head and neck cancers); LRC (loco-regional control); PFS (progression-free survival); SCC (squamous cell carcinoma); TFHX (Paclitaxel, 5-Fluorouracil, Hydroxyurea and Radiotherapy); TORS (trans-oral robotic surgery)

<u>Trial</u>	<u># Patients</u>	<u>Phase</u>	<u>Eligibility Criteria</u>	<u>Pathological Features</u>	<u>Intervention</u>	<u>Outcomes</u>
ECOG 3311 (2021) (85)	495	2	-p16+, stage III-IVA oropharyngeal SCC, resectable T1-2	Arm A: T1-2; RM >3 mm; N0-1 Arm B: T1-2; RM <3 mm; N1-2; ≤ECE, ≤4 LNs Arm C: as Arm B – randomised 1:1 Arm D: positive RM, >1mm ECE, ≥5 LNs	Arm A (low-risk): observation Arm B (intermediate-risk): 50 Gy/25 f over 5 weeks Arm C (intermediate Risk): 60 Gy/30 f over 6 weeks Arm D (high-risk): 66 Gy/33 f with concurrent weekly cisplatin (40 mg/m ²)	2-year PFS Arm A: 96.9% Arm B: 94.9% Arm C: 96% Arm D: 90.7%
ORATOR 2 (2021) (86)	61	2	-p16+, oropharyngeal SCC, T1-2, N0-2, no ECE	Adjuvant radiotherapy for T3-4, ECE, RM <3 mm, >1 LN or any LN >3 cm, LVI	Arm 1: radiotherapy alone OR CRT, 60 Gy/30 f over 6 weeks; CRT with weekly cisplatin (40 mg/m ²) Arm 2: TORS. If RM <1 mm or ECE, adjuvant 60 Gy/30 f only; If RM >1 mm and no ECE, 50 Gy/25 f only	<i>Trial ended early due to complications in TORS arm</i> 2 deaths in TORS arm G2-5 toxicities similar across both arms
ADEPT (2020) (87)	42	2	-p16+, oropharyngeal SCC, T1-4a, N+, ECE+	T1-4a, must be node and ECE positive	Arm A: adjuvant 60 Gy/30 f over 6 weeks only Arm B: adjuvant 60 Gy/30 f over 6 weeks with concurrent weekly cisplatin (40 mg/m ²)	Results awaited
SIRS (2021) (88)	54	2	-p16+ oropharyngeal SCC, T1-2, N0-2b, no ECE, ≤20 pack-year smoking	Arm 1: T1-2, N1-2b, no LVI/PNI/level 3 LNs Arm 2: LVI/PNI, ≤1mm ECE or RM Arm 3: >3 LNs, level 4/ contralateral LNs, RM+, >1 mm ECE	Arm 1: Observation Arm 2: 50 Gy/25 f over 5 weeks Arm 3: 56 Gy/28 f over 5.5 weeks with concurrent weekly cisplatin (40 mg/m ²)	Median follow up 43.9 months PFS: Arm 1: 91.3% Arm 2: 86.7% Arm 3: 93.3% (p-value >0.05)
AVOID (2019) (89)	60	2	-p16+ oropharyngeal SCC, T1-2, N0-3 No PNI/LVI/RM <2mm	all patients must have had LN disease	Single-arm: 60-66 Gy/30-33 f Concurrent cisplatin (weekly 40 mg/m ² or 3-weekly 100 mg/m ²) OR weekly cetuximab (250 mg/m ²)	2-year LRC 98.3% 2-year PFS 96.2% 2-year OS 100%
MC1273 (2017) (90)	80	2	-p16+ oropharyngeal SCC, ≤10 pack-year smoking, negative RM	≥T3, ≥N2, LVI, PNI	Arm A: 30 Gy/20 f (BD) over 12 days + weekly docetaxel (15 mg/m ²) Arm B: as above but integrated boost to LN with ECE to 36 Gy/20 f (BD)	5-year PFS/OS: Arm A: 91.7%/94.4% Arm B: 75.6%/95.3%
MC1675 (2021) (91)	194	3	-p16+ oropharyngeal SCC	Intermediate-risk included one of: LN >3 cm, ≥2 LNs, PNI, LVI, T3-4 High-risk: ECE	As per MR1273 (DART) protocol but compared against standard of care (SOC) 60 Gy/30 f over 6 weeks with concurrent weekly cisplatin (40 mg/m ²)	2-year PFS DART/SOC: ECE+/pN0-1: 89.6%/95.8% ECE+/pN2: 42.9%/100%
DIREKHT (2020) (92)	200	2	-Oral cavity, oropharyngeal or laryngeal SCC: -pT1-3, pN0-2b -Hypopharyngeal SCC: pT1-2, pN1	Arm A: pT2, RM ≥5 mm, no LVI/PNI, >3 ipsilateral LNs Arm B: pT2 +/- RM <5 mm +/- LVI/PNI, ≤3 ipsilateral LNs Arm C: pT2, RM ≥5 mm, no LVI/PNI, ≤3 ipsilateral LNs	Arm A: adjuvant 56 Gy/28 f over 5.5 weeks only with bilateral elective nodal irradiation Arm B: adjuvant 64 Gy/32 f over 6.5 weeks only with ipsilateral elective nodal irradiation Arm C: adjuvant 56 Gy/28 f over 5.5 weeks only with ipsilateral elective nodal irradiation	Still recruiting
DELPHI (2021) (NCT03396718)	384	2	-Oropharyngeal SCC	Intermediate risk: T3+R0 resection +/- 1-3 LNs without ECE High Risk: R1 resection +/- pT4 +/- >3 LNs +/- any ECE	p16+, intermediate risk: randomised to adjuvant radiotherapy 59.4 Gy/33 f or 55 Gy/25 f (+/- concurrent platinum) Any high-risk: adjuvant radiotherapy 66 Gy/33 f over 6.5 weeks with concurrent platinum	Still recruiting
PATHOS (2019) (93)	1100	3	-Oropharyngeal SCC -T1-2, N0-2b, suitable for TORS	Arm A: no adverse features Arm B: T1-3, N2a-2b, LVI/PNI, RM 1-5mm Arm C: RM <1 mm, +/- ECS	Arm A: No adjuvant treatment Arm B: Randomise to either adjuvant 60 Gy/30 f over 6 weeks or 50 Gy/25 f over 5.5 weeks Arm C: Randomise to adjuvant 60 Gy/30 f with or without concurrent cisplatin	Still recruiting

Table 1-3, Summary of studies investigating de-escalation of adjuvant therapy after primary surgery.

All staging as per AJCC TNM 7th Edition. BD (twice daily); CRT (concurrent chemoradiotherapy); ECE (extra-capsular extension); LN (lymph nodes); LRC (loco-regional control); LVI (lympho-vascular invasion); PFS (progression-free survival); PNI (peri-neural invasion); RM (resection margins); TORS (trans-oral robotic surgery);

1.4.3 Treatment Intensification

Treatment-intensification strategies have been investigated for HNCs with poorer control rates, such as laryngeal, hypopharyngeal and HPV-negative oropharyngeal SCCs. Prior to the study by Ang et al (71), approaches to treatment-escalation involved blanket increases of radiation dose or systemic therapy intensity without accounting for any degree of tumour risk. Studies that recently or are currently exploring treatment intensification using systemic therapy are summarised in Table 1-4.

1.4.3.1 Radiation Dose Intensification

Atwell et al reviewed the studies investigating radiation dose escalation for all HNCs (94). The majority of studies employed modest dose-escalation strategies, compared to current standard of care, however, the range of doses (equivalent dose in 2 Gy per fraction, EQD2) was 76.59 Gy to 90.2 Gy. Pooled control and survival data show that three-year LRC was 68.2 – 85.9% and 48.4 – 51.9% for OS, which reflect the survival data reported in the literature after standard of care radiation doses. There was no subgroup analysis performed for patients stratified by HPV and smoking status. In a phase 3 study, Tao et al compared dose-escalated IMRT (75 Gy in 35 fractions over 6 weeks) against 3-dimensional conformal radiotherapy (3D-CRT) (70 Gy in 30 fractions over 6 weeks) with concurrent cisplatin in stage III-IV non-nasopharyngeal HNC (95). Apart from xerostomia, their results, including after stratifying for p16 status, show no difference in LRC or survival between the two methods.

A lack of benefit of dose escalation is also reported in the phase 3 ART DECO study, which compared dose-escalated (chemo)radiotherapy (67.2 Gy in 28 fractions over 5.5 weeks) against standard of care (65 Gy in 30 fractions over 6 weeks) in laryngeal or hypopharyngeal SCCs (96). This study was closed after an interim analysis showed no benefit of dose escalation.

The ESCALOX study is also a phase 3 randomised study that is aiming to escalate dose with radiotherapy and concurrent cisplatin to gross tumour (97). The study is recruiting patients with HPV-negative oropharyngeal, hypopharyngeal or oral cavity SCCs. Patients will be randomised to receive either 80.5 Gy in 35 fractions over 7 weeks

or standard of care (70 Gy in 35 fractions over 7 weeks). The trial is yet to publish pre-study toxicity results before progressing to the main phase where the primary endpoint will be two-year LRC.

CompARE is a phase 3 randomised multi-arm multi-stage study that has been the successor to the ArChIMEDEs-Op study (98). CompARE is utilising a more stratified approach to treatment escalation by focusing on intermediate and high-risk oropharyngeal cancers. Standard of care CRT (Arm 1, 70 Gy in 35 fractions over 7 weeks) is compared against a hypofractionated CRT regimen (Arm 2, 64 Gy in 24 fractions over 5 weeks) or Arm 1 with the addition of induction and post-CRT durvalumab (Arm 3). Recruitment to Arm 3 was suspended due to a serious adverse event, but a planned interim analysis showed no benefit from hypofractionation.

The radiotherapy-based escalation strategies described in this section applied dose escalation to groups of patients stratified by primary site and tumour stage. It is now being realised that tumour response, even within these sub-groups, can differ due to underlying differences in tumour biology (99). Although the studies discussed in this section have not demonstrated a survival benefit from dose-escalation, data from the patients who could have benefited from dose escalation may have been diluted with data from patients grouped with the same tumour stage but with different disease biology that rendered them less likely to have benefited.

<u>Trial</u>	<u># Patients</u>	<u>Eligibility Criteria</u>	<u>Systemic Therapy Regimen</u>	<u>Radiation doses</u>	<u>Outcomes</u>
NRG-HN004 (100)	454 (Target)	-Locally-advanced stage III-IVb oropharyngeal, hypopharyngeal, laryngeal, oral cavity or unknown primary SCCs -Contraindication to cisplatin	Arm A: weekly cetuximab for 8 cycles Arm B: 4 weekly <i>Durvalumab</i> up to 7 cycles	70 Gy/35 f over 7 weeks	No DLT after safety review. Recruitment currently halted for planned interim analysis
RTOG 1216 (101)	613 (Target)	-Locally-advanced stage III-IVb oropharyngeal, hypopharyngeal, laryngeal or oral cavity SCC -Gross total surgical resection with resultant pathologically high-risk features (ECE and/or RM <1 mm)	Arm A: concurrent weekly cisplatin (40 mg/m ²) for 6 weeks Arm B: concurrent weekly docetaxel (15 mg/m ²) Arm C: concurrent once weekly cetuximab (400 mg/m ² loading dose pre-radiotherapy, then 250 mg/m ²) and docetaxel (15 mg/m ²) for 6 weeks Arm D: concurrent weekly cisplatin (40 mg/m ²) for 6 weeks and 3-weekly <i>Atezolizumab</i> for up to 8 doses	60 Gy/30 f over 6 weeks	Still recruiting
IMvoke010 (102)	406	-Locally-advanced stage III HPV-associated oropharyngeal SCC -Stage IVA-IVB HPV-negative oropharyngeal, hypopharyngeal, laryngeal or oral cavity SCC -Completed definitive local therapy (surgery or (chemo)radiotherapy)	Arm A: 3-weekly <i>Atezolizumab</i> 1200 mg for up to 52 weeks or ≤16 cycles Arm B: Placebo	-	Results awaited
NIVOSTOP (103)	680 (Target)	-Locally-advanced stage III-IV -Gross total surgical resection with resultant pathologically high-risk features (ECE, multiple PNI, ≥4 LNs. RM <1 mm)	Arm A: concurrent 3-weekly cisplatin (100 mg/m ²) for 3 cycles Arm B: concurrent cisplatin (as per Arm A) + <i>Nivolumab</i> (240 mg 3 weeks before radiotherapy, 360 mg 3-weekly concurrently, then 480 mg maintenance)	66 Gy/33 f over 6.5 weeks	Still recruiting
IMSTAR-HN (104)	276	-Locally-advanced stage III-IVb HPV-negative oropharyngeal SCC that is surgically resectable	Arm A: concurrent once weekly (40 mg/m ²) or 3-weekly (100 mg/m ²) Arm B: neoadjuvant <i>Nivolumab</i> (3 mg/kg) 2 weeks before surgery. Followed by concurrent CRT with cisplatin (as above) AND (Arm B1) 3-weekly <i>Nivolumab</i> (3 mg/kg) up to 6 months OR (Arm B2) <i>Nivolumab</i> + 6-weekly <i>Ipilimumab</i> (1 mg/kg) up to 6 months	66 Gy/33 f over 6.5 weeks	Results awaited
KEYNOTE 412 (105)	780	-Locally-advanced stage III-IVb oropharyngeal, hypopharyngeal, laryngeal or oral cavity SCC not suitable for surgical resection -Established PD-L1 status	Arm A: concurrent 3-weekly cisplatin (100 mg/m ²) + Placebo Arm B: concurrent 3-weekly cisplatin (as above) + 3-weekly <i>Pembrolizumab</i> (200 mg) (one dose pre-CRT, 2 doses concurrent with CRT, followed by up to 14 adjuvant doses)	70 Gy/35 f over 7 weeks	Median event-free survival at 4 years not reached for Arm B. Difference in survival failed to meet superiority thresholds.
REACH (106)	707	-Locally-advanced stage III-IVb oropharyngeal, hypopharyngeal, laryngeal or oral cavity SCC -Established PD-L1 status	Arm A1 (cisplatin fit): concurrent 3-weekly cisplatin (100 mg/m ²) Arm A2 (cisplatin fit): concurrent once weekly cetuximab (400 mg/m ² loading dose pre-radiotherapy, then 250 mg/m ²) + 3-weekly <i>Avelumab</i> (10 mg/kg) up to 12 months Arm B1 (cisplatin unfit): concurrent once weekly cetuximab (as above) Arm B2 (cisplatin unfit): concurrent cetuximab and <i>Avelumab</i> (as per Arm A2)	69.96 Gy/33 f over 6.5 weeks	PFS events not reached for Arm A; 1-year PFS Arm A1 (73%) vs A2 (64%) 2-year PFS: Arm B1 (31%) vs B2 (44%), p=0.34)
Javelin 100 (107)	697 (Target)	-Locally-advanced stage III-IVb oropharyngeal, hypopharyngeal, laryngeal or oral cavity SCC	Arm A: concurrent 3-weekly cisplatin (100 mg/m ²) + Placebo Arm B: concurrent cisplatin (as per Arm A) + 3-weekly <i>Avelumab</i> (10 mg/kg) up to 12 months	70 Gy/35 f over 7 weeks	Terminated after interim analysis as boundary for futility had been crossed. Median PFS not reached after median follow up of 14.8 months
KEYNOTE 689 (108)	704 (Target)	-Locally-advanced stage III-IVb oropharyngeal, hypopharyngeal, laryngeal or oral cavity SCC -Eligible for primary surgical resection	Arm A: adjuvant CRT with concurrent 3-weekly cisplatin (100 mg/m ²) Arm B: as per Arm A + 3-weekly <i>Pembrolizumab</i> (200 mg) (two doses pre-surgery, 2 doses concurrent with CRT, followed by up to 13 maintenance doses):	60-70 Gy/30-35 f over 5-7 weeks	Still recruiting

Table 1-4. Summary of current or recent phase-3 studies evaluating immunotherapy-based treatment intensification.

All staging as per AJCC TNM 7th Edition. CRT (concurrent chemoradiotherapy); ECE (extra-capsular extension); f (fraction); LN (lymph-node); PD-L1 status (programme death -ligand 1); PFS (progression-free survival); PNI (peri-neural invasion); RM (resection margin); SCC (squamous-cell carcinoma);

1.5 Adaptive Radiotherapy

The exploratory treatment approaches discussed in the previous sections analyse treatment de-escalation or intensification strategies based on patient stratification by pathological or clinical characteristics of disease and initial presentation. Adaptive radiotherapy (ART) is an umbrella term that describes treatment adjustments that may occur at pre-determined intervals or as a reactive response to weight loss, disease/contour changes or poor immobilisation (109). Anatomical-ART (A-ART) refers to treatment adaptation with the same target definitions adjusted for gross anatomical changes. Biological-ART (B-ART) describes the concept of a change in treatment intensity or target definition as a result of tumour response or change in biological parameters.

The shift from 3D-CRT to IMRT has resulted in an increased therapeutic ratio, as physicians are able to exercise improved control over placement of radiation dose, resulting in an improved tumour control probability (TCP) and stable or decreased normal tissue complication probability (NTCP) (110). It is also suggested that uniform dose to the primary tumour does not always give definitive local control (111). Dose-escalation strategies discussed in previous sections are largely limited by the doses to OARs and, ultimately, the NTCP. Conversely, dose de-escalation approaches or reducing target volumes may potentially compromise TCP in the event of target/contour changes or set-up errors (112).

Steep dose gradients with IMRT techniques make accurate target definition and consistency of patient set-up of paramount importance. ART, therefore, may compensate for anatomical changes that occur during treatment and prevent dose compromise to critical OARs or target structures (113). Image-guided radiotherapy (IGRT) using cone-beam Computed Tomography (CBCT) is currently in routine use to correct for daily random set-up errors. However, soft-tissue definition on kilo/megavoltage imaging is insufficient to detect detailed intra-treatment changes in tumour or OARs such as parotid glands (114).

1.5.1 Anatomical-Adaptive Radiotherapy

Weight loss is the most frequently occurring anatomical change that is seen during a course of radiotherapy (115). Weight loss causes progressively medial shifts of superficial structures and reduction of overall patient thickness with resultant changes in dosimetry (116). Bhide et al show that there are significant reductions in the primary tumour CTV (mean 11 cm³, 95% CI 3-14) and parotid (4.2 cm³, 95% CI 3-5.5) volumes, with the largest proportion of volume changes occurring within the first two weeks of radiotherapy (117). This study also demonstrated a mean medial shift of the parotid glands of 4 mm, with an additional 2.8 Gy of dose being delivered by week four of radiotherapy. These findings have been similarly demonstrated by Castadot et al, who show a mean rate of reduction in size of the primary and nodal GTVs of 3.2% and 2.2% per day, respectively (118). Their further work revealed increased dose to spinal cord planning risk volume (PRV) and oral cavity after anatomical modification (119).

Dosimetric analyses by Surucu et al aimed to compare the dose delivered to OARs with and without ART (120). A repeat CT scan was performed in the fourth week of radical radiotherapy for mostly oropharyngeal SCCs and median dose reductions in maximum dose to the spinal cord and brainstem and mean doses to the ipsilateral and contralateral parotid glands were 4.5, 3, 6.2 and 2.5 percent, respectively. Maximum dose increases to these OARs were 4.6, 19.9, 6.9 and 28.4 percent, respectively.

Primary tumour and nodal response rates may differ between HPV subtypes of HNC (121). HPV-associated primary tumours are noted to reduce in volume at a higher rate compared to HPV-negative disease. Surucu et al report that HPV-negative gross primary tumour may even increase in volume by up to 18% (122). A limited study of ten patients demonstrates a potentially larger proportion of shrinkage of the superficial parotid glands compared to the deep lobes (123). NTCP modelling shows differing responses to radiotherapy within sub-regions of the parotid and submandibular glands (121,124).

Such differential responses to radiation, warrant further improvement of existing NTCP models as well as the ideal time-points to repeat imaging and re-planning of radiotherapy. A systematic review implies that the second or third week is the most

popular time point (125). However, the included studies utilised a more reactive approach as adaptation was triggered by signs of weight loss (roughly 10%), ill-fitting mask and reduced neck separation (≥ 1 cm). Few studies in this review had set dosimetric criteria for replans, although some OAR dose constraints were inevitably breached after cases of severe weight loss.

1.5.2 Biological-Adaptive Radiotherapy

Not all patients with low-risk or high-risk disease respond to the same degrees. It is well described through Positron Emission Tomography (PET) and MRI (Magnetic Resonance Imaging)-based functional imaging studies that biological changes occur sooner than anatomical/volumetric, although they may not be recognised on conventional CT-based methods (126). The three facets of tumour biology that have received the most research attention are metabolism, proliferation and vascularity/hypoxia (127). B-ART may be employed to personalise therapy to counter this. Although dose-escalation has not yet proven to be a superior strategy for non-responsive tumours, functional image-guided ART and personalisation of management may find those patients who benefit most from such approaches, which the previously discussed dose-escalation studies may have failed to stratify.

1.5.2.1 PET/CT

PET-based exploration of tumour biology has been conducted using an array of variable radiotracers that assess different facets of tumour biology. Despite the interest that PET/CT has received for this purpose, there is no universal standardisation of segmentation or parameter reporting, limiting the interpretation of data between institutes.

2- ^{18}F fluoro-2-deoxyglucose (FDG)-PET/CT is routinely used for staging HNC (128). However, over the past 15 years, the use of FDG-PET/CT for radiotherapy planning or to assess tumour response in metabolism has received growing interest (129). Daisne et al compared GTV delineation between contrast-enhanced CT, MRI and FDG-PET/CT in patients with HNC (130). They demonstrated that the mean FDG-PET-derived

oropharyngeal SCC GTV volumes were the smallest (20.3 cm³) compared to CT (32 cm³) or MRI (27.9 cm³) and PET-derived volumes matched pathological disease most accurately, a finding replicated by Magalhaes et al (131). However, no imaging modality was sensitive to superficial mucosal disease.

Daisne et al used automated methods to delineate GTV using PET/CT, which utilised source to background ratios (132). They also demonstrate that GTV segmentation is heavily operator-dependent and variable based on what method of segmentation is chosen, as more recent studies have utilised one or a combination of metrics such as mean/max standardised uptake value (SUV_{mean/max}), metabolic tumour volume (MTV), total lesion glycolysis (TLG) or tumour to background ratio (TBR) (127).

Min et al demonstrate the predictive potential of SUV_{max}, MTV and TLG as FDG-PET/CT based biomarkers of response (both pre- and intra-treatment) in 100 patients with non-nasopharyngeal HNC (133). TLG was the strongest predictive factor, however, the combination of all three parameters strengthens the predictive potential.

Studies investigating FDG-PET/CT driven ART have provided limited outcome data due to small sample sizes and pooled data have been difficult to compare due to differences in scanning or segmentation protocols (134,135). However, the phase 2 study by Min et al, described above, has progressed to the phase 3 TEMPORAL study, which aims to evaluate the evolution of FDG-PET/CT related changes at baseline, week 2 and week 4 of standard-of-care CRT in 130 patients with non-nasopharyngeal HNC (NCT02469922, awaiting results). Smaller sample sized studies suggest FDG-PET/CT changes (TLG_{40%} and SUV_{max}) are deemed most significantly predictive of outcome to radiotherapy in the first (136) or second (137) weeks, although PET/CT findings later in treatment are likely to be confounded by inflammatory responses to radiation (138).

The first early-phase study exploring a “dose-painting by numbers” approach at three intervals during treatment demonstrates the feasibility and safety of dose-escalation to 85.9 Gy to the GTV without any grade-4 toxicities (139). A similar dose-escalation approach is currently being investigated in the phase 3 ARTFORCE study, which is comparing standard-of-care CRT with 70 Gy in 35 fractions over 7 weeks against a dose escalation to the SUV_{50%} as identified by FDG-PET/CT after the second week of

treatment only (140). Dose will be escalated as a simultaneous integrated boost to a maximum dose of 84 Gy to 2% of the Planning Target Volume (PTV), over 35 fractions in 7 weeks.

The failure rates after radical radiotherapy are 4.2 times higher when hypoxia is present (as defined by PET/CT-based SUV_{max} thresholds) (141). Detection and resolution of hypoxia has, therefore, been of great interest for many decades. Hypoxic imaging using PET is being explored by using an array of nitroimidazole-based radiotracers, such as ^{18}F -fluoromisonidazole (F-MISO) and ^{18}F -fluoroazomycin-arabinozide (F-AZA), which are the most widely used (129). Hypoxia is thought to be detectable using PET when the partial pressure of oxygen drops below 10 mmHg, seen in roughly 60% of tumours (142). Nehmeh et al demonstrate in an exploratory study of 14 patients with HNC that there is significant variability of spatial uptake of F-MISO PET in hypoxic zones, with a correlation coefficient between serial scans of 46% (143). Lin et al further investigated the dosimetric consequence of the spatial shifts in hypoxia in seven patients with HNC (144). The changes observed on F-MISO PET compromised the coverage of hypoxic tumour volumes in four patients, when trying to utilise non-adaptive dose-painting IMRT. Small-sample studies looking at spatial relations of local-tumour recurrences to hypoxia show conflicting results, where inconsistencies are likely related to non-standardised imaging, segmentation and delineation protocols (145,146).

The effectiveness and accuracy of PET for imaging of hypoxia is hampered by the poor resolution, where large voxel sizes provide averaged information on the hypoxic signals at microscopic levels (127). Therefore, hypoxic PET remains largely limited to imaging chronic and stable hypoxic regions, although new-generation tracers such as F-AZA or F-HX4 may mitigate some instability issues based on their improved lipophilic and pharmacodynamic properties (147). Despite this limitation, a hypoxia-directed dose-escalation approach is being evaluated in a phase 2 study that explores F-MISO PET/CT to dose-escalate to hypoxic tumour sub-volumes in the third week of radiotherapy for oropharyngeal or hypopharyngeal SCCs (148).

1.6 MRI-Guided Adaptive Radiotherapy

The integration of diagnostic Magnetic Resonance Imaging (MRI) and ^{18}F -FDG PET/CT into the CT-based radiotherapy workflow is in routine use for structure outlining, but its utilisation may be limited due to potential registration issues, due to differences in patient set-up or software and limited availability due to scanner demand for non-RT purposes (149). Conventional ART using CBCT or PET/CT-based approaches are costly, time- and labour-intensive and provide *offline* ART capabilities at most. A cost-analysis study by Vanderstraeten et al suggests that a three-phase adaptive treatment regimen over 30 fractions, involving FDG-PET/CT driven replanning twice during treatment, costs 30-45% more than standard-of-care IMRT (150).

The implementation of functional Magnetic Resonance Imaging (fMRI) allows more accurate soft-tissue definition and assessment of biological functions *in vivo*. For this purpose, the introduction of the MR-Linear Accelerator (MR-Linac) platform has greatly changed the ability to provide *online* MR-guided radiotherapy (MRgRT) (Figure 1-2) (151). The amalgamation of a linear accelerator and on-board 1.5 T MRI scanner on the MR-Linac offers the capability to acquire anatomical and functional imaging with patients in the treatment position and simultaneously deliver true online ART (152).

Techniques such as Diffusion-weighted/ Apparent Diffusion Coefficient imaging (DWI/ADC) and Blood Oxygenation-level Dependent (BOLD) MRI on diagnostic scanners have received great attention for their potential as prognostic or predictive biomarkers. However, these sequences on the MR-Linac platform are still being refined and clinically validated for some tumour sites (149).

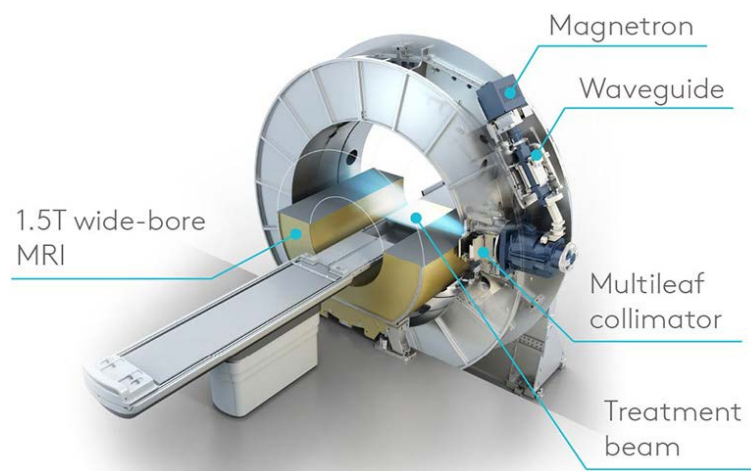


Figure 1-2, Schematic of the MR-Linear Accelerator.

The Elekta Unity system has a 7 MV photon linear accelerator built within a 1.5 T MRI with a split in the gradient coil to accommodate passage of radiation beams. Image from Medgadget (153).

1.6.1 MRI-Guided Anatomical ART

The use of CT and PET/CT modalities for ART are largely restricted to assessments at few and fixed time points due to limited resources, staff time and additional radiation exposure. The use of MRI may be at fixed or serial time points depending on the treatment platform used. MRgRT at fixed time points largely aims for similar outcomes to ART using CBCT or PET/CT based methods, by compensating for anatomical and/or biological changes over the course of radiotherapy (154).

Feasibility and small-sample-sized retrospective dosimetric studies demonstrated the underestimation of cumulative dose to OARs, such as parotid glands (155), and changes in tumour and OAR volumes (156). However, similarly to the PET/CT studies described earlier, the most appropriate time points for performing A-ART remains under debate.

The prospective phase 1 MARTHA study evaluated the role of once-weekly offline replanning for twelve patients receiving radical radiotherapy for HNC on an MR-Linac (157). Daily MRIs were acquired to assist with patient position adjustments, but no daily adaptations were made. The primary outcome was to assess the cumulative volumetric and dosimetric impacts on salivary glands and targets. The mean change in parotid volume was -31.9% (-8.2 ml) after five weeks of radiotherapy, with a mean distance of migration of 6.5 mm medially and the resultant cumulative-dose increase to the parotid glands was 0.5 Gy higher than original planned. They also suggested that once-weekly adaptation reduces the mean ipsilateral and contralateral parotid doses by 2.8 and 0.9 Gy,

respectively, compared to a single adaptation. However, this comparison against a single adaptation was performed at a very late stage in treatment (week 5), where the benefits of adaptation are likely to have been lost with limited fractions left to deliver. This study has now been extended to phase 2 and currently aims to recruit up to 44 patients.

The MR-ADAPTOR study is a similarly designed phase 2 study but utilising the Elekta Unity MR-Linac system, where a daily “Adapt-to-Position” workflow achieves a virtual couch shift to correct patient set-up (158). This study, however, will perform full once-weekly offline replanning with a new simulation CT and MRI. In contrast, the feasibility of an online ART approach is described using a modified “Adapt-to-Shape” approach on the same MR-Linac system, whereby daily MR is used to deformably propagate external patient contours with online plan re-optimisation (159). This daily adaptation is thought to reliably compensate for progressive weight loss experienced over a treatment course, although the impact of this on cumulative dose to target and OARs will be investigated as data from further patients are gathered.

1.6.2 MRI-guided Biological ART

Changes in MRI signals and contrast can provide additional information on biological function as well as anatomical detail. Factors such as tissue cellularity, perfusion and hypoxia have been investigated for their potentials as predictive or prognostic biomarkers. The majority of published work has taken place on diagnostic-MRI scanners. However, similar functions are now being explored on the various MR-Linac platforms that are available (160).

1.6.2.1 Diffusion-Weighted Imaging/Apparent Diffusion Coefficient

DWI is a form of fMRI that has been used in the diagnostic setting for many different tumour subtypes and pathological conditions (161). Differences in the degrees of diffusion of protons (from dissociated water molecules in solution) in soft-tissues are the bases for how contrast is generated in DWI (Figure 1-3). Restricted diffusion, in the oncological context, is more apparent when a relatively higher cell density is present (151). DWI can differentiate malignant from benign head and neck lesions as malignant

lesions produce increased signal (162,163). There is ongoing interest in exploring DW-MRI as a potential biomarker to identify response to radiotherapy (163).

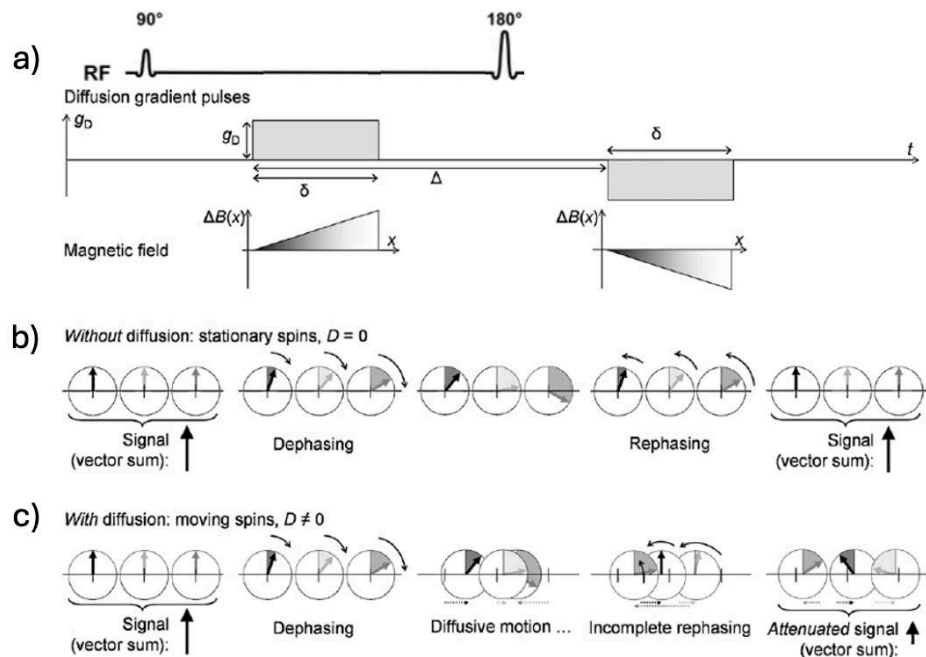


Figure 1-3, Single-Shot Spin-Echo Diffusion-Weighted MRI.

In a single-shot spin-echo sequence, a radiofrequency pulse is applied which induces proton spin at certain flip angles and frequency. a) A magnetic diffusion gradient pulse is then applied along a single direction that is of a specific amplitude (g_D) and of a certain duration (δ), the combination of which is called the “b-value.” The spin-echo component refers to an additional 180° radiofrequency pulse, which induces an inversion of the proton precession position. A subsequent diffusion gradient of equal strength and direction is applied. b) In a state of restricted diffusion, the anatomical and spin positions will have remained relatively stationary. The actions of the first and second diffusion gradient will have cancelled out each other’s effects as a result of the intervening 180° radiofrequency pulse. The resultant synchronised spins of the protons produce the characteristic signal seen with restricted diffusion. c) When water is diffusing freely, the shift in anatomical and spin positions relative to their initial state no longer results in a negating action when a second gradient field pulse is applied, resulting in an attenuated signal. Image from Dietrich et al (164).

Each b-value represents a combination of the strength and duration of the diffusion gradient applied. The higher the b-value, the greater the sensitivity of the sequence to diffusion effects. One drawback to stronger diffusion gradients may be distortion of the patient anatomy and so spatial correlation may be affected, particularly with older DWI sequences such as single-shot echo planar image (ssEPI) (165). A typical DWI sequence is sensitive to diffusion in both extravascular and intravascular compartments (166). Blood vessels within tissue, particularly neoplastic tissue, may have more permeable walls and a disorganised architecture compared to normal vasculature. Therefore, water flow within the intravascular compartments contributes to attenuation of signal due to freely diffusing water, referred to as “Intravoxel incoherent motion (IVIM)” (167). A

summary of the diffusivity of water can be summarised by the ADC, which is the biomarker that is more readily reported and analysed (Figure 1-4).

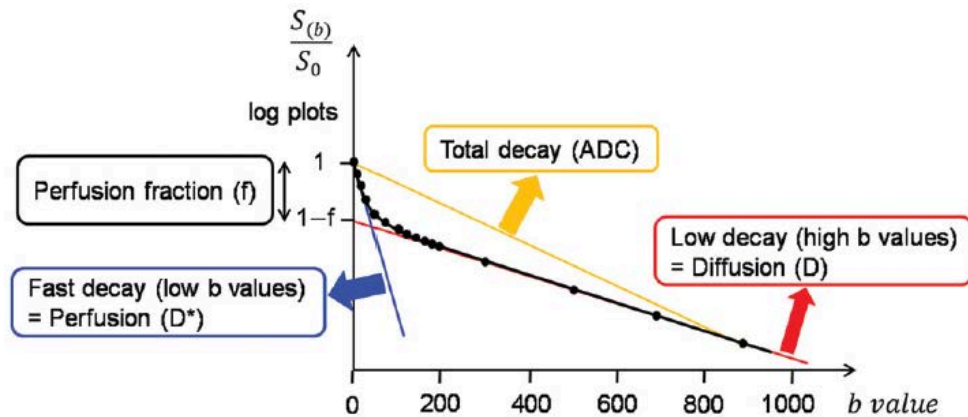


Figure 1-4. Apparent Diffusion Coefficient and Intra-Voxel Incoherent Motion.

The b -value (s/mm^2) refers to the strength of the diffusion gradient applied. Classic ADC (yellow line) is determined on a per voxel basis and described by the gradient of a line drawn between the natural logarithm of the signal intensities when no ($b=0$) and a high ($b \geq 500$) diffusion gradient is applied. This describes a mono-exponential function. The IVIM concept describes a more physiological bi-exponential concept, which separates the true ADC (red line), pseudo-diffusion (blue line) and the perfusion fraction (f), determined by the difference between the signal intensity at $b=0$ and the y -intercept (168).

With the ssEPI sequence, there is always a trade-off between resolution and signal-to-noise ratio (SNR). Therefore, ssEPI is prone to image artefact due to motion, which is particularly prominent around air-soft tissue interfaces (169). A potential solution to these distortions in ssEPI is a REadout Segmentation of Long Variable Echo-trains (RESOLVE) sequence, that is based on a multi-shot DWI sequence, with more efficient signal collection and non-linear completion of the k -space, which ultimately produces images with less anatomical distortion, improved SNR and resolution (170). For these reasons, RESOLVE has been favoured over ssEPI across various body sites that are particularly prone to motion or high blood flow velocity artefacts (170–173).

A functional image-guided study demonstrated the feasibility of performing DW-MRI in patients with HNC during radical CRT (136). A $>17\%$ increase in ADC between baseline and the second week of radiotherapy optimally distinguished responding from non-responding primary tumours. Tumours with a high baseline ADC ($>1.4 \times 10^{-3} \text{ mm}^2/\text{s}$) are less likely to respond to RT, as a high ADC may reflect presence of necrosis, low cellularity and tumour hypoxia (174,175). These findings are confirmed in a systematic review that focuses on patients receiving radical RT for HNC (176). Although there was much heterogeneity in scanning protocols and time points between individual studies, a

threshold for ADC change between 15.5-25% after two weeks of radiotherapy is determinant of a responding primary tumour. Therefore, there has been great interest in ADC-guided B-ART and is an aim of the phase 1/2 INSIGHT II trial (NCT04242459).

1.6.2.2 Intra-Voxel Incoherent Motion

The ADC describes a mono-exponential function. However, it is known that there are multiple anatomical compartments that can grossly be divided into intravascular and extra-vascular compartments. The diffusion and motion of water molecules in the intravascular compartment is less restricted and can skew the ADC value. The increased signal attenuation is more frequently observed at b-values below 100 s/mm² (177). Therefore, the IVIM concept describes the bi-exponential model by the separate factors that contribute to the overall signal intensities seen in DWI (Figure 1-4).

The IVIM effect can be mapped out by performing DWI MRI at a high number of b-values below 100 s/mm² to better define the portion of the curve where the exponential function changes. The gradient of the curve at b-values above 100 s/mm² represent the true ADC (D) and the gradient of the curve at lower b-values represents pseudo-diffusion (D*), which describes the flow of water within microvasculature.

Perfusion fraction (f) describes the percentage vascularity within a volume, which may be determined by two main methods as described by Marzi et al (178). One method is to model the differences in signal intensities as b-value increases, using the bi-exponential function, and solving for “f”:

$$S_b/S_0 = [(1-f) \times e^{-bD}] + [f \times e^{-b(D+D^*)}],$$

where S_b is the mean signal intensity with b-value b , S_0 is the mean signal intensity when b-value is 0 s/mm², D is the true ADC (mm²/s) and D^* is pseudo-diffusion (mm²/s). The alternative method described is referred to as the “extrapolation method” that is obtained from asymptotic fitting of the true diffusion (D) curve and measuring the difference between the signal intensity at the y-intercept (S_0^{extr}) and $b = 0$ s/mm² (S_0^{meas}):

$$f_{asym} = [(S_0^{meas} - S_0^{extr}) / S_0^{meas}] \times 100.$$

Marzi et al retrospectively compared these two methods of perfusion fraction in 43 patients with primary HNC and show small differences in the mean perfusion fraction, suggesting that either method is acceptable (178).

As understanding of the IVIM concept improves, studies have looked at the benefits of splitting the more conventional DWI/ADC components into IVIM metrics, by analysing true diffusion and perfusion fraction separately. Two studies, both analysing IVIM parameters in patients with HPV-associated oropharyngeal SCC show significant increases in ADC and true diffusion around week 3 of their radical RT (179,180). For perfusion fraction, Paudyal et al demonstrated an increasing trend whereas Ding et al reported a significant increase over a similar time period. The data for pre-treatment perfusion fraction are conflicting and it is not currently established whether, like ADC, pre-treatment perfusion fraction can predict responsive from non-responsive tumours (181). Unfortunately, data from multiple studies cannot be pooled for quantitative analyses due to heterogeneity in treatment, IVIM sequence and scanning protocols, although a systematic review suggests that the greatest prognostic strength of IVIM-MRI comes from the combination of ADC/true diffusion and perfusion fraction (182).

1.6.2.3 Blood Oxygenation-Level Dependent MRI

Susceptibility-weighted MRI is an umbrella term that describes the magnetic field perturbation created by either para-magnetic (attractant of magnets) or diamagnetic (repellent of magnets) compounds (183). The BOLD effect is a specific form of susceptibility-weighted MRI that is sensitive to the para-magnetic effects of deoxy-haemoglobin (d-Hb). The presence of d-Hb, results in a shortening of the T2* (and to a lesser degree T2) relaxation rate and this local disturbance of the magnetic field induces phase shifts in the spins of any protons immediately surrounding the blood vessels that contain d-Hb (184). The dephasing effect of d-Hb is seen as signal attenuation on a T2*-weighted MRI and may be used as a surrogate for measuring hypoxia within soft tissues on a voxel-by-voxel basis (183).

The presence of hypoxia and its detrimental impact on local control is well described in the context of HNC (185,186). Tumour neovasculature is morphologically and functionally abnormal, resulting in poor blood flow and oxygen delivery to cells (187).

Tumour hypoxia, like the vasculature, is heterogenous throughout the lesion, with regions of acute and chronic hypoxia (188). Potential strategies to circumvent tumour hypoxia have explored red blood cell transfusions, hyperbaric oxygen or carbogen inhalation and administration of drugs such as nicotinamide or nimorazole, with varying degrees of success (189–191). However, treatment strategies that target tumour hypoxia may not be relevant in HPV-associated tumours as a result of their inherently high response rates to RT (190).

A pre-clinical study investigated $R2^*$ ($=1 \div T2^*$) fluctuations in murine xenograft models of oral tongue SCC and correlated the findings with histopathological analyses (192). Mice had intraperitoneal injections of pimonidazole one hour before a 50 min $T2^*$ -MRI. After MRI completion, tumours were excised and immunohistochemical analyses performed for comparison to MRI findings. Their work showed that voxel-wise $R2^*$ values fluctuated, reflecting variations in blood flow and acute hypoxia. The locations of more stable chronic hypoxia correlated with those seen on histopathological analyses, a finding that has also been demonstrated in prostate cancer (193).

The impact of carbogen (95-98% O_2 and 2-5% CO_2) on tumour hypoxia is demonstrated using BOLD-MRI in a subset of patients from the accelerated radiotherapy with carbogen and nicotinamide (ARCON) study (194). Increase in $T2^*$ -signal intensity were seen in the cohort of patients that inhaled carbogen with no significant changes seen on dynamic contrast-enhanced MRI. A phase 3 study investigating the impact of ARCON in 345 patients randomised to accelerated RT alone or ARCON showed a significant benefit in LRC only with ARCON (195). A subset analysis showed that this benefit was more significant for hypoxic tumours, as determined by pimonidazole staining of biopsy samples. A separate analysis of patients from the phase 2 ARCON study with 215 patients with a variety of locally-advanced HNC, (47% larynx, 23% hypopharynx, 24% OPC and 6% oral cavity), demonstrated a high tolerability of the treatment and 3 and 5-year OS of 60% and 52%, respectively (196). Determination of HPV status was not a requirement at the time these studies were performed.

The BOLD effect has proven to be consistent and can demonstrate regions of chronic hypoxia. Although hypoxic modification has shown improvement in regional control for

laryngeal cancers, stratification by hypoxic and oxygenated tumours seems necessary to select patients most likely to benefit. Therefore, BOLD-MRI may help identify hypoxic radioresistant regions within tumour that not only serve as prognostic markers, but may be a target for dose-escalation or dose-painting strategies (197,198).

1.7 Adaptive Radiotherapy for Early-Stage Glottic Cancers

1.7.1 Background

SCC of the glottic is deemed low risk for regional or distant metastasis due to the limited lymphatic drainage of the vocal cords (199). SCCs of the glottis are slow growing and approximately two-thirds of tumours are contained at the level of the glottis at diagnosis (200). Accurate GTV identification can be difficult due to poor image resolution or inadequate tumour visualisation, particularly of the inferior vocal-cord surface, during laryngoscopy (201). However, a pathological analysis of 52 laryngectomy specimens demonstrated a common pattern of disease spread due to the vocal cord being composed of fibroelastic membranes and the conus elasticus, which forms a thick barrier against tumour spread (202).

The main treatment options for early-stage glottic SCC (ESGC, T1-2 N0, AJCC TNM 8th edition) are laser microsurgery or radical radiotherapy, both of which have similar LRC and OS (203). Traditional radiotherapy methods, such as parallel-opposed or anterior-oblique beam arrangements, are still utilised to treat PTVs that encompass the whole larynx without elective nodal irradiation (Figure 1-5). Treatment fields areas are approximately 25 cm² and 36 cm² for T1 and T2 tumours, respectively. Such large fields are utilised to ensure the target is not missed during motion such as swallowing (204).

IGRT techniques are readily available in the forms of CBCT and, more recently, MRgRT on the MR-Linac platform. As the precision of radiotherapy improves, the radiotherapy techniques for ESGC have evolved where IMRT/Volumetric-Modulated Arc Therapy (VMAT) may be used in some centres. However, the target definition has not changed, as the whole larynx is still delineated as the CTV (205).

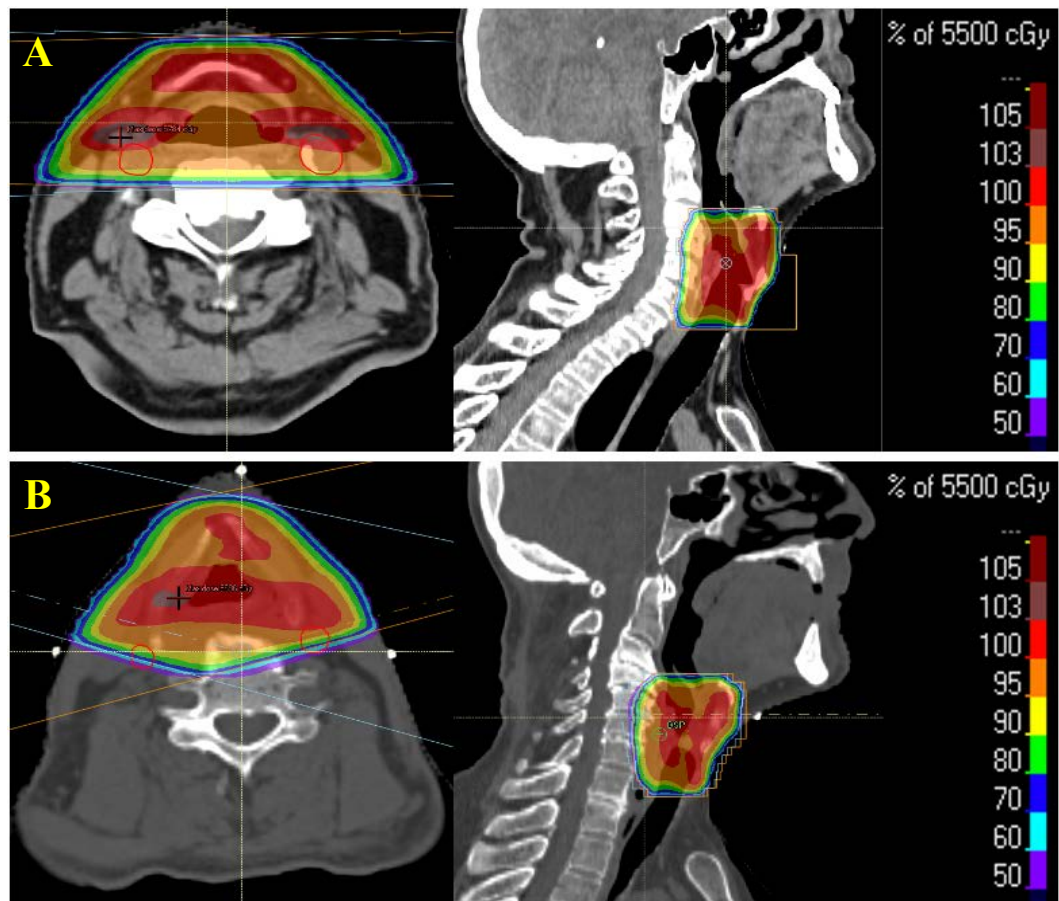


Figure 1-5, 3D-CRT Plan for Early-Stage Glottic Cancers.

Two patients with T1a glottic SCC treated with radical radiotherapy to a dose of 55 Gy in 20 fractions over 4 weeks. Axial and sagittal images show percentage dose coverage from A) bilateral parallel-opposed and B) anterior-oblique beam arrangements. Carotid arteries (red) highlight their proximity to the primary targets and doses received.

1.7.2 Dose-Volume Effects to Organs at Risk

Despite a 5-year DFS of 78% for ESGC, the radiation doses delivered to the OARs in close proximity to the larynx, and subsequent late radiation effects, warrant treatment approaches that limit the overall irradiated volume (206).

1.7.2.1 Deglutition

The pharyngeal constrictor muscles (superior and middle (SMPCM) and inferior (IPCM)) are key components of swallow and deemed “dysphagia aspiration-related structures (DARS)” (207). Peak dysfunction in deglutition is observed at roughly three months post-completion of radiotherapy, with variable extents of recovery between different muscle groups at twelve months (208). Pooled analyses from heterogeneous groups of studies and the DARS trial suggest that for a significant reduction in chronic

dysphagia and aspiration risk, mean-dose constraints of 50 Gy or 40 Gy (in 2 Gy per fraction) should be the limits for SMPCM or IPCM, respectively (46,209).

1.7.2.2 Voice

A study that compared 25 patients with ESGC who received accelerated hypofractionated radiotherapy showed poorer voice quality beyond 12 months post-radiotherapy, as measured by serial electroglottographic and acoustic analyses, compared to health volunteers (210). This finding is reflected in a study by Fung et al, which included patients with non-laryngeal SCC (211). Patients with T1a SCC of the glottis experienced global vocal dysfunction, as determined by measuring the harmonic-noise ratio. This is attributed to the impaired structural integrity of the vocal cords (212). Despite all objective measures demonstrating poorer outcomes in voice after radiotherapy, subjective scores are better compared to objective scores (211,213,214).

Prospective studies by Hocevar-Biltezar et al and Ma et al surveyed patients for over one year after completion of radical radiotherapy for ESGC where direct endoscopic visualisation of the larynx revealed chronic morphological defects in over 95% of patients (215,216). Roughly 50% of patients had contralateral vocal cord changes with ongoing evolution of changes that manifested as chronic dysphonia and vocal fatigue. Fu et al further established that 15% of patients receiving radical-dose radiotherapy for ESGC have persistent laryngeal oedema lasting three months or more with 11.7% of cases of oedema resolving within two years when the total dose delivered is below 70 Gy (217).

1.7.2.3 Carotid Arteries

Radiotherapy plans for HNC typically cover significant lengths of the carotid artery trees, particularly when neck nodes are irradiated. The consequences of radiation exposure have been described pathologically and clinically. Patients treated for a range of HNCs with doses between 40-74 Gy were noted to have carotid artery wall thickening within six months of radiation exposure (218). Histopathological analyses further showed acute vessel changes such as endothelial damage and disruption of the internal-elastic lamina (as early as 48 hours post-radiation), which leads to chronic vessel atherosclerosis

as seen from prolonged exposure to the Framingham risk factors and necrosis of the vasa vasorum, which is more typical of radiation related damage (219–222). The vessel wall intimal-medial layer thickness has been used as a surrogate for measuring the chronic radiation-related effects on carotid arteries (223).

Relative early pathological changes at 6-12 months have not been noted to cause impedance of blood flow, however, Cheng et al described a progressively increasing rate of carotid stenosis with a lifetime risk of >50% stenosis of 15.4% compared to 4.8% in non-irradiated arteries (224). Case-controlled studies in patients under the age of 60 years, who received radical radiotherapy for ESGC, showed a median interval to stroke event of 10.9 years with an exponential rate of increase in carotid-stenosis related events after this period (225–227).

Garcez et al demonstrated a statistically significant reduction in carotid artery dose by shifting from a parallel-opposed pair to an anterior-oblique beam arrangement for treating ESGC (228). Inverse-radiotherapy planning with IMRT or VMAT further reduces dose when placing dose-constraints on carotid arteries, although this results in increased dose to the spinal cord, which remains well within its known tolerance dose (229,230).

It has been difficult to establish clear dose-effect relationships due to the heterogeneity in treatment techniques and radiation doses between studies, but a single cross-sectional study of 14 patients suggested there was significant reduction in intimal-medial thickness for total doses below 35 Gy (231). Studies have since used V35 20% and V10 50% (volumes receiving up to 35 and 10 Gy, respectively) as dose-constraints and dose reporting in IMRT studies. Rosenthal et al and Zumsteg et al demonstrated no negative impact on 5-year OS or LRC when comparing carotid-sparing IMRT against 3D-CRT with these carotid artery dose constraints (232,233).

1.7.3 Laryngeal Motion

Patient set-up verification using portal-imaging systems was traditionally performed using cervical-vertebral matching. However, it has been shown that spatial relation between vertebrae and cartilages of the larynx were not consistent during swallow (234).

The impact of laryngeal motion in this context was realised when LRC rates were noted to be worse when matching patient set-up to vertebrae as opposed to laryngeal cartilages (235).

Laryngeal motion is shown to be greatest in the cranio-caudal direction (mean 25.5 mm), with limited motion in the anterior-posterior (8.3 mm) and negligible in the left-right directions (236). Total duration of each swallowing event is up to one second, where the highest frequency of swallow is thought to be during the first five fractions of treatment (237). The effects of swallowing have shown clinically insignificant impact on dosimetry, with a 0.5% dose reduction noted at the superior field edge when the whole larynx is defined as CTV (237). Therefore, there is much interest in evolving radiation techniques for ESGC. As a result, Bradley et al used MRI-based methods to evaluate laryngeal motion and their results reflected similar magnitudes of motion as described above, as well as more limited laryngeal motion at rest, (cranio-caudal 7.3 mm and anterior-posterior 3.4 mm) (238).

Individual swallow-related data have been derived between different centres, generating their own PTV volumes that do not account for the short duration of laryngeal excursion during swallow (238–241). The approaches to treatment personalisation and reduction of radiation volumes vary between centres. However, there is a common desire to shift away from whole-larynx irradiation.

1.7.4 Evolution of Radiotherapy for Early-Stage Glottic Cancers

The potential gains in OAR and normal tissue sparing have driven research towards irradiation of smaller overall treatment volumes using IMRT/VMAT techniques and a shift away from more traditional 3D-CRT techniques. The frequency of swallow varies between patients, however, instructing patients not to swallow during planning-CT acquisition helps reduce systematic errors by avoiding capture of the larynx in the swallow position (242). Instructing patients not to swallow at all during each fraction, or only to swallow at planned intervals also helps reduce errors and motion (242).

Reduction of treatment volumes have been attempted using different methods between centres. Kim et al utilised a more conservative approach to dose de-escalation

by maintaining 52.2 Gy in 33 fractions over 6.5 weeks to the larynx and a simultaneous boost to a smaller, high-risk, target to total 66 Gy (243). Five-year LRC for stage T1 disease was not significantly different to 3D-CRT methods. Princess Margaret Hospital employ a “5+5” approach, which is currently in routine use for pharyngeal HNCs (235). Despite limited patient numbers and follow-up period, 89% of all local failures reported in the IMRT group have been infield and within the ipsilateral vocal cord, although updated analyses report improvement on this LRC rate when adding radiotherapy acceleration (66-70 Gy in 33-35 fractions over 5.5-6 weeks) (244).

Osman et al have taken a further step by aiming to implement single vocal-cord irradiation using 4D-CT-based methods (245). 4D-CT planning aims to determine resting vocal-cord motion and nullify systematic errors on an individual patient level. With such stringent dose, planning and quality-assurance constraints they calculated and deemed a PTV margin of 2 mm as safe to deliver the prescribed dose. Two-year LRC for T1a glottis SCC, treated with single-vocal cord irradiation (66 Gy in 33 fractions over 6.5 weeks), has been reported as 100% with no worsening of late toxicities or voice quality when compared to whole-larynx IMRT (246).

1.8 Outline of Thesis

This thesis investigates the use of functional imaging to adapt radiotherapy for HNCs. It is hypothesised that the use of multiple functional MRI sequences (Diffusion-weighted, Intra-voxel incoherent motion, hypoxia/R2* and cine-MR), prior to and during radiotherapy, will personalise and adapt radiotherapy based on tumour response and motion. This can take place by longitudinally identifying biological changes before volumetric changes are apparent. Alternatively, measurement of anatomical motion will help personalise radiation treatment volumes.

The first part of Chapter 2 will aim to validate and compare two DWI sequences (ssEPI and RESOLVE). The second part of Chapter 2 will aim to explore anatomical and biological adaptive radiotherapy and the impact of such interventions on dosimetry to tumours and OARs.

Chapter 3 aims to compare DWI/ADC on the MR-Linac to determine whether patterns of ADC change correlate with that seen on a diagnostic-MRI scanner. This chapter will also explore MRI sequences such as IVIM and T2*/R2* to determine if there are any merits in their use as functional imaging biomarkers, like DWI/ADC.

Chapter 4 aims to utilise cine-MRI to explore laryngeal motion in patients who are receiving a course of radical radiotherapy with an aim to confirm the extent of motion described in the literature. This thesis will also investigate the longitudinal changes in frequency and extent of laryngeal motion that have not yet been as well described. The latter part of this project will aim to investigate the dosimetric gains to OARs such as the carotid arteries when utilising carotid-sparing IMRT/VMAT plans, with individualised treatment targets. Motion and dosimetric data will be analysed to determine whether dose delivery to more conformed targets can be safely delivered using both C-arm and MR-Linac platforms, with a view to implement target-tracking capabilities to further reduce overall treatment volumes.

1.9 References

1. CRUK. Head and Neck Cancer Statistics. Cancer Research UK. 2021;(https://www.cancerresearchuk.org/health-professional/cancer-statistics/statistics-by-cancer-type/head-and-neck-cancers#heading-Zero).
2. Fitzmaurice C, Abate D, Abbasi N, Abbastabar H, Abd-Allah F, Abdel-Rahman O, et al. Global, regional, and national cancer incidence, mortality, years of life lost, years lived with disability, and disability-Adjusted life-years for 29 cancer groups, 1990 to 2017: A systematic analysis for the global burden of disease study. *JAMA Oncol.* 2019 Dec 1;5(12):1749–68.
3. Johnson DE, Burtneß B, Leemans CR, Lui VWY, Bauman JE, Grandis JR. Head and neck squamous cell carcinoma. Vol. 6, *Nature Reviews Disease Primers.* Nature Research; 2020.
4. Haines GK. Pathology of head and neck cancer I: Epithelial and related tumors. In: *Head & Neck Cancer: Current Perspectives, Advances, and Challenges.* Springer Netherlands; 2013. p. 257–87.
5. Sood S, McGurk M, Vaz F. Management of Salivary Gland Tumours: United Kingdom National Multidisciplinary Guidelines. *J Laryngol Otol.* 2016 May 1;130(S2):S142–9.
6. Siegel RL, Miller KD, Jemal A. Cancer statistics, 2017. *CA Cancer J Clin.* 2017 Jan;67(1):7–30.
7. Aupérin A. Epidemiology of head and neck cancers: An update. Vol. 32, *Current Opinion in Oncology.* Lippincott Williams and Wilkins; 2020. p. 178–86.
8. Hashibe M, Brennan P, Benhamou S, Castellsague X, Chen C, Curado MP, et al. Alcohol drinking in never users of tobacco, cigarette smoking in never drinkers, and the risk of head and neck cancer: Pooled analysis in the international head and neck cancer epidemiology consortium. *J Natl Cancer Inst.* 2007 May 16;99(10):777–89.
9. Berthiller J, Straif K, Agudo A, Ahrens W, Dos Santos AB, Boccia S, et al. Low frequency of cigarette smoking and the risk of head and neck cancer in the INHANCE consortium pooled analysis. *Int J Epidemiol.* 2016 Jun 1;45(3):835–45.
10. Galbiatti ALS, Padovani-Junior JA, Maníglia JV, Rodrigues CDS, Pavarino ÉC, Goloni-Bertollo EM. Head and neck cancer: Causes, prevention and treatment. Vol. 79, *Brazilian Journal of Otorhinolaryngology.* Sociedade Brasileira de Otorrinolaringologia; 2013. p. 239–47.
11. National Cancer Institute. Head and Neck Cancers. Cancer.gov. 2021;(https://www.cancer.gov/types/head-and-neck/head-neck-fact-sheet).
12. Gillison ML, Koch WM, Capone RB, Spafford M, Westra WH, Wu L, et al. Evidence for a Causal Association Between Human Papillomavirus and a Subset of Head and Neck Cancers. *J Natl Cancer Inst* [Internet]. 2000; Available from: <https://academic.oup.com/jnci/article/92/9/709/2906131>
13. Klussmann JP, Weissenborn SJ, Wieland U, Dries V, Kolligs J, Jungehülsing M, et al. Prevalence, Distribution, and Viral Load of Human Papillomavirus 16 DNA in Tonsillar Carcinomas BACKGROUND. Oncogenic human papillomaviruses (HPV) DNA have repeatedly. American Cancer Society. 2001;
14. Sabatini ME, Chiocca S. Human papillomavirus as a driver of head and neck cancers. Vol. 122, *British Journal of Cancer.* Springer Nature; 2020. p. 306–14.
15. Cohen N, Fedewa S, Chen AY. Epidemiology and Demographics of the Head and Neck Cancer Population. Vol. 30, *Oral and Maxillofacial Surgery Clinics of North America.* W.B. Saunders; 2018. p. 381–95.

16. Kreimer AR, Viscidi R, Pawlita M, Fakhry C, Koch WM, Westra WH, et al. Case-Control Study of Human Papillomavirus and Oropharyngeal Cancer Abstract. *N Engl J Med* [Internet]. 2007; Available from: www.nejm.org
17. Howlader N, Noone AM, Krapcho M, Miller D, Bishop K, Kosary CL, et al. SEER cancer statistics review, 1975-2014. National Cancer Institute Bethesda, MD. 2017;(https://seer.cancer.gov/csr/1975_2014/).
18. Diana G, Corica C. Human Papilloma Virus vaccine and prevention of head and neck cancer, what is the current evidence? Vol. 115, *Oral Oncology*. Elsevier Ltd; 2021.
19. UK Health Security Agency. Human papillomavirus (HPV) vaccination coverage in adolescent females and males in England: 2020 to 2021. *Health Protection Report*. 2021;15.
20. Gillison ML, Chaturvedi AK, Anderson WF, Fakhry C. Epidemiology of human papillomavirus-positive head and neck squamous cell carcinoma. Vol. 33, *Journal of Clinical Oncology*. American Society of Clinical Oncology; 2015. p. 3235–42.
21. Rettig EM, D'Souza G. Epidemiology of Head and Neck Cancer. Vol. 24, *Surgical Oncology Clinics of North America*. W.B. Saunders; 2015. p. 379–96.
22. Anand R, Dhingra C, Prasad S, Menon I. Betel nut chewing and its deleterious effects on oral cavity. Vol. 10, *Journal of Cancer Research and Therapeutics*. Wolters Kluwer Medknow Publications; 2014. p. 499–505.
23. Wong KCW, Hui EP, Lo KW, Lam WKJ, Johnson D, Li L, et al. Nasopharyngeal carcinoma: an evolving paradigm. Vol. 18, *Nature Reviews Clinical Oncology*. Nature Research; 2021. p. 679–95.
24. Gupta B, Johnson NW, Kumar N. Global Epidemiology of Head and Neck Cancers: A Continuing Challenge. Vol. 91, *Oncology (Switzerland)*. S. Karger AG; 2016. p. 13–23.
25. Gianfaldoni S, Gianfaldoni R, Wollina U, Lotti J, Tchernev G, Lotti T. An overview on radiotherapy: From its history to its current applications in dermatology. *Open Access Maced J Med Sci*. 2017;5(4 Special Issue *GlobalDermatology*):521–5.
26. Grégoire V, De Neve W, Eisbruch A, Lee N, Van Den Weyngaert D, Van Gestel D. Intensity-Modulated Radiation Therapy for Head and Neck Carcinoma LEARNING OBJECTIVES *Oncologist*® Head and Neck Cancers. *TheOncologist* [Internet]. 2014; Available from: www.TheOncologist.com
27. Pajonk F, Vlashi E, McBride WH. Radiation resistance of cancer stem cells: The 4 R's of radiobiology revisited. Vol. 28, *Stem Cells*. 2010. p. 639–48.
28. Herskind C, Ma L, Liu Q, Zhang B, Schneider F, Veldwijk MR, et al. Biology of high single doses of IORT: RBE, 5 R's, and other biological aspects. Vol. 12, *Radiation Oncology*. BioMed Central Ltd.; 2017.
29. Sanganalmath P, Lester JE, Bradshaw AG, Das T, Esler C, Roy AEF, et al. Continuous Hyperfractionated Accelerated Radiotherapy (CHART) for Non-small Cell Lung Cancer (NSCLC): 7 Years' Experience From Nine UK Centres. *Clin Oncol*. 2018 Mar 1;30(3):144–50.
30. Dearnaley D, Syndikus I, Mossop H, Khoo V, Birtle A, Bloomfield D, et al. Conventional versus hypofractionated high-dose intensity-modulated radiotherapy for prostate cancer: 5-year outcomes of the randomised, non-inferiority, phase 3 CHHiP trial. *Lancet Oncol*. 2016 Aug 1;17(8):1047–60.
31. Murray Brunt A, Haviland JS, Wheatley DA, Sydenham MA, Alhasso A, Bloomfield DJ, et al. Hypofractionated breast radiotherapy for 1 week versus 3 weeks (FAST-Forward): 5-year efficacy and late normal tissue effects results from a multicentre, non-inferiority, randomised, phase 3 trial. *The Lancet*. 2020 May 23;395(10237):1613–26.

32. Jens Overgaard, Hanne Sand Hansen, Lena Specht, Marie Overgaard, Cai Grau, Elo Andersen, et al. Five compared with six fractions per week of conventional radiotherapy of squamous-cell carcinoma of head and neck: DAHANCA 6&7 randomised controlled trial. *The Lancet* [Internet]. 2003; Available from: www.thelancet.com
33. Lacas B, Bourhis J, Overgaard J, Zhang Q, Grégoire V, Nankivell M, et al. Role of radiotherapy fractionation in head and neck cancers (MARCH): an updated meta-analysis. *Lancet Oncol*. 2017 Jan 1;18(9):1221–37.
34. Rey J, Tobias S, Monson K, Gupta N, Macdougall H, Glaholm J, et al. Chemoradiotherapy for locally advanced head and neck cancer: 10-year follow-up of the UK Head and Neck (UKHAN1) trial. *Lancet Oncology* [Internet]. 2010;11:66–74. Available from: www.thelancet.com/oncology
35. Jacinto AA, Batalha Filho ES, Viana LDS, De Marchi P, Capuzzo RDC, Gama RR, et al. Feasibility of concomitant cisplatin with hypofractionated radiotherapy for locally advanced head and neck squamous cell carcinoma 11 Medical and Health Sciences 1112 Oncology and Carcinogenesis. *BMC Cancer*. 2018 Oct 23;18(1).
36. Hawkins PG, Kadam AS, Jackson WC, Eisbruch A. Organ-Sparing in Radiotherapy for Head-and-Neck Cancer: Improving Quality of Life. Vol. 28, *Seminars in Radiation Oncology*. W.B. Saunders; 2018. p. 46–52.
37. Onjukka E, Mercke C, Björgevinnson E, Embring A, Berglund A, Alexandersson von Döbeln G, et al. Modeling of Xerostomia After Radiotherapy for Head and Neck Cancer: A Registry Study. *Front Oncol*. 2020 Aug 14;10.
38. Logemann JA, Pauloski BR, Rademaker AW, Lazarus CL, Mittal B, Gaziano J, et al. Xerostomia: 12-Month changes in saliva production and its relationship to perception and performance of swallow function, oral intake, and diet after chemoradiation. *Head Neck*. 2003 Jun 1;25(6):432–7.
39. Nutting CM, Morden JP, Harrington KJ, Sydenham MA, Emson M, Hall E, et al. Parotid-sparing intensity modulated versus conventional radiotherapy in head and neck cancer (PARSPORT): a phase 3 multicentre randomised controlled trial. *Lancet Oncology* [Internet]. 2011;12:127–36. Available from: www.thelancet.com/oncology
40. Saarilahti K, Kouri M, Collan J, Kangasmäki A, Atula T, Joensuu H, et al. Sparing of the submandibular glands by intensity modulated radiotherapy in the treatment of head and neck cancer. *Radiotherapy and Oncology*. 2006;78(3):270–5.
41. Little M, Schipper M, Feng FY, Vineberg K, Cornwall C, Murdoch-Kinch CA, et al. Reducing xerostomia after chemo-IMRT for head-and-neck cancer: Beyond sparing the parotid glands. *Int J Radiat Oncol Biol Phys*. 2012 Jul 1;83(3):1007–14.
42. Wang ZH, Yan C, Zhang ZY, Zhang CP, Hu HS, Tu WY, et al. Impact of salivary gland dosimetry on post-IMRT recovery of saliva output and xerostomia grade for head-and-neck cancer patients treated with or without contralateral submandibular gland sparing: A longitudinal study. *Int J Radiat Oncol Biol Phys*. 2011 Dec 1;81(5):1479–87.
43. Matsuo K, Palmer JB. *Anatomy and Physiology of Feeding and Swallowing: Normal and Abnormal*. Vol. 19, *Physical Medicine and Rehabilitation Clinics of North America*. 2008. p. 691–707.

44. Chiu YH, Tseng WH, Ko JY, Wang TG. Radiation-induced swallowing dysfunction in patients with head and neck cancer: A literature review. Vol. 121, *Journal of the Formosan Medical Association*. Elsevier B.V.; 2022. p. 3–13.
45. Duprez F, Madani I, De Potter B, Boterberg T, De Neve W. Systematic review of dose-volume correlates for structures related to late swallowing disturbances after radiotherapy for head and neck cancer. Vol. 28, *Dysphagia*. 2013. p. 337–49.
46. Petkar I, Rooney K, Roe JWG, Patterson JM, Bernstein D, Tyler JM, et al. DARS: A phase III randomised multicentre study of dysphagia- optimised intensitymodulated radiotherapy (Do-IMRT) versus standard intensity- modulated radiotherapy (S-IMRT) in head and neck cancer. *BMC Cancer*. 2016;16(1).
47. Christopher Nutting, Keith Rooney, Bernadette Foran, Laura Pettit, Matthew Beasley, Laura Finneran, et al. Results of a randomized phase III study of dysphagia-optimized intensity modulated radiotherapy (Do-IMRT) versus standard IMRT (S-IMRT) in head and neck cancer. *Journal of Clinical Oncology*. 2020;
48. Breglio AM, Rusheen AE, Shide ED, Fernandez KA, Spielbauer KK, McLachlin KM, et al. Cisplatin is retained in the cochlea indefinitely following chemotherapy. *Nat Commun*. 2017 Dec 1;8(1).
49. Nutting CM, Morden JP, Beasley M, Bhide S, Cook A, De Winton E, et al. Results of a multicentre randomised controlled trial of cochlear-sparing intensity-modulated radiotherapy versus conventional radiotherapy in patients with parotid cancer (COSTAR; CRUK/08/004). *Eur J Cancer*. 2018 Nov 1;103:249–58.
50. Price J, Hall E, West C, Thomson D. TORPEdO – A Phase III Trial of Intensity-modulated Proton Beam Therapy Versus Intensity-modulated Radiotherapy for Multi-toxicity Reduction in Oropharyngeal Cancer. Vol. 32, *Clinical Oncology*. Elsevier Ltd; 2020. p. 84–8.
51. Lang P, Contreras J, Kalman N, Paterson C, Bahig H, Billfalk-Kelly A, et al. Preservation of swallowing in resected oral cavity squamous cell carcinoma: Examining radiation volume effects (PRESERVE): Study protocol for a randomized phase II trial. *Radiation Oncology*. 2020 Aug 14;15(1).
52. Steel GG, Peckham MJ. Exploitable mechanisms in combined radiotherapy-chemotherapy: the concept of additivity. *Int J Radiat Oncol Biol Phys*. 1979;5:0.
53. Vokes EE, Weichselbaum RR. Concomitant Chemoradiotherapy: Rationale and Clinical Experience in Patients With Solid Tumors. *Journal of Clinical Oncology*. 1990;
54. Pignon JP, Maître A le, Maillard E, Bourhis J. Meta-analysis of chemotherapy in head and neck cancer (MACH-NC): An update on 93 randomised trials and 17,346 patients. *Radiotherapy and Oncology*. 2009 Jul;92(1):4–14.
55. van der Kamp MF, Muntinghe FOW, Iepsma RS, Plaat BEC, van der Laan BFAM, Algassab A, et al. Predictors for distant metastasis in head and neck cancer, with emphasis on age. *European Archives of Oto-Rhino-Laryngology*. 2021 Jan 1;278(1):181–90.
56. Hiyama T, Kuno H, Nagaki T, Sekiya K, Oda S, Fujii S, et al. Extra-nodal extension in head and neck cancer: how radiologists can help staging and treatment planning. Vol. 38, *Japanese Journal of Radiology*. Springer; 2020. p. 489–506.
57. Spence T, Bruce J, Yip KW, Liu FF. HPV associated head and neck cancer. Vol. 8, *Cancers*. MDPI AG; 2016.
58. Huang SH, O’Sullivan B, Xu W, Zhao H, Chen DD, Ringash J, et al. Temporal nodal regression and regional control after primary radiation therapy for N2-N3 head-and-neck cancer stratified by HPV status. *Int J Radiat Oncol Biol Phys*. 2013 Dec 1;87(5):1078–85.

59. Ang KK, Harris J, Wheeler R, Weber R, Rosenthal DI, Nguyen-Tân PF, et al. Human Papillomavirus and Survival of Patients with Oropharyngeal Cancer. *New England Journal of Medicine*. 2010 Jul;363(1):24–35.
60. Shao Hui Huang, Wei Xu, John Waldron, Lillian Siu, Xiaowei Shen, Li Tong, et al. Refining American Joint Committee on Cancer/Union for International Cancer Control TNM Stage and Prognostic Groups for Human Papillomavirus-Related Oropharyngeal Carcinomas. *Journal of Clinical Oncology*. 2015 Mar 10;33(8):817–8.
61. Kobayashi K, Hisamatsu K, Suzui N, Hara A, Tomita H, Miyazaki T. A review of HPV-related head and neck cancer. Vol. 7, *Journal of Clinical Medicine*. MDPI; 2018.
62. Zandoni DK, Patel SG, Shah JP. Changes in the 8th Edition of the American Joint Committee on Cancer (AJCC) Staging of Head and Neck Cancer: Rationale and Implications. Vol. 21, *Current Oncology Reports*. Current Medicine Group LLC 1; 2019.
63. Oksuz DC, Prestwich RJ, Carey B, Wilson S, Senocak MS, Choudhury A, et al. Recurrence patterns of locally advanced head and neck squamous cell carcinoma after 3D conformal (chemo)-radiotherapy. *Radiation Oncology*. 2011 May 24;6(1).
64. Bollen H, van der Veen J, Laenen A, Nuyts S. Recurrence Patterns After IMRT/VMAT in Head and Neck Cancer. *Front Oncol*. 2021 Sep 16;11.
65. Begg AC. Predicting Recurrence After Radiotherapy in Head and Neck Cancer. Vol. 22, *Seminars in Radiation Oncology*. 2012. p. 108–18.
66. Nevens D, Duprez F, Daisne JF, Schatteman J, Van der Vorst A, De Neve W, et al. Recurrence patterns after a decreased dose of 40 Gy to the elective treated neck in head and neck cancer. *Radiotherapy and Oncology*. 2017 Jun 1;123(3):419–23.
67. van der Kamp MF, Muntinghe FOW, Iepma RS, Plaat BEC, van der Laan BFAM, Algassab A, et al. Predictors for distant metastasis in head and neck cancer, with emphasis on age. *European Archives of Otorhinolaryngology*. 2021 Jan 1;278(1):181–90.
68. Ferlito A, Shaha AR, Silver CE, Rinaldo A, Mondin V. Incidence and Sites of Distant Metastases from Head and Neck Cancer [Internet]. Vol. 63, *ORL*. 2001. Available from: www.karger.com/journals/orl
69. Economopoulou P, Kotsantis I, Psyrris A. De-escalating strategies in hpv-associated head and neck squamous cell carcinoma. *Viruses*. 2021 Sep 1;13(9).
70. Nguyen-Tan PF, Zhang Q, Ang KK, Weber RS, Rosenthal DI, Soulieres D, et al. Randomized phase III trial to test accelerated versus standard fractionation in combination with concurrent cisplatin for head and neck carcinomas in the radiation therapy oncology group 0129 trial: Long-term report of efficacy and toxicity. *Journal of Clinical Oncology*. 2014 Dec 1;32(34):3858–67.
71. Ang KK, Harris J, Wheeler R, Weber R, Rosenthal DI, Nguyen-Tân PF, et al. Human Papillomavirus and Survival of Patients with Oropharyngeal Cancer. *New England Journal of Medicine*. 2010 Jul;363(1):24–35.
72. O’Sullivan B, Huang SH, Siu LL, Waldron J, Zhao H, Perez-Ordóñez B, et al. Deintensification candidate subgroups in human papillomavirus-related oropharyngeal cancer according to minimal risk of distant metastasis. *Journal of Clinical Oncology*. 2013 Feb 10;31(5):543–50.
73. Rosenberg AJ, Vokes EE. Optimizing Treatment De-Escalation in Head and Neck Cancer: Current and Future Perspectives. *Oncologist*. 2021 Jan 1;26(1):40–8.

74. Atwell D, Elks J, Cahill K, Hearn N, Vignarajah D, Lagopoulos J, et al. A Review of Modern Radiation Therapy Dose Escalation in Locally Advanced Head and Neck Cancer. *Clin Oncol*. 2020 May 1;32(5):330–41.
75. O’Sullivan B, Huang SH, Perez-Ordóñez B, Massey C, Siu LL, Weinreb I, et al. Outcomes of HPV-related oropharyngeal cancer patients treated by radiotherapy alone using altered fractionation. *Radiotherapy and Oncology*. 2012 Apr;103(1):49–56.
76. Chen AM, Zahra T, Daly ME, Farwell DG, Luu Q, Gandour-Edwards R, et al. Definitive radiation therapy without chemotherapy for human papillomavirus-positive head and neck cancer. *Head Neck*. 2013 Nov 1;35(11):1652–6.
77. Sher DJ, Pham NL, Shah JL, Sen N, Williams KA, Subramaniam RM, et al. Prospective Phase 2 Study of Radiation Therapy Dose and Volume De-escalation for Elective Neck Treatment of Oropharyngeal and Laryngeal Cancer. In: *International Journal of Radiation Oncology Biology Physics*. Elsevier Inc.; 2021. p. 932–40.
78. Bratman S, Berthelet E, Butler J, de Almeida J, Karam I, Metser U, et al. De-Escalation Radiotherapy in Patients With Low-Risk HPV-Related Oropharyngeal Squamous Cell Carcinoma (EVADER). *Journal of Clinical Oncology*. 2020;38(15).
79. Villafior VM, Melotek JM, Karrison TG, Brisson RJ, Blair EA, Portugal L, et al. Response-adapted volume de-escalation (RAVD) in locally advanced head and neck cancer. *Annals of Oncology*. 2016 May 1;27(5):908–13.
80. Chen AM, Felix C, Wang PC, Hsu S, Basehart V, Garst J, et al. Reduced-dose radiotherapy for human papillomavirus-associated squamous-cell carcinoma of the oropharynx: a single-arm, phase 2 study. *Lancet Oncol*. 2017 Jun 1;18(6):803–11.
81. Marur S, Li S, Cmelak AJ, Gillison ML, Zhao WJ, Ferris RL, et al. E1308: Phase II trial of induction chemotherapy followed by reduced-dose radiation and weekly cetuximab in patients with HPV-associated resectable squamous cell carcinoma of the oropharynx- ECOG-ACRIN cancer research group. *Journal of Clinical Oncology*. 2017 Feb 10;35(5):490–7.
82. Seiwert TY, Foster CC, Blair EA, Karrison TG, Agrawal N, Melotek JM, et al. Optima: A phase II dose and volume de-escalation trial for human papillomavirus-positive oropharyngeal cancer. *Annals of Oncology*. 2019 Feb 1;30(2):297–302.
83. Rosenberg A, Agrawal N, Pearson A, Seiert T, Gooi Z, Blair E, et al. Nivolumab, nabpaclitaxel, and carboplatin followed by risk/response adaptive de-escalated locoregional therapy for HPV-associated oropharyngeal cancer: OPTIMA II trial. *Journal of Clinical Oncology*. 2021;39(15):6011–6011.
84. Misiukiewicz K, Gupta V, Miles BA, Bakst R, Genden E, Selkridge I, et al. Standard of care vs reduced-dose chemoradiation after induction chemotherapy in HPV+ oropharyngeal carcinoma patients: The Quarterback trial. *Oral Oncol*. 2019 Aug 1;95:170–7.
85. Ferris RL, Flamand Y, Weinstein GS, Li S, Quon ; Harry, Mehra R, et al. Phase II Randomized Trial of Transoral Surgery and Low-Dose Intensity Modulated Radiation Therapy in Resectable p161 Locally Advanced Oropharynx Cancer: An ECOG-ACRIN Cancer Research Group Trial (E3311). *J Clin Oncol [Internet]*. 2021;40:138–49. Available from: <https://doi>.

86. Nichols AC, Lang P, Prisman E, Berthelet E, Tran E, Hamilton S, et al. Treatment de-escalation for HPV-associated oropharyngeal squamous cell carcinoma with radiotherapy vs. trans-oral surgery (ORATOR2): Study protocol for a randomized phase II trial. *BMC Cancer*. 2020 Feb 14;20(1).
87. Rich J. Post Operative Adjuvant Therapy De-intensification Trial for Human Papillomavirus-related, p16+ Oropharynx Cancer (ADEPT). Secondary Post Operative Adjuvant Therapy De-intensification Trial for Human Papillomavirus-related, p16+ Oropharynx Cancer (ADEPT). <https://clinicaltrials.gov/ct2/show/NCT01687413>. 2020;
88. Miles BA, Posner MR, Gupta V, Teng MS, Bakst RL, Yao M, et al. De-Escalated Adjuvant Therapy After Transoral Robotic Surgery for Human Papillomavirus-Related Oropharyngeal Carcinoma: The Sinai Robotic Surgery (SIRS) Trial. *Oncologist*. 2021 Jun 1;26(6):504–13.
89. Swisher-McClure S, Lukens JN, Aggarwal C, Ahn P, Basu D, Bauml JM, et al. A Phase 2 Trial of Alternative Volumes of Oropharyngeal Irradiation for De-intensification (AVOID): Omission of the Resected Primary Tumor Bed After Transoral Robotic Surgery for Human Papilloma Virus–Related Squamous Cell Carcinoma of the Oropharynx. *Int J Radiat Oncol Biol Phys*. 2020 Mar 15;106(4):725–32.
90. Ma DJ, Price K, Eric MJ, Patel SH, Hinni ML, Ginos BF, et al. Long-Term Results for MC1273, A Phase II Evaluation of De-Escalated Adjuvant Radiation Therapy for Human Papillomavirus Associated Oropharyngeal Squamous Cell Carcinoma (HPV+ OPSCC). *Oral Scientific Session Abstracts*. 2021;111(3S).
91. Ma DM, Price K, Moore EJ, Patel SH, Hinni ML, Fruth B, et al. MC1675, a Phase III Evaluation of De-Escalated Adjuvant Radiation Therapy (DART) vs. Standard Adjuvant Treatment for Human Papillomavirus Associated Oropharyngeal Squamous Cell Carcinoma. *ASTRO's 63rd Annual Meeting [Internet]*. 2021; Available from: www.redjournal.org
92. Haderlein M, Speer S, Ott O, Lettmaier S, Hecht M, Semrau S, et al. Dose reduction to the swallowing apparatus and the salivary glands by de-intensification of postoperative radiotherapy in patients with head and neck cancer: First (treatment planning) results of the prospective multicenter DIREKHT trial. *Cancers (Basel)*. 2020 Mar 1;12(3).
93. Hargreaves S, Beasley M, Hurt C, Jones TM, Evans M. Deintensification of Adjuvant Treatment After Transoral Surgery in Patients With Human Papillomavirus-Positive Oropharyngeal Cancer: The Conception of the PATHOS Study and Its Development. Vol. 9, *Frontiers in Oncology*. Frontiers Media S.A.; 2019.
94. Atwell D, Elks J, Cahill K, Hearn N, Vignarajah D, Lagopoulos J, et al. A Review of Modern Radiation Therapy Dose Escalation in Locally Advanced Head and Neck Cancer. *Clin Oncol*. 2020 May 1;32(5):330–41.
95. Tao Y, Auperin A, Blanchard P, Alfonsi M, Sun XS, Rives M, et al. Concurrent cisplatin and dose escalation with intensity-modulated radiotherapy (IMRT) versus conventional radiotherapy for locally advanced head and neck squamous cell carcinomas (HNSCC): GORTEC 2004-01 randomized phase III trial. *Radiotherapy and Oncology*. 2020 Sep 1;150:18–25.
96. Nutting CM, Griffin CL, Sanghera P, Foran B, Beasley M, Bernstein D, et al. Dose-escalated intensity-modulated radiotherapy in patients with locally advanced laryngeal and hypopharyngeal cancers: ART DECO, a phase III randomised controlled trial. *Eur J Cancer*. 2021 Aug 1;153:242–56.

97. Pigorsch SU, Wilkens JJ, Kampfer S, Kehl V, Hapfelmeier A, Schläger C, et al. Do selective radiation dose escalation and tumour hypoxia status impact the loco-regional tumour control after radio-chemotherapy of head & neck tumours? The ESCALOX protocol. *Radiation Oncology*. 2017 Mar 1;12(1).
98. Mehanna H, Sen M, Chester J, Sanghera P, Paleri V, Gaunt P, et al. Phase III randomised controlled trial (RCT) comparing alternative regimens for escalating treatment of intermediate and high-risk oropharyngeal cancer (CompARE). *Journal of Clinical Oncology*. 2017;35(15).
99. Belgioia L, Morbelli SD, Corvò R. Prediction of Response in Head and Neck Tumor: Focus on Main Hot Topics in Research. Vol. 10, *Frontiers in Oncology*. Frontiers Media S.A.; 2021.
100. Mell L, Torres-Saavedra P, Wong S, Chang S, Kish J, Minn A, et al. Safety of radiotherapy with concurrent and adjuvant MEDI4736 (durvalumab) in patients with locoregionally advanced head and neck cancer with a contraindication to cisplatin: NRG-HN004. *Journal of Clinical Oncology*. 2019;37(15).
101. Le QT, Jordan R, Bauman JE, Blvd H. Testing Docetaxel-Cetuximab or the Addition of an Immunotherapy Drug, Atezolizumab, to the Usual Chemotherapy and Radiation Therapy in High-Risk Head and Neck Cancer (NCT01810913). <https://clinicaltrials.gov/ct2/show/NCT01810913> [Internet]. 2023; Available from: www.rtog.org
102. Haddad R, Wong D, Guo Y, Fayette J, Cohen E, Kowgier M, et al. IMvoke010: Randomized Phase III Study of Atezolizumab (atezo) as Adjuvant Monotherapy After Definitive Therapy of Squamous Cell Carcinoma of the Head and Neck. *ESMO Abstract*. 2018;1052.
103. Trial Evaluating the Addition of Nivolumab to Cisplatin-RT for Treatment of Cancers of the Head and Neck (NIVOPOSTOP) (NCT03576417). <https://clinicaltrials.gov/ct2/show/NCT03576417>. 2021;
104. Zech HB, Moeckelmann N, Boettcher A, Muenscher A, Binder M, Vettorazzi E, et al. Phase III study of nivolumab alone or combined with ipilimumab as immunotherapy versus standard of care in resectable head and neck squamous cell carcinoma. *Future Oncology*. 2020 Dec 1;16(36):3035–43.
105. MacHiels JP, Tao Y, Burtness B, Tahara M, Licitra L, Rischin D, et al. Pembrolizumab given concomitantly with chemoradiation and as maintenance therapy for locally advanced head and neck squamous cell carcinoma: KEYNOTE-412. *Future Oncology*. 2020 Jun 1;16(18):1235–43.
106. Bourhis J, Tao Y, Sun X, Sire C, Martin L, Liem X, et al. Avelumab-cetuximab-radiotherapy versus standards of care in patients with locally advanced squamous cell carcinoma of head and neck (LA-SCCHN): Randomized phase III GORTEC-REACH trial. *Annals of Oncology Abstract* [Internet]. 2021;32(S5). Available from: <https://doi.org/10.1016/j.annonc.2021.08.2112>
107. Lee NY, Ferris RL, Psyrrri A, Haddad RI, Tahara M, Bourhis J, et al. Avelumab plus standard-of-care chemoradiotherapy versus chemoradiotherapy alone in patients with locally advanced squamous cell carcinoma of the head and neck: a randomised, double-blind, placebo-controlled, multicentre, phase 3 trial [Internet]. Vol. 22, *Articles Lancet Oncol*. 2021. Available from: www.thelancet.com/oncology
108. Cohen E, Uppaluri R, Lee N, Westra W, Haddad R, Temam S, et al. Neoadjuvant and adjuvant pembrolizumab (pembro) plus standard of care (SOC) in patients (pts) with resectable locally advanced (LA) head and neck squamous cell carcinoma (HNSCC): The phase III KEYNOTE-689 study. *Annals of Oncology*. 2019 Nov;30:ix106.

109. Morgan HE, Sher DJ. Adaptive radiotherapy for head and neck cancer. *Cancers Head Neck* [Internet]. 2020 Dec 9;5(1):1. Available from: <https://cancersheadneck.biomedcentral.com/articles/10.1186/s41199-019-0046-z>
110. Jakobi A, Lühr A, Stützer K, Bandurska-Luque A, Löck S, Krause M, et al. Increase in tumor control and normal tissue complication probabilities in advanced head-and-neck cancer for dose-escalated intensity-modulated photon and proton therapy. *Front Oncol*. 2015;5(NOV).
111. Minn H, Sulamo S, Seppala J. Impact of PET/CT on planning of radiotherapy in head and neck cancer Imaging expression of HSV thymidine kinase gene therapy in experimental glioma with 18F-FHBG PET/CT View project Rotating frame relaxation and diffusion weighted imaging of human gliomas View project. *The Quarterly Journal of Nuclear Medicine and Molecular Imaging* [Internet]. 2010;54(5). Available from: <https://www.researchgate.net/publication/47357818>
112. Veresezan O, Troussier I, Lacout A, Kreps S, Maillard S, Toulemonde A, et al. Adaptive radiation therapy in head and neck cancer for clinical practice: state of the art and practical challenges. Vol. 35, *Japanese Journal of Radiology*. Springer Tokyo; 2017. p. 43–52.
113. Margalit DN, Schoenfeld JD, Tishler RB. Radiation Oncology-New Approaches in Squamous Cell Cancer of the Head and Neck. Vol. 29, *Hematology/Oncology Clinics of North America*. W.B. Saunders; 2015. p. 1093–106.
114. Dawson LA, Jaffray DA. Advances in image-guided radiation therapy. Vol. 25, *Journal of Clinical Oncology*. 2007. p. 938–46.
115. Farina E, Ferioli M, Castellucci P, Farina A, Rambaldi GZ, Cilla S, et al. 18F-Fdg-PET-guided Planning and Re-Planning (Adaptive) Radiotherapy in Head and Neck Cancer: Current state of art. Vol. 37, *Anticancer Research*. International Institute of Anticancer Research; 2017. p. 6523–32.
116. Ho KF, Marchant T, Moore C, Webster G, Rowbottom C, Penington H, et al. Monitoring dosimetric impact of weight loss with kilovoltage (KV) cone beam CT (CBCT) during parotid-sparing IMRT and concurrent chemotherapy. *Int J Radiat Oncol Biol Phys*. 2012 Mar 1;82(3).
117. Bhide SA, Davies M, Burke K, McNair HA, Hansen V, Barbachano Y, et al. Weekly Volume and Dosimetric Changes During Chemoradiotherapy With Intensity-Modulated Radiation Therapy for Head and Neck Cancer: A Prospective Observational Study. *Int J Radiat Oncol Biol Phys*. 2010 Apr;76(5):1360–8.
118. Castadot P, Geets X, Lee JA, Christian N, Grégoire V. Assessment by a deformable registration method of the volumetric and positional changes of target volumes and organs at risk in pharyngo-laryngeal tumors treated with concomitant chemo-radiation. *Radiotherapy and Oncology*. 2010;95(2):209–17.
119. Castadot P, Geets X, Lee JA, Grégoire V. Adaptive functional image-guided IMRT in pharyngo-laryngeal squamous cell carcinoma: Is the gain in dose distribution worth the effort? *Radiotherapy and Oncology*. 2011 Dec;101(3):343–50.
120. Surucu M, Shah KK, Roeske JC, Choi M, Small W, Emami B. Adaptive Radiotherapy for Head and Neck Cancer: Implications for Clinical and Dosimetry Outcomes. *Technol Cancer Res Treat*. 2017 Apr 1;16(2):218–23.
121. Kupelian P, Sonke JJ. Magnetic Resonance-Guided Adaptive Radiotherapy: A Solution to the Future. Vol. 24, *Seminars in Radiation Oncology*. W.B. Saunders; 2014. p. 227–32.

122. Surucu M, Shah KK, Mescioglu I, Roeske JC, Small W, Choi M, et al. Decision Trees Predicting Tumor Shrinkage for Head and Neck Cancer: Implications for Adaptive Radiotherapy. *Technol Cancer Res Treat*. 2016 Feb 1;15(1):139–45.
123. Vásquez Osorio EM, Hoogeman MS, Al-Mamgani A, Teguh DN, Levendag PC, Heijmen BJM. Local Anatomic Changes in Parotid and Submandibular Glands During Radiotherapy for Oropharynx Cancer and Correlation With Dose, Studied in Detail With Nonrigid Registration. *Int J Radiat Oncol Biol Phys*. 2008 Mar 1;70(3):875–82.
124. Mulder SL, Heukelom J, McDonald BA, Van Dijk L, Wahid KA, Sanders K, et al. MR-Guided Adaptive Radiotherapy for OAR Sparing in Head and Neck Cancers. Vol. 14, *Cancers*. MDPI; 2022.
125. Avgousti R, Antypas C, Armpilia C, Simopoulou F, Liakouli Z, Karaiskos P, et al. Adaptive radiation therapy: When, how and what are the benefits that literature provides? Vol. 26, *Cancer/Radiotherapie*. Elsevier Masson s.r.l.; 2022. p. 622–36.
126. Schinagl DA, Kaanders JH, Oyen WJ. From anatomical to biological target volumes: the role of PET in radiation treatment planning. *Cancer Imaging*. 2006;6.
127. Hamming-Vrieze O, Navran A, Al-Mamgani A, Vogel W V. Biological PET-guided adaptive radiotherapy for dose escalation in head and neck cancer: A systematic review. *Quarterly Journal of Nuclear Medicine and Molecular Imaging*. 2018 Dec 1;62(4):349–68.
128. Mehanna H, Wong WL, McConkey CC, Rahman JK, Robinson M, Hartley AGJ, et al. PET-CT Surveillance versus Neck Dissection in Advanced Head and Neck Cancer. *New England Journal of Medicine*. 2016 Apr 14;374(15):1444–54.
129. Bussink J, Kaanders AM, Bussink J. PET-CT for response assessment and treatment adaptation in head and neck cancer. *Lancet Oncology* [Internet]. 2010;11:661–9. Available from: www.thelancet.com/oncology
130. Daisne JF, Duprez T, Weynand B, Lonneux M, Hamoir M, Reyckler H, et al. Tumor volume in pharyngolaryngeal squamous cell carcinoma: Comparison at CT, MR imaging, and FDG PET and validation with surgical specimen. *Radiology*. 2004 Oct;233(1):93–100.
131. Caldas Magalhaes J, Kasperts N, Kooij N, van den Berg C, Terhaard C, Raaijmakers C, et al. Validation of Imaging with Pathology in Laryngeal Cancer: Accuracy of the Registration Methodology. *International Journal of Radiation Oncology*Biography*Physics*. 2011 Oct;81(2):S29.
132. Daisne JF, Sibomana M, Bol A, Doumont T, Lonneux M, Grégoire V. Tri-dimensional automatic segmentation of PET volumes based on measured source-to-background ratios: Influence of reconstruction algorithms. *Radiotherapy and Oncology*. 2003;69(3):247–50.
133. Min M, Lin P, Lee M, Shon IH, Lin M, Forstner D, et al. 18F-FDG PET-CT performed before and during radiation therapy of head and neck squamous cell carcinoma: Are they independent or complementary to each other? *J Med Imaging Radiat Oncol*. 2016 Jun 1;60(3):433–40.
134. Hentschel M, Appold S, Schreiber A, Abramyuk A, Abolmaali N, Kotzerke J, et al. Serial FDG-PET on patients with head and neck cancer: Implications for radiation therapy. *Int J Radiat Biol*. 2009 Sep;85(9):796–804.
135. Vernon MR, Maheshwari M, Schultz CJ, Michel MA, Wong SJ, Campbell BH, et al. Clinical Outcomes of Patients Receiving Integrated PET/CT-Guided Radiotherapy for Head and Neck Carcinoma. *Int J Radiat Oncol Biol Phys*. 2008 Mar 1;70(3):678–84.

136. Wong KH, Panek R, Dunlop A, Mcquaid D, Riddell A, Welsh LC, et al. Changes in multimodality functional imaging parameters early during chemoradiation predict treatment response in patients with locally advanced head and neck cancer. *Eur J Nucl Med Mol Imaging*. 2018 May 1;45(5):759–67.
137. Thureau S, Briens A, Decazes P, Castelli J, Barateau A, Garcia R, et al. PET and MRI guided adaptive radiotherapy: Rational, feasibility and benefit. Vol. 24, *Cancer/Radiotherapie*. Elsevier Masson s.r.l.; 2020. p. 635–44.
138. Mohamed ASR, Cardenas CE, Garden AS, Awan MJ, Rock CD, Westergaard SA, et al. Patterns-of-failure guided biological target volume definition for head and neck cancer patients: FDG-PET and dosimetric analysis of dose escalation candidate subregions. *Radiotherapy and Oncology*. 2017 Aug 1;124(2):248–55.
139. Duprez F, De Neve W, De Gersem W, Coghe M, Madani I. Adaptive dose painting by numbers for head-and-neck cancer. *Int J Radiat Oncol Biol Phys*. 2011 Jul 15;80(4):1045–55.
140. Heukelom J, Hamming O, Bartelink H, Hoebbers F, Giralt J, Herlestam T, et al. Adaptive and innovative Radiation Treatment FOR improving Cancer treatment outcOME (ARTFORCE); a randomized controlled phase II trial for individualized treatment of head and neck cancer. *BMC Cancer*. 2013;13.
141. Chirla R, Marcu LG. PET-based quantification of statistical properties of hypoxic tumor subvolumes in head and neck cancer. Vol. 32, *Physica Medica*. Associazione Italiana di Fisica Medica; 2016. p. 23–35.
142. Lapi SE, Voller TF, Welch MJ. PET Imaging of Hypoxia. Vol. 4, *PET Clinics*. 2009. p. 39–47.
143. Nehmeh SA, Lee NY, Schröder H, Squire O, Zanzonico PB, Erdi YE, et al. Reproducibility of Intratumor Distribution of 18F-Fluoromisonidazole in Head and Neck Cancer. *Int J Radiat Oncol Biol Phys*. 2008 Jan 1;70(1):235–42.
144. Lin Z, Mechalakos J, Nehmeh S, Schoder H, Lee N, Humm J, et al. The Influence of Changes in Tumor Hypoxia on Dose-Painting Treatment Plans Based on 18F-FMISO Positron Emission Tomography. *Int J Radiat Oncol Biol Phys*. 2008 Mar 15;70(4):1219–28.
145. Boeke S, Thorwarth D, Mönnich D, Pfannenbergs C, Reischl G, La Fougère C, et al. Geometric analysis of loco-regional recurrences in relation to pre-treatment hypoxia in patients with head and neck cancer. *Acta Oncol (Madr)*. 2017 Nov 2;56(11):1571–6.
146. Zschaecck S, Haase R, Abolmaali N, Perrin R, Stützer K, Appold S, et al. Spatial distribution of FMISO in head and neck squamous cell carcinomas during radio-chemotherapy and its correlation to pattern of failure. *Acta Oncol (Madr)*. 2015 Oct 21;54(9):1355–63.
147. Hoeben BAW, Bussink J, Troost EGC, Oyen WJG, Kaanders JHAM. Molecular PET imaging for biology-guided adaptive radiotherapy of head and neck cancer. Vol. 52, *Acta Oncologica*. 2013. p. 1257–71.
148. Welz S, Mönnich D, Pfannenbergs C, Nikolaou K, Reimold M, La Fougère C, et al. Prognostic value of dynamic hypoxia PET in head and neck cancer: Results from a planned interim analysis of a randomized phase II hypoxia-image guided dose escalation trial. *Radiotherapy and Oncology*. 2017 Sep 1;124(3):526–32.
149. Datta A, Aznar MC, Dubec M, Parker GJM, O'Connor JPB. Delivering Functional Imaging on the MRI-Linac: Current Challenges and Potential Solutions. *Clin Oncol*. 2018 Nov 1;30(11):702–10.
150. Vanderstraeten B, Berwouts D, Goddeeris B, Duprez F, De Neve W, Lievens Y. Adaptive Intensity-Modulated Radiation Therapy for Head and Neck Cancer: Is it Affordable? *International Journal of Radiation Oncology*Biography*Physics*. 2014 Sep;90(1):S107–8.

151. Chawla S, Kim S, Wang S, Poptani H. Diffusion-weighted imaging in head and neck cancers. *Future Oncology*. 2009;5(7):959–75.
152. Dietrich O, Biffar A, Baur-Melnyk A, Reiser MF. Technical aspects of MR diffusion imaging of the body. Vol. 76, *European Journal of Radiology*. 2010. p. 314–22.
153. Matoba M, Tuji H, Shimode Y, Toyoda I, Kuginuki Y, Miwa K, et al. Fractional change in apparent diffusion coefficient as an imaging biomarker for predicting treatment response in head and neck cancer treated with chemoradiotherapy. *American Journal of Neuroradiology*. 2014 Feb;35(2):379–85.
154. Glitzner M, Crijns SPM, Denis De Senneville B, Kontaxis C, Prins FM, Lagendijk JJW, et al. On-line MR imaging for dose validation of abdominal radiotherapy. *Phys Med Biol*. 2015 Nov 4;60(22):8869–83.
155. Zhang P, Simon A, Rigaud B, Castelli J, Ospina Arango JD, Nassef M, et al. Optimal adaptive IMRT strategy to spare the parotid glands in oropharyngeal cancer. *Radiotherapy and Oncology*. 2016 Jul 1;120(1):41–7.
156. Raghavan G, Kishan AU, Cao M, Chen AM. Anatomic and dosimetric changes in patients with head and neck cancer treated with an integrated MRI-tri-60Co teletherapy device. *British Journal of Radiology*. 2016;89(1067).
157. van Timmeren JE, Chamberlain M, Bogowicz M, Ehrbar S, Dal Bello R, Schüler HG, et al. MR-guided adaptive radiotherapy for head and neck cancer: Prospective evaluation of migration and anatomical changes of the major salivary glands. *Cancers (Basel)*. 2021 Nov 1;13(21).
158. Bahig H, Yuan Y, Mohamed ASR, Brock KK, Ng SP, Wang J, et al. Magnetic Resonance-based Response Assessment and Dose Adaptation in Human Papilloma Virus Positive Tumors of the Oropharynx treated with Radiotherapy (MR-ADAPTOR): An R-IDEAL stage 2a-2b/Bayesian phase II trial. *Clin Transl Radiat Oncol*. 2018 Nov 1;13:19–23.
159. Gupta A, Dunlop A, Mitchell A, McQuaid D, Nill S, Barnes H, et al. Online adaptive radiotherapy for head and neck cancers on the MR linear Accelerator: Introducing a novel modified Adapt-to-Shape approach. *Clin Transl Radiat Oncol*. 2022 Jan 1;32:48–51.
160. Boeke S, Mönnich D, van Timmeren JE, Balermipas P. MR-Guided Radiotherapy for Head and Neck Cancer: Current Developments, Perspectives, and Challenges. *Front Oncol*. 2021 Mar 19;11.
161. Bhatt N, Gupta N, Soni N, Hooda K, Sapire JM, Kumar Y. Role of diffusion-weighted imaging in head and neck lesions: Pictorial review. Vol. 30, *Neuroradiology Journal*. SAGE Publications Inc.; 2017. p. 356–69.
162. Wang J, Takashima S, Takayama F, Kawakami S, Saito A, Matsushita T, et al. Head and neck lesions: Characterization with diffusion-weighted echo-planar MR imaging. *Radiology*. 2001;220(3):621–30.
163. Surov A, Meyer HJ, Wienke A. Apparent Diffusion Coefficient for Distinguishing Between Malignant and Benign Lesions in the Head and Neck Region: A Systematic Review and Meta-Analysis. *Front Oncol*. 2020 Jan 8;9.
164. Dietrich O, Biffar A, Baur-Melnyk A, Reiser MF. Technical aspects of MR diffusion imaging of the body. Vol. 76, *European Journal of Radiology*. 2010. p. 314–22.
165. Yoshida T, Urikura A, Shirata K, Nakaya Y, Terashima S, Hosokawa Y. Image quality assessment of single-shot turbo spin echo diffusion-weighted imaging with parallel imaging technique: A phantom study. *British Journal of Radiology*. 2016;89(1065).
166. Fouad Y, Aanei C. Revisiting the hallmarks of cancer. *Am J Cancer Res*. 2017;7(5):1016–36.
167. Le Bihan D. What can we see with IVIM MRI? *Neuroimage*. 2019 Feb 15;187:56–67.

168. Kim HS, Suh CH, Kim N, Choi CG, Kim SJ. Histogram analysis of intravoxel incoherent motion for differentiating recurrent tumor from treatment effect in patients with glioblastoma: Initial clinical experience. *American Journal of Neuroradiology*. 2014;35(3):490–7.
169. Le Bihan D, Poupon C, Amadon A, Lethimonnier F. Artifacts and pitfalls in diffusion MRI. Vol. 24, *Journal of Magnetic Resonance Imaging*. 2006. p. 478–88.
170. Porter DA, Heidemann RM. High resolution diffusion-weighted imaging using readout-segmented echo-planar imaging, parallel imaging and a two-dimensional navigator-based reacquisition. *Magn Reson Med*. 2009;62(2):468–75.
171. Hayes L, Porter D, Jones R, Palasis S, Grattan-Smith D. RESOLVE- A Powerful Tool for Imaging the Pediatric Spine. *Clinical Neurology* [Internet]. 2014 [cited 2023 Mar 4]; Available from: <https://www.magnetomworld.siemens-healthineers.com/clinical-corner/case-studies/tool-imaging-pediatric-spine.html>
172. Qian W, Chen Q, Zhang Z, Wang H, Zhang J, Xu J. Comparison between readout-segmented and single-shot echo-planar imaging in the evaluation of cervical cancer staging. *British Journal of Radiology*. 2019;92(1094).
173. Bogner W, Pinker-Domenig K, Bickel H, Chmelik M, Weber M, Helbich TH, et al. readout-segmented echo-planar imaging improves the Diagnostic Performance of Diffusion-weighted Mr Breast examinations at 3.0 T 1 Division of Molecular and Gender Imaging (K. radiology.rsna.org n Radiology [Internet]. 2012;263(1). Available from: <http://radiology.rsna.org/lookup/suppl/doi:10.1148/radiol.12111494/-/DC1>
174. Vandecaveye V, Dirix P, De Keyzer F, Op De Beeck K, Vander Poorten V, Roebben I, et al. Predictive value of diffusion-weighted magnetic resonance imaging during chemoradiotherapy for head and neck squamous cell carcinoma. *Eur Radiol*. 2010 Jul;20(7):1703–14.
175. Srinivasan A, Chenevert TL, Dwamena BA, Eisbruch A, Watcharotone K, Myles JD, et al. Utility of Pretreatment Mean Apparent Diffusion Coefficient and Apparent Diffusion Coefficient Histograms in Prediction of Outcome to Chemoradiation in Head and Neck Squamous Cell Carcinoma. *Comput Assist Tomogr* [Internet]. 2012;36(1). Available from: www.jcat.org
176. Chung SR, Choi YJ, Suh CH, Lee JH, Baek JH. Diffusion-weighted magnetic resonance imaging for predicting response to chemoradiation therapy for head and neck squamous cell carcinoma: A systematic review. *Korean J Radiol*. 2019 Apr 1;20(4):649–61.
177. Pieper CC, Sprinkart AM, Meyer C, König R, Schild HH, Kukuk GM, et al. Evaluation of a Simplified Intravoxel Incoherent Motion (IVIM) Analysis of Diffusion-Weighted Imaging for Prediction of Tumor Size Changes and Imaging Response in Breast Cancer Liver Metastases Undergoing Radioembolization. *Medicine (United States)*. 2016 Apr 1;95(14).
178. Marzi S, Piludu F, Vidiri A. Assessment of diffusion parameters by intravoxel incoherent motion MRI in head and neck squamous cell carcinoma. *NMR Biomed*. 2013 Dec;26(12):1806–14.
179. Paudyal R, Oh JH, Riaz N, Venigalla P, Li J, Hatzoglou V, et al. Intravoxel incoherent motion diffusion-weighted MRI during chemoradiation therapy to characterize and monitor treatment response in human papillomavirus head and neck squamous cell carcinoma. *Journal of Magnetic Resonance Imaging*. 2017 Apr 1;45(4):1013–23.
180. Ding Y, Hazle JD, Mohamed ASR, Frank SJ, Hobbs BP, Colen RR, et al. Intravoxel incoherent motion imaging kinetics during chemoradiotherapy for human papillomavirus-associated squamous cell carcinoma of

- the oropharynx: Preliminary results from a prospective pilot study. *NMR Biomed.* 2015 Dec 1;28(12):1645–54.
181. Hauser T, Essig M, Jensen A, Gerigk L, Laun FB, Münter M, et al. Characterization and therapy monitoring of head and neck carcinomas using diffusion-imaging-based intravoxel incoherent motion parameters - Preliminary results. *Neuroradiology.* 2013 May;55(5):527–36.
 182. Noij DP, Martens RM, Marcus JT, de Bree R, Leemans CR, Castelijns JA, et al. Intravoxel incoherent motion magnetic resonance imaging in head and neck cancer: A systematic review of the diagnostic and prognostic value. Vol. 68, *Oral Oncology.* Elsevier Ltd; 2017. p. 81–91.
 183. Matthews PM. Functional magnetic resonance imaging [Internet]. Vol. 75, *J Neurol Neurosurg Psychiatry.* 2004. Available from: www.jnnp.com
 184. Barth M, Poser BA. Advances in high-field bold fmri. *Materials.* 2011;4(11):1941–55.
 185. Vaupel P, Mayer A. Hypoxia in cancer: Significance and impact on clinical outcome. Vol. 26, *Cancer and Metastasis Reviews.* 2007. p. 225–39.
 186. Brizel DM, Sibley GS, Prosnitz LR, Scher RL, Dewhirst MW. Tumor hypoxia adversely affects the prognosis of carcinoma of the head and neck. Vol. 38, *Oncology Biol. Phys.* Elsevier Science Inc; 1997.
 187. De Ridder M, Verellen D, Verovski V, Storme G. Hypoxic tumor cell radiosensitization through nitric oxide. Vol. 19, *Nitric Oxide - Biology and Chemistry.* 2008. p. 164–9.
 188. Begg K, Tavassoli M. Inside the hypoxic tumour: reprogramming of the DDR and radioresistance. Vol. 6, *Cell Death Discovery.* Springer Nature; 2020.
 189. Welsh L, Panek R, Riddell A, Wong K, Leach MO, Tavassoli M, et al. Blood transfusion during radical chemo-radiotherapy does not reduce tumour hypoxia in squamous cell cancer of the head and neck. *Br J Cancer.* 2017 Jan 3;116(1):28–35.
 190. Overgaard J. Hypoxic modification of radiotherapy in squamous cell carcinoma of the head and neck - A systematic review and meta-analysis. Vol. 100, *Radiotherapy and Oncology.* 2011. p. 22–32.
 191. Kaanders JHAM, Popa LAM, Marresb HAM, Van Der Maazen RWM, Van Der Kogela AJ, Van Daala WAJ. Radiotherapy with carbogen breathing and nicotinamide in head and neck cancer: feasibility and toxicity. Vol. 37, *Radiotherapy and Oncology.* 1995.
 192. Panek R, Welsh L, Baker LCJ, Schmidt MA, Wong KH, Riddell AM, et al. Noninvasive imaging of cycling hypoxia in head and neck cancer using intrinsic susceptibility MRI. *Clinical Cancer Research.* 2017 Aug 1;23(15):4233–41.
 193. Alonzi R, Padhani AR, Maxwell RJ, Taylor NJ, Stirling JJ, Wilson JI, et al. Carbogen breathing increases prostate cancer oxygenation: A translational MRI study in murine xenografts and humans. *Br J Cancer.* 2009 Feb 24;100(4):644–8.
 194. Rijpkema M, Ham Kaanders J, M Joosten FB, Van Der Kogel AJ, Heerschap A. Effects of breathing a hyperoxic hypercapnic gas mixture on blood oxygenation and vascularity of head-and-neck tumors as measured by magnetic resonance imaging. *Int J Radiation Oncology Biol Phys.* 2002;53(5):1185–91.
 195. Janssens GO, Rademakers SE, Terhaard CH, Doornaert PA, Bijl HP, Van Ende P Den, et al. Accelerated radiotherapy with carbogen and nicotinamide for laryngeal cancer: Results of a phase III randomized trial. *Journal of Clinical Oncology.* 2012 May 20;30(15):1777–83.

196. A M Kaanders JH, M Pop LA, M Marres HA, Bruaset I, A Van Den Hoogen FJ, W Merckx MA, et al. ARCON-experience in 215 patients with advanced head-and-neck cancer. *Int J Radiation Oncology Biol Phys.* 2002;52(3):769–78.
197. Hoskin PJ. Hypoxia dose painting in prostate and cervix cancer. Vol. 54, *Acta Oncologica.* Taylor and Francis Ltd; 2015. p. 1259–62.
198. Dirix P, Vandecaveye V, De Keyzer F, Stroobants S, Hermans R, Nuyts S. Dose painting in radiotherapy for head and neck squamous cell carcinoma: Value of repeated functional imaging with 18F-FDG PET, 18F-fluoromisonidazole PET, diffusion-weighted MRI, and dynamic contrast-enhanced MRI. *Journal of Nuclear Medicine.* 2009 Jul 1;50(7):1020–7.
199. Waldfahrer F, Hauptmann B, Iro H. Lymph node metastasis of glottic laryngeal carcinoma. *Laryngo-Rhino-Otol.* 2005;84:96–100.
200. Mucha-Małecka A, Chrostowska A, Urbanek K, Małecki K. Prognostic factors in patients with T1 glottic cancer treated with radiotherapy. *Strahlentherapie und Onkologie.* 2019 Sep 1;195(9):792–804.
201. Merlotti A, Alterio D, Vigna-Taglianti R, Muraglia A, Lastrucci L, Manzo R, et al. Technical guidelines for head and neck cancer IMRT on behalf of the Italian association of radiation oncology - head and neck working group. Vol. 9, *Radiation Oncology.* BioMed Central Ltd.; 2014.
202. Kirchner J. Two hundred laryngeal cancers- patterns of growth and spread as seen in serial section. *American Laryngological, Rhinological and Otological Society Meeting.* 1976;
203. Guimarães AV, Dedivitis RA, Matos LL, Aires FT, Cernea CR. Comparison between transoral laser surgery and radiotherapy in the treatment of early glottic cancer: A systematic review and meta-analysis. *Sci Rep.* 2018 Dec 1;8(1).
204. Kim JW, Byeon HK, Choi HS, Lee IJ. Dose de-escalation to the normal larynx using conformal radiotherapy reduces toxicity while maintaining oncologic outcome for T1/T2 glottic cancer. *Sci Rep.* 2017 Dec 1;7(1).
205. Gupta A, Wong KH, Newbold K, Bhide S, Nutting C, Harrington KJ. Early-Stage Glottic Squamous Cell Carcinoma in the Era of Image-Guided Radiotherapy. Vol. 11, *Frontiers in Oncology.* Frontiers Media S.A.; 2021.
206. Bradford CR, Ferlito A, Devaney KO, Mäkitie AA, Rinaldo A. Prognostic factors in laryngeal squamous cell carcinoma. Vol. 5, *Laryngoscope Investigative Otolaryngology.* John Wiley and Sons Inc; 2020. p. 74–81.
207. Van Der Molen L, Heemsbergen WD, De Jong R, Van Rossum MA, Smeele LE, Rasch CRN, et al. Dysphagia after chemoradiotherapy Dysphagia and trismus after concomitant chemo-Intensity-Modulated Radiation Therapy (chemo-IMRT) in advanced head and neck cancer; Dose-effect relationships for swallowing and mastication structures. *Radiotherapy and Oncology.* 2013 Mar;106(3):364–9.
208. Wall LR, Ward EC, Cartmill B, Hill AJ. Physiological changes to the swallowing mechanism following (chemo)radiotherapy for head and neck cancer: A systematic review. Vol. 28, *Dysphagia.* 2013. p. 481–93.
209. Duprez F, Madani I, De Potter B, Boterberg T, De Neve W. Systematic review of dose-volume correlates for structures related to late swallowing disturbances after radiotherapy for head and neck cancer. Vol. 28, *Dysphagia.* 2013. p. 337–49.
210. Kazi R, Venkitaraman R, Johnson C, Prasad V, Clarke P, Newbold K, et al. Prospective, longitudinal electroglottographic study of voice recovery following accelerated hypofractionated radiotherapy for T1/T2 larynx cancer. *Radiotherapy and Oncology.* 2008 May;87(2):230–6.

211. Fung K, Yoo J, Leeper A, Hawkins S, Heeneman H, Doyle PC, et al. Vocal Function Following Radiation for Non-Laryngeal Versus Laryngeal Tumors of the Head and Neck. *Laryngoscope*. 2001;111.
212. Mekis J, Strojjan P, Boltezar IH. Factors affecting voice quality in early glottic cancer before and after radiotherapy. *Radiol Oncol*. 2019;
213. Bibby JRL, Cotton SM, Perry A, Corry JF. Voice outcomes after radiotherapy treatment for early glottic cancer: Assessment using multidimensional tools. *Head Neck*. 2008 May;30(5):600–10.
214. Heijnen BJ, Speyer R, Kertscher B, Cordier R, Koetsenruijter KWJ, Swan K, et al. Dysphagia, Speech, Voice, and Trismus following Radiotherapy and/or Chemotherapy in Patients with Head and Neck Carcinoma: Review of the Literature. Vol. 2016, BioMed Research International. Hindawi Limited; 2016.
215. Ma Y, Green R, Pan S, McCabe D, Goldberg L, Woo P. Long-term Voice Outcome Following Radiation Versus Laser Microsurgery in Early Glottic Cancer. *Journal of Voice*. 2019 Mar 1;33(2):176–82.
216. Hočevár-Boltežar I, Žargi M, Strojjan P. Risk factors for voice quality after radiotherapy for early glottic cancer. *Radiotherapy and Oncology*. 2009 Dec;93(3):524–9.
217. Fu KK, Woodhouse RJ, Quivey JM, Phillips TL, Dedo HH. The Significance of Laryngeal Edema Following Radiotherapy of Carcinoma of the Vocal Cord. *Cancer*. 1982;49:655–8.
218. Chung T, Yousem D, Lexa F, Markiewicz D. MRI of carotid angiopathy after therapeutic radiation. *J Comput Assist Tomogr*. 1994;18(4):533–8.
219. Carmody B, Arora S, Avena R, Curry K, Simpkins J, Cosby K, et al. Accelerated carotid artery disease after high-dose head and neck radiotherapy- is there a role for routine carotid duplex surveillance. *J Vasc Surg*. 1993;30:1045–51.
220. Plummer C, Henderson RD, O'Sullivan JD, Read SJ. Ischemic stroke and transient ischemic attack after head and neck radiotherapy: A review. Vol. 42, *Stroke*. 2011. p. 2410–8.
221. Murros KE, Toole JF. The Effect of Radiation on Carotid Arteries A Review Article. *Arch Neurol* [Internet]. 1989;46. Available from: <http://archneur.jamanetwork.com/>
222. Abayomi OK. Neck irradiation, carotid injury and its consequences. Vol. 40, *Oral Oncology*. 2004. p. 872–8.
223. Gujral DM, Shah BN, Chahal NS, Senior R, Harrington KJ, Nutting CM. Clinical features of radiation-induced carotid atherosclerosis. *Clin Oncol*. 2014 Feb;26(2):94–102.
224. Cheng SWK, Ting ACW, Ho P, Wu LLH. Accelerated progression of carotid stenosis in patients with previous external neck irradiation. *J Vasc Surg*. 2004;39(2):409–15.
225. Dorresteijn LDA, Kappelle AC, Boogerd W, Klokman WJ, Balm AJM, Keus RB, et al. Increased Risk of Ischemic Stroke After Radiotherapy on the Neck in Patients Younger Than 60 Years. *J Clin Oncol*. 2001;20:282–8.
226. Fernández-Alvarez V, López F, Suárez C, Strojjan P, Eisbruch A, Silver CE, et al. Radiation-induced carotid artery lesions. Vol. 194, *Strahlentherapie und Onkologie*. Urban und Vogel GmbH; 2018. p. 699–710.
227. Gujral DM, Chahal N, Senior R, Harrington KJ, Nutting CM. Radiation-induced carotid artery atherosclerosis. *Radiotherapy and Oncology*. 2014;110(1):31–8.
228. Garcez K, Lim CC, Whitehurst P, Thomson D, Ho KF, Lowe M, et al. Carotid dosimetry for T1 glottic cancer radiotherapy. *British Journal of Radiology*. 2014 Jun 1;87(1038).
229. Chatterjee S, Guha S, Prasath S, Mallick I, Achari R. Carotid sparing hypofractionated tomotherapy in early glottic cancers: Refining image guided IMRT to improve morbidity. *J Cancer Res Ther*. 2013 Jul;9(3):452–5.

230. Chera BS, Amdur RJ, Morris CG, Mendenhall WM. Carotid-sparing intensity-modulated radiotherapy for early-stage squamous cell carcinoma of the true vocal cord. *Int J Radiat Oncol Biol Phys.* 2010 Aug 1;77(5):1380–5.
231. Martin JD, Buckley AR, Graeb D, Walman B, Salvian A, Hay JH. Carotid artery stenosis in asymptomatic patients who have received unilateral head-and-neck irradiation. *Int J Radiat Oncol Biol Phys.* 2005 Nov 15;63(4):1197–205.
232. Rosenthal DI, Fuller CD, Barker JL, Mason B, Garcia JA, Lewin JS, et al. Simple Carotid-Sparing Intensity-Modulated Radiotherapy Technique and Preliminary Experience for T1-2 Glottic Cancer. *Int J Radiat Oncol Biol Phys.* 2010 Jun 1;77(2):455–61.
233. Zumsteg ZS, Riaz N, Jaffery S, Hu M, Gelblum D, Zhou Y, et al. Carotid sparing intensity-modulated radiation therapy achieves comparable locoregional control to conventional radiotherapy in T1-2N0 laryngeal carcinoma. *Oral Oncol.* 2015 Jul 1;51(7):716–23.
234. Shelton RL, Bosma JF, Sheets B V. Tongue, hyoid and larynx displacement in swallow and phonation'. *J Appl Physiol* [Internet]. 1960;15(2):283–8. Available from: www.physiology.org/journal/jappl
235. Tiong A, Huang SH, O'Sullivan B, Mallick I, Kim J, Dawson LA, et al. Outcome following IMRT for T2 glottic cancer: the potential impact of image-guidance protocols on local control. *J Radiat Oncol.* 2014 Sep;3(3):267–75.
236. Hamlet S, Ezzell G, Aref A. Larynx motion associated with swallowing during radiation therapy. Vol. 28, *Oncology BioL Phys.* 1993.
237. Van Asselen B, Raaijmakers CPJ, Lagendijk JJW, Terhaard CHJ. Intrafraction motions of the larynx during radiotherapy. *Int J Radiat Oncol Biol Phys.* 2003 Jun 1;56(2):384–90.
238. Bradley JA, Paulson ES, Ahunbay E, Schultz C, Li XA, Wang D. Dynamic MRI analysis of tumor and organ motion during rest and deglutition and margin assessment for radiotherapy of head-and-neck cancer. *Int J Radiat Oncol Biol Phys.* 2011 Dec 1;81(5).
239. Osman SOS, de Boer HCJ, Heijmen BJM, Levendag PC. Four-dimensional CT analysis of vocal cords mobility for highly focused single vocal cord irradiation. *Radiotherapy and Oncology.* 2008 Oct;89(1):19–27.
240. Kwa SLS, Al-Mamgani A, Osman SOS, Gangsaas A, Levendag PC, Heijmen BJM. Inter- and intrafraction target motion in highly focused single vocal cord irradiation of t1a larynx cancer patients. *Int J Radiat Oncol Biol Phys.* 2015 Sep 1;93(1):190–5.
241. Bruijnen T, Stemkens B, Terhaard CHJ, Lagendijk JJW, Raaijmakers CPJ, Tijssen RHN. Intrafraction motion quantification and planning target volume margin determination of head-and-neck tumors using cine magnetic resonance imaging. *Radiotherapy and Oncology.* 2019 Jan 1;130:82–8.
242. Bahig H, Nguyen-Tan PF, Filion É, Roberge D, Thanomsack P, de Guise J, et al. Larynx motion considerations in partial larynx volumetric modulated arc therapy for early glottic cancer. *J Med Imaging Radiat Oncol.* 2017 Oct 1;61(5):666–73.
243. Kim JW, Byeon HK, Choi HS, Lee IJ. Publisher Correction: Dose deescalation to the normal larynx using conformal radiotherapy reduces toxicity while maintaining oncologic outcome for T1/T2 glottic cancer (Scientific Reports DOI: 10.1038/s41598-017-15974-6). Vol. 8, *Scientific Reports.* Nature Publishing Group; 2018.

244. Rock K, Huang SH, Tiong A, Lu L, Xu W, Ringash J, et al. Partial Laryngeal IMRT for T2N0 Glottic Cancer: Impact of Image Guidance and Radiation Therapy Intensification. *Int J Radiat Oncol Biol Phys.* 2018 Nov 15;102(4):941–9.
245. Osman SOS, Astreinidou E, De Boer HCJ, Keskin-Cambay F, Breedveld S, Voet P, et al. IMRT for image-guided single vocal cord irradiation. *Int J Radiat Oncol Biol Phys.* 2012 Feb 1;82(2):989–97.
246. Al-Mamgani A, Kwa SLS, Tans L, Moring M, Fransen D, Mehilal R, et al. Single vocal cord irradiation: Image guided intensity modulated hypofractionated radiation therapy for T1a glottic cancer: Early clinical results. *Int J Radiat Oncol Biol Phys.* 2015 Oct 1;93(2):337–43.

2 CHAPTER 2: FUNCTIONAL MRI-GUIDED ADAPTIVE RADIOTHERAPY FOR HEAD AND NECK CANCERS

2.1 Introduction

The original INSIGHT study investigated the role of functional imaging in the forms of ^{18}F -FDG PET/CT, DWI, BOLD and dynamic contrast-enhanced MRIs (1). The results showed that PET/CT-derived SUV_{max} and TLG parameters have predictive powers in the first week of CRT. ADC was the most powerful MRI-based parameter that was able to predict response in the second week of CRT (2). The DWI-MRI findings have been echoed in a systematic review, where the threshold for ADC increase between 15.5-25% after two weeks of commencing CRT is deemed predictive of a responding primary tumour (3).

The INSIGHT II study aims to further explore the role of DWI-guided ART in patients with locally-advanced HNC who are receiving radical CRT. INSIGHT II also investigates and compares the differences between RESOLVE and ssEPI DWI sequences, as RESOLVE is reported to offer a better signal to noise ratio and less anatomical distortion than ssEPI, although RESOLVE has not yet been tested as an imaging biomarker (4). In addition, the INSIGHT II study puts the published DWI-MRI findings into practice by investigating the role of DWI-guided ART in patients with intermediate-/high-risk locally-advanced oropharyngeal, hypopharyngeal and laryngeal SCCs.

Comparisons between DWI findings from different centres are difficult due to the heterogeneity in MRI scanners, sequence protocols/parameters and definitions of target volumes. However, the trends in ADC changes are of similar proportion as the exponential rate of signal decay with increasing b-values should not differ. The MR-Linac provides the ideal platform for performing MRgRT by allowing DWI and session imaging and treatment without having to move the patient, improving registration and treatment accuracy. This project additionally evaluates the patterns and repeatability of DWI on the MR-Linac to determine whether they reflect the patterns of change seen on the diagnostic-MRI scanner.

One of the potential gains from ART for HNC is maximally to spare OARs from dose by adjusting for tumour size, position and shape. Functional imaging can also potentially guide intra-treatment strategy changes to improve local control for non-responding tumours. Both scenarios will also be evaluated in the INSIGHT II study. In addition, this project aims to explore the resultant dosimetry to targets and OARs when adopting such strategies.

2.2 Aims and Hypotheses

i) **Aims:**

- To validate ADC values using ssEPI DWI in the INSIGHT II-study patient cohort and determine how RESOLVE DWI compares to ssEPI.

Hypothesis:

- Changes in ADC values using ssEPI and RESOLVE DWI will be of similar magnitude to those reported using ssEPI in the original INSIGHT study.

ii) **Aim:**

- To assess the repeatability of DW-MRI parameters on the MR-Linac platform to determine whether ADC-guided ART can be replicated on the MR-Linac.

Hypothesis:

- The MR-Linac will provide similar ADC measurements to diagnostic MRI and, therefore, allow ADC-guided ART.

iii) **Aims:**

- To compare the cumulative doses to tumour targets and OARs with and without MRgRT.
- To investigate the feasibility and safety of RT dose-escalation for non-responding tumours as determined by DWI.

Hypotheses:

- Reduction of high-dose volumes for responding tumours will result in reduced dose to the OARs.
- Dose-escalation for non-responding primary tumours will allow safe delivery of dose without compromising critical OAR tolerances.

2.3 Materials and Methods

2.3.1 Patient Criteria

INSIGHT II (NCT04242459) is a phase 1/2 study investigating functional image-guided ART using MRI in patients with locally-advanced (stage III-IVb AJCC 7th Edition) oropharyngeal, hypopharyngeal or laryngeal SCC receiving radical CRT. Data from patients recruited to this study will be used for DWI/ADC and ART analyses. Other inclusion criteria included age 18-70, World Health Organisation performance status 0, creatinine clearance >50 mL/min, neutrophils $\geq 1500/\text{mm}^3$, platelets $\geq 100000/\text{mm}^3$ and haemoglobin ≥ 9 g/dl. Exclusion criteria included any patient with any prior malignancy except for non-melanoma skin cancer, any prior head and neck radiotherapy or contraindications to MRI or intravenous contrast agents.

To investigate DW-MRI changes on the MR-Linac, additional patients with measurable primary tumour undergoing radical radiotherapy were recruited into the PRIMER (NCT0297382) and PERMIT (NCT03727698) studies. Patients in PRIMER were limited to five total scanning sessions and patients in PERMIT were able to have baseline plus weekly DW-MRIs. To investigate the stability of ADC parameters on the MR-Linac, consenting patients were requested to have double-baseline DW-MRIs over two consecutive days.

2.3.2 INSIGHT II Study Design

The INSIGHT II trial workflow is displayed in Figure 2-1. All patients received planning-CT and MRI-Neck scans at baseline (pre-radiotherapy), fraction 8-9 (week 2) and fraction 18-19 (week 4) of CRT. The feasibility phase of the study aimed to demonstrate in ten patients that MRIs and radiotherapy replans could be generated within the designated time frame.

Patients in the feasibility phase of the trial received standard CRT without any changes to the clinically delivered radiotherapy plans, unless clinically indicated. However, the week 2 and 4 planning-CT and MRI scans were used to simulate adaptive-radiotherapy plans at each time point. Patients in the main phase of the trial were stratified into two cohorts based on primary site and tumour risk group and clinically delivered

adaptive radiotherapy plans produced based on tumour response (Table 2-1). Radiotherapy for all patients was prescribed at 65 Gy in 30 fractions over 6 weeks with concurrent cisplatin (100 mg/m²) or carboplatin (AUC 5) on days 1 and 29.

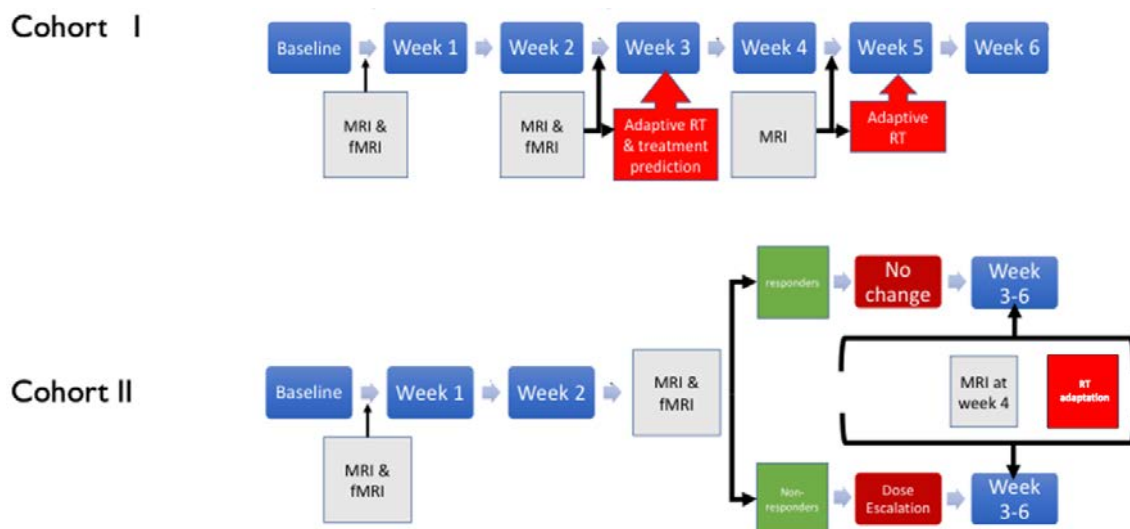


Figure 2-1, INSIGHT II trial workflow.

Patients were stratified by risk groups based on stage and smoking history. All patients received a planning CT and functional-MRI (fMRI) pre-treatment, at week 2 and 4 of treatment. Patients in cohort 1 had primary target volumes adjusted depending on response. Patients in cohort 2 had DWI/ADC measurements at the week 2 time point, where non-responding tumours received dose escalation. The week 4 scan in cohort 2 allowed adjustment of all targets to account for any evolving anatomical changes.

<u>Risk Groups</u>	<u>Cohort 1</u>	<u>Cohort 2</u>	
	Low-Risk p16-positive	Intermediate-/High-Risk p16-positive	Intermediate-/High-Risk p16-negative
<u>Stage (AJCC 7th)</u>	T1-3, N0-2c	T1-3, N0-2c (≥10 pack-yr) T4, N3 (incl <10 pack-yr)	T1-4, N0-3
<u>Smoking History</u>	<10 pack-yr	See above	any
<u>Tumour size</u>	any	≤ 5 cm	≤ 5 cm

Table 2-1, Patient Risk Stratification.

Patients with stage III-IVb disease were stratified by the initial TNM stage (AJCC 7th Edition), HPV and smoking status, based on the risk stratification as described by Ang et al (5). HPV status is considered in the AJCC 8th edition. Primary tumour size for intermediate-/high-risk disease is required to be ≤ 5 cm to allow boost dose to be delivered safely, if required.

Patients in cohort 1 underwent adaptation of radiotherapy volumes to the primary and nodal targets depending on the degree of response at each time point. As per the original INSIGHT study (1), patients in cohort 2 were stratified into responder or non-responder groups based on the percentage change in the primary-target ADC compared to baseline. A change in ADC $\leq 15\%$ on ssEPI DWI-MRI at week 2 classified a tumour as unresponsive to treatment and resulted in a 9% total dose escalation to the primary tumour PTV only. A rise in ADC $>15\%$ defined a tumour as responsive and there were no changes in the dose to primary target. Target and OAR contour adaptations were performed at week 4 for both cohorts.

2.3.3 CT and MRI Scan Protocols

All planning CT scans were performed with patients immobilised in the supine position with a five-point thermoplastic head shell and knee fix. Shoulder wedge was occasionally used to assist in achieving an extended neck position. Planning CT was performed on a large-bore scanner (Philips Medical, Cleveland, OH, USA) with intravenous contrast and images acquired at 2 mm slices from the vertex to the carina. Intravenous contrast was not administered for the week 2 and 4 planning CTs.

For the INSIGHT II study, a non-contrast-enhanced MRI of the neck was performed with patients immobilised in the same head and neck shell as for their planning CTs. T2, fat suppression (Turbo Inversion Recovery Magnitude, TIRM) and DWI (both single-shot echo planar image (ssEPI) and RESOLVE) sequences were performed on a Siemens MAGNETOM Aera 1.5 T MRI scanner (scan parameters listed in Appendix A).

DW-MRI scans on the Elekta AB. (Stockholm, Sweden) Unity MR-Linac were also performed with patients immobilised in the treatment position (Appendix A). However, scanning time points varied between patients due to MR-Linac availability.

ADC maps were generated using b-values of 50-800 s/mm² or 30-500 s/mm² for the diagnostic MR and MR-Linac scanners, respectively.

2.3.4 DWI/ ADC Analysis

DWI image sets were imported into the RayStation treatment planning system (TPS) (12.0.0.932, RaySearch Laboratories AB, Sweden). Primary and dominant nodal targets were contoured on DWI b50 s/mm² images for both DWI sequences because these had the least anatomical distortion. Necrotic regions in the lymph nodes were excluded (Figure 2-2 (A-E)). Regions of interest were translated onto the corresponding ADC maps and histograms of ADC values per voxel were generated. ADC value maps were generated using a mono-exponential function between b50 - b800 s/mm², on a voxel-by-voxel basis. Median ADC values were recorded after eliminating all values below 0.5 x 10⁻³ mm²s⁻¹, as these were considered to be related to signal noise (Figure 2-2F). MR-Linac-generated DWIs were analysed using the same method, except that b30 s/mm² images were used as the reference.

Percentage change in median-ADC values were determined as follows:

$$\Delta \text{ADC (\%)} = [\text{ADC (time point } x) \div \text{ADC (baseline)}] \times 100.$$

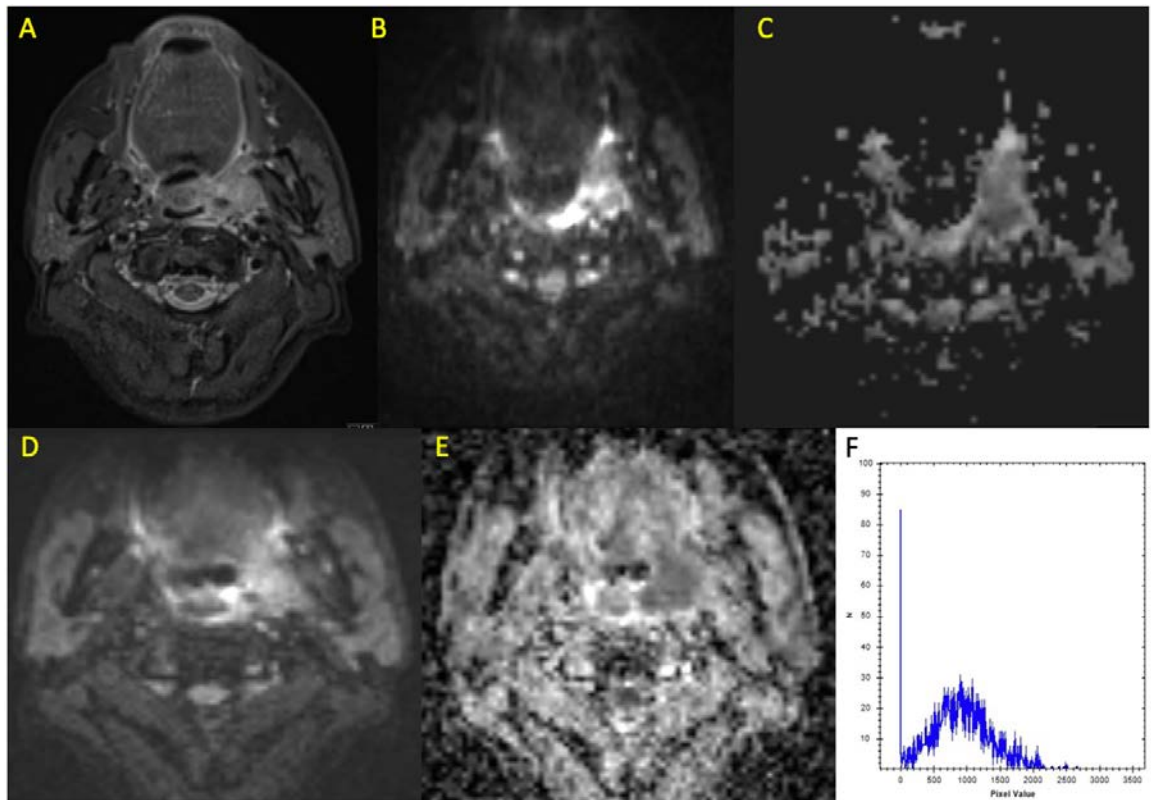


Figure 2-2, Diagnostic DW-MRI sequences.

A) Turbo Inversion Recovery Magnitude, TIRM. B)/C) single-shot Echo-Planar Image (ss-EPI)/Apparent Diffusion Coefficient (ADC), respectively. ADC voxel threshold of 40 mm²s⁻¹ to exclude noise. D)/E) Readout Segmentation of Long Variable Echo-trains DWI/ADC, respectively. No threshold was applied on ADC. E) Histogram generated for ss-EPI DWI demonstrates significant noise with voxels below 50 mm²s⁻¹.

2.3.5 Target Delineation, Radiotherapy Planning and Replanning

The GTV included the primary tumour and involved lymph node(s). The high-dose CTV (65 Gy) was generated using a 5 mm isotropic expansion of the GTV, edited off natural barriers such as air and bone. An additional low-dose CTV (54 Gy) for microscopic disease was created using a 10 mm isotropic expansion of the primary tumour GTV only, which was also edited off natural barriers. Nodal levels at risk of microscopic disease were treated to 54 Gy. Superior, middle and inferior pharyngeal constrictor muscles sparing were performed and any intersecting elective-nodal coverage was compromised as per the “Dysphagia-Aspiration Related Structures” study (6).

If patients in cohort 1 had regressing primary or nodal tumours seen on the week 2 or 4 MRIs, the GTV would be adjusted to encompass the remaining visible gross disease. Any voxel defined as primary or nodal tumour at baseline would receive a minimum of 1.8 Gy per fraction on the replans. Therefore, CTVs would receive doses between 54 – 65 Gy in total. Patients in cohort 2 who were identified as “non-responders” at week 2 would receive dose escalation to the primary tumour only. Dose was escalated by producing a 20-fraction plan (fractions 11-30) at a dose of 2.36 Gy/fraction to total 68.9 Gy in 30 fractions over six weeks. No further adjustments to dose were made at week 4.

Radiotherapy plans at all time points were created by members of the physics team on the RayStation TPS. Planning objectives and target constraints for the baseline plans were as per standard-of-care objectives currently used in the clinic. All planning objectives and constraints, including those for the dose-escalation cohort, are listed in Appendix B. All plans were produced using a collapsed cone dosimetry algorithm (V5.6). A VMAT technique was utilised with a dual 360° arc of 6 MV flattening-filter-free photons, maximum 90 seconds per beam, maximum 180 segments with gantry spacing of 2°, 60 maximum optimisation loops, dose-grid resolution of 0.25 cm³ and a single isocentre.

To assist with target delineation speeds, the ANAtomically CONstrained Deformation image registration Algorithm (ANACONDA), described by Weistrand et al (7) and investigated by Hin et al (8), was used. Firstly, the CTs were rigidly co-registered, followed by deformable registration. OARs and primary/nodal GTV and CTV contours

from the previous CT were transferred using default RayStation TPS intensity-based methods. Targets were checked and amended, if necessary, by me and a Clinical Oncology consultant before being replanned.

Final dose reporting was performed by accumulating dose cubes from the 3 plans (fractions 1-10, 11-20 and 21-30) on the baseline CT for more consistent comparisons between baseline plans and ART. The original baseline contours for the primary and lymph-node tumours were used for all dose reporting.

2.3.6 Statistical Analyses

In order to validate ssEPI and RESOLVE DWI-MRI, minimums of 22 responding and 6 non-responding patients were required. This is based on a power of 0.8 (alpha 5%) to detect a maximum percentage difference in week 2 ADC change of up to 10%, to be deemed equivalent (based on previous data).

For the purposes of DW-MRI sequence comparisons, ssEPI was assigned as the control modality against which RESOLVE and MR-Linac DWI results were compared. Pearson's correlation tests between different sequences were initially performed to determine the linearity of any relationships between the different DWI modalities.

Stability and repeatability of DWI parameters were assessed by performing Bland-Altman analyses using the SPSS Stats Package (V23.0, 2015, IBM). For each subject pair, the differences between the values and mean of both values were calculated. The differences were plotted against the paired value means. The mean of all the differences was used as the mean reference line, with 1.96 standard deviations of this mean determining the limits of agreement. A 95% confidence interval of the reference mean line was calculated as: $[\sqrt{(SD^2 \div n)}] \times (t\text{-value for } (n-1))$.

Dosimetric comparisons between baseline and ART plans for the relevant targets and OARs for patients in cohort 1 were analysed with the paired t-test using Microsoft Excel (V16.49, 2021). Bonferroni correction was applied, (original alpha level 0.05 divided by 22 to give new alpha of <0.023), to account for the multiple testing. Data for patients in cohort 2 were similarly analysed but due to the limited patient numbers, the non-parametric Wilcoxon signed-rank sum test was used.

2.4 Results

2.4.1 Patient Demographics

Nine and ten patients were recruited into the feasibility and main phases of the INSIGHT II study, respectively, (Table 2-2a). Twenty-five patients were recruited to have scans on the MR-Linac (Table 2-2b). One patient's images were of unsuitable quality for use and another patient withdrew from the study and they were not included in analyses.

2.4.1.1 INSIGHT II Study

Sixteen patients (84.2%) had HPV-associated oropharyngeal primaries with a single non-oropharyngeal (larynx) primary. Seven (36.8%) patients were deemed to be low-risk. Sixteen (84.2%) patients were male and the whole cohort mean age was 57.3 years (SD 8.3). All patients in the feasibility phase successfully had ART plans created in the second and fourth weeks of CRT. All ten patients in the main phase of the study had these ART plans clinically delivered. All patients across the feasibility and main phases who reached the 3-month follow-up point received an ¹⁸F-FDG PET/CT, which showed complete metabolic responses to CRT. At the time of write up, three patients ("mH-J") were yet to have their post-treatment PET/CT scans.

2.4.1.2 MR-Linac

Twenty-two patients (95.7%) had oropharyngeal and one patient had laryngeal (4.3%) SCCs. Nineteen patients (82.6%) had HPV-associated SCCs. All patients except one (mrQ) had locally-advanced disease. This group was predominantly of male gender (82.6%) and the whole cohort mean age was 64.5 years (SD 8.3). For all the 3-month post-radiotherapy PET/CTs that were performed, a single patient with HPV-negative left base-of-tongue SCC ("mrI") had residual primary and nodal disease. Four patients (17.4%) were still within the 3-month post-treatment period and had not had their PET/CT scans.

a)

<u>Patient ID</u>	<u>Age</u>	<u>Gender</u>	<u>Primary Site</u>	<u>Subsite</u>	<u>T</u>	<u>N</u>	<u>AJCC Stage (7th)</u>	<u>Smoking Status</u>	<u>Risk Group</u>	<u>PET Outcome</u>
fA	65	Male	Oropharynx (HPV)	Left BOT	1	1	3	<10 pck-yr	1	CR
fB	58	Male	Oropharynx (HPV)	Right Tonsil	2	1	3	>10 pck-yr	2	CR
fC	67	Male	Oropharynx (HPV)	Right BOT	1	1	3	<10 pck-yr	1	CR
fD	55	Male	Oropharynx (HPV)	Right Tonsil	4	1	4a	<10 pck-yr	2	CR
fE	61	Male	Oropharynx (HPV)	Left BOT	1	1	3	> 10 pck-yr	2	CR
fF	56	Male	Oropharynx (HPV)	Right BOT	2	1	3	<10 pck-yr	1	CR
fG	33	Male	Larynx	Supraglottis	3	0	3	>10 pck-yr	2	CR
fH	68	Male	Oropharynx (HPV)	Left BOT	4	1	4a	>10 pck-yr	2	CR
fI	65	Male	Oropharynx (HPV)	Soft Palate	4	2	4a	<10 pck-yr	2	CR
mA	59	Male	Oropharynx (HPV)	Right Tonsil	2	1	3	<10 pck-yr	1	CR
mB	62	Male	Oropharynx (non-HPV)	Right Pharyngeal Wall	3	0	3	>10 pck-yr	2	CR
mC	56	Male	Oropharynx (HPV)	Left Tonsil	2	1	3	>10 pck-yr	2	CR
mD	48	Male	Oropharynx (HPV)	Left Tonsil	3	1	3	<10 pck-yr	1	CR
mE	65	Male	Oropharynx (HPV)	Left Tonsil	4	1	4a	<10 pck-yr	2	CR
mF	55	Female	Oropharynx (HPV)	Left BOT	4	1	4a	<10 pck-yr	2	CR
mG	47	Female	Oropharynx (HPV)	Right Tonsil	4	0	4a	>10 pck-yr	2	CR
mH	59	Male	Oropharynx (non-HPV)	Left Pharyngeal Wall	3	2b	4a	>10 pck-yr	2	NA
mI	52	Male	Oropharynx (HPV)	Right BOT	2	1	3	<10 pck-yr	1	NA
mJ	58	Female	Oropharynx (HPV)	Right BOT	2	1	3	<10 pck-yr	1	NA

b)

Patient ID	Age	Gender	Primary Site	Subsite	T	N	AJCC Stage (7th)	PET Outcome
mrA	70	Male	Oropharynx (HPV)	Left BOT	3	2	4a	CR
mrB	71	Male	Oropharynx (HPV)	Right BOT	4a	2	4a	CR
mrC	67	Male	Oropharynx (HPV)	Left Tonsil	3	1	3	CR
mrD	76	Male	Oropharynx (HPV)	Right Tonsil	4	1	4a	CR
mrE	71	Male	Oropharynx (HPV)	Left Tonsil	3	1	3	CR
mrF	54	Male	Oropharynx (HPV)	Left Tonsil	2	1	3	CR
mrG	61	Male	Oropharynx (HPV)	Left Tonsil	1	1	3	CR
mrH	64	Male	Oropharynx (HPV)	Left BOT	4	1	4a	CR
mrI	58	Female	Oropharynx (non-HPV)	Left BOT	4	2c	4a	Residual disease
mrJ	59	Male	Oropharynx (HPV)	Right Tonsil	2	1	3	CR
mrK	48	Male	Oropharynx (HPV)	Left Tonsil	3	1	3	CR
mrL	56	Male	Oropharynx (HPV)	Right BOT	4	2	4a	CR
mrM	77	Male	Oropharynx (HPV)	Left BOT	2	1	3	CR
mrN	75	Male	Oropharynx (HPV)	Right Tonsil	3	1	3	CR
mrO	62	Male	Oropharynx (non-HPV)	Epiglottis	3	0	3	CR
mrP	74	Male	Oropharynx (HPV)	Left BOT	3	1	2	CR
mrQ	67	Female	Larynx	Supraglottis	2	0	2	CR
mrR	52	Male	Oropharynx (non-HPV)	Left Tonsil	3	2b	4a	CR
mrS	57	Female	Oropharynx (HPV)	Right Tonsil	4	0	4a	CR
mrT	72	Male	Oropharynx (HPV)	Left Tonsil	4	1	4a	NA
mrU	68	Male	Oropharynx (HPV)	Left BOT	4	0	4a	NA
mrV	68	Female	Oropharynx (HPV)	Right BOT	2	1	3	NA
mrW	57	Male	Oropharynx (HPV)	Right Tonsil	2	2	4a	NA

Table 2-2, Patient Characteristics and Treatment Outcomes.

Patient details are displayed for those recruited to the a) INSIGHT II trial and b) MR-Linac. The prefixes “f, m” and “mr” refer to patients in the feasibility, main and MR-Linac parts of the various studies, respectively. PET/CT was performed at 3 months post-treatment to establish outcomes. Some patients did not reach this time point before concluding data collection (“NA”). Risk groups in Table 2-2 refer to those described in Table 2-1. Patients are assigned IDs for reference in the main text. BOT-Base of Tongue, HPV-Human Papilloma Virus, CR-Complete Response, T-Tumour, N-Node.

2.4.2 ADC Data

2.4.2.1 INSIGHT II study

All individual-level ADC data are provided for the primary tumours and lymph nodes in Appendix C. In the feasibility phase, patient “fH” was the only non-responder with a consistent ADC increase $<15\%$ for the primary and lymph-node diseases on both ssEPI and RESOLVE sequences at week 2. The only discrepancy was for patient “fF,” who was deemed a non-responder on ssEPI (Δ ADC $+3.38\%$) but a responder on RESOLVE (Δ ADC $+20.16\%$) for the primary lesion at week 2. Responders were consistently identified on both ssEPI and RESOLVE for primary tumours in all other patients in the feasibility phase.

In the main phase, patients “mB, mG, mH and mJ” were all deemed non-responders for the primary tumours on both ssEPI and RESOLVE sequences. Patients “mB, mG and mH” had intermediate-/high-risk disease (cohort 2) and subsequently received radiation dose escalation to 68.9 Gy. “mB, mH and mJ” had lymph node disease. For “mB and mH,” Δ ADC was $<15\%$ on ssEPI, but “mB” was the only patient with Δ ADC $<15\%$ on RESOLVE. “mJ” was deemed a responder on both ssEPI (Δ ADC $+35.1\%$) and RESOLVE (Δ ADC $+24.8\%$) sequences.

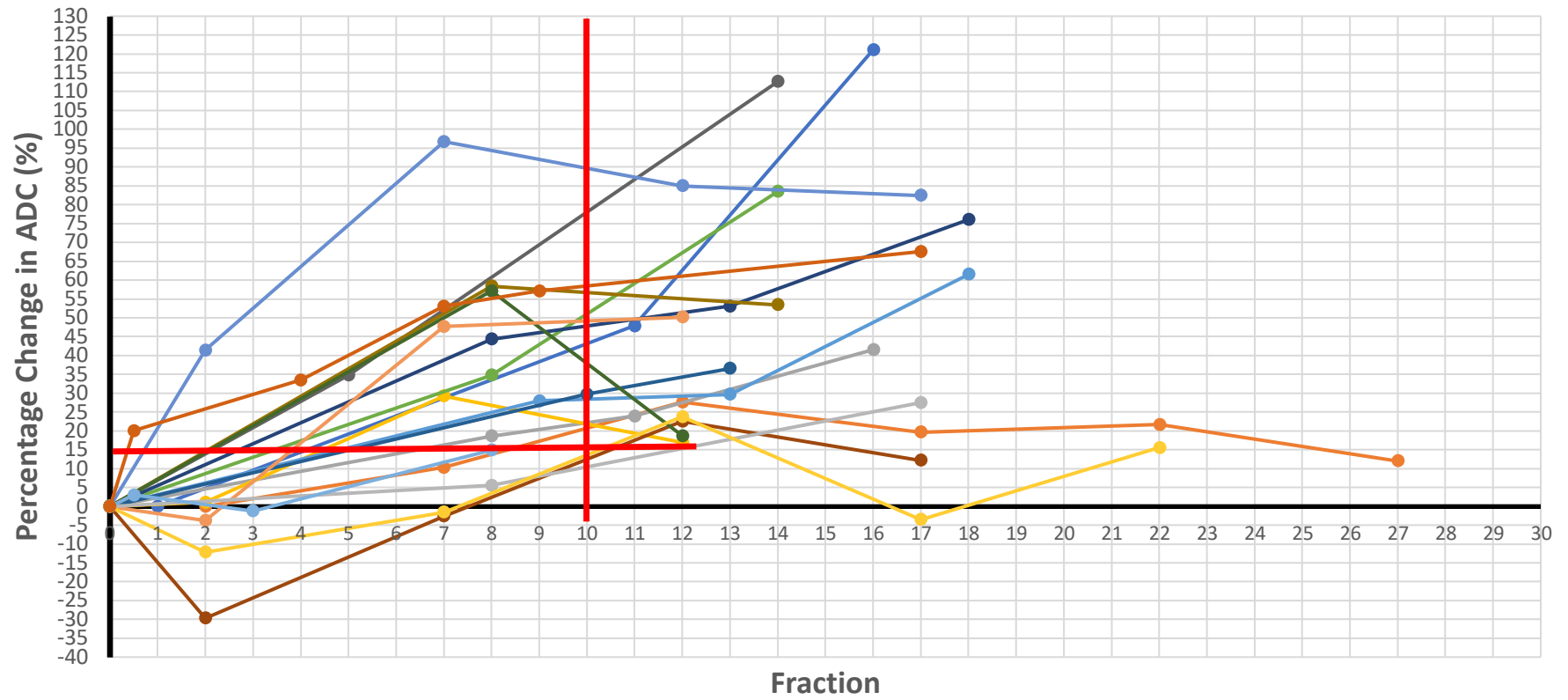
2.4.2.2 MR-Linac

Individual-level ADC data for MR-Linac DWIs are provided in Appendix D, however, the data are summarised in Figures 2-3a+b. The red threshold lines in Figure 2-3 denote the 15% ADC threshold as used on the diagnostic-MRI scanner and the 10th fraction, which marks the end of week 2 of radiotherapy. Trend lines immediately entering the lower-right quadrant around the intersecting red thresholds are highlighted as potentially non-responding tumours.

“mrI” was the only patient found to have residual disease in both the primary and lymph node sites. Percentage change ADC data show that for this patient, her primary lesion Δ ADC was $>15\%$, but lymph node lesion Δ ADC was $<15\%$. Primary lesions for patients “mrH, mrO and mrP” had Δ ADC $<15\%$ by the 10th fraction yet they have all had complete metabolic responses on post-treatment PET/CT.

a)

Percentage change in ADC (Primary Tumour)



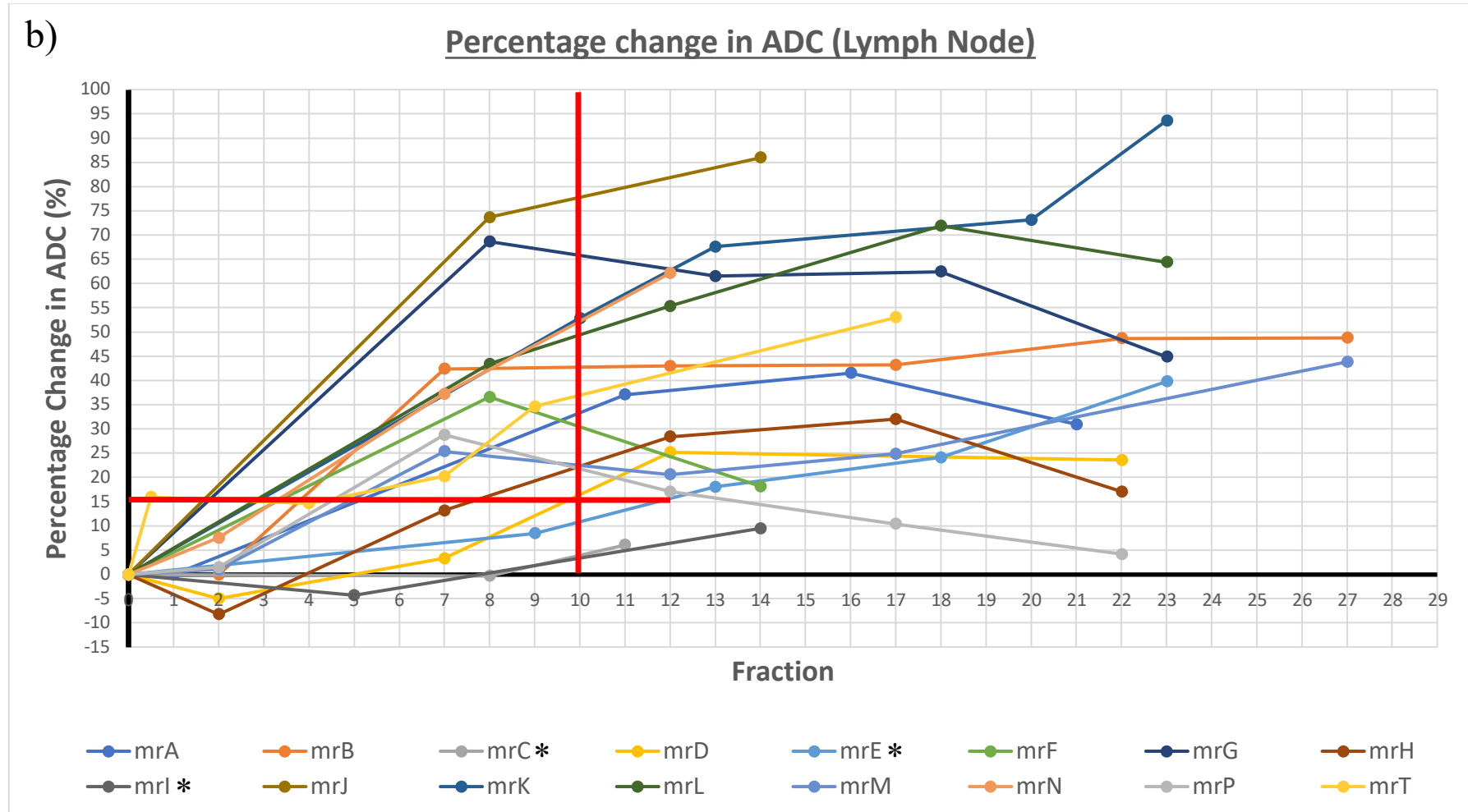


Figure 2-3, Percentage ADC changes for Primary and Lymph Node disease.

Percentage ADC changes are shown for a) primary tumours and b) lymph node disease. Red lines denote the ADC threshold of 15% change at 10 fractions (2 weeks) into treatment to distinguish those patients who would have been deemed non-responders based on diagnostic-MR ssEPI DWI-MRI criteria. The relevant non-responding patients have been highlighted in the corresponding legends (*).

2.4.3 DWI-MRI Sequence Agreements

2.4.3.1 Diagnostic DW-MRI

Correlations between the percentage changes in ssEPI and RESOLVE parameters were initially assessed to confirm linear relationships (raw ADC data are in Appendix C). Figures 2-4a+b show scatter plots to display these trends for the primary and lymph node targets, respectively. Table 2-3 shows the Pearson's correlation coefficients.

For the primary tumour, correlation was significantly strong at baseline ($p < 0.01$) but lost this strength at the week 2 and 4 time points. For the involved lymph node, correlation remained consistently and significantly strong at each time point. The percentage change in ADC was measured between "baseline vs week 2" and "baseline vs week 4," for both ssEPI and RESOLVE DWIs. The correlations between ssEPI and RESOLVE were significantly strong for percentage changes at week 2 and 4 ($p < 0.05$) and it is these values of percentage change that are used for the following Bland-Altman analyses.

The agreement between values of percentage change (for baseline vs week 2 or 4) were assessed using Bland-Altman analyses (Table 2-4 and Figures 2-5). For all Bland-Altman plots, the differences of the means for the primary and lymph node tumours are small and close to zero, with confidence intervals overlapping zero. For the differences in percentage change in ADCs of the primary tumours at week 2, there is good agreement between ssEPI and RESOLVE. However, there is proportional bias between the difference of the means as linear regression analysis shows a significant positive correlative relationship ($p < 0.05$). The differences in percentage change between ssEPI and RESOLVE for primary tumour at week 4 are statistically significant and different from zero, so there is disagreement between the two methods at this time point ($p < 0.05$, 95% CI of the mean difference 0.86-15.1). Therefore, Bland-Altman analysis was not performed for the week 4 time point.

For lymph nodes, Bland-Altman analyses show good agreement between ssEPI and RESOLVE at both week 2 and 4 time points, with no proportional biases measured. Coefficients of variation and limits of agreement had wide values for all three Bland-Altman plots.

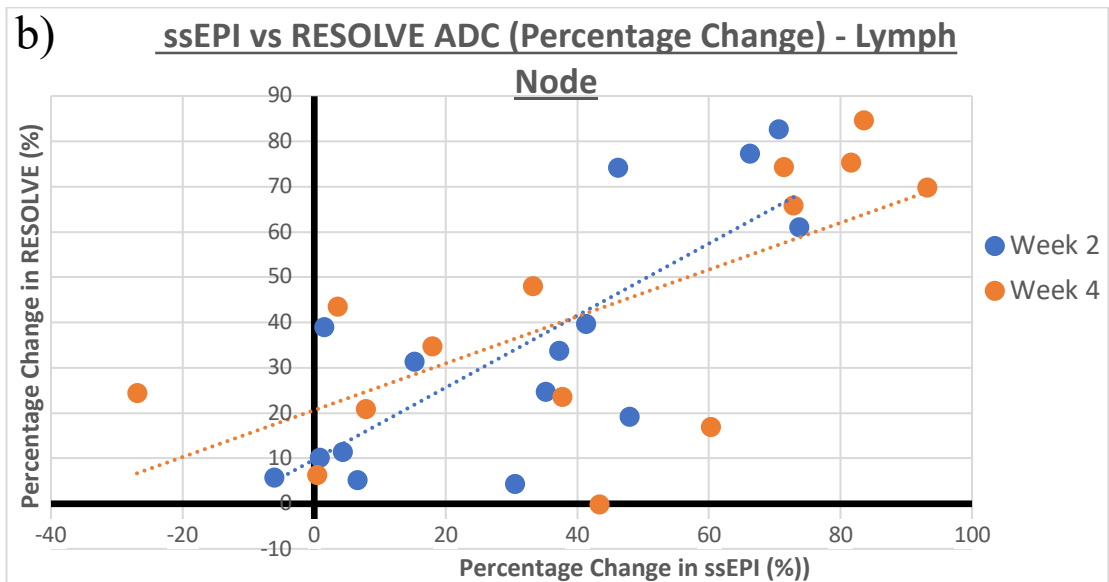
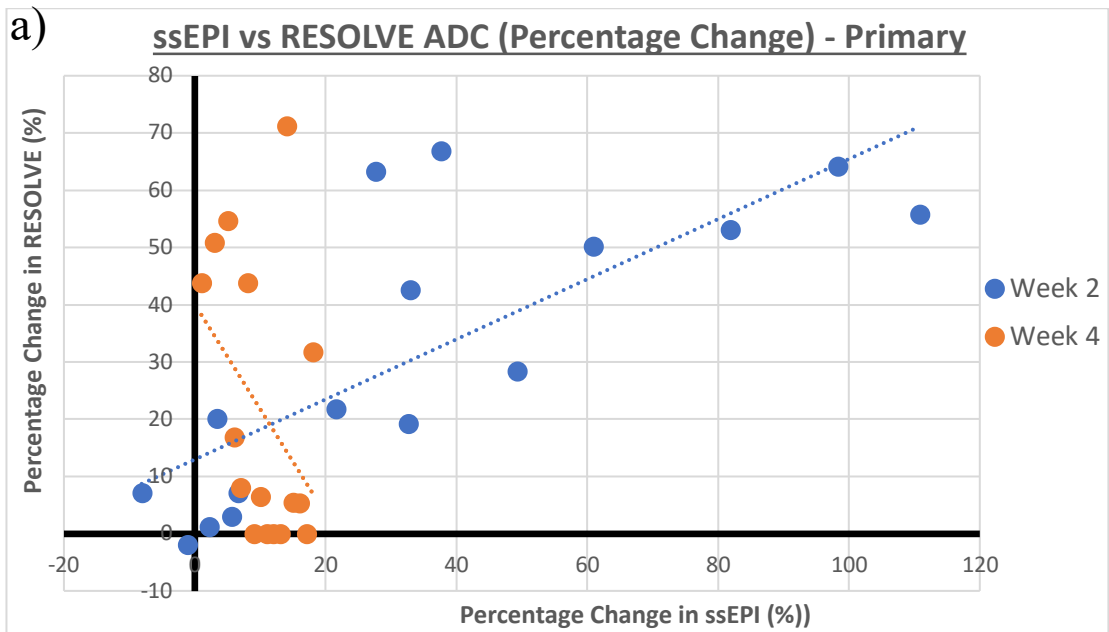


Figure 2-4, ssEPI vs. RESOLVE ADCs for Primary and Lymph Node disease.
Correlations between percentage change in ssEPI and RESOLVE ADC are displayed for a) primary and b) lymph node targets.

Pearson's Correlation Coefficients (p-value)					
	Baseline	Week 2	Week 4	% Change Week 2	% Change Week 4
Primary	0.85 (<0.01)	0.21 (0.44)	0.57 (0.07)	0.77 (<0.01)	0.95 (<0.01)
Lymph Node	0.82 (<0.01)	0.87 (<0.01)	0.73 (<0.01)	0.77 (<0.01)	0.69 (<0.01)

Table 2-3, Pearson's Correlation Coefficients for ssEPI vs RESOLVE ADC.
Pearson's correlation coefficients are presented for the raw ADC values with corresponding p-values. Percentage change values for baseline-week 2 and baseline-week 4 are also shown.

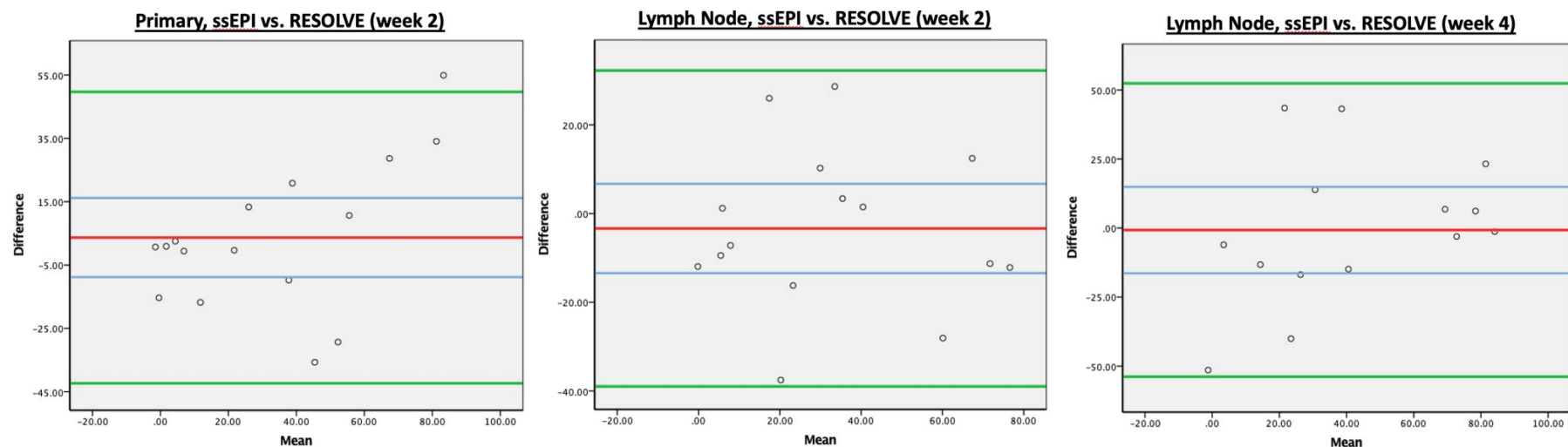


Figure 2-5, Bland-Altman Plots for Primary and Lymph Node Tumours.

The percentage change in ADC ($\times 10^{-3}$) was measured for baseline vs week 2 and baseline vs week 4 time points. The differences in these changes for each patient are plotted against the means of each pair of ADC values. Red line denotes the mean of the differences with the 95% confidence interval of this mean in blue, (calculation described by Giavarina D, (9)). Green lines denote limits of agreement (i.e. $\pm 1.96 \times$ standard deviations). Graphs are shown for the primary tumour (at week 2) and lymph nodes (at weeks 2 and 4).

ADC (Time point)	Mean	Standard Deviation	Coefficient of Variation (%)	Limits of Agreement
Primary (week 2)	3.68	23.47	638.31	-42.32 – 49.67
Lymph Node (week 2)	-3.36	18.18	-541	-38.98 – 32.26
Lymph Node (week 4)	-0.72	27.1	-3752.46	-53.84 – 52.39

Table 2-4, Bland-Altman data.

The data shown are for the corresponding Bland-Altman charts in Figure 2-5. Mean, standard deviation and limits of agreement numbers refer to percentage changed in ADC values.

2.4.3.2 MR-Linac DWI Repeatability

Seven patients had double-baseline DW-MRIs on the MR-Linac. Four of these patients had lymph node disease. Primary lesion (Pearson’s method, $r = 0.77$, $p < 0.05$) and lymph node (Spearman method, $r = 0.99$, $p < 0.01$) correlation analyses between ADC values show significantly strong relationships, (Figure 2-6). Patients “mrV and mrW” were outliers with ADC differences between 32-38%. Bland-Altman analysis of the primary tumour only reveals good agreement but with wide limits of agreement ($-569.4 - 421.9 \text{ mm}^2\text{s}^{-1}$) and a coefficient of variation of 342.9% (Figure 2-7). There were not enough patients with lymph node disease for a similar analysis.

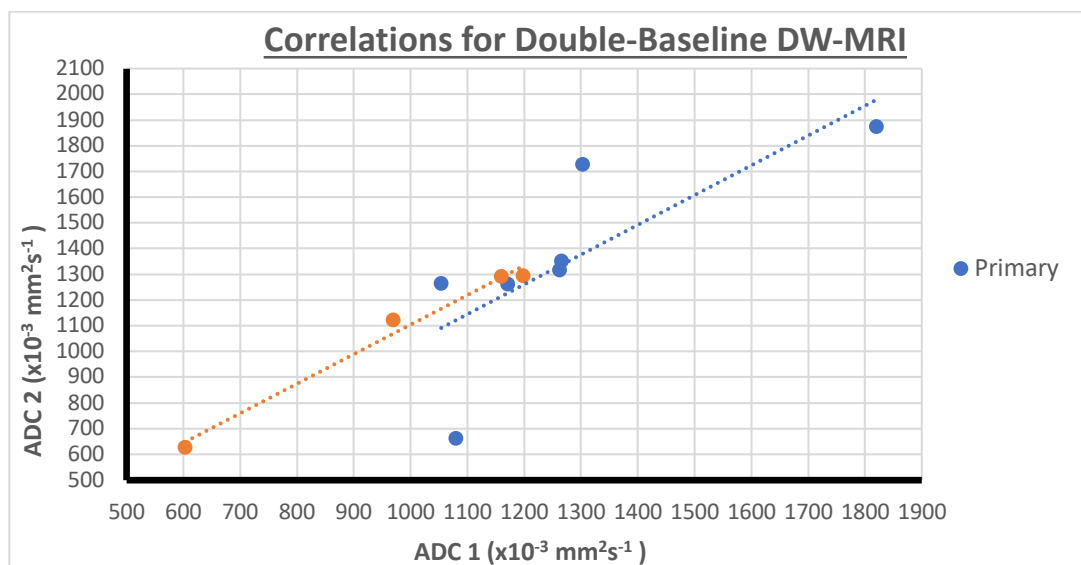


Figure 2-6, Correlation Analyses for Double-Baseline DW-MRIs on MR-Linac. Correlations between ADC values are displayed for both primary and lymph-node lesions that had two DW-MRIs 1 day apart.

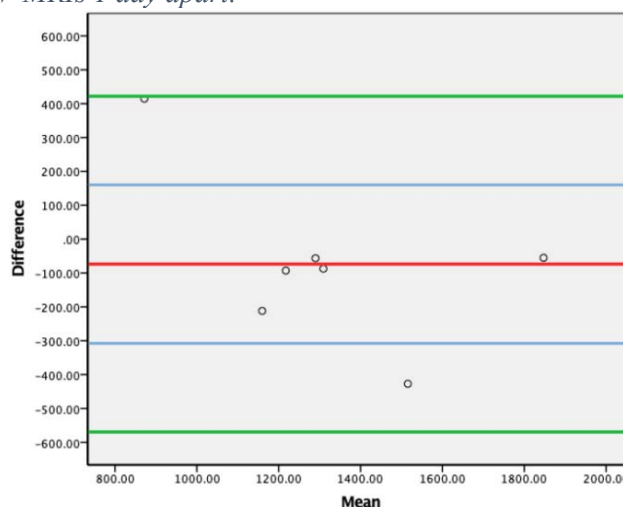


Figure 2-7, Bland-Altman Plot for MR-Linac ADC Repeatability ($\times 10^{-3} \text{ mm}^2\text{s}^{-1}$). Red line denotes the mean of the differences with the 95% confidence interval of this mean in blue ($-307.6 - 160.1 \text{ mm}^2\text{s}^{-1}$). Green lines denote limits of agreement (i.e. $\pm 1.96 \times$ standard deviations).

2.4.4 MRI-Guided Adaptive Planning

2.4.4.1 Target Volume Adaptation

Data from 14 patients are available who had non-dose escalated plans created (Figure 2-8). Standard deviations for each bar are tabulated and shown separately due to large variation (Table 2-5). Absolute dose difference data are shown in Appendix E.

For all high-dose PTV targets, there were statistically significant lower doses delivered with ART compared than non-adapted RT plans. No statistically significant differences in doses were found for any of the OARs or elective nodal targets, including the ipsilateral parotid glands. There were high degrees of variation with large standard deviations of dose differences for the OARs.

Patients had weekly body weights recorded during on-treatment follow up. Patients lost a mean weight of 7.31 kg (9.0%) between baseline and week 6 of treatment. Mean depth of external contour change at week 4 (latest measurable time point) was 9.6 mm, (measured in the left-right direction, at the level of the anterior/inferior border of the C1-vertebral body). There was a poor correlation ($r = 0.21$, $p\text{-value} > 0.05$) between degree of weight loss and change in patient depth (Figure 2-9).

There was a statistically significant reduction in parotid gland volumes in both ipsilateral (mean 4.35 ml (15.6%), SD 2.4 (5%)) and contralateral (mean 3.68 ml (13.3%), SD 3.3 (9.1%)) parotids ($p\text{-value} < 0.01$). The loss in parotid volumes did not correlate with changes in patient weight or depth.

2.4.4.2 Dose Escalation

Three patients (“mB, mG and mH”) had dose-escalated plans generated and delivered (Figure 2-10, raw data in Appendix F). The trends show a decrease in ipsilateral parotid and increase in contralateral parotid gland doses, but merged parotid data show no differences between adapted and non-adapted plans. Primary PTV doses are higher with dose-escalated plans, as expected, but dose constraints to critical OARs such as spinal cord and brainstem were within the set constraints. Only two patients had involved nodal disease and the related data are not shown. The difference in elective nodal dose was negligible.

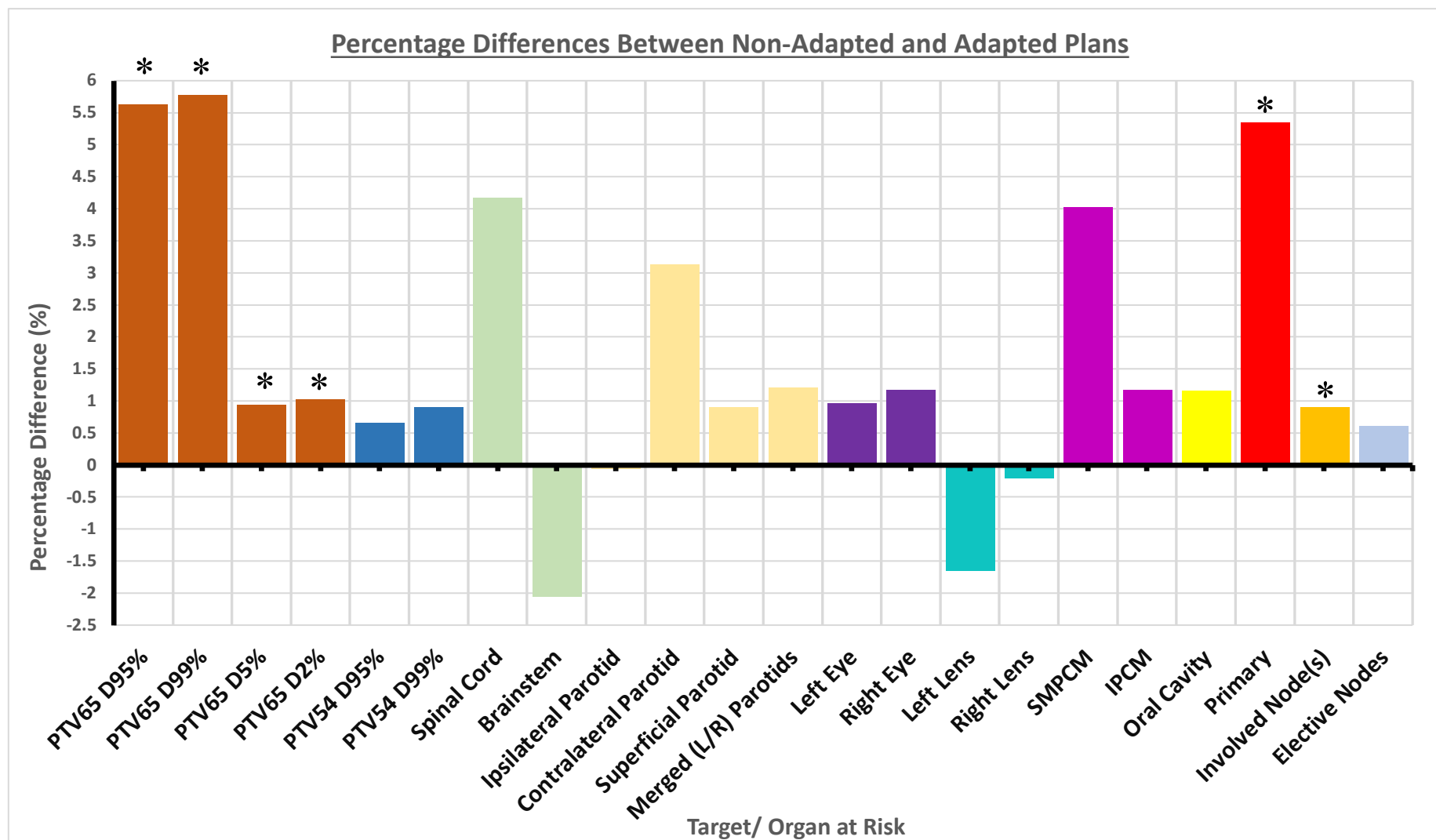


Figure 2-8, Percentage Dose Difference between Adapted and Non-Adapted Radiotherapy Plans.

Dose differences are displayed for relevant structures. Positive value denotes x% higher dose on a non-adapted plan. Data for primary, involved lymph nodes and elective nodes are also shown separately. Significant differences are highlighted (*). SMPCM-Superior/Middle pharyngeal constrictor muscle; IPCM-Inferior pharyngeal constrictor muscle.

Target/Organ at Risk	Mean Dose Difference (Gy) (Percentage Differences(%))	Standard Deviations (Gy)	p-values
PTV 65 D95%	3.57 (5.63)	1.88	<0.0023*
PTV 65 D99%	3.59 (5.78)	1.62	<0.0023*
PTV 65 D5%	0.63 (0.94)	0.25	<0.0023*
PTV 65 D2%	0.68 (1.02)	0.27	<0.0023*
PTV 54 D95%	0.35 (0.66)	1.08	0.23
PTV 54 D99%	0.48 (0.91)	2.67	0.55
Spinal Cord	1.7 (4.17)	1.7	0.19
Brainstem	0.15 (-2.05)	4.18	0.96
Ipsilateral Parotid	0.15 (-0.05)	1.52	0.93
Contralateral Parotid	0.38 (3.13)	0.66	0.83
Superficial Parotid	0.19 (0.9)	0.72	0.89
Merged Whole Parotids	0.27 (1.21)	0.69	0.84
Left Eye	0.05 (0.97)	0.15	0.91
Right Eye	0.07 (1.17)	0.22	0.87
Left Lens	-0.02 (-1.65)	0.06	0.92
Right Lens	0.01 (-0.21)	0.1	0.95
SMPCM	2.13 (4.02)	1.85	0.2
IPCM	0.47 (1.17)	1.96	0.77
Oral Cavity	0.62 (1.17)	1.58	0.77
Primary Tumour	3.44 (5.35)	2.11	<0.0023*
Involved Node(s)	0.59 (0.9)	0.52	<0.0023*
Elective Nodes	0.33 (0.61)	0.39	0.017

Table 2-5, Mean Percentage Differences and Corresponding Standard Deviations.

Data are shown for Figure 2-8, with standard deviations included. Statistically significant results are highlighted ().*

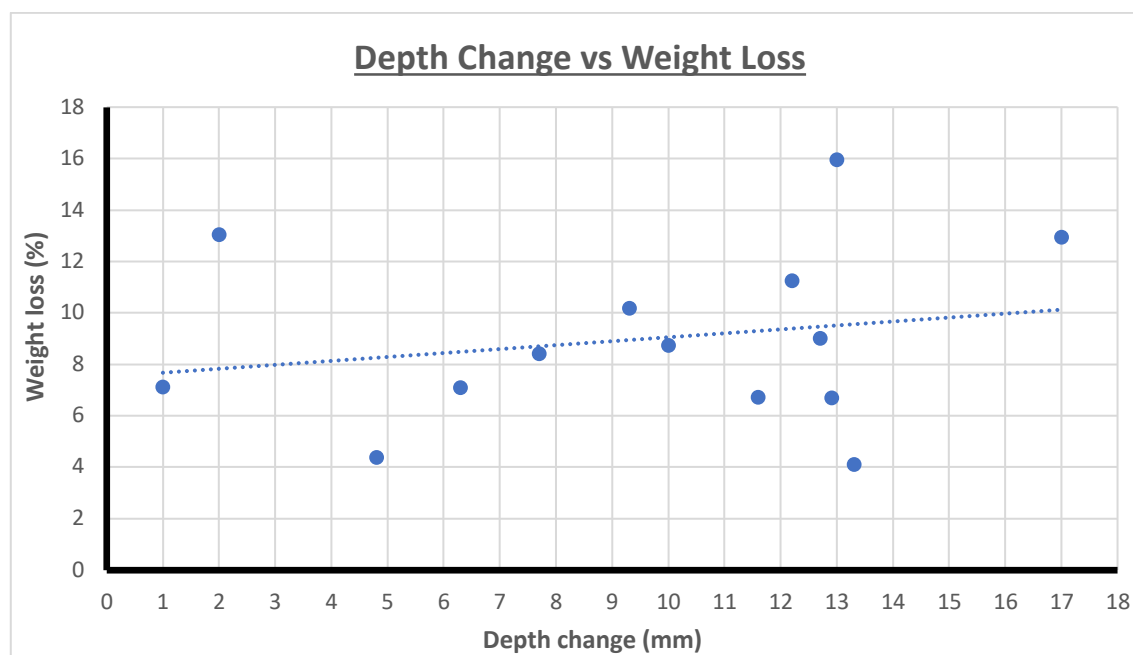


Figure 2-9, Correlation Between Depth Change (mm) and Weight Loss (%).

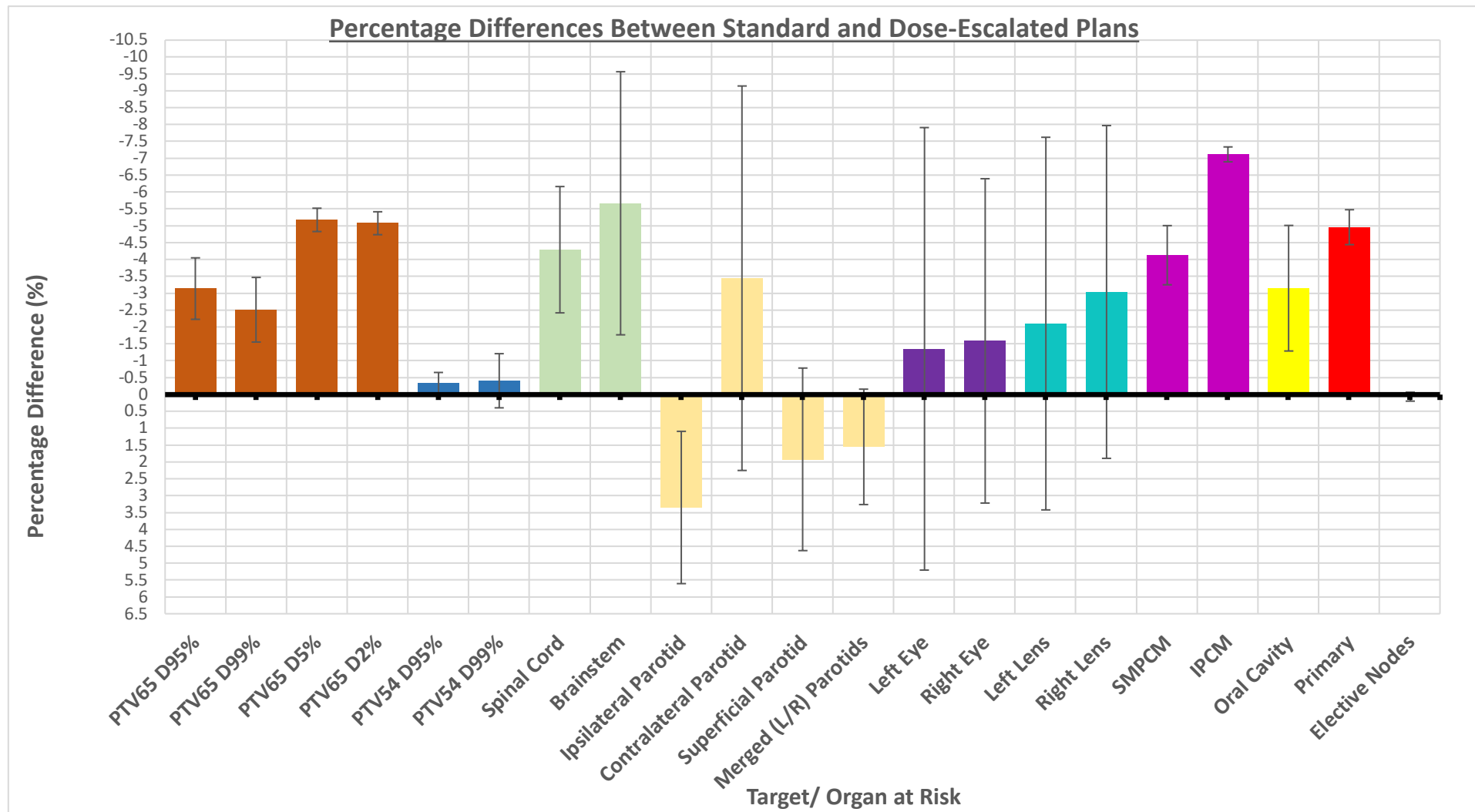


Figure 2-10, Percentage Dose Difference between Standard and Dose-Escalated Radiotherapy Plans.

Dose differences are displayed for relevant structures. Positive value denotes x% higher dose on the standard plan. Data for primary, involved lymph nodes and elective nodes are also shown separately. Error bars denote standard error of the means. **NOTE: y-axis reversed for ease of interpretation.** SMPCM-Superior/Middle pharyngeal constrictor muscle; IPCM-Inferior pharyngeal constrictor muscle.

2.5 Discussion

2.5.1 Diagnostic-MR and MR-Linac DWI/ADC

2.5.1.1 Diagnostic MRI and INSIGHT II DWI

The data presented in this chapter show that the raw ADC values are markedly different between ssEPI and RESOLVE sequences, as demonstrated in Figure 2-4. However, the magnitudes of percentage change observed, when compared to the baseline ADC values, can be deemed to be correlated according to the Bland-Altman analyses. This is based on the strong positive correlations shown between both DWI sequences for both primary and lymph node disease. It is for this reason that percentage change values were used for subsequent Bland-Altman analyses, rather than raw ADC, as they ought to be more consistent and comparable between studies. When applying the 15% threshold to determine a primary tumour responder from a non-responder, there was only one discrepancy between ssEPI and RESOLVE.

However, when assessing for agreement between the DWI sequences, there was significant proportional bias for the primary tumour, suggesting that the agreement between the two parameters may not be as strong at higher values. This is also evidenced by the wide limits of agreement and large coefficient of variation. Although the agreements for lymph node changes were better, the coefficients of variation were just as large.

This can be, partly, attributed to the limited sample size, but also the fact that there is marked image distortion in the ssEPI sequence. These distortions lead to difficulties, and inconsistencies, in head and neck tumour delineation. This is particularly apparent around air-soft tissue interfaces, where most HNCs are situated. RESOLVE image quality is more consistent and accurate for patient anatomy. This may also explain the loss of correlation between ssEPI and RESOLVE for primary tumours in the 4th week, as responding tumours were more difficult to identify and distinguish from surrounding oedema/normal tissue.

When the previously determined threshold of a change in ADC <15% is applied at the week-2 time point, there were only two instances where there was disagreement

between ssEPI and RESOLVE sequences. For non-RESOLVE DWI sequences, the sensitivity and specificity for a change in ADC threshold of 15.5-25% are reported to be between 75-100% and 69-95%, respectively (3,10,11). The original INSIGHT study calculates an optimal threshold change in ssEPI ADC of 17%, with a sensitivity and specificity of 100% and 86%, respectively (2). The INSIGHT II study applied a 15% threshold to distinguish responders from non-responders, which was a more conservative threshold to avoid overestimation of patients as non-responders.

It was not possible to validate the ssEPI or RESOLVE sequences using the current cohort, as there were no patients with residual/recurrent disease. Therefore, regression analyses or receiver operating characteristic curves could not be generated. With the initiation of the main-phase of the INSIGHT II study, there is now clinical intervention being applied in response to Δ ADC <15% for intermediate-/high-risk disease (in the form of dose escalation), which may have already affected the treatment outcomes for the 3 patients that were designated non-responders in this project.

2.5.1.2 MR-Linac DWI

Data from patients scanned on the MR-Linac could not be compared against the diagnostic scanner because the patient population was different. The scanning time points on the MR-Linac were also inconsistent between patients as the machine was not as readily available as the diagnostic scanner. However, three patients were identified with both primary and lymph node tumours that would have been deemed non-responders when applying the diagnostic-MR ssEPI criteria of Δ ADC <15%. Despite this, none of these patients had residual disease on their post-treatment PET/CTs. In fact, the one patient who had residual disease in the primary tumour would have been deemed a responder based on the week 2 Δ ADC.

This project also aimed to evaluate the repeatability of DWI measurements on the MR-Linac platform, which has previously been investigated by Habrich J et al (12). Their study protocol was different in that they scanned patients on two occasions, 10 minutes apart, before and during/after patients receiving radiotherapy, performed twice a week

throughout treatment. They analysed the consistency of ADC readings of various head and neck structures, including tumour and OARs. Their repeatability coefficient was 31.3% and 23.5% for the GTV and lymph node, respectively. However, it is not clear how immediate and/or confounding the effects of radiation were on DWI values within their patient group.

The difference in this project is that all patients had their repeat DWIs before exposure to radiation and each scan was 24 hours apart, which could have allowed physiological/intra-tumour changes to occur. The data show a strong correlation between both ADC readings. However, the wide limits of agreement and coefficient of variation may be attributed to two outliers who had markedly different ADCs. Diffusion depends on water content and can be affected by vascularity, as described by the IVIM concept discussed in the next chapter. It is also possible that in the 24 hours between scans, there have been perfusion-related changes occurring that alter the diffusivity of water within tissue.

The MR-Linac also uses ssEPI-type parameters to acquire images and its images are, therefore, prone to the similar issues related to anatomical distortion around air-soft tissue interfaces. Inconsistent contouring and mis-registration between scans may also have influenced the accuracy of readings, but it is unlikely that this explains differences of up to 38% as seen in this dataset.

Shukla-Dave et al, members of the “Quantitative Imaging Biomarkers Alliance (QIBA),” describe the importance of establishing the variability of measurements within any imaging modality prior to investigating longitudinal changes and treatment effects (13). Measuring the repeatability coefficient by establishing within-subject standard deviations allows one to determine how much difference is required before a change can be interpreted as significant, and the number of publications on “test-retest” of such metrics are limited.

Based on the QIBA recommendations, (which were originally written for diagnostic-MR systems), McDonald et al also investigated DWI repeatability on their Elekta Unity MR-Linac system in ten patients (14). In addition to the standardised Elekta-approved ssEPI sequence, they investigated other DWI sequences such as SPLICE, BLADE and

RESOLVE. Each participant in their study (patients and volunteers) underwent two repeat scans per imaging session (with a 10-minute gap between scans), for 2 sessions with a mean 8-day gap between sessions. They found that the within-subject coefficient of variation was greater for tumour and lymph nodes than for parotid glands, with statistically significant proportional biases for all MR-Linac DWI sequences except for BLADE and RESOLVE. A similar interrogation of phantom models shows that ADC values vary substantially for models that have a static diffusivity value.

McDonald et al suggested that these differences in ADC measurements result from the split-coil design of the MR-Linac, that may result in eddy currents that affect the homogeneity of the magnetic field. Kooreman et al further explained that the time delay between application of the different gradients (b-values) can impact the signal-to-noise ratio and create variations in ADC values (15). This effect occurs because a longer time between application of different b-values, (termed the “gradient-change time”), allows water within structured tissues to reach the boundaries of diffusion, particularly in a restricted environment. For this reason, the gradient-change time should remain as short as possible. However, the gradient strength is lower and slew rates used on the Elekta Unity system are longer than that on diagnostic-MR systems, with the resultant effect being longer gradient-change times and a worsened signal-to-noise ratio.

Another factor that may affect comparability between studies is target definition methods. In this project, the whole primary tumour was outlined by me, with difficult cases checked by a consultant clinical oncologist or a consultant radiologist. However, it is well established that target delineation, whether on T1/T2-weighted imaging or DWI, varies within/between oncologists and radiologists, with a significant number of target alterations being made during peer review (16,17). Although, it was decided to include necrotic regions within the primary target definition on DWI, it is not known how the presence of necrosis affects the interpretation and comparability of mean ADC between studies.

In this context, the repeatability results seen in this study fit with the patterns described elsewhere, including phantom only studies (18,19). However, the limited

within-subject measurements performed have likely affected the precision of the results. A dedicated study with more scanning time points would be required to scan patients on more sessions. Similarly, for the reasons just discussed, the longitudinal MR-Linac DWI changes seen in this project would need to be re-examined once the variability of measurements has been established, to determine how much of the observed change can be deemed biologically significant.

2.5.2 Adaptive Radiotherapy Planning

For low-risk or intermediate-/high-risk tumours that are responding, adjusting GTV/CTV volumes at two time-points is a feasible strategy and no instances of residual disease were seen on the 3-month post-treatment PET/CTs.

2.5.2.1 Weight loss

Patient depth change of ≥ 1 cm generally results in increased dose to more central structures, with particular concern about the spinal cord (20). Mean weight loss across the cohort in this study was 7.3 kg (SD 3.1 kg), with a resultant mean depth change of 9.6 mm (SD 4.6 mm). The lack of correlation observed between weight loss and depth change could be explained by the fact that patients may lose weight in different positions and measuring changes in depth at the same anatomical levels across all patients may miss larger degrees of change in depth more inferiorly.

Another caveat was that the maximum weight loss was recorded between the start and sixth week of treatment, but the maximum depth change was measured on the week-4 CT scan at fraction 18. Toxicities and its resultant impact on the nutritional state progressively worsens and reaches a peak towards the end of radiotherapy, where any reduction in patient thickness is also at its maximum. The lack of correlation noted, therefore, may be confounded by this issue and there may be a direct relationship between the two parameters, as demonstrated by Ahn et al (21).

2.5.2.2 Primary and Lymph Node Targets

After target adaptations, the doses to the primary target PTVs were significantly reduced, with a mean primary tumour D95% of 59.7 Gy (SD 1.7 Gy). The mean D95% to the primary target, when the baseline plan was applied to the week-2 and -4 CT scans

(cumulative and non-adapted plan) was 63.27 Gy (SD 0.58 Gy). This equates to a mean primary dose reduction of 3.44 Gy. Studies looking at a dose de-escalation approach for low-risk tumours explore doses as low as 60 Gy in 25 fractions (22) or 50 Gy in 25 fractions in the adjuvant setting (23). The dose reductions in this study are modest by comparison. However, this is a consequence of the fact that a minimum of 1.8 Gy per fraction was still delivered to any region defined as tumour at baseline, even if gross tumour was no longer being seen on subsequent anatomical imaging. This conservative approach to dose reduction was adopted as it is described that tumour does not shrink towards a central core, but in fact there are microscopic tumour colonies likely still present within the original perimeter of tumour (24). The typical dose fall-off distances in VMAT plans would still cover these peripheral regions with adequate microscopic doses, but local recurrence patterns would need to be examined before complete omission of this mandatory 1.8 Gy per fraction coverage could be considered.

Weight loss and depth-related changes have previously been described to result in increased dose to the primary target in HNC and other central tumours such as prostate cancer, with varying magnitudes of dose difference up to 6% (25–28). However, cumulative dosimetric analyses suggest conflicting outcomes for HNCs (29).

All primary tumours in this study arose from largely central structures, but there were no significant differences in doses between baseline plans and cumulative non-adapted plans (i.e. the dose that would have been delivered when the baseline plan accounts for evolving anatomies at weeks 2 and 4). Some tumours in this cohort were exophytic in nature. With progressive radiotherapy-related response, areas of soft tissue may have become air space, where there is no dose deposition, resulting in compensatory and artificial decreases in dose within the baseline primary target volume. Final primary target dose reporting was also based on all dose cubes being accumulated onto the baseline-CT scan. Any resolving tumour that is now air space or altered anatomy may compensate for weight loss-related dose increases.

2.5.2.3 Spinal Cord

The mean maximum spinal cord dose in the baseline plans was 38.4 Gy (SD 3.6 Gy). When the actual dose delivered is calculated with the baseline plan applied to patient anatomies on the weeks-2 and 4 CT scans, the mean maximum spinal cord dose was measured as 38.9 Gy (SD 3.5 Gy). There was a trend for a reduction in maximum spinal cord dose to 37.2 Gy (SD 3. Gy) when adapting dose to responding primary targets and contour changes, however, these findings were not statistically significant due to the variability between patients. These findings were of a similar pattern for the brainstem.

The increase in spinal cord dose without dose adaptation was expected, but modest, based on the average magnitudes of weight loss and depth differences that were observed. When analysing individual-level data, patient “mA” had the greatest depth loss of 13 mm and weight loss of 15.2 kg, with an increase from a baseline plan maximum spinal cord dose of 42.17 Gy to 42.38 Gy with cumulative non-adapted plans. For this patient, adapting primary target volumes resulted in an adapted maximum spinal cord dose of 40.91 Gy, which is lower than the planned baseline dose.

Comparisons between similar studies are difficult because different descriptions of dose or targets were utilised. For example, Noble et al utilised deformably-registered daily image-guidance scans in 113 patients having radical radiotherapy for HNC (28). Castadot et al re-scanned patients at four separate time points but additionally utilised auto-contouring software to delineate targets, as well as applying a PRV border to the spinal cord before recording dose (30). Bhide et al performed repeat planning-CT scans at 5 time points and analysed the spinal cord without a PRV (31). Despite the differences, all these studies demonstrate progressively increasing mean maximum dose being delivered to the spinal cord when no adaptations are applied.

Interestingly, Castadot et al also analysed spinal cord dose with and without the PRV and report significantly increased dose for the PRV structure only (30). This may occur in situations where the TPS optimises for PRV structures and attains a homogenous dose to the spinal cord, with steep dose fall off within the PRV boundary, providing a buffer to the non-PRV spinal cord structure against reductions in photon path length secondary to weight loss. This finding was echoed by Noble et al (28).

2.5.2.4 Parotid Glands

Significant reductions in the volume of both ipsilateral and contralateral parotid glands did not result in any statistically significant difference in parotid doses between baseline plans and the cumulative non-adaptive plans, despite the reductions in patient thickness at the level of the parotids. Dose-adapted plans showed a trend for modest reduction in parotid glands, with greater reduction for the contralateral parotid. The lack of significant impact on parotid gland dose was unexpected but has been demonstrated in a very limited number of other studies.

Raghavan et al analysed change in parotid volumes and subsequent impact on dose in just six patients (32). Despite a mean parotid volume loss of 38.7%, there were no differences in parotid dose between planned and truly delivered scenarios. The primary tumour sites varied greatly and four patients had oropharyngeal SCCs. The contradictory outcomes of the impact of anatomical changes on parotid gland dosimetry likely arise from the variability in parotid volume and the limited patient numbers in individual studies (33).

Bhide et al showed a 2.7 Gy increase to the ipsilateral parotid gland in the 4th week of radiotherapy because of the significant medial shift and reduced volume of the gland, although doses remained within parotid tolerance (31). However, this was not a cumulative value and did not consider dose delivered in prior fractions. A dose-accumulation study by Lee et al showed that 3 patients (30%) saw an increase in the parotid dose by a mean 11% (34). The 3 patients had the greatest amount of weight loss and they had oropharyngeal cancers, where medialisation of the parotid glands could have occurred into areas where there is usually steep dose fall-off as optimisation protocols attempt to spare parotid glands as much as possible.

Castelli et al estimated that for a dose prescription at 70 Gy in 35 fractions, a reduction in 1 cm³ of the CTV₇₀ or a reduction in neck thickness of 1mm would lead to a 0.3 Gy increase in dose to the parotid glands (35). They applied a more aggressive approach to adaptive radiotherapy, where in the event of a complete primary tumour response, primary target delineations did not maintain a minimum dose to the periphery of the baseline tumour, resulting in lower “splash” dose to parotid glands. With this once-

weekly replanning method they noted a mean dose reduction to the parotid glands of 4 Gy, which was estimated to decrease the risk of xerostomia by 3% based on their NTCP model.

The dose differences seen in this study are very modest in comparison to the majority of literature that is published including the studies mentioned. However, one potential reason for the small differences in parotid doses seen in this study, as for the primary tumours described earlier, is the way the dose was accumulated and reported. Dose accumulations occurred at the week 2 and 4 time points, however, dose cubes were then imported back on to the baseline planning-CT scan. The baseline parotid gland volumes were used to report the non-adapted and adapted plan doses. From baseline to the week 4 CT, there were mean parotid volume decreases of 4.1 and 4.3 cm³ for the left and right glands, respectively. If an increase in dose had truly occurred without plan adaptation at later time-points in treatment (as described by Bhide et al (31)), the effect may have been diluted by displaying this dosimetry on the baseline parotid volumes, as superficial lobes on baseline volumes may have consistently received a lower overall dose. This effect could perhaps be mitigated by reporting dose to superficial and deep parotid lobes separately or comparing the differences in dose reporting between dose accumulations on the baseline versus the week-4 CT scans.

2.5.2.5 Pharyngeal Constrictor Muscles

With target volume adaptation, there were modest and non-significant dose reductions in the SMPCM (2.1 Gy) and IPCM (0.5 Gy). These are central structures and the SMPCM frequently overlapped or abutted the high-dose CTV. Therefore, the dose sparing effects on the PCMs were largely dependent on the rate of response in the primary tumour within the first two weeks. However, even if a total response in the primary tumour had occurred by the second week scan, the benefit from ART in this study may have been limited by the mandatory 1.8 Gy per fraction to voxels originally defined as tumour at baseline.

The INSIGHT II radiotherapy planning script on RayStation was originally developed before PCM sparing was incorporated into routine clinical practice. Once PCM sparing was introduced, the revised planning objective for SMPCM or IPCM specified a

mean dose < 50 or <20 Gy, respectively. The TPS did not attempt to reduce the dose beyond this objective and future work would aim to improve this planning script to further optimise PCM sparing.

2.6 Further work

Validation of the RESOLVE DWI sequence could not be performed due to lack of patients with residual disease after chemoradiotherapy, which would have allowed determination of an appropriate ADC threshold. Further recruitment of patients that are not receiving any trial intervention would be required, as in the original INSIGHT study, to help validate the RESOLVE DWI and ssEPI sequences on the diagnostic and MR-Linac scanners, respectively.

For the patients that completed their chemoradiotherapy, follow-up for this analysis ended at 3 months, when they had their post-treatment PET/CTs performed. Longer term follow-up would be required to assess for late locoregional recurrences, which could provide further information on the specificity of the ADC biomarker for determination of durable response to treatment.

Adaptive planning with a view to de-escalation of treatment was carried out with an intent to demonstrate clinically meaningful reductions to OARs. This project showed that, with the limited number of patients recruited, that dose changes to parotid glands and spinal cord were insignificant. The study assumed patient anatomy was static between scanning time points, which would not be the actual case. There was much variability between the degree of dose sparing to OARs and this is likely a result of the differences in tumour location and lymph-node involvement. Further work would require ongoing recruitment, where data analyses could be stratified for primary site and whether patients received bilateral or ipsilateral neck irradiation. This may allow identification of patient groups that are more likely to benefit from dose de-escalation.

Longer term follow-up would also allow analysis of recurrence patterns and locations that would perhaps allow adjustment or reduction of the dose to resolving tumour regions, where the currently modest dose reductions could be much greater and better at preserving OAR doses.

2.7 References

1. Welsh L, Panek R, McQuaid D, Dunlop A, Schmidt M, Riddell A, et al. Prospective, longitudinal, multi-modal functional imaging for radical chemo-IMRT treatment of locally advanced head and neck cancer: The INSIGHT study. *Radiation Oncology*. 2015 May 15;10(1).
2. Wong KH, Panek R, Dunlop A, Mcquaid D, Riddell A, Welsh LC, et al. Changes in multimodality functional imaging parameters early during chemoradiation predict treatment response in patients with locally advanced head and neck cancer. *Eur J Nucl Med Mol Imaging*. 2018 May 1;45(5):759–67.
3. Chung SR, Choi YJ, Suh CH, Lee JH, Baek JH. Diffusion-weighted magnetic resonance imaging for predicting response to chemoradiation therapy for head and neck squamous cell carcinoma: A systematic review. *Korean J Radiol*. 2019 Apr 1;20(4):649–61.
4. Ding Y, M Meheissen MA, Zhou K, R Mohamed AS, Wen Z, Ping Ng S, et al. Evaluation of different diffusion-weighted image techniques for head and neck radiation treatment: phantom and volunteer studies Corresponding Author. medRxiv [Internet]. 2022; Available from: <https://doi.org/10.1101/2022.03.22.22272705>
5. Ang KK, Harris J, Wheeler R, Weber R, Rosenthal DI, Nguyen-Tân PF, et al. Human Papillomavirus and Survival of Patients with Oropharyngeal Cancer. *New England Journal of Medicine*. 2010 Jul;363(1):24–35.
6. Petkar I, Rooney K, Roe JWG, Patterson JM, Bernstein D, Tyler JM, et al. DARS: A phase III randomised multicentre study of dysphagia- optimised intensitymodulated radiotherapy (Do-IMRT) versus standard intensity- modulated radiotherapy (S-IMRT) in head and neck cancer. *BMC Cancer*. 2016;16(1).
7. Westrand O, Svensson S. The ANACONDA algorithm for deformable image registration in radiotherapy. *Med Phys*. 2015 Jan 1;42(1):40–53.
8. Ng-Cheng-Hin B, Mcquaid D, Dunlop A, Court S, Petkar I, Nutting C, et al. Structure delineation using a deformable image registration-based contour propagation in HNC. *Radiotherapy and Oncology*. 2019;133(S654).
9. Giavarina D. Understanding Bland Altman analysis. *Biochem Med (Zagreb)*. 2015;25(2):141–51.
10. Kim S, Loevner L, Quon H, Sherman E, Weinstein G, Kilger A, et al. Diffusion-weighted magnetic resonance imaging for predicting and detecting early response to chemoradiation therapy of squamous cell carcinomas of the head and neck. *Clinical Cancer Research*. 2009 Feb 1;15(3):986–94.
11. King AD, Thoeny HC. Functional MRI for the prediction of treatment response in head and neck squamous cell carcinoma: Potential and limitations. *Cancer Imaging*. 2016 Aug 19;16(1).
12. Habrich J, Boeke S, Nachbar M, Nikolaou K, Schick F, Gani C, et al. Repeatability of diffusion-weighted magnetic resonance imaging in head and neck cancer at a 1.5 T MR-Linac. *Radiotherapy and Oncology*. 2022 Sep 1;174:141–8.
13. Shukla-Dave A, Obuchowski NA, Chenevert TL, Jambawalikar S, Schwartz LH, Malyarenko D, et al. Quantitative imaging biomarkers alliance (QIBA) recommendations for improved precision of DWI and DCE-MRI derived biomarkers in multicenter oncology trials. Vol. 49, *Journal of Magnetic Resonance Imaging*. John Wiley and Sons Inc.; 2019. p. e101–21.
14. McDonald B, Salzillo T, Mulder S, Ahmed S, Dresner A, Preston K, et al. In Vivo and Phantom Repeatability of Diffusion-Weighted MRI Sequences on 1.5T MRI Linear Accelerator (MR-Linac) and MR Simulator Devices for Head and Neck Cancers- Results from a Prospective R-IDEAL Stage 2a Evaluation of Tumor. medRxiv. 2022;

15. Kooreman ES, van Houdt PJ, Keesman R, Pos FJ, van Pelt VWJ, Nowee ME, et al. ADC measurements on the Unity MR-linac – A recommendation on behalf of the Elekta Unity MR-linac consortium. *Radiotherapy and Oncology*. 2020 Dec 1;153:106–13.
16. Njeh CF. Tumor delineation: The weakest link in the search for accuracy in radiotherapy. Vol. 33, *Journal of Medical Physics*. 2008.
17. Chiu K, Hoskin P, Gupta A, Butt R, Terparia S, Codd L, et al. The quantitative impact of joint peer review with a specialist radiologist in head and neck cancer radiotherapy planning. *British Journal of Radiology*. 2022;95(1130).
18. Thorwarth D, Ege M, Nachbar M, Mönnich D, Gani C, Zips D, et al. Quantitative magnetic resonance imaging on hybrid magnetic resonance linear accelerators: Perspective on technical and clinical validation. *Phys Imaging Radiat Oncol*. 2020 Oct 1;16:69–73.
19. Kooreman ES, van Houdt PJ, Nowee ME, van Pelt VWJ, Tijssen RHN, Paulson ES, et al. Feasibility and accuracy of quantitative imaging on a 1.5 T MR-linear accelerator. *Radiotherapy and Oncology*. 2019 Apr 1;133:156–62.
20. Belshaw L, Agnew CE, Irvine DM, Rooney KP, McGarry CK. Adaptive radiotherapy for head and neck cancer reduces the requirement for rescans during treatment due to spinal cord dose. *Radiation Oncology*. 2019 Nov 1;14(1).
21. Ahn PH, Chen CC, Ahn AI, Hong L, Sripes PG, Shen J, et al. Adaptive planning in intensity-modulated radiation therapy for head and neck cancers: Single-institution experience and clinical implications. *Int J Radiat Oncol Biol Phys*. 2011 Jul 1;80(3):677–85.
22. O’Sullivan B, Huang SH, Perez-Ordonez B, Massey C, Siu LL, Weinreb I, et al. Outcomes of HPV-related oropharyngeal cancer patients treated by radiotherapy alone using altered fractionation. *Radiotherapy and Oncology*. 2012 Apr;103(1):49–56.
23. Hargreaves S, Beasley M, Hurt C, Jones TM, Evans M. Deintensification of Adjuvant Treatment After Transoral Surgery in Patients With Human Papillomavirus-Positive Oropharyngeal Cancer: The Conception of the PATHOS Study and Its Development. Vol. 9, *Frontiers in Oncology*. Frontiers Media S.A.; 2019.
24. Rafat M, Ali R, Graves EE. Imaging radiation response in tumor and normal tissue [Internet]. Vol. 5, *Am J Nucl Med Mol Imaging*. 2015. Available from: www.ajnmml.us/ISSN:2160-8407/ajnmml0008827
25. Aly F, Miller AA, Jameson MG, Metcalfe PE. A prospective study of weekly intensity modulated radiation therapy plan adaptation for head and neck cancer: improved target coverage and organ at risk sparing. *Australas Phys Eng Sci Med*. 2019 Mar 15;42(1):43–51.
26. D’Souza H, Weatherburn H, Dwivedi A, Ganesh T. Volumetric arc therapy treatment plan dosimetry correction method to account patient weight loss during a course of radiation therapy. *J Med Phys*. 2020 Jan 1;45(1):1–6.
27. Stauch Z, Zoller W, Tedrick K, Walston S, Christ D, Hunzeker A, et al. An evaluation of adaptive planning by assessing the dosimetric impact of weight loss throughout the course of radiotherapy in bilateral treatment of head and neck cancer patients. *Medical Dosimetry*. 2020 Mar 1;45(1):52–9.
28. Noble DJ, Yeap PL, Seah SYK, Harrison K, Shelley LEA, Romanchikova M, et al. Anatomical change during radiotherapy for head and neck cancer, and its effect on delivered dose to the spinal cord. *Radiotherapy and Oncology*. 2019 Jan 1;130:32–8.
29. Height R, Khoo V, Lawford C, Cox J, Joon DL, Rolfo A, et al. The dosimetric consequences of anatomic changes in head and neck radiotherapy patients. *J Med Imaging Radiat Oncol*. 2010 Oct;54(5):497–504.

30. Castadot P, Geets X, Lee JA, Grégoire V. Adaptive functional image-guided IMRT in pharyngo-laryngeal squamous cell carcinoma: Is the gain in dose distribution worth the effort? *Radiotherapy and Oncology*. 2011 Dec;101(3):343–50.
31. Bhide SA, Davies M, Burke K, McNair HA, Hansen V, Barbachano Y, et al. Weekly Volume and Dosimetric Changes During Chemoradiotherapy With Intensity-Modulated Radiation Therapy for Head and Neck Cancer: A Prospective Observational Study. *Int J Radiat Oncol Biol Phys*. 2010 Apr;76(5):1360–8.
32. Raghavan G, Kishan AU, Cao M, Chen AM. Anatomic and dosimetric changes in patients with head and neck cancer treated with an integrated MRI-tri-60Co teletherapy device. *British Journal of Radiology*. 2016;89(1067).
33. Morgan HE, Sher DJ. Adaptive radiotherapy for head and neck cancer. *Cancers Head Neck* [Internet]. 2020 Dec 9;5(1):1. Available from: <https://cancersheadneck.biomedcentral.com/articles/10.1186/s41199-019-0046-z>
34. Lee C, Langen KM, Lu W, Haimerl J, Schnarr E, Ruchala KJ, et al. Assessment of Parotid Gland Dose Changes During Head and Neck Cancer Radiotherapy Using Daily Megavoltage Computed Tomography and Deformable Image Registration. *Int J Radiat Oncol Biol Phys*. 2008 Aug 1;71(5):1563–71.
35. Castelli J, Simon A, Louvel G, Henry O, Chajon E, Nassef M, et al. Impact of head and neck cancer adaptive radiotherapy to spare the parotid glands and decrease the risk of xerostomia. *Radiation Oncology*. 2015 Jan 9;10(1).

3 CHAPTER 3: NOVEL FUNCTIONAL MRI-BASED BIOMARKERS FOR HEAD AND NECK CANCER

3.1 Introduction

The tumour microenvironment is a complex matrix consisting of normal and tumour cells, vasculature and extracellular matrix, which is manipulated by cancerous cells during tumourigenesis (1). Tumour growth results in an imbalance between the supply and consumption of oxygen resulting in a constant state of hypoxia, the distribution and magnitude of which is constantly fluctuating (2). The Hypoxia Inducible Factor-1 response ultimately results in upregulation of a network of over 70 genes involved in oxygen homeostasis and changes in metabolism (3). The presence of tumour hypoxia is linked to a poor prognosis and is inextricably linked to neo-angiogenesis through the upregulation of vascular endothelial growth factor transcription (4)

In over 60% of tumour types, hypoxia exists with pO_2 values below 2.5 mmHg, with whole tumour median oxygen partial pressure below 10 mmHg (5). Tumour oxygen partial pressure between 0.5 to 20 mmHg may be the most crucial when it comes to determine the response to fractionated radiotherapy because this intermediate range of oxygenation induces adaptation towards a more aggressive phenotype (6). Cells living under the conditions of oxygen partial pressures below 0.5 mmHg are not deemed viable.

Polarographic needle electrodes have been described as the most accurate and widely used method for direct measurement of tissue oxygen partial pressures (7,8). This method has consistently shown correlation between hypoxia and poor response to radiotherapy (9). However, the major drawbacks are the invasive nature of this procedure and the inability to distinguish necrosis from severe hypoxia, as both conditions exist in low oxygen environments (10).

Histological analyses of tissue samples from head and neck cancers showed that cellular proliferation generally took place in close proximity to blood vessels and pimonidazole (an injectable hypoxia marker) was consistently bound at distances away from vessels (11,12). As such, this relation between perfusion or vascularity and hypoxia is important as it directly affects tumour repopulation and re-oxygenation rates during a

course of fractionated radiotherapy (13). Therefore, establishing the relationship between hypoxia and vasculature using non-invasive methods would be informative when it comes to radiotherapy planning and identify potentially radio-resistant regions that may warrant dose-escalation.

Dynamic contrast-enhanced (DCE)-MRI has been considered the current gold standard technique when it comes to imaging tissue perfusion and vascularity (14). However, this is also an invasive technique as it requires injection of exogenous contrast that may accumulate within tissues such as brain with repeated injections (15). Analysis and calculation of DCE-MRI is also a time-consuming and laborious process that is not clinically feasible with repeated measurements during a single course of radiotherapy. The IVIM technique, therefore, offers a non-invasive solution to establishing such information.

The MR-Linac has been designed and developed to provide RT by adapting to both evolving anatomy and biology. The capabilities of the MR-Linac in terms of delivering *anatomically*-adapted radiotherapy for HNCs have been described in an early evaluation of the Elekta Unity workflow (16). This project was undertaken to further explore the potential for *biologically*-adapted radiotherapy by investigating some novel biomarkers on this platform.

The aim of this project is to evaluate a form of susceptibility-weighted imaging (in the form of T2*-MRI) and IVIM-MRI sequences in patients with HNC, to determine how these factors evolve over the course of radiotherapy. Other aims included testing the repeatability of measurements of hypoxia and vascularity and whether these factors have the ability to stratify disease into risk and prognostic groups. The long-term aim is to determine whether additional radiological biomarkers can provide additive predictive information to DWI/ADC in order to provide biologically-adaptive radiotherapy.

3.2 Aims and Hypotheses

i) **Aims:**

- To determine how IVIM parameters correlate with DWI/ADC as predictors and indicators of tumour response to (chemo)radiotherapy.

Hypotheses:

- IVIM parameters, such as perfusion fraction, will be complementary to ADC in terms of predicting tumour response to (chemo)radiotherapy.
- Tumours with high baseline perfusion fraction will be more responsive to (chemo)radiotherapy due to improved oxygenation and delivery of chemotherapy.

i) **Aims:**

- To determine repeatability of hypoxia measurements using T2* MRI on the MR-Linac.
- To correlate tumour hypoxia with tumour response and treatment outcome.

Hypotheses:

- T2* MRI will be able to map tumour hypoxia spatially on a voxel-by-voxel basis.
- Hypoxia, if present at baseline, will reduce in responding tumours, as reoxygenation occurs over the course of radiotherapy.
- Residual tumour hypoxia will highlight potentially radioresistant regions and may be a site of residual disease in patients that fail radiotherapy.

ii) **Aim:**

- To assess the correlation between IVIM-derived perfusion maps with T2*-derived tumour hypoxia.

Hypothesis:

- Hypoxic tumour regions will have significantly lower perfusion fraction.

3.3 Materials and Methods

3.3.1 Patient Criteria

Patients for the IVIM analyses were acquired through the INSIGHT II (NCT04242459) and PRIMER (NCT0297382)/PERMIT (NCT03727698) studies. Patients in the INSIGHT II study had DW-MRI scans on the diagnostic-MRI scanner as described in Chapter 2. Patients recruited into the PRIMER/PERMIT studies all had fMRI scans on the MR-Linac.

3.3.2 Scan Protocols

Patients on the INSIGHT II study were scanned at baseline (pre-radiotherapy), week 2 (fraction 8-9) and week 4 (fraction 18-19) of CRT. DWI protocols are described in Chapter 2/Appendix A.

Patients having scans on the Elekta Unity MR-Linac had scans at baseline (pre-radiotherapy), then once weekly scans during their (chemo)radiotherapy (Appendix A). Patients in the PRIMER study had T2, SPectral Attenuated Inversion Recovery (SPAIR), DWI and T2* MRIs at a maximum of five time points, with up to two baseline scans pre-treatment. The time points for the intra-treatment scans varied between patients due to MR-Linac availability.

Patients in the PERMIT study were able to have more frequent scans, however, due to the limited total scanning time per treatment session, patients were limited to one sequence per day. Therefore, SPAIR, T2* and DWI MRIs were performed on different days of the treatment week.

3.3.3 Image Post-Processing

Perfusion maps and T2* images were acquired from the MR-Linac platform only. Perfusion maps and R2* image formation was automated using a Matlab script (V2020b, MathWorks, Massachusetts, United States) written by Dr Andreas Wetscherek (The Institute of Cancer Research, U.K.). All images were analysed using the RayStation TPS.

Perfusion maps were created by fitting the biexponential decay IVIM model to anatomically corresponding voxels on the DWI image sets (b-values 0,30,150 and 500 s/mm²) and related ADC maps. The voxels on the output images displayed the perfusion fractions (“f”) as a percentage value (Figure 3-1C).

Multi-echo images were taken from 5 to 40 ms in 5 ms increments. A T2* map was initially created by calculating the gradient of a semi-logarithmic plot between the echo time (x-axis) against the natural logarithm of signal value (y-axis) on a voxel-by-voxel basis. R2* maps were created using “R2* = 1 ÷ T2*” on a voxel-by-voxel basis (Figure 3-1D).

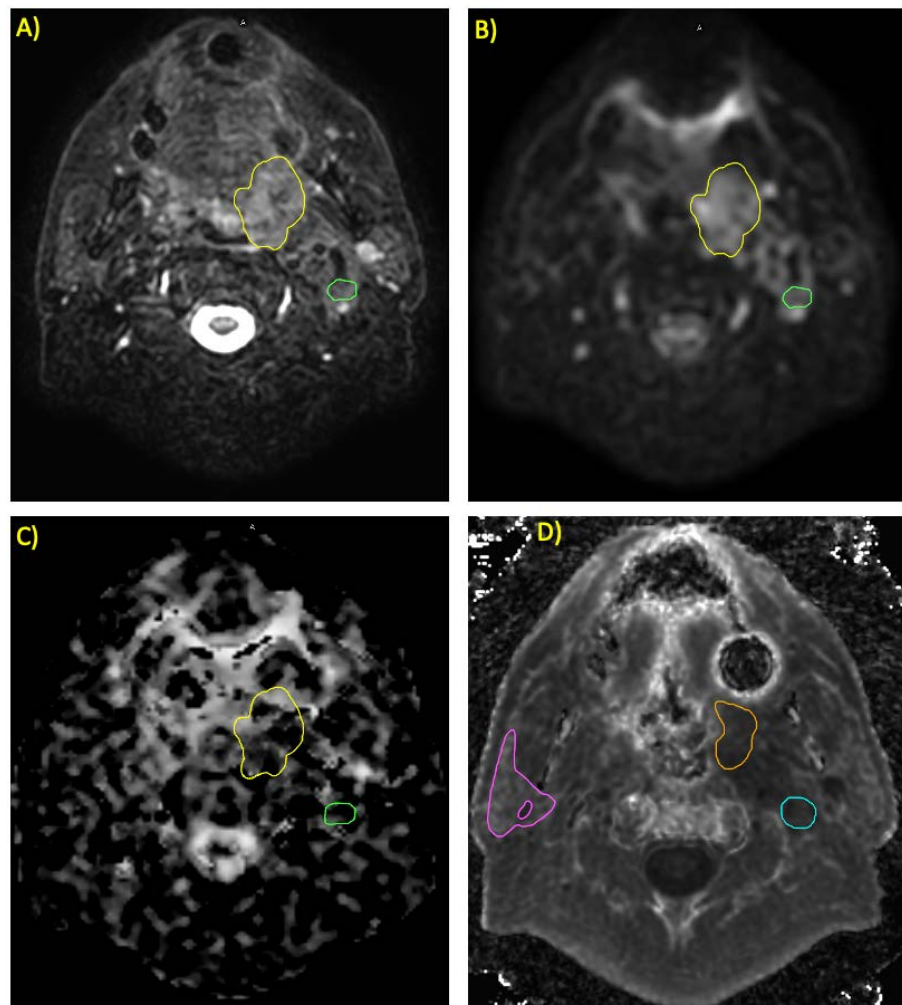


Figure 3-1, Example of perfusion and R2* maps.

A) SPectral Attenuated Inversion Recovery MR sequence was performed to assist with delineation; B) Diffusion-Weighted Image (b30 s/mm²); C) Perfusion map, produced with original image-registration details in place to allow propagation of volumes from DWI; Yellow – primary tumour, green – involved lymph node; D) R2 image, where contours were amended to avoid areas of distortion or loss of signal due to implants or air-tissue interface-related interference; orange – primary tumour, blue – involved lymph node, pink – contralateral parotid gland (with excluded blood vessel).*

3.3.4 Image Analyses

3.3.4.1 DWI, Intra-Voxel Incoherent Motion and Perfusion scans

For both diagnostic and MR-Linac DW-MRIs, ROIs were drawn around the primary and largest involved lymph node on each b-value image. A semi-logarithmic plot of the b-value (x-axis) against the natural logarithm of the DWI signal intensity (y-axis) was created (Figure 3-2). The perfusion fraction (“f”) was calculated as:

$$f = [(S_{b0} - e^{S(y-int)}) \div S_{b0}] \times 100,$$

where S_{b0} is signal intensity at b-value 0 s/mm^2 and $S_{(y-int)}$ is signal intensity at the y-intercept. Perfusion maps, created from DWIs on the MR-Linac were contoured and whole volume perfusion fraction data were extracted as a Microsoft Excel spreadsheet (V16.63.1).

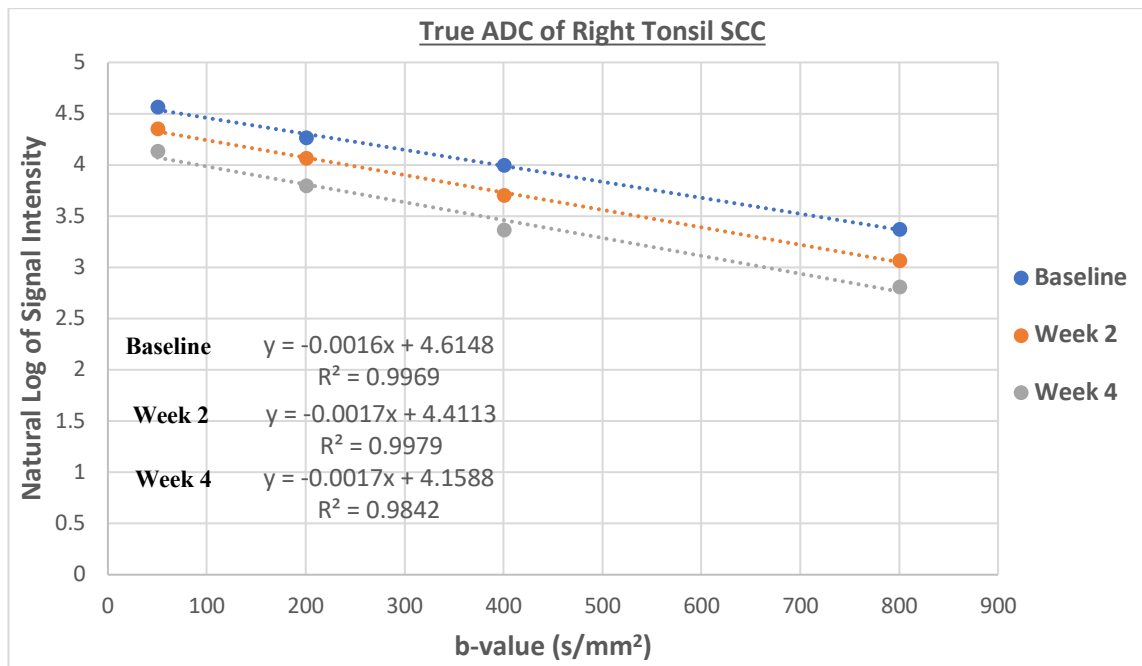


Figure 3-2, IVIM plot of b-value against natural logarithm of signal intensity.

Example case of a right tonsil tumour. Natural logarithm of signal intensities from b-values 50-800 s/mm^2 plotted against the b-value at 3 time-points. y-intercepts were used to calculate perfusion fractions. b-value 0 s/mm^2 omitted as it was not required to determine the y-intercept and to avoid skewing the trend line. High R^2 coefficients demonstrate that the signal intensities measured on individual b-value sequences were accurate as an exponential relation is expected.

3.3.4.2 R2* scans

Primary and lymph-node targets were outlined on RayStation. The contralateral parotid gland was contoured as a control as parotid glands have inherently high R2* value and it was not expected that the contralateral parotid value would change over the course of radiotherapy. Therefore, due to intra-patient variation in R2* image quality, mean whole-tumour volume R2* values were normalised to the contralateral parotid gland. Similarly, mean R2* values of tumour volumes were also measured. Areas of signal distortion (particularly around air-soft tissue interfaces) or vessels were excluded. Whole volume data were extracted as a Microsoft Excel spreadsheet.

To establish the fraction of hypoxia within whole-tumour volumes, thresholds of R2* at 60 s^{-1} and 50 s^{-1} were utilised for primary and lymph-node disease, respectively. These thresholds were based on quantitative susceptibility-weighted imaging studies in HNC xenograft models and patients by Panek et al (17).

3.3.4.3 Correlation between Perfusion and R2*

To investigate the correlation between tissue perfusion and hypoxia, a Matlab script was generated by Dr Wajiha Bano, (post-doctoral researcher at The Institute of Cancer Research, U.K.), to register both perfusion and R2* maps and compare the voxel values. Only scans from the PRIMER study were used because DWI and multi-echo sequences were taken in a single imaging session and it was expected that different sequences would be co-registered. To ensure accuracy of image fusion, Matlab presented the perfusion and R2* map fusions for screening and confirmation of accuracy, prior to completing the analysis.

Data were extracted as a Microsoft Excel spreadsheet. Scans performed in PERMIT were not utilised as they were acquired on separate days and despite patient immobilisation, image registrations between scans were not accurate enough to allow correlative analyses.

3.3.5 Statistical Analyses

All data are presented as percentage changes from baseline. This allowed comparability between sequences with different units. This also allowed comparison

against ADC, which was originally measured as the percentage change from baseline measurements.

All comparisons between MRI-sequence data sets were made using Pearson's correlation analyses (Spearman rank test for non-parametric data) using Microsoft Excel (V16.49, 2021). Bland-Altman analyses on SPSS Stats Package (V23.0, 2015, IBM) was used to compare the agreement between different sequences, if a significant correlation was found.

To compare the spatial correlation between perfusion fraction and hypoxia, the Repeated Measures Correlation (rmcorr) package for R (R Core team (2022), Vienna, Austria) was used as it better handled the larger number of data-points (18).

3.4 Results

3.4.1 Patient Demographics

All functional MRI scans performed in this project were on the same group of patients as described in Chapter 2 (Table 2-2). Patients recruited into either the PERMIT or PRIMER studies are also specified in Table 2-2b.

3.4.2 IVIM on the Diagnostic-MR Scanner

Figure 3-3 shows the percentage changes in the perfusion fractions for both primary tumour and lymph nodes, when IVIM-MRI is performed on the diagnostic-MR scanner. Raw perfusion fraction values and percentage changes are presented in Appendix G. All patients with resolving primary tumour (mA, mC, mD, mE and mI), where no residual disease was seen on the fourth-week CT, show trends for increasing perfusion fractions between baseline and the second week. There were no patients in the entire cohort that had residual disease after chemo-radiotherapy and there were no trends or patterns of changes in perfusion fractions that could stratify patients or their diseases into risk groups as defined in Table 2-1.

Perfusion fractions in involved lymph nodes were of similar magnitude at baseline and there were indistinct patterns with variable degrees of percentage change between patients. Like primary tumours, there were no patients who had residual nodal disease to differentiate between risk groups based on perfusion fraction.

3.4.2.1 Perfusion Fraction compared to ADC

Perfusion fraction data were compared against ADC to determine the agreement between these two sequences (Figure 3-4a). At week 2, there is a strong correlation between perfusion fraction and ADC for the primary tumour (Pearson's correlation 0.73, p-value 0.001), but the correlation weakens by week 4 (Pearson's correlation 0.4, p-value 0.22).

For lymph nodes, there was no correlation between perfusion fraction and ADC at week 2 (Pearson's correlation 0.42, p-value 0.12) (Figure 3-4b) or week 4 (Pearson's correlation 0.06, p-value 0.85).

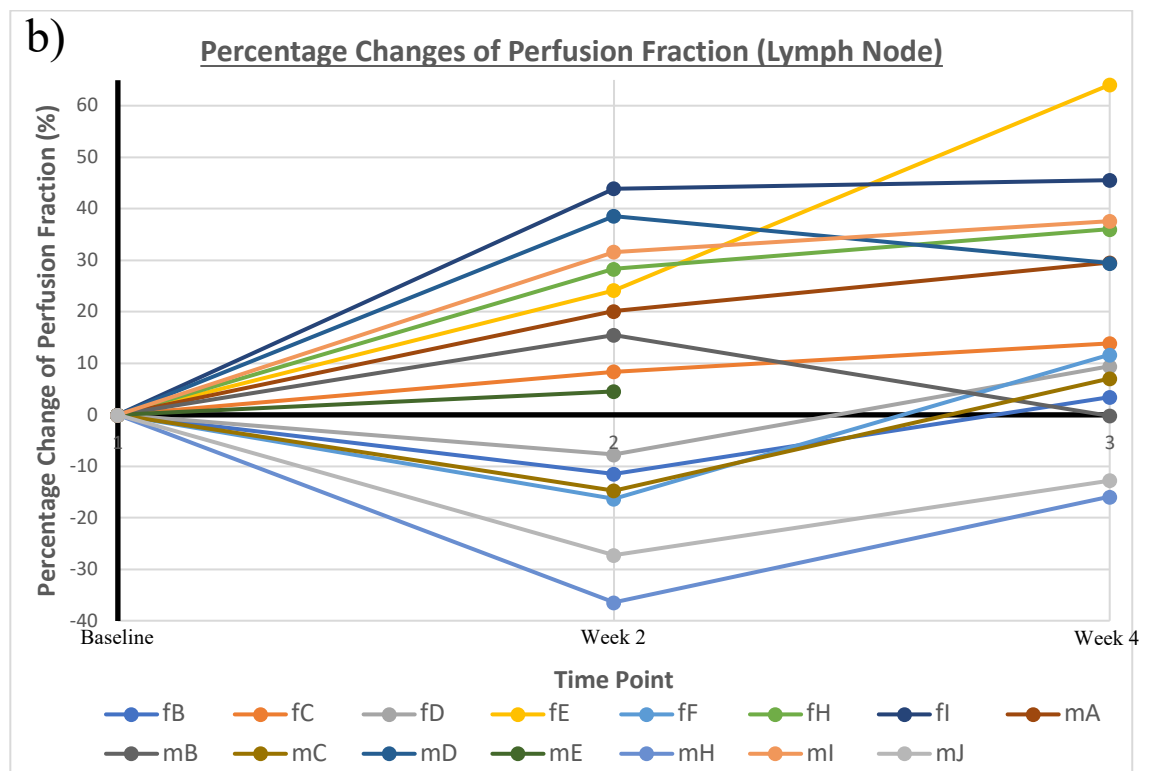
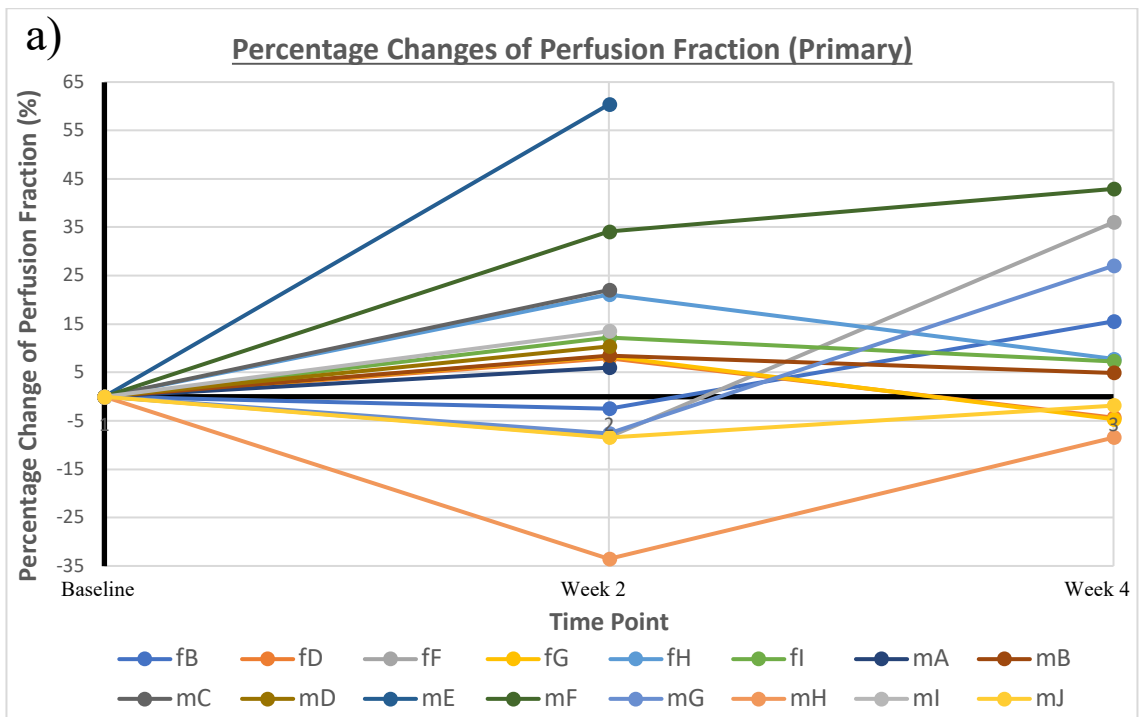


Figure 3-3, Percentage Changes of Perfusion Fractions for Primary and Lymph Node Disease.

Changes in perfusion fractions are presented as percentage changes at baseline, week 2 and week 4 of chemo-radiotherapy for a) Primary and b) Lymph node disease. Patient identifiers relate to those as presented in Table 2-2. Patients with fully resolving tumours before the week 4 CT have no data points at this stage.

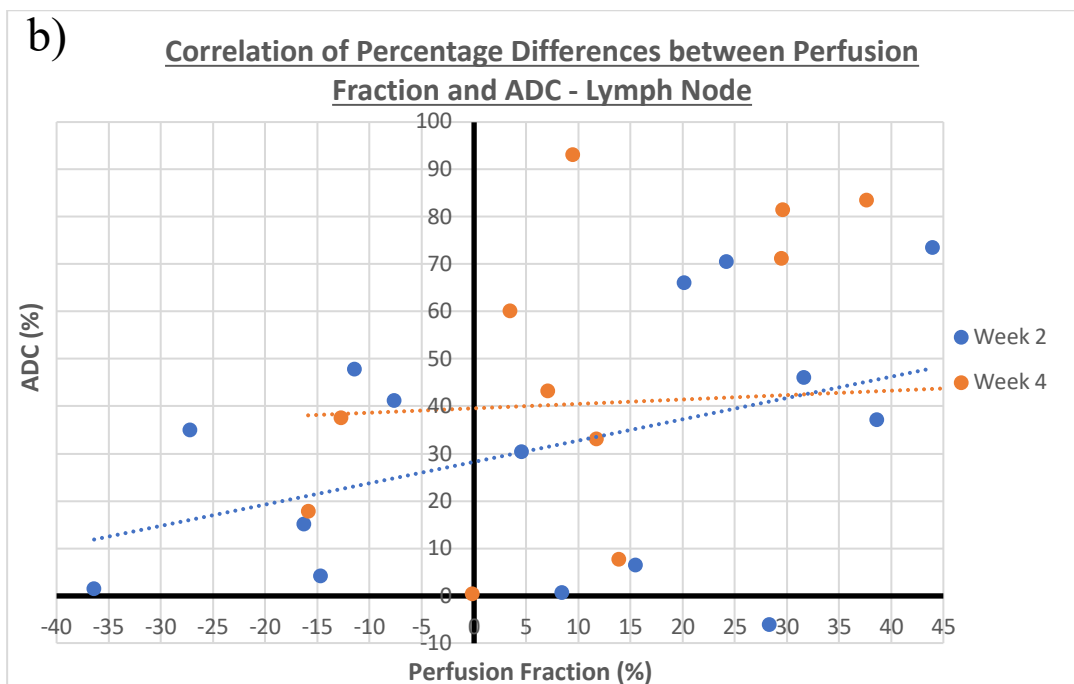
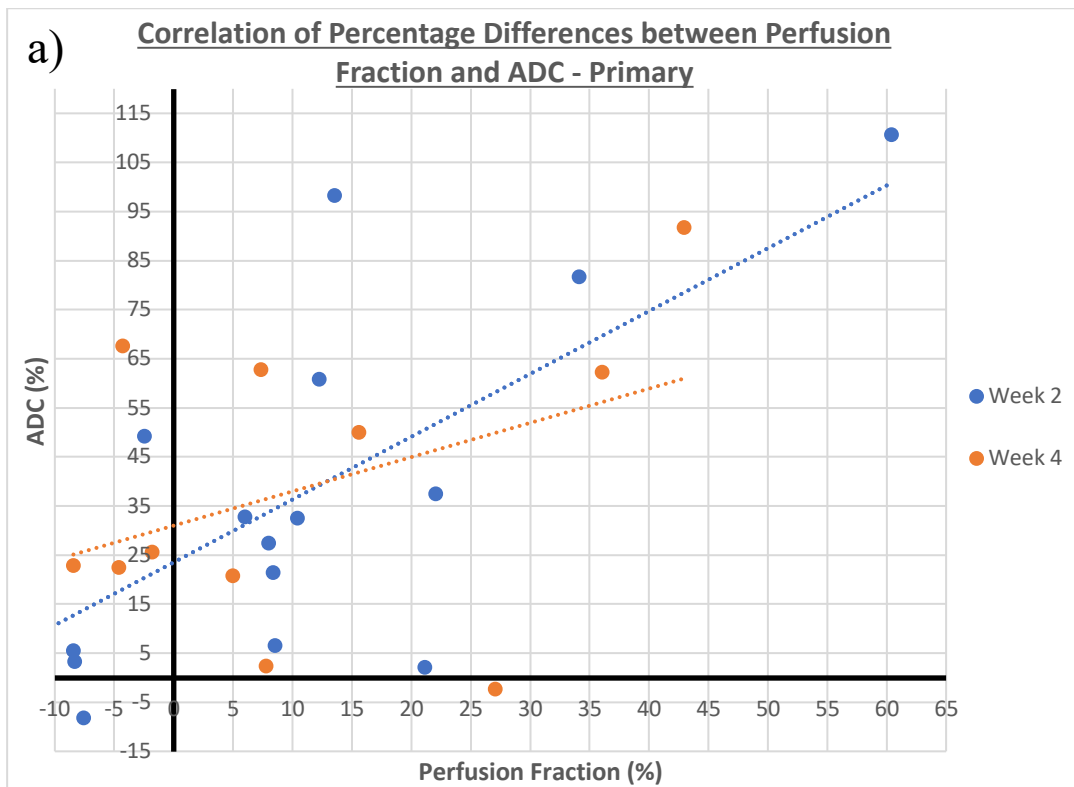


Figure 3-4, Correlations of Percentage Changes Between Perfusion Fraction and ADC. Correlations between the percentage changes for the perfusion fraction and ADC (ssEPI) are shown for patients scanned on the diagnostic-MR scanner for a) Primary and b) Lymph Node disease.

A Bland-Altman plot for the differences between the primary tumour ADC and perfusion fraction at week 2 suggests good agreement between these two parameters (coefficient of variation = -98.5%; limits of agreement -76.5–24.3), (Figure 3-5). However, there is proportional bias between the difference of the means as linear

regression analysis shows a significant positive correlative relationship (p-value <0.05) and this limits interpretability of this plot.

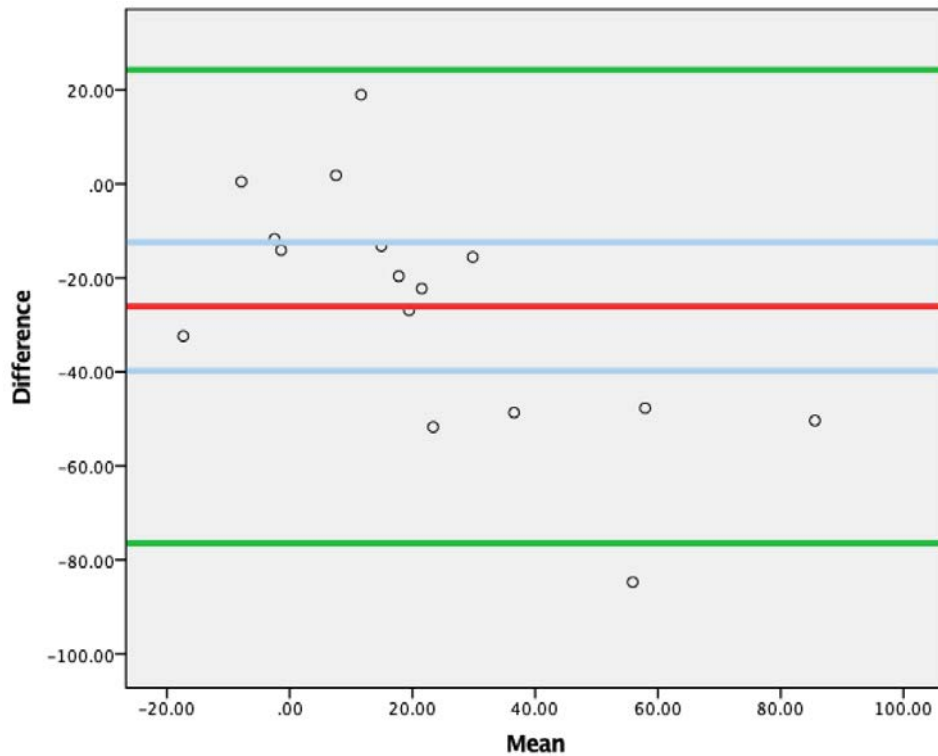


Figure 3-5, Bland Altman Plot For Primary Tumour ADC vs. Perfusion Fraction Percentage Changes at Week 2.

The differences between the percentage changes of ADC and Perfusion Fractions (for each patient) are plotted against the mean. Red line denotes the mean of the differences with the 95% confidence interval of this mean in blue. Green lines denote limits of agreement (i.e. $\pm 1.96 \times$ standard deviations).

3.4.3 IVIM on the MR-Linac

Figure 3-6 displays the percentage changes of perfusion fractions on the MR-Linac (raw data shown in Appendix H). Residual disease in the primary and lymph node was observed in patient mrl only. There were no discernible trends or patterns noted in perfusion fractions at baseline or over the course of radiotherapy for primary tumours or lymph nodes. There were no statistically significant differences between the mean baseline values of perfusion fraction between low-risk and intermediate-/high-risk disease, (risk groups defined in Table 2-1).

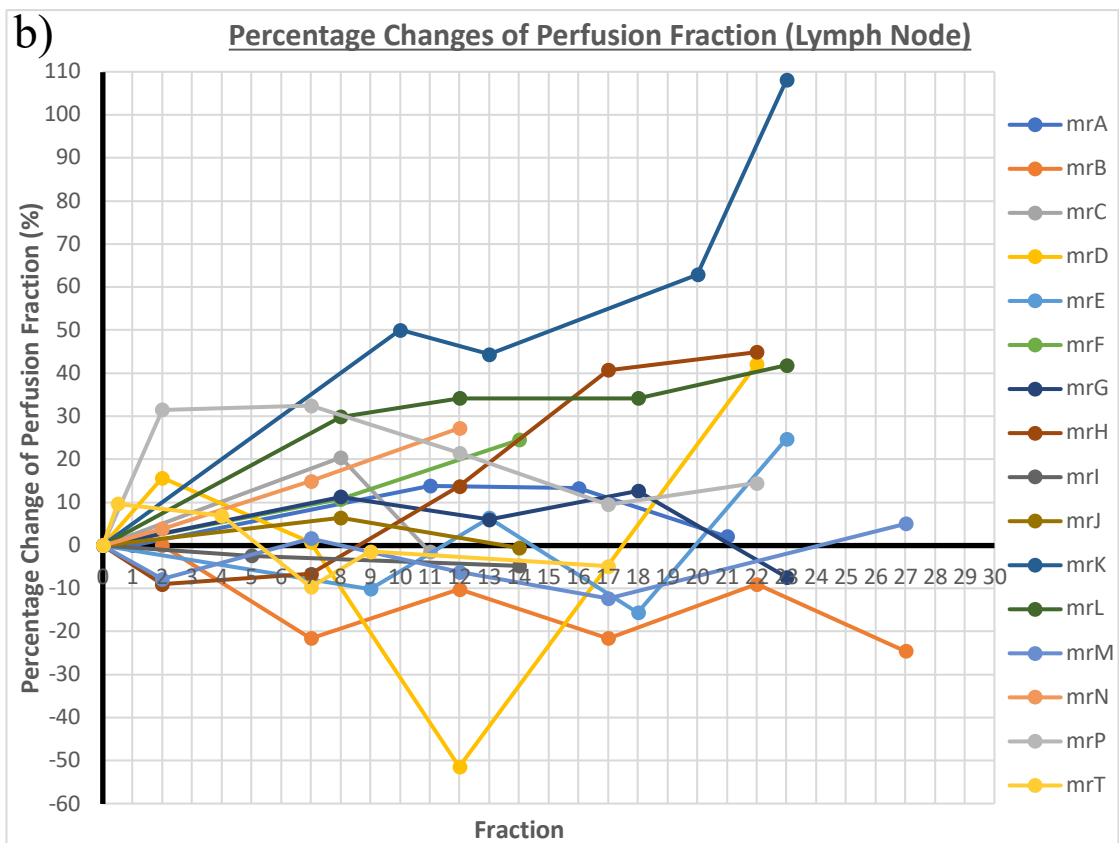
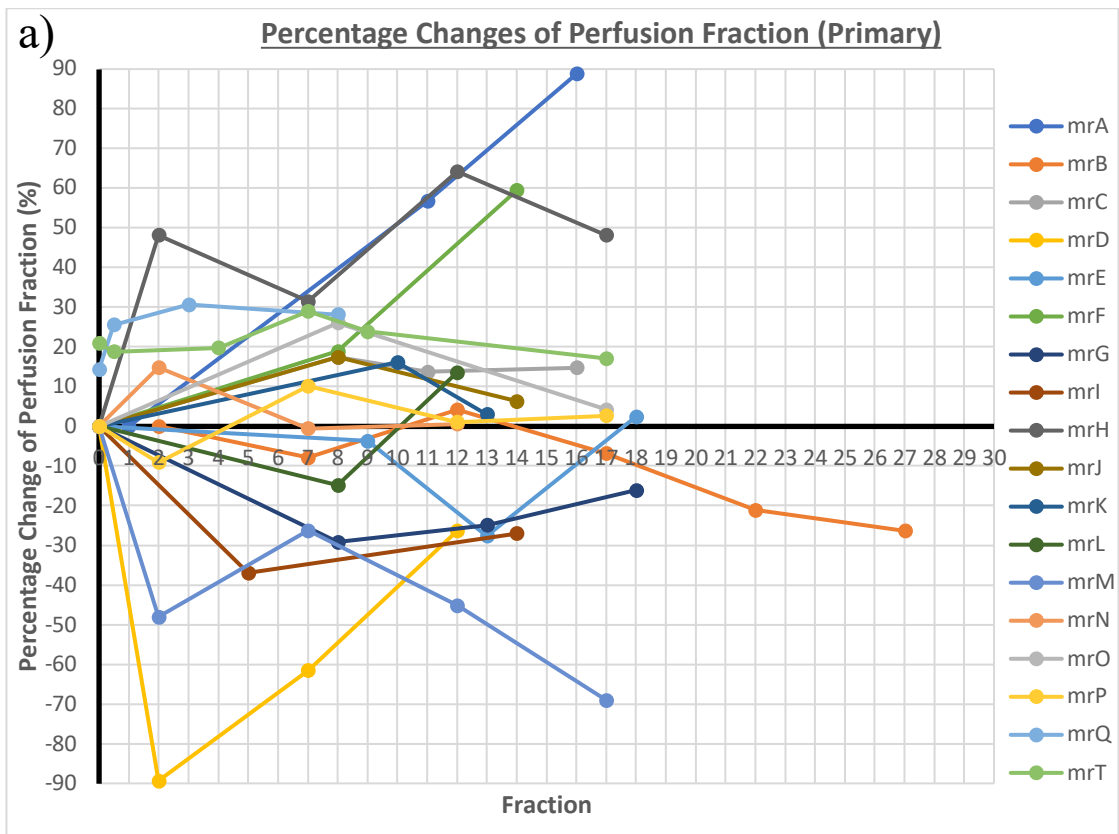


Figure 3-6, Percentage Changes of Perfusion Fractions for Primary and Lymph Node Disease.

Changes in perfusion fraction are presented as percentage changes during chemo-radiotherapy for a) Primary and b) Lymph node disease. Patient identifiers relate to those as listed in Table 2-2.

3.4.3.1 Perfusion Fraction compared to ADC

The correlations between the percentage change in perfusion fraction and ADC were analysed (Figure 3-7). There were no correlations between these parameters for the primary tumour at all time points (Pearson's correlations at week 1 = -0.44; week 2 = -0.35; week 3 = -0.18; week 4 = 0.1, p-value >0.05 at all time points).

Pearson's correlations for lymph node disease were only statistically significant at week 3 (week 1 = 0.2; week 2 = 0.19; week 3 = 0.57 (p-value <0.05); week 4 = 0.52; week 5 = -0.48).

3.4.3.2 Tumour Hypoperfusion

In order to investigate the proportion of tumour tissue that was under-perfused, the volume of tumour that contained a perfusion fraction below 15% was analysed using the perfusion maps. The raw data are presented in Appendix I, but there were neither significant nor consistent trends in the percentage changes of under-perfused primary tumour or lymph-node tissues. Some primary tumours saw a reduction as much as 100% by the second week (mrQ) or an increase in hypoperfusion volume as much as 670% (mrL).

3.4.3.3 MR-Linac IVIM Repeatability

Seven patients had double-baseline DW-MRIs on the MR-Linac. Four of these patients had lymph-node disease. Primary lesion (Pearson's method, $r = 0.94$, p-value <0.01) and lymph-node (Spearman method, $r = 1.00$, p-value <0.01) correlation analyses between ADC values show significantly strong relationships, (Figure 3-8). The measured line of best fit in Figure 3-8 included an anomaly result and generated a seemingly negative correlation. After exclusion of the anomalous data point, the correlation was in fact positive.

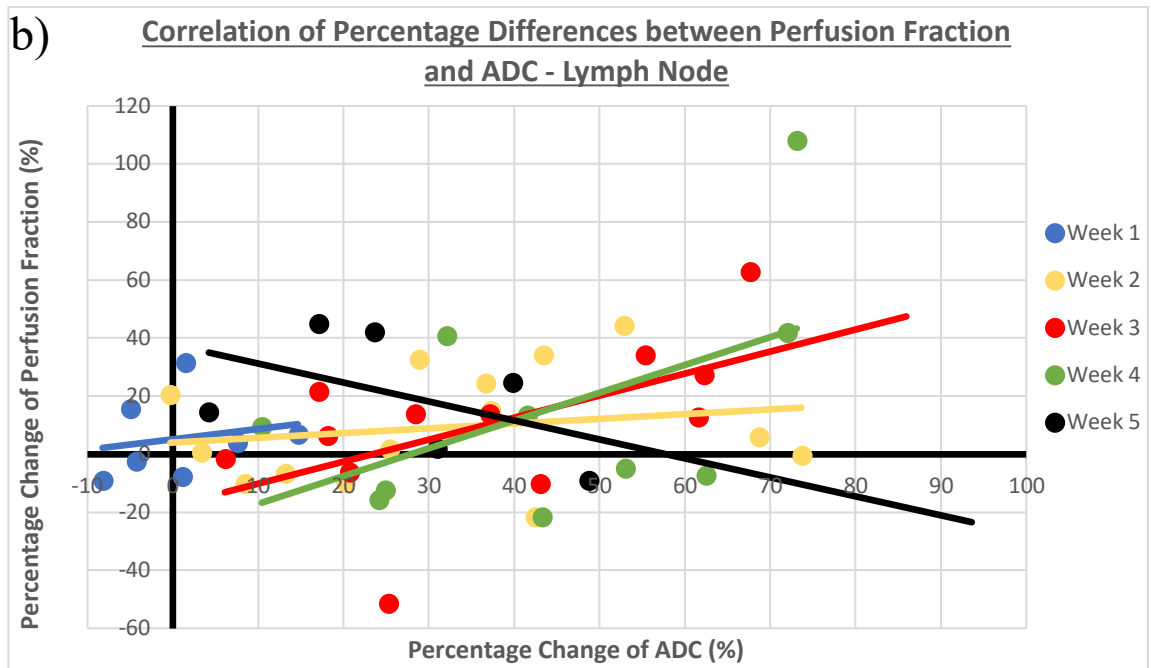
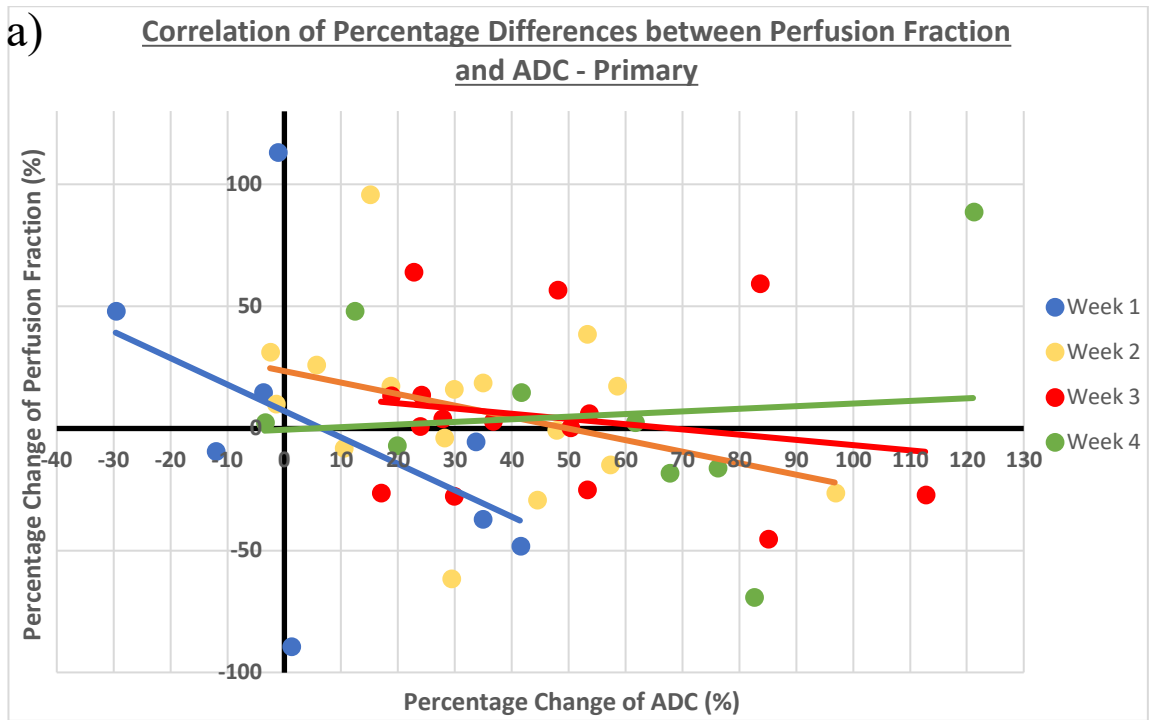


Figure 3-7, Correlations between Perfusion Fraction and ADC.

Correlations are plotted between the percentage changes in perfusion fraction and ADC (ssEPI) for both a) primary and b) lymph node. Each week is plotted as a separate curve.

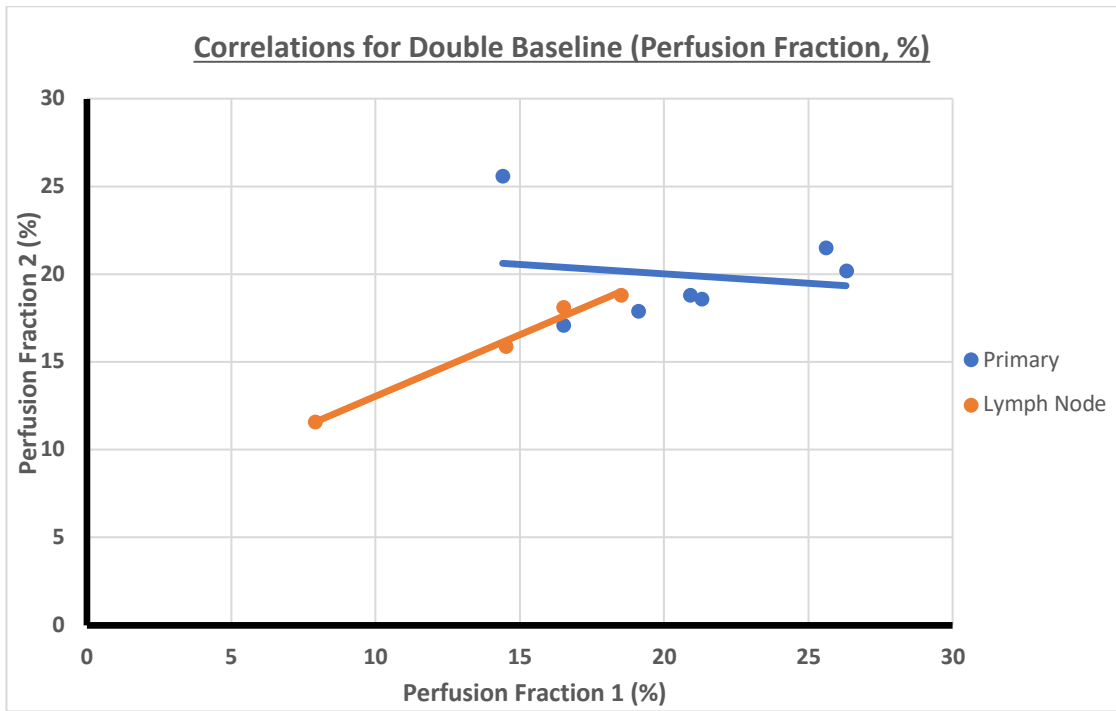


Figure 3-8, Double-baseline comparisons for Perfusion Fractions.
The correlations between double-baseline readings for perfusion fractions are plotted for both primary and lymph node disease.

3.4.4 Hypoxic-MRI on the MR-Linac

Twenty-two patients had T2* MRIs performed. An example of the MATLAB-generated R2* map is shown in Figure 3-9. The proportion of tissue within the volume deemed hypoxic ($R2^* > 60 \text{ s}^{-1}$ and 50 s^{-1} for primary tumour and lymph-node disease, respectively) was expressed as a percentage of the whole volume. The percentage changes in these hypoxic fractions are presented in Figure 3-10, with raw data presented in Appendix J.

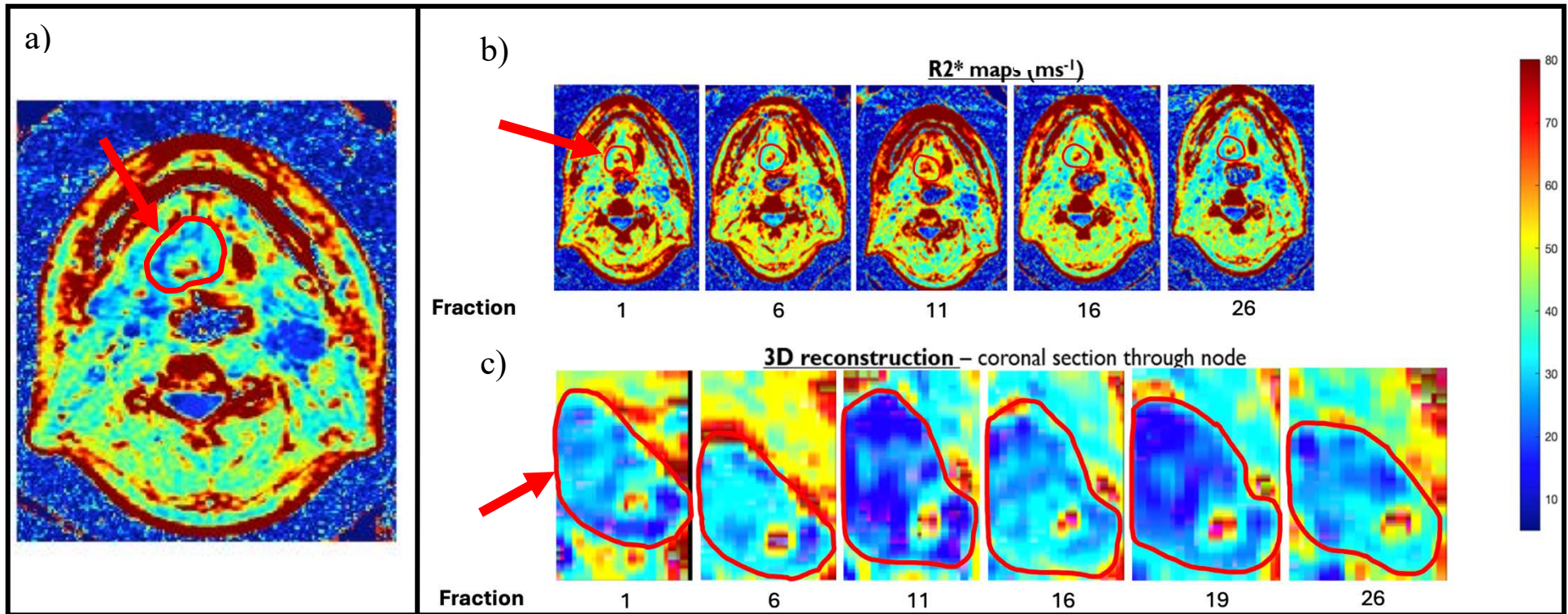


Figure 3-9, Example R2* Map.

Patient mrB is shown as an example of the R2 maps that were generated in MATLAB. a) Tumours are demarcated in red contours (red arrows) for reference. b) The top row qualitatively demonstrates the evolution of R2* changes over the course of radiotherapy, where there is variation in the R2* value within the central region of the primary target. c) The bottom row displays a coronal section through the involved lymph node, where there was a persistent focus of raised R2*.*

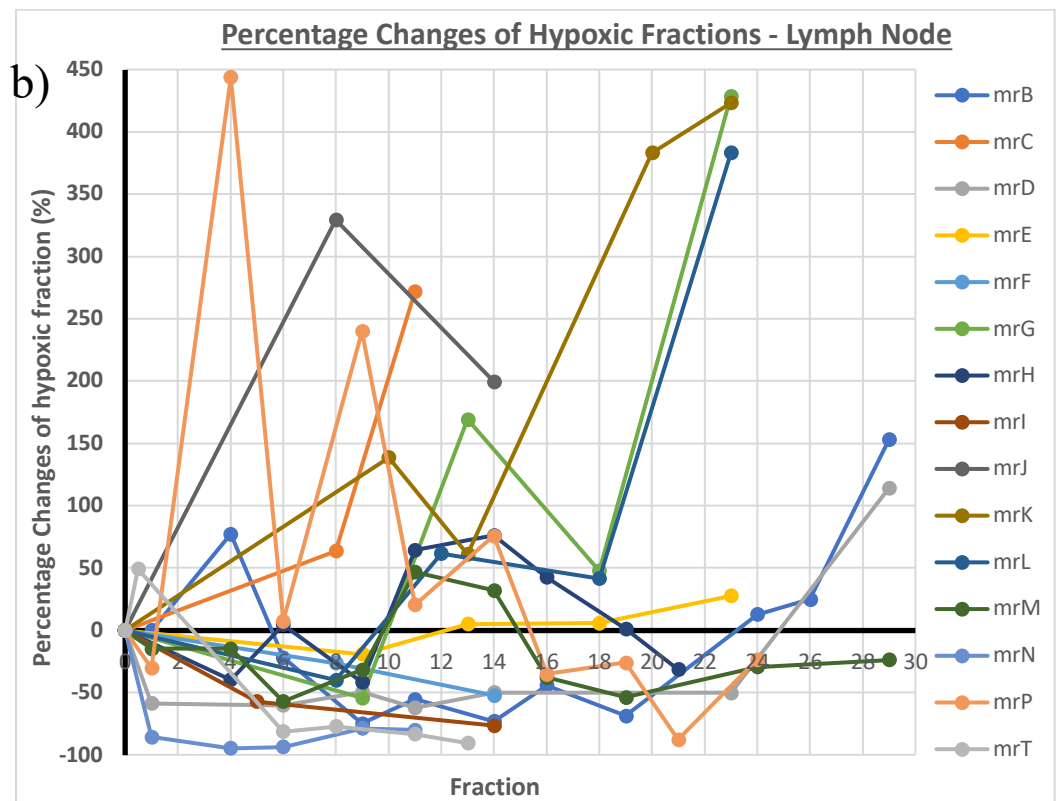
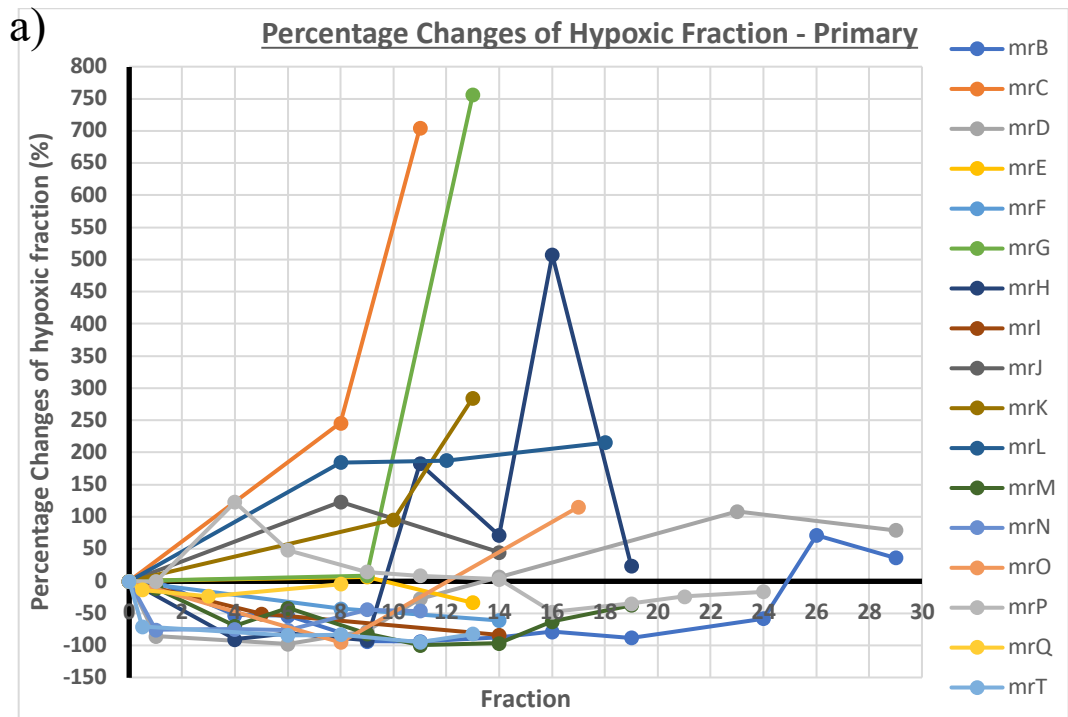


Figure 3-10, Percentage Changes of Hypoxic Fraction for Primary and Lymph Node Diseases.

The percentage changes in hypoxic fraction (percentage volume of tumour that is deemed hypoxic) are plotted against fractions for a) Primary and b) Lymph node disease. All percentage changes are relative to baseline values.

Three patients had baseline primary tumour hypoxic fractions above 30%. Although the percentage change graphs in Figure 3-10 suggest increases in hypoxic fractions of large magnitudes for some patients, the raw hypoxic fractions are still relatively small. Four patients had an increase in the hypoxic fractions after the first week of radiotherapy and the remainder saw decreasing trends for hypoxic fractions. The single patient with residual disease did not show a pattern of change in hypoxic fraction that could distinguish them from other patients. Patient mrQ's R2* MRI contained spuriously high R2* values, with resultant hypoxic fractions above 100%.

3.4.4.1 Hypoxia compared to ADC

The percentage change in the fraction of primary tumour or lymph node with a hypoxic fraction above a certain R2* value (R2* >60 s⁻¹ and 50 s⁻¹ for primary tumour and lymph-node disease, respectively) were compared against the corresponding ADC value for that week (Figure 3-11).

For the primary tumour, there were no correlations throughout the course of radiotherapy (Pearson's correlations week 1 = 0.39; week 2 = 0.26; week 3 = -0.25; week 4 = -0.36, p-value >0.05), (Figure 3-11a).

For the lymph node, there was a range of strengths of correlations between weeks, with statistically significant strong correlation at week 5 only, (week 1 -0.28; week 2 0.43; week 3 0.23; week 4 0.64 and week 5 0.81 (p-value < 0.05)), (Figure 3-11b).

3.4.4.2 MR-Linac Hypoxic Imaging Repeatability

There was a significantly strong correlation between double-baseline measurements for the primary tumour (Pearson's correlation 0.9, p-value < 0.05) (Figure 3-12). There was no correlation between double-baseline measurements for lymph-node disease (Spearman method -0.2, p-value > 0.05).

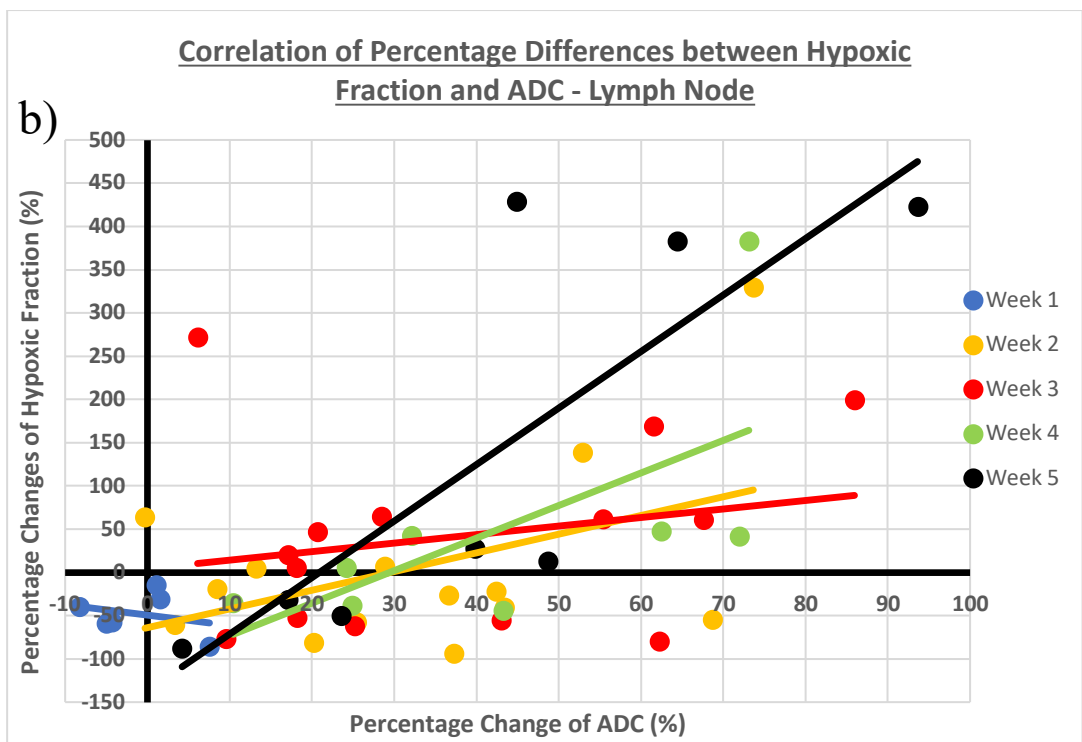
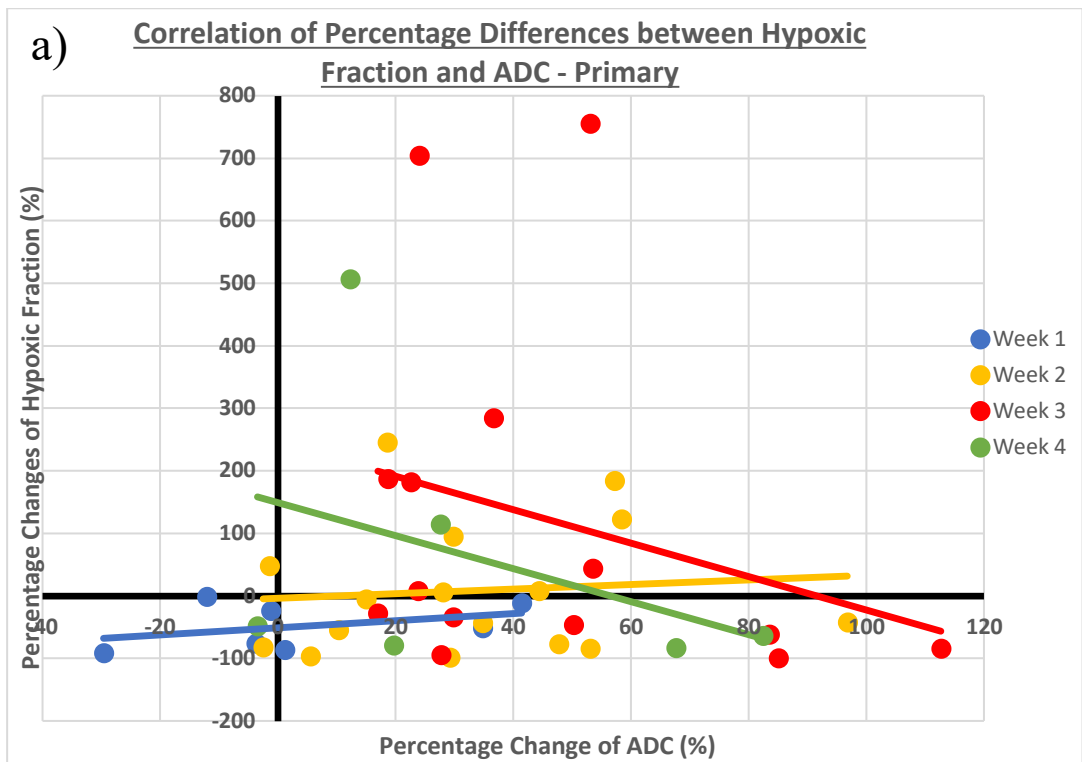


Figure 3-11, Correlations between Hypoxic Fraction and ADC.

The correlations between the percentage changes in hypoxic fractions and ADC are plotted for both a) Primary and b) Lymph Node disease. Correlations are plotted separately for each week of radiotherapy. Lymph Node disease responded more slowly and has a set of data points for the fifth week.

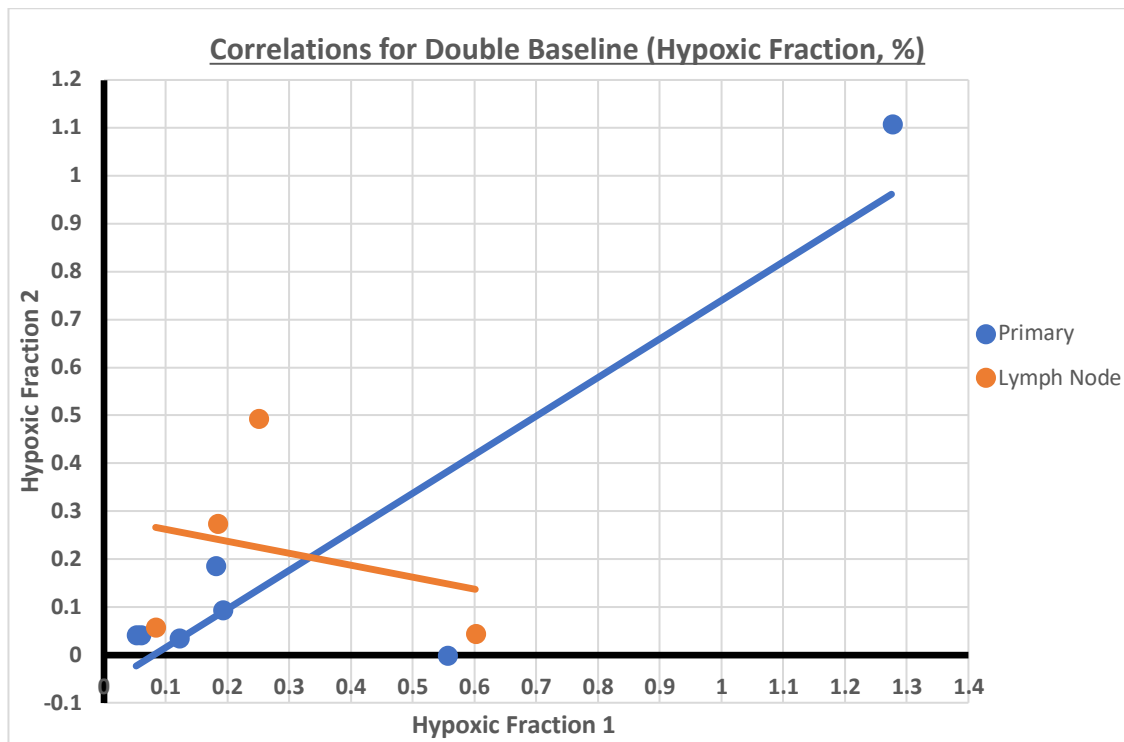


Figure 3-12, Correlations between Double-Baseline Hypoxic Fraction Images.
 Plotted are the double-baseline values between hypoxic fractions for both primary and lymph node tumours. The raw hypoxic fractions ($R2^*$ above threshold values) are plotted.

3.4.5 MR-Linac Perfusion Fraction vs. Hypoxia

So far, functional-MRI on the MR-Linac has been compared against DWI/ADC as the standard sequence. In this section, the percentage changes in tumour perfusion and hypoxic fractions are compared against each other (Figure 3-13).

There were no statistically significant correlations between the percentage change in perfusion fraction (defined as mean perfusion within whole-tumour volume) and hypoxic fraction (defined as the proportion of tumour with $R2^*$ value $>60 \text{ s}^{-1}$) for the primary tumour (Figure 3-13a). There were no correlations between weeks 1-4 (Pearson's correlations week 1 = 0.11; week 2 = 0.04; week 3 = 0.08; week 4 = 0.78, p-value >0.05).

For involved lymph nodes, correlation was strong for week 4 only. There were no correlations at other time points (Figure 3-13b), (Pearson's correlations week 1 = -0.04; week 2 = 0.15; week 3 = 0.18; week 4 = 0.89 (p-value <0.05); week 5 = -0.29).

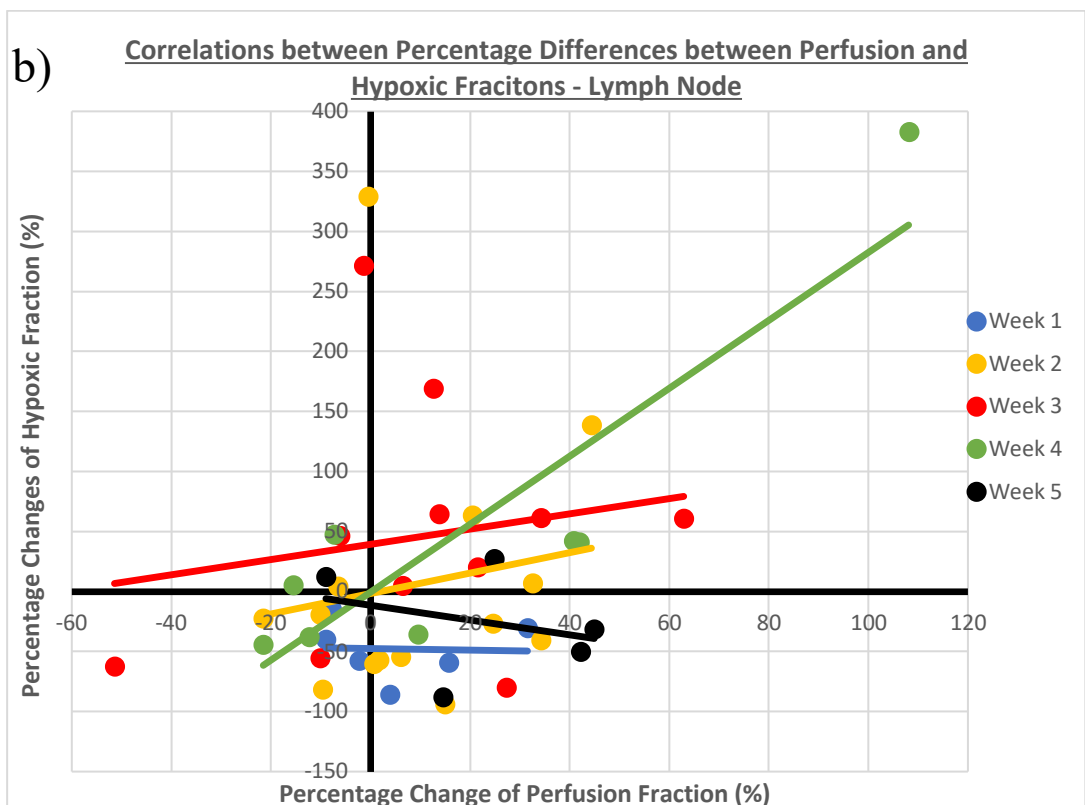
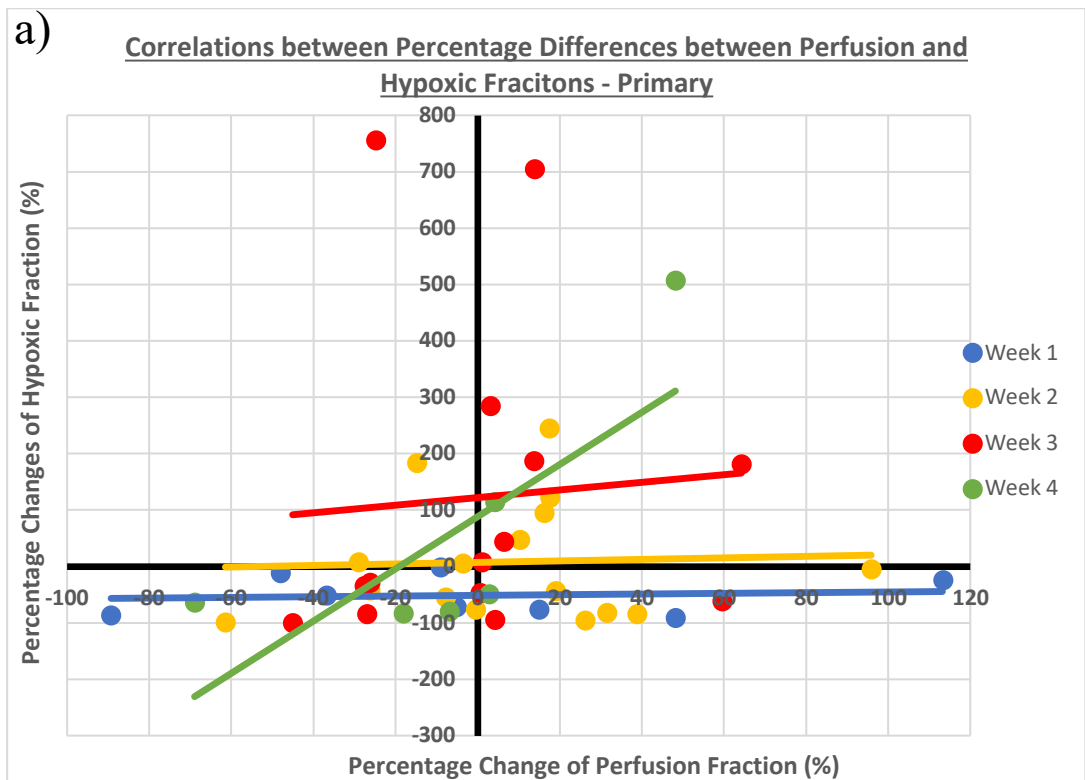


Figure 3-13, Perfusion against Hypoxic Fractions.
 The correlations between perfusion fraction (fraction of tumour with perfusion below 15%) and hypoxia (fraction of tumour above a threshold $R2^*$ value) are displayed for a) Primary and b) Lymph Node tumours.

3.4.6 Spatial Correlation between Perfusion and Hypoxic MRI

In this final section, voxel-by-voxel matching was performed to establish whether there was any correlation between perfusion and R2* on the MR-Linac for the primary tumour only. Figure 3-14 displays the correlations on individual patient levels (image fusions were not available for all patients). There were no correlations between perfusion and R2* when comparing matched voxels, with the highest Pearson's value of 0.3 for patient mrL. No correlation was seen when voxel data from all patients were combined (data not shown).

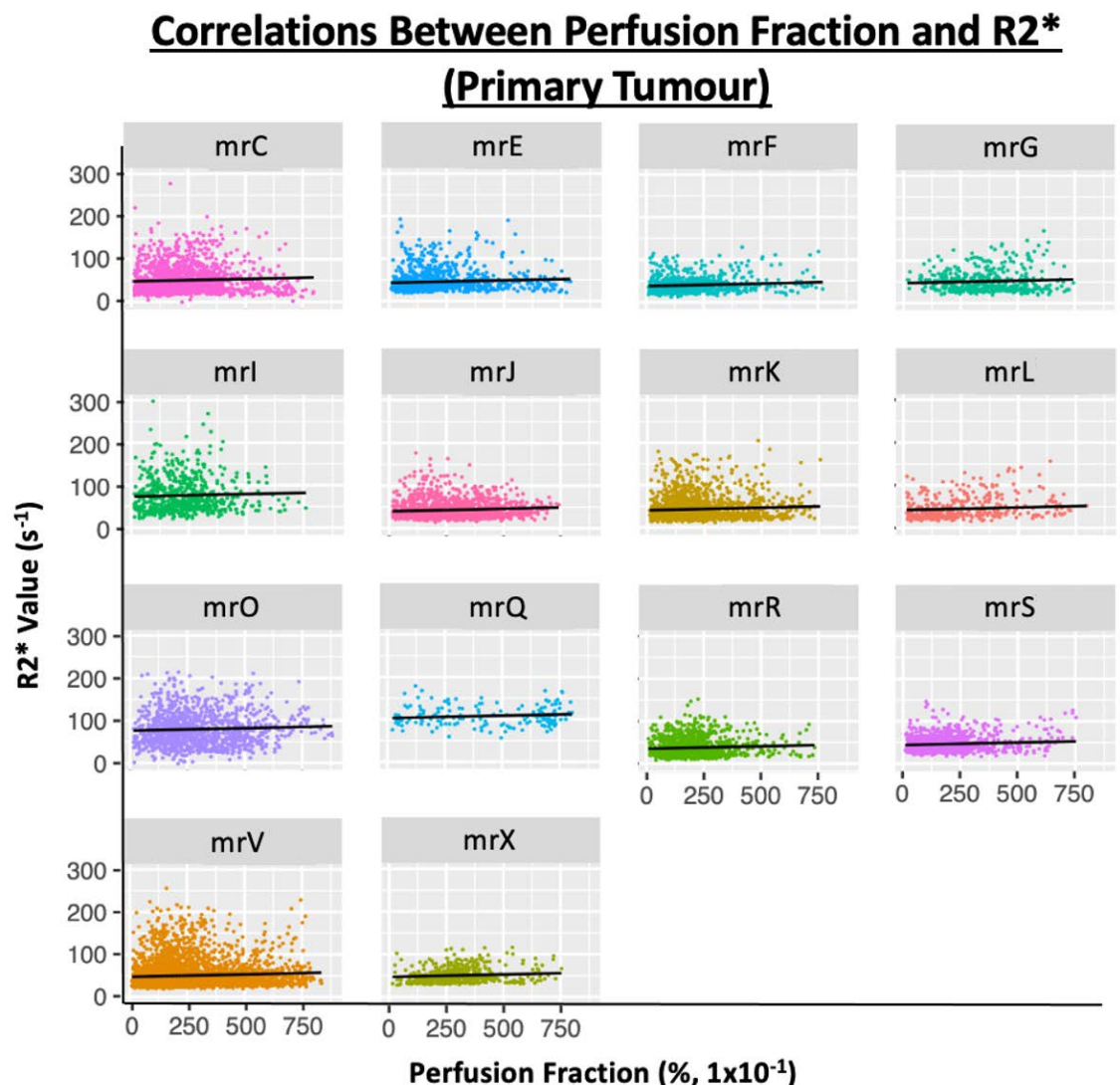


Figure 3-14, Spatial Correlations Between Perfusion fraction and R2*.
Displayed are the correlations between perfusion fraction and R2 values for matched voxels on an individual-patient level.*

3.5 Discussion

3.5.1 Intravoxel Incoherent Motion

IVIM is an extension of the DWI/ADC concept. As such, at any time point a strong correlation was expected between these two parameters for primary and lymph-node disease. However, the correlation was significantly strong only when assessing primary tumours in the second week of radiotherapy. Although this relationship was also strong for the lymph nodes, it was not statistically significant. The data was limited in that only a single patient had residual disease on the post-treatment PET, meaning that stratification of findings into risk groups was not possible.

Perfusion fraction is a surrogate marker for the vascular compartment within tissues. It does not reflect the proportions of haemoglobin to plasma. Inflammation, which induces hyper-perfusion, may also contribute to the signal changes in IVIM, making confirmation and comparison against definitive DCE-MRI studies very difficult. IVIM sequences are also affected by the T2 and susceptibility-weighted signals of the surrounding anatomy, which is a significant consequence of head and neck anatomy (19).

There is consistent evidence of the utility of IVIM-MRI in the diagnostic setting for differentiating between SCC, lymphomas and benign or malignant salivary gland tumours (20,21). Noji D et al performed the largest systematic review of the literature on IVIM for HNCs, involving 17 studies with a total of 882 patients (22). Despite the heterogeneity between included studies, they concluded that combination of IVIM parameters (including perfusion fraction (f), pseudo-diffusion (D^*) and true diffusion (D)) resulted in superior diagnostic accuracy and consistency. The recommendation was also to utilise a minimum of four b-values below 200 s/mm^2 . The combined sensitivity and specificity to distinguish between benign and malignant diseases were 85-87% and 80-100%, respectively. The clinical context of all the studies in this systematic review were predominantly in the diagnostic setting and there are, currently, few studies looking at the evolution of changes of IVIM parameters during treatment.

A more recent systematic review included a greater number of prospective studies to determine the utility of IVIM to predict early response during radiotherapy for HNCs

(23). However, despite their attempts to establish the role of perfusion fraction, this particular analysis of the available data demonstrated that the literature surrounding perfusion fraction is generally lacking.

Ding et al explored the feasibility of measuring serial IVIM-related changes during a course of CRT for stage 3/4 HPV-associated oropharyngeal SCCs (24). They scanned patients one week before starting CRT and 3-4 weeks into treatment, followed by a final response assessment with both PET/CT and IVIM-MRI at three months post-CRT. Their IVIM protocol included twelve b-values and used a 3-Tesla MRI scanner, with eight b-values below 200 s/mm². After recruitment of 31 patients, pre-treatment pseudo-diffusion and perfusion fraction were not able to significantly predict complete response to CRT. In those patients that eventually achieved complete responses, ADC and perfusion fraction significantly increased mid-treatment. However, similarly to the data presented in this chapter, all patients had achieved primary tumour complete responses, with a small subset of residual nodal disease. Reproducibility of the technique was not assessed in their study.

Hauser et al similarly investigated the role of IVIM in predicting recurrence risk. However, the difference in their methodology, compared to Ding et al and this chapter, was that they only performed post-treatment MRIs (25). They concluded that to distinguish between high and low recurrence risk, the differences in proportional change in perfusion fractions post-radiotherapy had to be large between both risk groups. This finding has been echoed by Cao et al (26). However, there is less coherent consensus on the baseline tumour blood volumes and the relevance of this in terms of complete response prediction.

The results in this chapter reflect the inconsistent results described in published literature. Despite recruitment of patients with a variety of disease risk, baseline perfusion fraction or patterns of change during treatment did not demonstrate any distinguishing trends. The strong and significant correlation between perfusion fraction and ADC in the second week of treatment may be due to the fact that a significant volume of tumour remains and, therefore, the two radiologically-related factors of ADC and perfusion fraction demonstrate similar findings. However, by the fourth week, distinction of tumour

volume from inflammation and/or necrosis is difficult. The consistent perfusion fraction measurements for both primary and lymph nodes, on double-baseline measurements, is suggestive that the accuracy of measurements is consistent and reliable, although this requires a higher number of patients for confirmation.

3.5.2 Imaging Hypoxia on the MR-Linac

The T2*-MRI signal describes a complex biological function in living tissues and the technique was initially explored in the central nervous system and for assessments of cognitive function (27,28). Hypoxia in cancer is a continuous interplay between acute (a consequence of lack of perfusion) and chronic (a consequence of lack of diffusion) forms (29). Oxygen delivery from a vessel is deemed optimal within a 70 μm radius, beyond which, hypoxia and ultimately necrosis (at roughly 300 μm) can develop (30).

Therefore, compared to acute hypoxia, chronic hypoxia is more stable and more consistently imaged using T2*/BOLD-MRI. Due to the irregular, immature and poorly compliant blood vessels that are created in the neo-angiogenic process, imaging tumour hypoxia may not provide consistent results because acute hypoxia affects the mean voxel T2* signal. For the susceptibility-weighted effect to take place, deoxygenated haemoglobin needs to reach close to the hypoxic region to create the magnetic field gradients and signal dephasing, although the dephasing effect can take place at a distance up to five times the vessel radius (31). Necrosis may also contribute to the reduced signal seen on T2* MRI (31).

The benefits of accelerated radiotherapy, carbogen (carbon dioxide and oxygen mixture) and nicotinamide (ARCON) on local disease control has been demonstrated in a phase 3 study (32). However, capturing the response to inhalation of carbogen using R2*/BOLD-MRI in murine prostate cancer xenograft models has been demonstrated by Alonzi et al (33). They also suggested that tumours which show the greatest reduction in R2* signal in response to carbogen tend to be the most hypoxic tumours.

The air and soft-tissue interface, local magnetic field inhomogeneities, local haematocrit, vascular geometry, local T2 sensitivity and vascular volumes all contribute to the basal value of the R2* signal in the head and neck region (34). For this reason, the

validity of the BOLD technique for specifically measuring partial pressures of oxygen was questioned by Rijpkema et al, particularly because interpretation of the individually contributing effects of carbon dioxide and oxygen inhalation on microregional physiology are challenging to define radiologically (35). Furthermore, a weak correlation has been demonstrated between the partial pressure of oxygen and T2* MRI in healthy mice (36) and men with prostate cancers (37). In a similar pattern to the carbogen experiments described, there are some proportional relationships demonstrated with T2*/R2*, but these do not directly relate to actual partial pressures of oxygen (38).

Hypoxic fraction data in this chapter are presented as proportions of whole tumour volume above a threshold R2* value (60 s⁻¹ and 50 s⁻¹ for primary and lymph-node diseases, respectively). These thresholds were based on 3-Tesla MRI-based experiments on head and neck xenograft models (17). The R2* variability is known to be significantly affected by the background magnetic field strength (39). However, there is lacking data on the R2* thresholds for HNCs on 1.5-Tesla MRI systems and it is possible that the thresholds defined in this chapter are unsuitable to establish the true hypoxic fraction, which potentially contributed to the inconsistent results.

The intra-tumour regional differences between arteriole, capillary and venule spatial distribution and the different deoxy-haemoglobin and free oxygen content should warrant a more detailed description of the range of R2* values, such as in a histogram format (35,40). This could also mitigate the issues of inappropriate thresholding. Voxel-wise R2* data were available from the image-sets in this study, but it was not reported in the results as the voxel size was large (5.8 mm²). The physiological processes mentioned above occur on a sub-voxel level and so the reported voxel values represent a mean measure of total activity.

Double-baseline measurements in this study reflected a strong correlation for the primary tumour, however this was most likely a skewed result based on a single outlier with a much larger pair of R2* values. It is more likely the case that repeatability measurements for this parameter are poor, perhaps as a result of the acute hypoxic changes in the 24 hours between MRI scans. Despite being able to visualise gross regions

of tumour that gave high $R2^*$ values (Fig 3-9), the resolution of this sequence was not good enough to determine how the spatial changes of acute hypoxia evolve over time.

Due to the large number of biological processes contributing to the $T2^*$ signal, it has been suggested that changes in $T2^*$ in response to oxygen/carbogen are key to highlight the regions of tissue that can be affected by higher partial pressures of oxygen and, therefore, the most hypoxic regions (41). O'Connor et al established their technique of oxygen-enhanced MRI (OE-MRI), which allows quantification of oxygen within tumour using $T1/R1$ -MRI (42). The level of molecular oxygen dissolved in plasma or interstitial tissue affects $T1$ (or $R1$, s^{-1}). Tissues that are well perfused typically have completely saturable haemoglobin, so surplus oxygen stays dissolved in plasma and increases $R1$ when hyperoxic gas is inhaled. The variations in $R1$ should alter in direct proportion to variations in dissolved oxygen. However, because haemoglobin oxygen saturations are thought to be lower in hypoxic sub-regions that are resistant to oxygen challenge and because extra oxygen binds preferentially to haemoglobin, this approach is unable to detect tissue hypoxia (or dissolved oxygen) directly. To deduce hypoxic fractions both quantitatively and spatially, O'Connor et al employed the use of DCE-MRI to identify regions that are both perfused and refractory to oxygen-challenge, indicating hypoxia.

Combination OE- and DCE-MRIs (at 1.5 Tesla) in murine tumour xenograft models for colorectal and renal cell cancers (42) and non-small cell lung adenocarcinoma (43) demonstrated a good sensitivity to changes in oxygen concentration with good accuracy. They were also able to spatially determine the locations of both perfused and oxygen enhancing, perfused and non-oxygen enhancing and non-perfused regions, which histologically correlated with regions of normoxia, hypoxia and necrosis, respectively.

Conversely, based on multiple murine xenograft models for different cell lines, it seems that changes in native $T2^*$ values are able to provide (at best) temporary correlation with changes in tumour partial pressures of oxygen rather than an absolute $T2^*$ value correlating with a specific value of oxygen concentration (44). As such, the lack of correlation with ADC seen in this chapter may be related to the fact that during radiotherapy, the changes imposed on $T2^*$ by factors unrelated to oxygen/haemoglobin (such as haemorrhage, changes in blood volume or perfusion) may affect the overall

signal change observed during the course of radiotherapy. This lack of correlation has also been implied for other more specific and sensitive hypoxia biomarkers such as the F-MISO tracer for PET/CT (45).

3.5.3 Biomarker Development

The approach to exploring new functional-MRI biomarkers was based on the utilisation of IVIM and T2* sequence parameter cards created for pelvic tumour sites or developed at another institute. The IVIM sequence was set by Elekta after collaboration and agreement by the 'Elekta Unity MR-Linac Biomarker Group' and it included just one b-value significantly below 200 s/mm². A b-value of 150 s/mm² was chosen for the DWI/IVIM protocol on the MR-Linac as it was deemed equivalent b-value to 200 s/mm² on a diagnostic system. The R2* sequence card originated from The University of Texas MD Anderson Cancer Centre (Houston, Texas) and has not been further optimised since its first use.

Due to the number of sequences per individual patient scanning session and the total number of MRIs per patient, minimising the time per scanning session was deemed of paramount importance to allow patients to comply with the whole scan in a head shell. This limited the number of b-values (for IVIM) and echo times (for T2*) that could be implemented.

Cancer Research UK and European Organisation for Research and Treatment of Cancer describe fourteen recommendations for the validation and qualification of imaging biomarkers, which encompass two phases, biomarker discovery and validation (46). In the context of MRI-based biomarkers, they emphasised the importance of sequence parameter optimisations prior to assessing its ability to accurately capture biological functions with high repeatability and reproducibility. This step should be completed before attempting assessments of clinical utility, sensitivity and specificity of the imaging biomarker.

The study in this chapter was carried out in the opposite manner, in that it applied the IVIM and T2* sequences on clinical cases, to first establish any correlative relationships. However, without confirming if the sequence parameters were optimised and fit to

function as valid biomarkers, or suitable to determine tumour biology, it is not possible to ensure that there are in fact no relationships between $T2^*/R2^*$ and IVIM (as the results of this study would otherwise imply). Similarly, the poor image resolution for the perfusion maps limited their use to help determine spatial correlative relationships with tissue hypoxia or $R2^*$ values.

Optimal parameters to capture the $T2^*$ -weighted effect are thought to be a low flip angle and long echo and repetition times (to minimise T1-effect) (47). Increasing the voxel resolution and resting magnetic field strength (to 3 Tesla) are thought to increase the sensitivity to $T2^*$ effects and may reduce deleterious effects at air-tissue interfaces (48). The maximum echo time employed in our $T2^*$ sequence was 40 ms and should be increased with future work.

Quantitative BOLD (qBOLD) is a further extension of the conventional $T2^*/BOLD$ sequence that was conceptualised at a similar time to $T2^*$ (49). Multiparametric qBOLD non-invasively measures and separates the different contributors to the $T2^*$ signal (by implementing gradient-echo sampling under the spin-echo sequence) and acquires independent measurements of T1/T2 effects, blood volume, oxygen saturation and deoxy-haemoglobin induced dephasing effects, with high spatial resolution and good correlation with experiments using blood gas measurements (50).

3.5.4 Conclusions

The $T2^*/BOLD$ function cannot be taken as a simple voxel based mean measure of tissue oxygenation because of the multitude of components that can generate and manipulate the $T2^*$ signal. It depends on a complex relationship between tissue content in terms of vasculature and oxygen status. Tissue oxygenation is also not in equilibrium with vascular or haemoglobin oxygenation due to the constant diffusion gradient towards mitochondria (44). It seems that OE-MRI may be a more reliable measure of tissue oxygenation and hypoxia but this does not obviate the need for some sort of invasive intervention (in the form of contrast administration for DCE-MRI).

In addition, rather than static measurements of $T2^*$, dynamic measurements using oxygen challenge should be employed to mitigate issues of spatial and temporal

heterogeneity. From a clinical and radiotherapy planning perspective, deciphering an average measurement of what areas to dose-escalate should be used for dose-painting indications.

In this chapter, combination of $R2^*$ and IVIM did not demonstrate any correlative findings, which was not originally hypothesised. Whether the findings in this study were due to the sequence parameters being of poor optimisation, or whether there is a true lacking effect is not clear. However, based on the current evidence base, it seems that rather than direct measurement of hypoxia, the response or changes in $T2^*/R2^*$ to varying oxygenation conditions may be a more appropriate use for this functional-MRI sequence.

3.6 Further Work

MRI remains an important and ideal platform for non-invasive measurements of biological functions and processes. Dedicated studies to explore the true IVIM effect, with better signal-to-noise ratio to produce more accurate perfusion maps are necessary, before comparisons with T2*/BOLD and DWI can be made. Future IVIM sequences will likely need to include a higher number of sub-200 s/mm² b-values to fully map the contribution of perfusion fraction to the overall diffusion effect. This requires the involvement of a dedicated specialist MR-physicist to lend their expertise in MR-sequence development and optimisation.

OE-MRI is an alternative and exciting modality that is informative of the elements of perfusion and hypoxia. If perfusion fraction from IVIM can substitute the need for contrast-based DCE-MRI, this could potentially be an ideal method for exploring these biological functions and deliverable on the MR-Linac platform.

3.7 References

1. Jin MZ, Jin WL. The updated landscape of tumor microenvironment and drug repurposing. Vol. 5, *Signal Transduction and Targeted Therapy*. Springer Nature; 2020.
2. Qiu GZ, Jin MZ, Dai JX, Sun W, Feng JH, Jin WL. Reprogramming of the Tumor in the Hypoxic Niche: The Emerging Concept and Associated Therapeutic Strategies. Vol. 38, *Trends in Pharmacological Sciences*. Elsevier Ltd; 2017. p. 669–86.
3. Ziello JE, Jovin IS, Huang Y. Hypoxia-Inducible Factor (HIF)-1 Regulatory Pathway and its Potential for Therapeutic Intervention in Malignancy and Ischemia. Vol. 80, *YALE JOURNAL OF BIOLOGY AND MEDICINE*. 2007.
4. Fukumura D, Xu L, Chen Y, Gohongi T, Seed B, Jain RK. Hypoxia and Acidosis Independently Up-Regulate Vascular Endothelial Growth Factor Transcription in Brain Tumors in Vivo 1. *Cancer Res [Internet]*. 2001;61:6020–4. Available from: <http://aacrjournals.org/cancerres/article-pdf/61/16/6020/2486038/ch1601006020.pdf>
5. Vaupel P, Mayer A. Hypoxia and anemia: Effects on tumor biology and treatment resistance. *Transfusion Clinique et Biologique*. 2005;12(1):5–10.
6. Hoogsteen IJ, Marres HAM, Bussink J, van der Kogel AJ, Kaanders JHAM. Tumor microenvironment in head and neck squamous cell carcinomas: Predictive value and clinical relevance of hypoxic markers. A review. Vol. 29, *Head and Neck*. 2007. p. 591–604.
7. Kooreman ES, van Houdt PJ, Keesman R, van Pelt VWJ, Nowee ME, Pos F, et al. Daily Intravoxel Incoherent Motion (IVIM) In Prostate Cancer Patients During MR-Guided Radiotherapy—A Multicenter Study. *Front Oncol*. 2021 Aug 13;11.
8. Terris DJ. Head and Neck Cancer: The Importance of Oxygen. *Laryngoscope*. 2000;110:696–707.
9. Nordmark M, Bentzen SM, Rudat V, Brizel D, Lartigau E, Stadler P, et al. Prognostic value of tumor oxygenation in 397 head and neck tumors after primary radiation therapy. An international multi-center study. *Radiotherapy and Oncology*. 2005 Oct;77(1):18–24.
10. Milosevic M, Fyles A, Hedley D, Hill R. The human tumor microenvironment: Invasive (needle) measurement of oxygen and interstitial fluid pressure. *Semin Radiat Oncol*. 2004;14(3):249–58.
11. Wijffels KIEM, Marres HAM, Peters JPW, Rijken PFJW, van der Kogel AJ, Kaanders JHAM. Tumour cell proliferation under hypoxic conditions in human head and neck squamous cell carcinomas. *Oral Oncol*. 2008 Apr;44(4):335–44.
12. Ljungkvist ASE, Bussink J, Rijken PFJW, Kaanders JHAM, van der Kogel AJ, Denekamp J. Vascular architecture, hypoxia, and proliferation in first-generation xenografts of human head-and-neck squamous cell carcinomas. *Int J Radiation Oncology Biol Phys*. 2002;54(1).
13. Pajonk F, Vlashi E, McBride WH. Radiation resistance of cancer stem cells: The 4 R's of radiobiology revisited. Vol. 28, *Stem Cells*. 2010. p. 639–48.
14. Gaddikeri S, Gaddikeri RS, Taylor T, Anzai Y. Dynamic contrast-enhanced MR imaging in head and neck cancer: Techniques and clinical applications. Vol. 37, *American Journal of Neuroradiology*. American Society of Neuroradiology; 2016. p. 588–95.
15. Rogosnitzky M, Branch S. Gadolinium-based contrast agent toxicity: a review of known and proposed mechanisms. Vol. 29, *BioMetals*. Springer Netherlands; 2016. p. 365–76.

16. Gupta A, Dunlop A, Mitchell A, McQuaid D, Nill S, Barnes H, et al. Online adaptive radiotherapy for head and neck cancers on the MR linear Accelerator: Introducing a novel modified Adapt-to-Shape approach. *Clin Transl Radiat Oncol*. 2022 Jan 1;32:48–51.
17. Panek R, Welsh L, Baker LCJ, Schmidt MA, Wong KH, Riddell AM, et al. Noninvasive imaging of cycling hypoxia in head and neck cancer using intrinsic susceptibility MRI. *Clinical Cancer Research*. 2017 Aug 1;23(15):4233–41.
18. Bakdash JZ, Marusich LR. Repeated measures correlation. *Front Psychol*. 2017 Apr 7;8(MAR).
19. Lu Y, Jansen JFA, Mazaheri Y, Stambuk HE, Koutcher JA, Shukla-Dave A. Extension of the intravoxel incoherent motion model to non-gaussian diffusion in head and neck cancer. *Journal of Magnetic Resonance Imaging*. 2012 Nov;36(5):1088–96.
20. Xu XQ, Choi YJ, Sung YS, Yoon RG, Jang SW, Park JE, et al. Intravoxel incoherent motion MR imaging in the head and neck: Correlation with dynamic contrast-enhanced MR imaging and diffusion-weighted imaging. *Korean J Radiol*. 2016 Sep 1;17(5):641–9.
21. Sumi M, Nakamura T. Head and neck tumors: Assessment of perfusion-related parameters and diffusion coefficients based on the intravoxel incoherent motion model. *American Journal of Neuroradiology*. 2013 Feb;34(2):410–6.
22. Noij DP, Martens RM, Marcus JT, de Bree R, Leemans CR, Castelijns JA, et al. Intravoxel incoherent motion magnetic resonance imaging in head and neck cancer: A systematic review of the diagnostic and prognostic value. Vol. 68, *Oral Oncology*. Elsevier Ltd; 2017. p. 81–91.
23. Song Q, Li F, Chen X, Wang J, Liu H, Cheng Y. Early detection treatment response for head and neck carcinomas using intravoxel incoherent motion-magnetic resonance imaging: A meta-analysis. Vol. 50, *Dentomaxillofacial Radiology*. British Institute of Radiology; 2020.
24. Ding Y, Hazle JD, Mohamed ASR, Frank SJ, Hobbs BP, Colen RR, et al. Intravoxel incoherent motion imaging kinetics during chemoradiotherapy for human papillomavirus-associated squamous cell carcinoma of the oropharynx: Preliminary results from a prospective pilot study. *NMR Biomed*. 2015 Dec 1;28(12):1645–54.
25. Hauser T, Essig M, Jensen A, Gerigk L, Laun FB, Münter M, et al. Characterization and therapy monitoring of head and neck carcinomas using diffusion-imaging-based intravoxel incoherent motion parameters - Preliminary results. *Neuroradiology*. 2013 May;55(5):527–36.
26. Cao Y, Popovtzer A, Li D, Chepeha DB, Moyer JS, Prince ME, et al. Early Prediction of Outcome in Advanced Head-and-Neck Cancer Based on Tumor Blood Volume Alterations During Therapy: A Prospective Study. *Int J Radiat Oncol Biol Phys*. 2008 Dec 1;72(5):1287–90.
27. Logothetis NK. The Underpinnings of the BOLD Functional Magnetic Resonance Imaging Signal. *The Journal of Neuroscience*. 2003;23(10).
28. Robinson SP, Rijken PFJW, Howe FA, McSheehy PMJ, van der Sanden BPJ, Heerschap A, et al. Tumor vascular architecture and function evaluated by non-invasive susceptibility MRI methods and immunohistochemistry. *Journal of Magnetic Resonance Imaging*. 2003 Apr 1;17(4):445–54.
29. Lee P, Chandel NS, Simon MC. Cellular adaptation to hypoxia through hypoxia inducible factors and beyond. Vol. 21, *Nature Reviews Molecular Cell Biology*. Nature Research; 2020. p. 268–83.
30. Sebestyén A, Kopper L, Dankó T, Tímár J. Hypoxia Signaling in Cancer: From Basics to Clinical Practice. Vol. 27, *Pathology and Oncology Research*. Frontiers Media S.A.; 2021.
31. O'Connor JPB, Robinson SP, Waterton JC. Imaging tumour hypoxia with oxygen-enhanced MRI and BOLD MRI. Vol. 92, *British Journal of Radiology*. British Institute of Radiology; 2019.

32. Janssens GO, Rademakers SE, Terhaard CH, Doornaert PA, Bijl HP, van Ende P den, et al. Accelerated radiotherapy with carbogen and nicotinamide for laryngeal cancer: Results of a phase III randomized trial. *Journal of Clinical Oncology*. 2012 May 20;30(15):1777–83.
33. Alonzi R, Padhani AR, Maxwell RJ, Taylor NJ, Stirling JJ, Wilson JI, et al. Carbogen breathing increases prostate cancer oxygenation: A translational MRI study in murine xenografts and humans. *Br J Cancer*. 2009 Feb 24;100(4):644–8.
34. Punwani S, Ordidge RJ, Cooper CE, Amess P, Clemence M. MRI measurements of cerebral deoxyhaemoglobin concentration [dHb]Dcorrelation with near infrared spectroscopy (NIRS). *NMR Biomed*. 1998;11:281–9.
35. Rijpkema M, Ham Kaanders J, M Joosten FB, van der Kogel AJ, Heerschap A. Effects of breathing a hyperoxic hypercapnic gas mixture on blood oxygenation and vascularity of head-and-neck tumors as measured by magnetic resonance imaging. *Int J Radiation Oncology Biol Phys*. 2002;53(5):1185–91.
36. Baudelet C, Gallez B. How does blood oxygen level-dependent (BOLD) contrast correlate with oxygen partial pressure (pO₂) inside tumors? *Magn Reson Med*. 2002 Dec 1;48(6):980–6.
37. Chopra S, Foltz WD, Milosevic MF, Toi A, Bristow RG, Ménard C, et al. Comparing oxygen-sensitive MRI (BOLD R₂*) with oxygen electrode measurements: A pilot study in men with prostate cancer. *Int J Radiat Biol*. 2009 Sep;85(9):805–13.
38. Baudelet C, Gallez B. How does blood oxygen level-dependent (BOLD) contrast correlate with oxygen partial pressure (pO₂) inside tumors? *Magn Reson Med*. 2002 Dec 1;48(6):980–6.
39. Głowiczki ML, Glockner J, Gomez SI, Romero JC, Lerman LO, McKusick M, et al. Comparison of 1.5 and 3 T BOLD MR to study oxygenation of kidney cortex and medulla in human renovascular disease. *Invest Radiol*. 2009;44(9):566–71.
40. Mueller-klieser W, Vaupel P, Manz R, Schmidseder R. Intracapillary oxyhemoglobin saturation of malignant tumors in humans. *Int J Radiat Oncology Biol Phys*. 1981;7:1397–404.
41. Hoskin PJ, Carnell DM, Taylor NJ, Smith RE, Stirling JJ, Daley FM, et al. Hypoxia in Prostate Cancer: Correlation of BOLD-MRI With Pimonidazole Immunohistochemistry-Initial Observations. *Int J Radiat Oncol Biol Phys*. 2007 Jul 15;68(4):1065–71.
42. O'Connor JPB, Boulton JKR, Jamin Y, Babur M, Finegan KG, Williams KJ, et al. Oxygen-enhanced MRI accurately identifies, quantifies, and maps tumor hypoxia in preclinical cancer models. *Cancer Res*. 2016 Feb 15;76(4):787–95.
43. Little RA, Jamin Y, Boulton JKR, Naish JH, Watson Y, Cheung S, et al. Mapping hypoxia in renal carcinoma with oxygen-enhanced MRI: Comparison with intrinsic susceptibility MRI and pathology. *Radiology*. 2018 Sep 1;288(3):739–47.
44. Connor O, Robinson JP, Waterton SP. Imaging tumour hypoxia with oxygen-enhanced MRI and BOLD MRI. Vol. 92, *Br J Radiol*. 2019.
45. Wiedenmann N, Bunea H, Rischke HC, Bunea A, Majerus L, Bielak L, et al. Effect of radiochemotherapy on T₂* MRI in HNSCC and its relation to FMISO PET derived hypoxia and FDG PET. *Radiation Oncology*. 2018 Aug 29;13(1).
46. O'Connor JPB, Aboagye EO, Adams JE, Aerts HJWL, Barrington SF, Beer AJ, et al. Imaging biomarker roadmap for cancer studies. *Nat Rev Clin Oncol*. 2017 Feb 20;14(3):169–86.
47. Christen T, Bolar DS, Zaharchuk G. Imaging brain oxygenation with MRI using blood oxygenation approaches: Methods, validation, and clinical applications. Vol. 34, *American Journal of Neuroradiology*. 2013. p. 1113–23.

48. Chavhan GB, Babyn PS, Thomas B, Shroff MM, Mark Haacke E. Principles, techniques, and applications of T2*-based MR imaging and its special applications. *Radiographics*. 2009 Sep;29(5):1433–49.
49. Dmitriy J, Yablonskiy A. Quantitation of Intrinsic Magnetic Susceptibility-Related Effects in a Tissue Matrix. *Phantom Studv. Magn Reson Med* . 1998;39(3).
50. Sohlin MC, Schad LR. Susceptibility-related MR signal dephasing under nonstatic conditions: Experimental verification and consequences for qBOLD measurements. *Journal of Magnetic Resonance Imaging*. 2011 Feb;33(2):417–25.

4 CHAPTER 4: ANATOMICAL-ADAPTIVE RADIOTHERAPY FOR EARLY-STAGE SQUAMOUS CELL CANCERS OF THE GLOTTIS

4.1 Introduction

Treatment of early-stage glottic SCC (ESGC, T1-2, N0) in the United Kingdom traditionally involves irradiation of the whole larynx, with PTV typically defined from the inferior edge of the hyoid to the inferior edge of the cricoid cartilages. The resultant irradiation fields are typically used to treat a CTV that covers any potential microscopic disease within the supra/sub-glottic regions and an Internal Target Volume (ITV) that accounts for any laryngeal and tumour motion during deglutition, although an ITV is not typically defined during delineation. The equivalent surgical management option for visible and accessible disease is more focal transoral laser microsurgery. There are no randomised-controlled trials comparing surgery against radiotherapy, but cancer-specific survival outcomes are deemed equivalent between the two strategies (1,2). Therefore, there is interest in shifting towards personalised target delineation to either account for or totally exclude swallow-related motion and minimise irradiation of normal tissues and OARs.

The whole larynx is not a fixed structure as its components, such as the vocal cords or thyroid cartilage, move independently of other surrounding soft tissues. The rationale for this project was to investigate the motion of the hyoid bone and laryngeal structures including the evolution of motion-related changes over the course of a patient's radiotherapy. The findings from these analyses can subsequently help to determine whether individualised patient treatment volumes that account for gross disease and any motion can improve the dosimetry to surrounding OARs, when compared to conventional radiotherapy volumes that cover the whole larynx.

4.2 Aims and Hypotheses

i) **Aim:**

- To retrospectively analyse cases of ESGC previously treated with 3D-CRT at The Royal Marsden Hospital to determine toxicity rates and the dose to OARs.

Hypothesis:

- Dose to both carotid arteries, IPCM and thyroid gland will be above OAR constraints for grade ≥ 3 toxicities.

ii) **Aims:**

- To quantify the motion of laryngeal structures in three dimensions using cine-MRI on the MR-Linac.
- To assess prospectively longitudinal changes in laryngeal motion over the course of radiotherapy.

Hypotheses:

- Laryngeal motion in ESGC will be greatest in the cranio-caudal and least in the left-right axes.
- Laryngeal motion will reduce over the course of radiotherapy due to radiotherapy-related odynophagia.

iii) **Aims:**

- To determine patient-specific ITV margins based on the motion studies.
- To produce and compare whole-larynx and individualised radiotherapy plans using the C-arm and MR-Linac-based modalities to analyse the dosimetry to critical OARs.

Hypothesis:

- VMAT/IMRT plans on the C-arm linear accelerator/MR-Linac are feasible and can be delivered to treat ESGC with smaller targets that account for patient-specific laryngeal motion, with reduction of dose to OARs, such as the carotid arteries.

4.3 Methods

4.3.1 Patient Selection

4.3.1.1 Radiotherapy Audit

The local HNC database was screened for all patients with ESGC (T1-2 N0) who received radical radiotherapy (55 Gy in 20 fractions over 4 weeks or 50 Gy in 16 fractions over 3 weeks) using a 3D-CRT technique since 2016. RayStation (V12.0.0.932, RaySearch Laboratories AB, Stockholm, Sweden) TPS was utilised to acquire dosimetry data for the relevant OARs. Electronic patient record systems were utilised to acquire patients' demographics, toxicities (as per the National Cancer Institute Common Terminology Criteria for Adverse Events version 3.0) and outcome data.

4.3.1.2 Laryngeal Motion Study

Patient with ESGC receiving radical radiotherapy, at doses of either 55 Gy in 20 fractions over 4 weeks or 50 Gy in 16 fractions over 3 weeks, were recruited into PRIMER (NCT02973828) and MOMENTUM (NCT04075305) studies. Patients were consented for up to three cine-MRI sessions on the Elekta Unity MR-Linac (Elekta AB, Stockholm, Sweden) at the beginning (fractions 1-4), middle (fractions 9-11) and end (fractions 16-20) of radiotherapy. Patients were positioned using the same setup instructions as for their planning CTs, in five-point thermoplastic head shells and knee rests (Figure 4-1).

4.3.2 PHASE 1: Image Acquisition and Analyses

4.3.2.1 Cine-MRI

The cine-MR sequence allowed imaging of a single anatomical slice in a single plane at any time point. To capture the full extent of motion, each imaging session scanned three anatomical planes separately (axial, coronal and sagittal) for three minutes each, ensuring the selected scanning plane captured the relevant laryngeal structures. Each three-minute scan session consisted of two minutes of scanning at rest, (where the patient was free to swallow at their natural rate), and one minute of active swallowing every 10-15 seconds (Figure 4-2).



Figure 4-1, Patient setup on the Elekta Unity MR-Linear Accelerator.

a) standard patient setup, with head rest, knee rest and standardised head and neck coil; b)+c) volunteer with head shell, ear guards and flex coils in position.

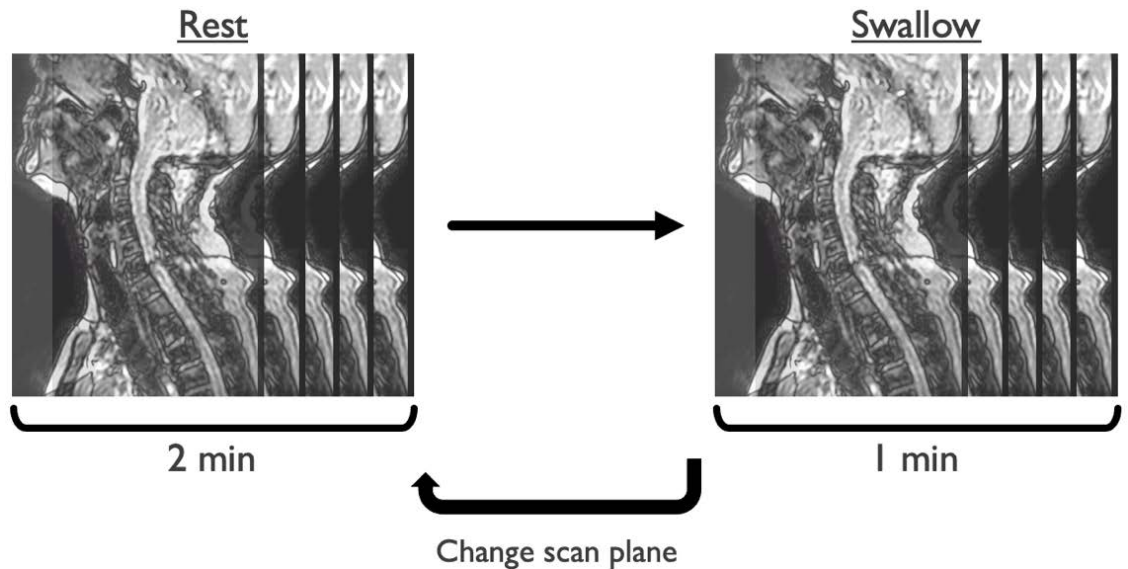


Figure 4-2, Cine-MR imaging protocol.

The larynx is imaged for a total of three minutes in each anatomical plane. Two minutes of respiratory motion and swallow frequency capture, followed by 1 minute of active swallowing to ensure the full extent of swallow is captured. The scanning plane is then changed and the process repeated, for a total scan time of 9 minutes. The same images were then used to contour structures for motion analyses and define individualised ITVs.

All cine-MRIs were performed on the Philips (Best, The Netherlands) 1.5 T MRI scanner, part of the Elekta Unity MR-Linac with a standardised head and neck receiver

coil (Figure 4-1). Cine-MRI parameters were set as the flip angle (FA) 35° , Echo Time (TE)/Repetition Time (TR) 2.298/4.577 ms, matrix 120, Bandwidth (BW) 479 Hz, Number of Signal Averages (NSA) 1 and pixel spacing of 0.8x0.8 mm. Cine-MRIs are taken at a rate of 4 frames per second.

4.3.2.2 Motion Analysis

Prior in-house analyses of cine-MRIs of static phantoms demonstrated no geometric or anatomical distortions during image post-processing or importing (unpublished data). Therefore, cine-MRIs were anonymised and imported into RayStation TPS for all analyses.

Motion of the vocal cords, hyoid bone, cricoid and thyroid cartilages were measured in the cranio-caudal direction (Figure 4-3). Cranio-caudal motion was measured from the most inferior to the most superior position (Figure 4-4). Due to respiration-related tidal-wave motion of the larynx, this distance was halved to estimate the baseline position of each laryngeal substructure. It was from this baseline position that the maximal swallow distance was recorded.

The thyroid cartilage was noted to have a rotational component during deglutition because of the anterior pull on the superior aspect of the cartilage by the thyro-hyoid ligament. Therefore, the superior and inferior points of the thyroid cartilage were measured independently. Left-right motion of both vocal cords and carotid arteries were measured on the axial image sets. Patients' vertebral alignments were not always parallel to the treatment couch. Motion data in RayStation TPS would reflect superior-inferior motion along the plane of the couch rather than the true anatomical superior-inferior motion along the plane of the vertebrae. Therefore, actual spatial motion was captured to account for any anterior as well as superior components of motion of all laryngeal structures. Straight-line distances were calculated and reported using Pythagorean methods.

For each rest and active swallow image set, all measurements were performed in triplicate and a mean calculated. Swallow distances were measured from the one-minute active swallow image sets only. Frequencies of deglutition and respiration-related motion at rest were measured on the two-minute rest sequences only.

4.3.2.3 Duration of Deglutition

The cricoid cartilage had the best visibility on the cine-MRIs and was chosen as the surrogate for measuring duration of swallow. The starting position for swallow was defined as the baseline position of the cricoid cartilage as seen during rest. End of swallow was defined as the return of the cricoid cartilage to its starting position. The excursion time of the cricoid was measured in number of frames (0.25 seconds per frame) and the time recorded to the nearest quarter of a second.

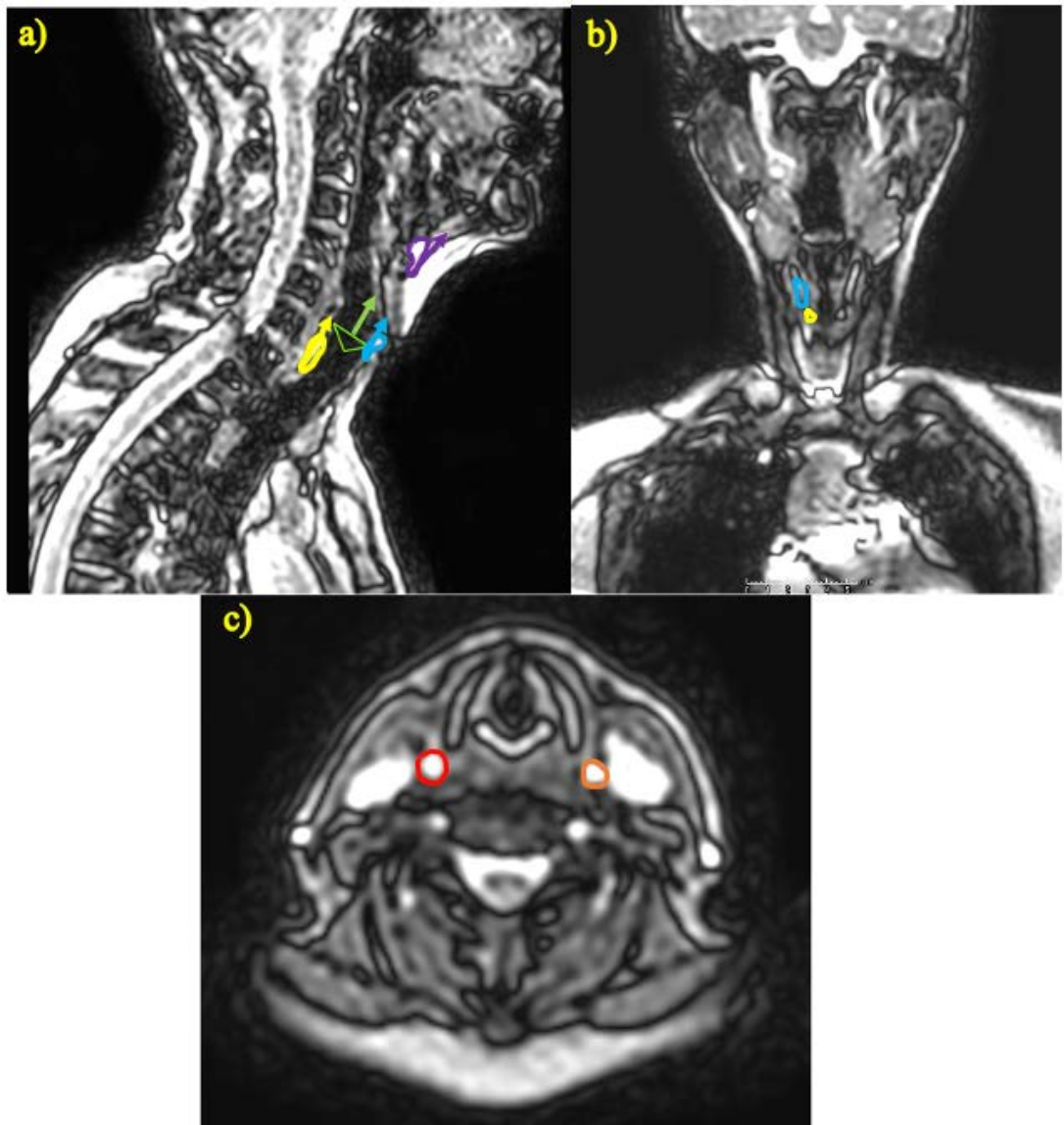


Figure 4-3, Motion analysis of laryngeal structures.

Scans in a) sagittal, b) coronal and c) axial planes captured motion of the vocal cords, carotid arteries, hyoid, cricoid and superior/inferior thyroid cartilages. The complete thyroid cartilage was not contoured as the points of measurements were either from the most superior or inferior points of this structure. Arrows denote vocal cords (green), right (red) and left (orange) carotid arteries, cricoid (yellow), thyroid (blue) cartilages and hyoid (purple) bone.

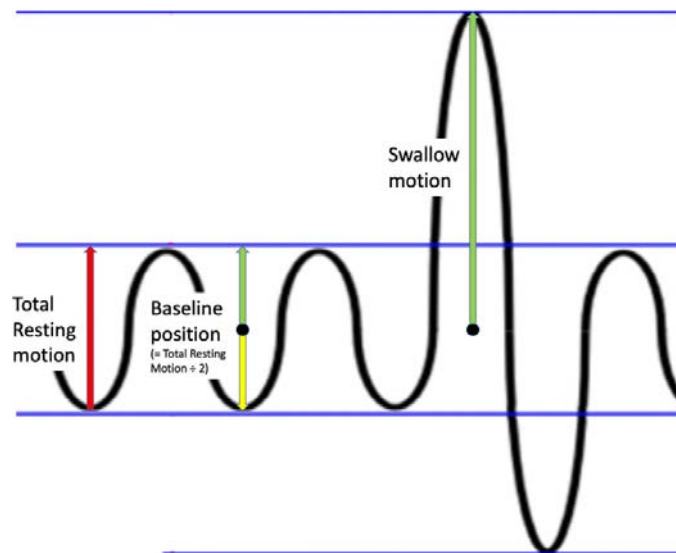


Figure 4-4, Definition of motion measurements.

Respiratory-related motion was recorded from the inferior-most to the superior-most position. This distance was halved and designated the baseline position. Swallow distances were also measured from the inferior most positions of each structure, however, half the resting distance was subtracted to determine swallow motion from baseline position.

4.3.3 PHASE 2: Radiotherapy Planning Studies

All patients were positioned supine with arms down. Patients were immobilised with a five-point thermoplastic head shell with neck neutral and a knee rest. A shoulder wedge was used if required to assist with neck positioning. A non-contrast enhanced planning CT scan from the vertex to carina was taken in 2 mm slices and 1x1 mm pixel size. All patients received radical radiotherapy for their ESGC using 3D-CRT plans designed by dosimetrists/physicists.

Three additional plans were created for each patient by me, under supervision by a dosimetrist. A non-adapted VMAT plan, termed “VMAT_NA,” was created to treat the standard-of-care volume that encompasses the whole larynx. After motion data analyses it was deemed unnecessary to incorporate swallow-related motion. Therefore, individualised resting motion and swallow frequency data were used to formulate personalised target volumes. Adapted-volume VMAT plans (“VMAT_A”) were created on RayStation to simulate treatment on a C-arm linear accelerator and IMRT plans (“IMRT_A”) on Research Monaco (V 5.59.02, Elekta AB, Stockholm, Sweden) to simulate treatment on the MR-Linac. All plans aimed to deliver 55 Gy in 20 fractions over 4 weeks.

The GTV was the involved vocal cord(s) (T1) including any disease extending into supraglottic or subglottic regions (T2). CTV was expanded from GTV using 0.5 cm (T1) or 1 cm (T2), edited off natural air and bone barriers. Based on the acquired motion data, individualised ITVs were used to account for respiratory-related motion only. Target definitions and planning parameters/constraints are listed in Table 4-1. Dose constraints for carotid arteries were based on suggested constraints after a literature review (3). The IPCM volume intersecting with the PTV was subtracted from IPCM to create a “Plan_IPCM,” which was used for optimisation in the VMAT_NA, VMAT_A and IMRT_A plans. A Plan_IPCM constraint of mean dose 47 Gy was based on the “Dysphagia-Aspiration Related Structures” study (D_{mean} 50 Gy), but adjusted for the higher dose per fraction of 2.75 Gy and alpha:beta ratio of 10 for acute toxicities (4). Final mean dose was reported for the complete IPCM structure.

4.3.3.1 3D-Conformal Radiotherapy Plans

Radiation plans were created using a virtual-simulation technique with 6 MV parallel-opposed fields or anterior-oblique fields for patients with a short neck. Field borders were adjusted to cover the PTV. Soft-tissue equivalent bolus (0.5 – 1 cm) was used over the midline anterior neck for cases with anterior commissure involvement if dosimetry coverage was poor. Dose was prescribed to the ICRU reference point, which was typically at the isocentre placed in the centre of the PTV. Except for the PTV, there were no dose objectives or constraints for any OARs with this modality.

4.3.3.2 Volumetric-Modulated Arc Radiotherapy Plans

All VMAT plans were produced using a collapsed-cone algorithm (V5.6) on RayStation TPS. Plan parameters included a single-beam arc (360°) using 6 MV flattening-filter-free photons, maximum 180 segments with gantry spacing of 2° , 40 maximum optimisation loops, dose-grid resolution of 0.25 cm^3 and a single isocentre. Dose was scaled and prescribed to the median (50%) of the PTV.

a) 3D-CRT/VMAT (VMAT NA) (conventional volumes)		
Structure	Recipe	Notes
CTV	Whole Larynx	
PTV	CTV + 3 mm isocentrically	
IPCM	Inferior Hyoid to superior Cricoid cartilages	For dose reporting only
Plan_IPCM	IPCM minus PTV	
Thyroid	Whole Thyroid gland	
Thyroid PRV	Thyroid gland + 3 mm	For dose reporting only
Spinal Cord	2 cm superior and inferior to PTV	
Spinal Cord PRV	Spinal Cord + 3 mm	
Ipsilateral & Contralateral carotid arteries (separate ROIs)	1 cm superior and inferior to PTV	
Ipsilateral & Contralateral carotid arteries PRV	Ipsilateral & Contralateral carotid arteries + 3 mm	
b) VMAT (VMAT A)/IMRT (IMRT A) (adapted volumes)		
Structure	Recipe	Notes
GTV	- Involved vocal cord for T1a/b - Full tumour extent for T2	
CTV	GTV + 0.5 cm (T1)/1 cm (T2)	
ITV	CTV + respiratory-related motion	
PTV	(CTV + ITV) + 3 mm isocentrically	
IPCM	Inferior Hyoid to superior Cricoid cartilages	For dose reporting only
Plan_IPCM	IPCM minus PTV	
Thyroid	Whole Thyroid gland	
Thyroid PRV	Thyroid gland + 3 mm	For dose reporting only
Spinal Cord	2 cm superior and inferior to PTV	
Spinal Cord PRV	Spinal Cord + 3 mm	
Ipsilateral & Contralateral carotid arteries (separate ROIs)	1 cm superior and inferior to PTV	
Ipsilateral & Contralateral carotid arteries PRV	Ipsilateral & Contralateral carotid arteries + 3 mm	
c) Planning Optimisation Objectives (for VMAT NA, VMAT A and IMRT A plans)		
Structure	Recipe	
PTV	Dmin 53.9 Gy Dmax 56.1 Gy Uniform Dose 55 Gy V54.85 Gy ≥ 50% V55.15 Gy ≤ 50% D95 ≥ 52.25 Gy Target EUD 55 Gy	
Spinal Cord	Dmax 25 Gy to 0.10 cm ³	
Spinal Cord PRV	Dmax 30 Gy to 0.10 cm ³	
Ipsilateral & Contralateral Carotid Arteries PRVs	Dmax 35 Gy to 0.10 cm ³ D50 < 10 Gy	
Plan IPCM	Dmean < 47 Gy	

Table 4-1, Radiotherapy planning target definitions.

a) volumes for conventional volumes, planned using either 3D-conformal radiotherapy (3D-CRT) or volumetric-modulated arc therapy (VMAT) techniques and, b) volumes for adapted volumes, planned using either VMAT or intensity-modulated radiotherapy (IMRT) techniques. Thyroid gland and inferior pharyngeal constrictor muscles (IPCM) were contoured for dose-reporting purposes only. c) Planning objectives were kept the same for all non-3D-CRT modalities. However, VMAT_{NA}, VMAT_A and IMRT_A plans were optimised to the “Plan_IPCM” structure. CTV (Clinical Target Volume); EUD (Equivalent Uniform Dose); GTV (Gross Tumour Volume); ITV (Internal Target Volume); PRV (Planning Risk Volume); PTV (Planning Target Volume); ROI (Region of Interest).

4.3.3.3 Intensity-Modulated Radiotherapy Plans

IMRT_A plans were created on Research Monaco using a Monte Carlo dose engine. Treatment plans consisted of nine-field step-and-shoot IMRT utilising 7 MV flattening-filter-free photons, (beam angles 145°, 95°, 65°, 30°, 0°, 330°, 295°, 265° and 215°). Maximum segments per beam 60, minimum segment width/area/monitor units 0.5 cm/4 cm²/6 and fluence smoothing set to medium. Plans were calculated with dose uncertainties of 2% and dose-grid resolution of 3 mm, with dose prescriptions to 50% of the PTV.

4.3.3.4 Impact of Swallow on Target Dosimetry

Individual-level data on swallow distance, frequency and duration, monitor units delivered per minute, total fraction delivery time and dosimetry data for 3D-CRT, VMAT_NA and IMRT_A were acquired. The percentage dose at the point of maximal ITV displacement during swallow was recorded. Based on this information, the percentage dose received by the superior ITV edge for the duration of swallow was calculated. Despite the trend for reduced frequency of swallow, it was assumed that the baseline frequency was maintained and the worst-case scenario was calculated. This was reported as the total dose delivered after 20 fractions.

4.3.4 Statistical Analysis

OAR dosimetry and outcome data from the audit were pooled and mean values reported with single standard deviations. Paired longitudinal data from motion of separate laryngeal structures were compared using Wilcoxon signed rank-sum test to assess for differences in motion between the start and end of radiotherapy. Swallow motion, frequency and duration data were presented as the mean of motion at each scanning time point (beginning, middle and end of radiotherapy) with single standard deviations. Motion directional data for each sub-structure are presented as the mean and single standard deviations. Wilcoxon signed rank-sum test was used to assess the significance of any differences in the dosimetry between the various planning modalities. All analysis was performed on Microsoft Excel (V16.33).

4.4 Results

4.4.1 Patient Demographics and Previous Dosimetry

One hundred and two patients were treated for ESGC between August 2017 and April 2022. Complete data from 38 patients were available for the retrospective analysis of radiation dosimetry and toxicities (Table 4-2). The mean duration of documented follow up was 23.9 months (SD 12.8 months). All patients received 3D-CRT with either parallel-opposed (n=26) or anterior-oblique (n=12) beam arrangements. Seventy-nine percent of patients were male, with 84% of patients having been current or previous smokers. Seventy-one percent of patients reported a pain score of ≥ 5 (out of 10), with 47% of patients experiencing up to grade-2 dysphagia. Feeding tube data were available for all 102 patients and 8% of patients required either a nasogastric tube or radiologically-inserted gastrostomy.

Mean dose to both carotid arteries was 45.43 Gy (SD 4.83 Gy) and maximum point dose to both carotid arteries was 57.2 Gy (SD 1.22 Gy). Compared to the anterior-oblique beam arrangement, mean carotid doses were 3 Gy higher with parallel-opposed beam arrangement (Table 4-2). Maximum spinal cord doses were consequently higher with anterior-oblique (17.67 Gy) than with parallel-opposed (5.7 Gy) beam arrangements. Structures more central and proximal to the CTV such as the arytenoid cartilages and IPCM received full prescription doses across both 3D-CRT planning techniques. Mean dose to the thyroid gland was variable due to anatomical differences in size of the organ between individuals.

a) Patient Demographics and Toxicity Data (n)						
Mean Age (range, years)	67.58 (41-94)					
Gender	Male (30) Female (8)					
Smoking History	Never smoked (6) Ex-smoker (22) Current smoker (10)					
T-Stage	1a (19) 1b (3) 2 (16)					
Anterior Commissure involvement	Yes (16) No (22)					
Feeding tube placement	Yes (8, median duration 23 days (range 4 - 82 days)) No (79)					
Dysphagia	Intra-treatment: Grade 0 (2); Grade 1 (13); Grade 2 (18); Grade 3 (2)					
	Post-treatment: Grade 0 (29); Grade 1 (5); Grade 2 (1); Grade 3 (0)					
Pain Score	Intra-treatment: Score ≥ 5 (27)					
	Post-treatment: Scores ≥ 5 (0)					
Skin Toxicity	Grade 0 (2); Grade 1 (15); Grade 2 (16); Grade 3 (2)					
Xerostomia	Intra-treatment: Grade 0 (29); Grade 1 (5); Grade 2 (1); Grade 3 (0)					
	Post-treatment: Grade 0 (31); Grade 1 (2); Grade 2 (2); Grade 3 (0)					
b) Radiation Dosimetry Data						
<u>Organs at Risk</u>	3D-CRT (n=38)		Parallel-opposed pair (n=26)		Anterior-Oblique (n=12)	
	Dmean (SD, Gy)	Dmax to 1cm ³ (SD, Gy)	Dmean (SD, Gy)	Dmax to 1cm ³ (SD, Gy)	Dmean (SD, Gy)	Dmax to 1cm ³ (SD, Gy)
Carotid (ipsilateral)	45.49 (4.67)	57.24 (1.16)	46.48 (4.22)	57.28 (1.3)	43.21 (4.88)	57.14 (0.85)
Carotid (contralateral)	45.37 (4.99)	57.16 (1.28)	46.38 (4.53)	57.16 (1.45)	43.18 (5.43)	57.15 (0.84)
Arytenoid (ipsilateral)	55.84 (1.24)	-	55.76 (1.43)	-	56.01 (0.67)	-
Arytenoid (contralateral)	55.94 (0.97)	-	55.92 (1.11)	-	55.99 (0.64)	-
Inferior pharyngeal constrictor muscle	54.68 (1.15)	-	54.47 (1.20)	-	55.14 (0.89)	-
Spinal Cord	-	10.05 (9.86)	-	5.7 (3.32)	-	17.67 (12.77)
Thyroid Gland	27.14 (8.94)	-	25.43 (8.47)	-	17.68 (12.77)	-

Table 4-2, Patient demographics and radiation dosimetry.

Historic data from patients treated with 3D-Conformal Radiotherapy (3D-CRT). a) Patient demographics and toxicity data are reported. The total number of evaluable patients was 38, with 3 patients still on treatment at the time of data capture, for which reason post-treatment toxicity data is not available. Feeding tube data were available for 102 patients. b) Radiation dosimetry data shown for patients receiving 55 Gy in 20 fractions over 4 weeks.

4.4.2 PHASE 1: Laryngeal Motion

Fifteen patients were prospectively recruited for laryngeal motion analyses. Seven patients had T1 (T1a = 6 and T1b = 1) and seven patients had T2 SCCs of the glottis. One patient had very limited metastatic laryngeal SCC, with a single mediastinal node only. This patient was recruited for motion capture study only and subsequently excluded from the phase 2 ART-planning studies. Eleven patients were male and three females. All patients completed their course of radical radiotherapy. Seven patients had cine-MRI at all 3 time points, five patients had 2 and three patients had 1.

Tables 4-3a and b display the motion data from the different laryngeal components at rest and swallow, respectively. Figure 4-5 displays the swallow-related motion data only. Swallow-related data show the greatest extent of motion in the cranio-caudal plane, with mean motion of the laryngeal structures between 20.2 – 24.8 mm. The mean cranio-caudal motion of the hyoid bone was 17.1 mm. The differences in swallow-related motion between the beginning and end of patients' radiotherapy were significant in the left-right directions for the ipsilateral and contralateral carotid arteries only (p-value <0.05). There were no significant differences or trends in swallow-related motion for any other structures in the cranio-caudal direction.

Due to variations in patient set-up positions and vertebral alignments, the true spatial motion of structures, with data on any anterior components of motion, were also captured (Figure 4-6). Motion of the superior (mean 20.6 mm, SD 2.2 mm) and inferior (mean 21.2 mm, SD 1.7 mm) components of the thyroid and cricoid (mean 22.7 mm, SD 0.7 mm) cartilages were predominantly in the cranial direction. However, there was an anterior component of motion in all these structures (grouped mean 6.6 mm, SD 1.5 mm). The hyoid bone had greater anterior (mean 9.9 mm, SD 1.2 mm) and lesser cranial (mean 13.4 mm, SD 1.2 mm) motion compared to the laryngeal structures.

Table 4-3c displays the data on the frequency and duration of swallow. A trend for decreasing number of swallows per minute was noted (p-value >0.05). The maximum mean rate of swallow across all patients was 1 per minute (SD 1). The mean duration of each swallow event was 1.5 seconds (SD 0.4 seconds) with no significant change during radiotherapy (p-value >0.05).

a)	Structure	REST		
		Time-point		
		1 (mm (SD)) (n=15)	2 (mm (SD)) (n=11)	3 (mm (SD)) (n=9)
	Hyoid	1.8 (0.9)	1.5 (1.4)	1.4 (1.0)
	Thyroid	3.0 (2.4)	3.1 (1.7)	3.0 (2.3)
	Cricoid	3.0 (2.4)	3.2 (2.3)	3.3 (2.3)
	Vocal Cords (cranio-caudal)	2.8 (2.4)	2.9 (2.1)	2.8 (2.8)
	Vocal Cord (ipsilateral, left-right)	1.8 (1.2)	1.7 (1.1)	1.6 (0.8)
	Vocal Cord (contralateral, left-right)	1.8 (0.6)	1.5 (1.0)	1.4 (0.6)
b)	Structure	SWALLOW		
		Time-point		
		1 (mm (SD)) (n=15)	2 (mm (SD)) (n=11)	3 (mm (SD)) (n=9)
	Hyoid	16.9 (4.4)	17.1 (4.6)	13.6 (7.9)
	Thyroid (superior pole)	20.2 (7.1)	23.4 (5.7)	22.8 (3.3)
	Thyroid (inferior pole)	20.6 (5.5)	23.1 (5.5)	22.1 (3.8)
	Cricoid	23.4 (5.9)	23.8 (5)	21.6 (4.8)
	Vocal Cords (cranio-caudal)	22.6 (5.3)	24.8 (5.1)	22.1 (3.4)
	Carotid Artery (ipsilateral, left-right)	3.8 (2.5)	4.6 (3.6)	5.4 (3.6)
	Carotid Artery (contralateral, left-right))	3.4 (2.3)	4.0 (2.7)	5.0 (2.0)
c)		Time Point		
		1 (n=15)	2 (n=11)	3 (n=9)
	Mean number of swallows per minute (SD)	1 (1)	0.6 (0.8)	0.3 (0.4)
	Mean duration of swallows (s, (SD))	1.5 (0.3)	1.5 (0.4)	1.5 (0.3)

Table 4-3, Laryngeal Motion (mm), Duration and Frequency Data.

Data are shown for laryngeal sub-structure motion at a) rest and b) swallow at three time points spread over the course of patients' radiotherapy. Unless stated otherwise, all measurements are cranio-caudal motion for each structure. The mean numbers and durations of swallows across all patients are shown in c).

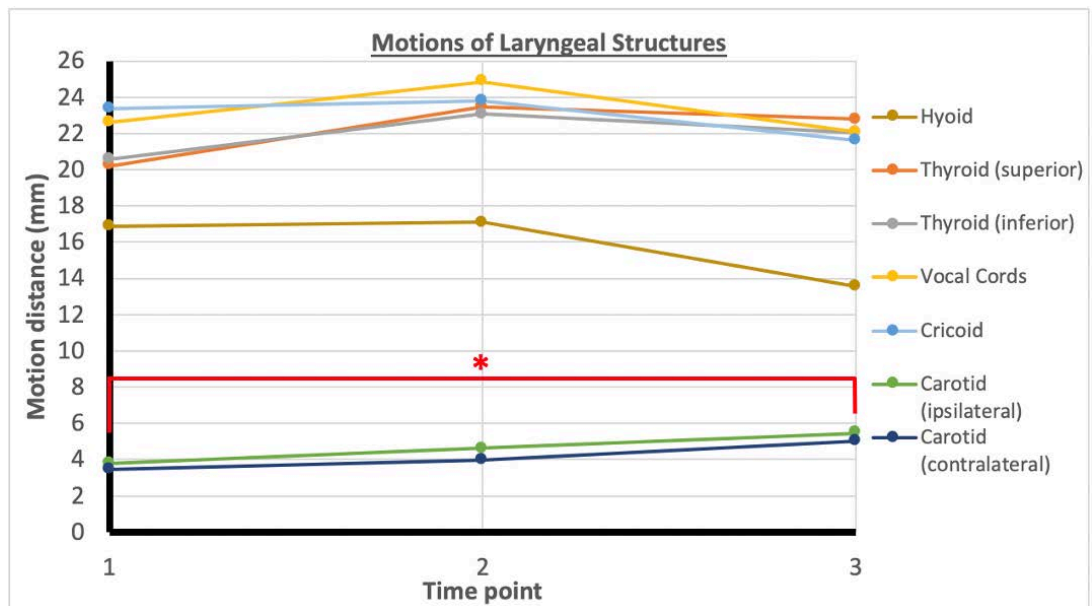


Figure 4-5, Swallow-Related Motion Data.

Swallow-related motion for laryngeal sub-structures, hyoid bone and both carotid arteries are shown. Motion for carotid arteries is measured in the left-right direction and all other structures are cranio-caudal directions. Standard deviations for the mean measurements are reported in Table 4-3b. *Differences in motion of both carotid arteries were significant between the start and end of radiotherapy.

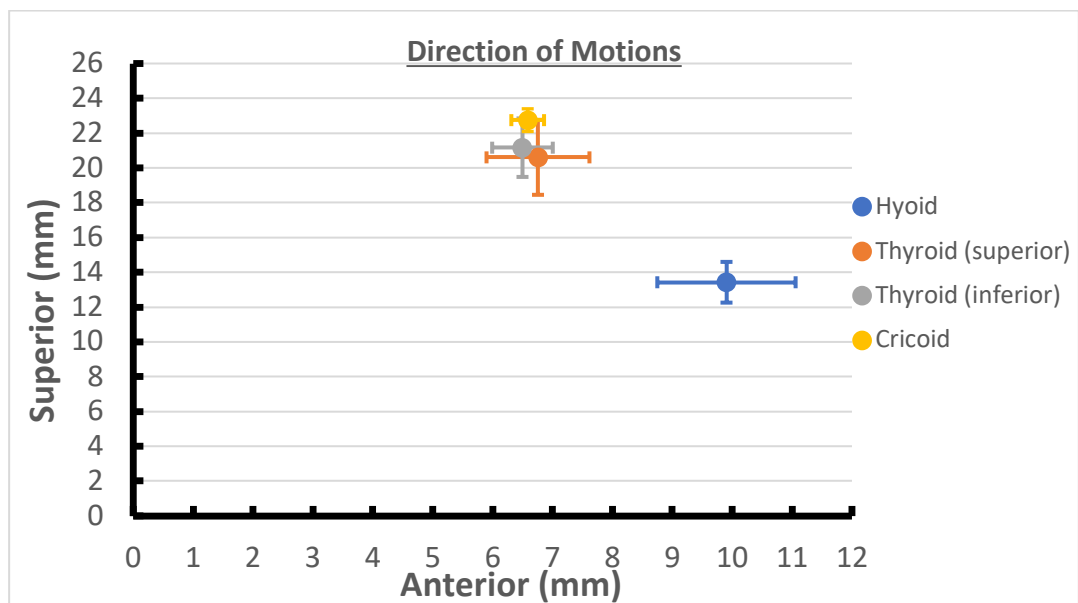


Figure 4-6, Motion Breakdown into Anterior and Superior Components.

Motion of laryngeal sub-components and hyoid bone are separated into cranial and anterior elements to demonstrate the variations in patient set-up and to highlight the lack of perpendicular vertebral alignment with the treatment couch. Error bars denote single standard deviations.

4.4.3 PHASE 2: Adaptive-Radiotherapy Planning

Fourteen patients with ESGC were recruited and had ART plans generated. 3D-CRT and VMAT_NA failed 5 constraints each. VMAT_A was the best performing modality with failures only occurring in the ipsilateral carotid artery V10 constraint. IMRT_A

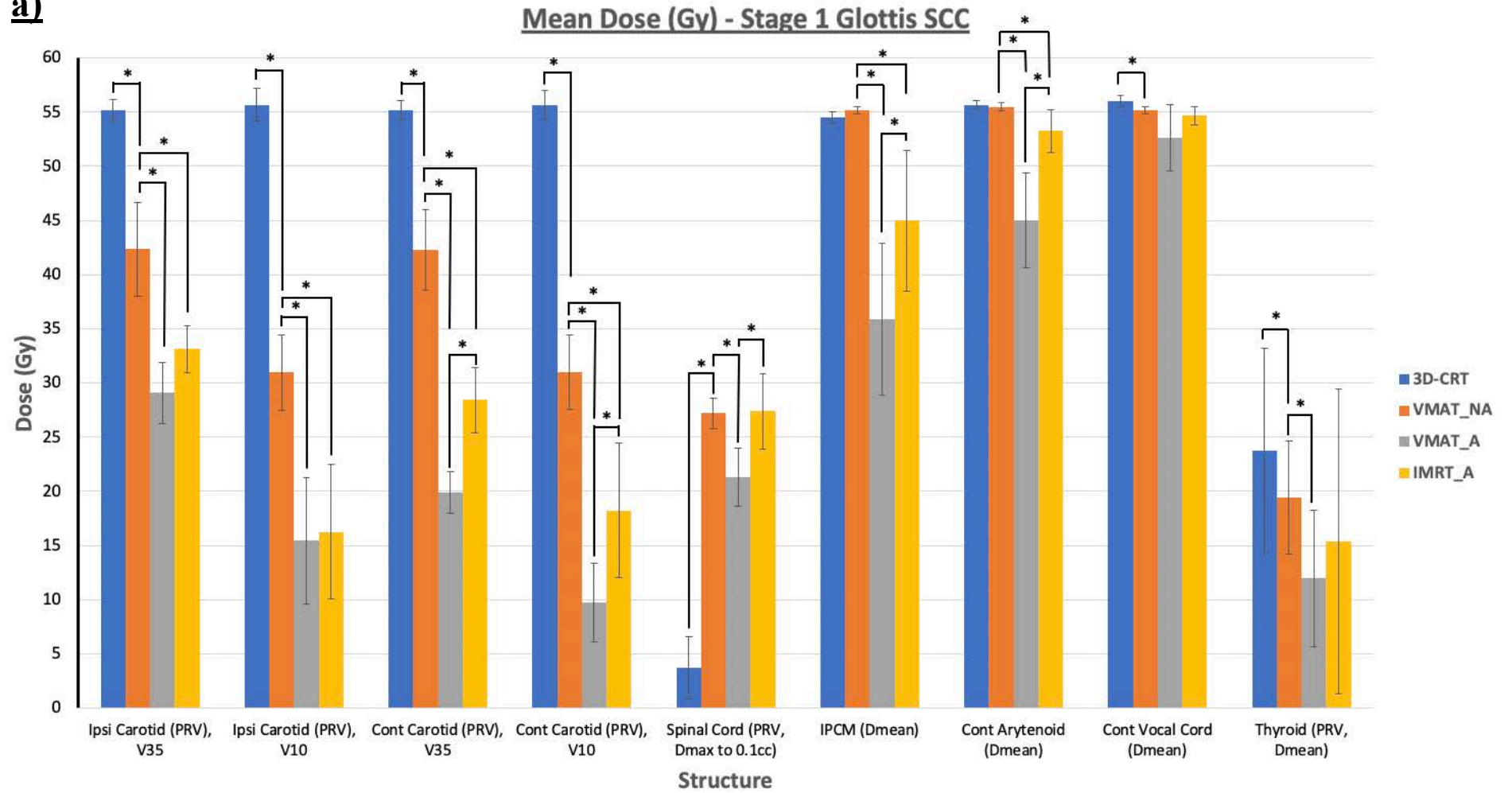
failed both ipsilateral and contralateral carotid artery V10 constraints. The mean dose by which constraints failed (or passed) are displayed in Table 4-4. The number of all-constraint failures were similar for stages T1 and T2.

T-Stage	Structure	Dose Constraint	Planning Modality			
			3D-CRT (Gy)	VMAT_NA (Gy)	VMAT_A (Gy)	IMRT_A (Gy)
T1	PTV	D99 \geq 49.5	1.7 (1.3)	0.2 (1.1)	1.3 (0.3)	1.6 (1.0)
		D95 \geq 52.25	0.6 (0.9)	0.1 (0.4)	0 (0.2)	0.4 (0.3)
		D5 \leq 57.75	-1.1 (0.3)	-1.3 (0.3)	-1.8 (0.1)	-0.3 (0.4)
		D2 \leq 60.5	-3.6 (0.3)	-3.6 (0.3)	-4.3 (0.2)	-2.5 (0.5)
	Ipsilateral Carotid Artery (PRV)	V35 < 20%	20.2 (1.0)	7.3 (4.4)	-5.9 (2.9)	-1.9 (2.2)
		V10 < 50%	45.7 (1.5)	21.0 (3.5)	5.5 (5.8)	6.3 (6.2)
	Contralateral Carotid Artery (PRV)	V35 < 20%	20.1 (0.9)	7.3 (3.7)	-15.1 (1.9)	-6.6 (3.0)
		V10 < 50%	45.7 (1.4)	21.0 (3.4)	-0.2 (3.6)	8.2 (6.2)
	Spinal Cord (PRV)	Dmax 30 Gy to 0.1cm ³	-26.3 (2.8)	-2.8 (1.4)	-8.7 (2.7)	-2.6 (3.5)
	IPCM	Dmean < 50 Gy	4.5 (0.5)	5.2 (0.3)	-14.1 (7.0)	-5.0 (6.5)
Sum of optimal constraints failed			5	5	1	2
T2	PTV	D99 \geq 49.5	2.9 (0.6)	0.3 (1.0)	1.1 (0.6)	1.4 (2.3)
		D95 \geq 52.25	1.4 (0.4)	0.2 (0.4)	0.4 (0.7)	0.4 (0.7)
		D5 \leq 57.75	-1.1 (0.5)	-1.5 (0.4)	-1.9 (0.1)	-0.3 (0.2)
		D2 \leq 60.5	-3.6 (0.5)	-4.0 (0.5)	-4.4 (0.3)	-2.4 (0.3)
	Ipsilateral Carotid Artery (PRV)	V35 < 20%	20.1 (1.9)	7.1 (5.1)	0 (5.8)	-1.0 (5.9)
		V10 < 50%	46.0 (1.2)	21.7 (3.9)	13.8 (5.0)	5.8 (4.3)
	Contralateral Carotid Artery (PRV)	V35 < 20%	19.7 (3.0)	8.2 (4.1)	-9.6 (7.4)	-5.0 (4.2)
		V10 < 50%	45.7 (1.7)	22.1 (3.7)	-0.1 (0.5)	11.8 (3.1)
	Spinal Cord (PRV)	Dmax 30 Gy to 0.1cm ³	-19.9 (7.7)	-3.4 (2.6)	-7.0 (2.5)	-1.8 (4.4)
	IPCM	Dmean < 50 Gy	5.0 (0.7)	5.3 (0.5)	-5.3 (6.7)	-1.1 (4.8)
Sum of optimal constraints failed			5	5	1	2

Table 4-4, Dose Statistics for Patients Separated by T-Stage.

The mean dose deficits or surplus for each dose constraint are displayed, separated by T-stage. For example, in T1-stage tumours planned with 3D-CRT, the ipsilateral carotid artery V35 constraint failed by mean 20.2 Gy above the threshold. All doses are displayed in Gray with standard deviations in parentheses. Green cells denote dose constraints that were satisfied and yellow cells denote dose constraints that did not achieve optimal constraints. IPCM (Inferior Pharyngeal Constrictor Muscle); PRV (Planning Risk Volume).

a)



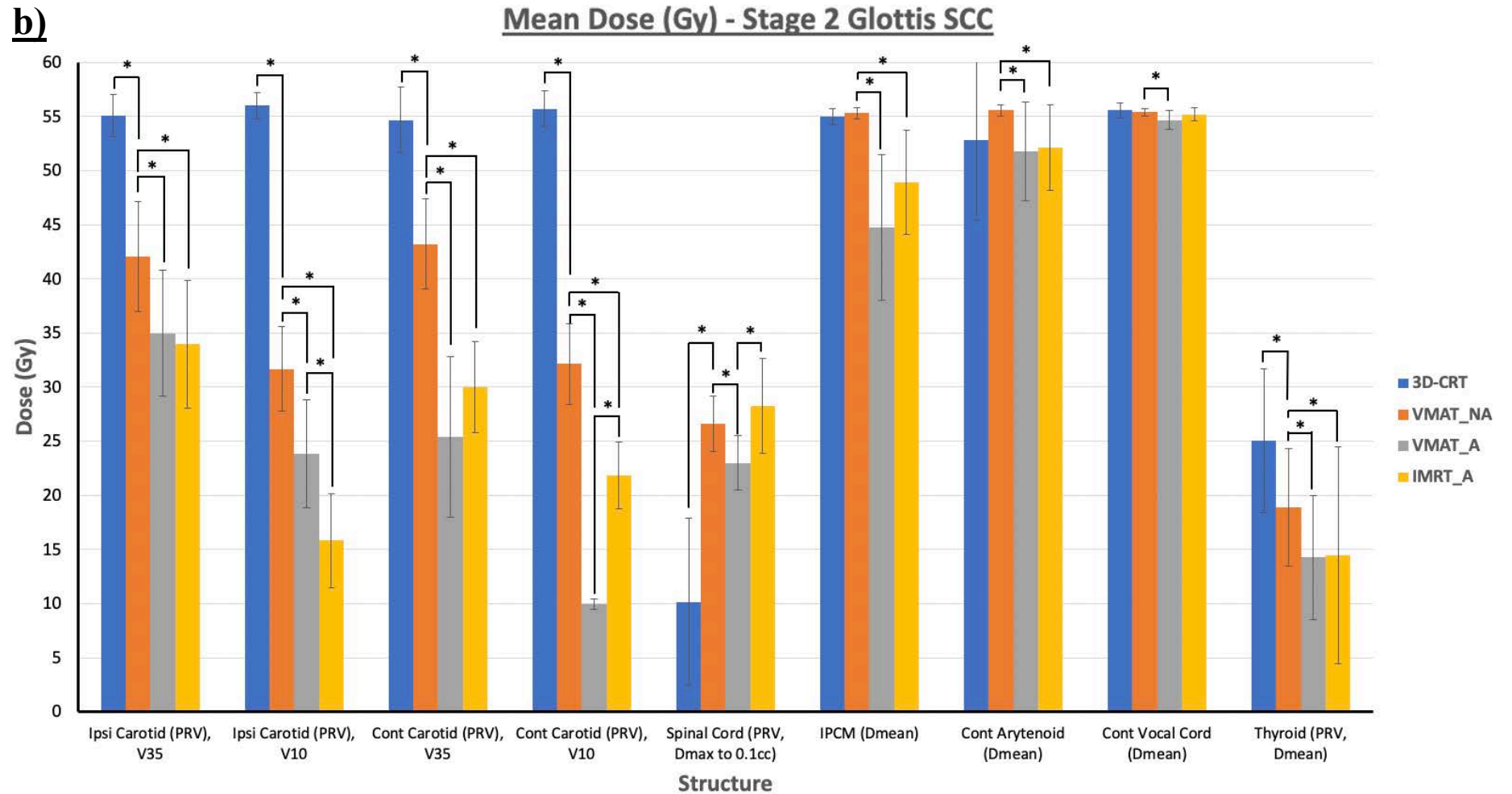


Figure 4-7, Mean doses for Organ at Risks.

Mean doses for a) Stage 1 (T1) and b) Stage 2 (T2) SCCs of the glottis are graphed with single standard deviations. *Significant difference ($p < 0.05$). Cont/Ipsi (Contralateral/Ipsilateral); IPCM (Inferior Pharyngeal Constrictor Muscle); PRV (Planning Risk Volume).

Dosimetric comparisons were made between (3D-CRT vs VMAT_NA), (VMAT_NA vs VMAT_A/IMRT_A) and (VMAT_A vs IMRT_A). Whole larynx volumes planned with either 3D-CRT or VMAT_NA delivered significantly higher mean doses to the ipsilateral and contralateral carotid arteries (Figures 4-7a and b). Detailed dosimetry data are listed in Appendix K. IMRT_A delivered a significantly lower mean ipsilateral carotid artery V35 (33.98 Gy) and V10 (15.81 Gy) doses in T2-stage tumours compared to VMAT_A (V35 34.96 Gy and V10 23.83 Gy), ($p < 0.05$). Conversely, VMAT_A delivered significantly lower doses to the contralateral carotid arteries in both T1 and T2-stage tumours ($p < 0.05$).

Mean maximum spinal cord doses were significantly higher with VMAT/IMRT techniques, with 3D-CRT delivering the lowest maximum spinal cord dose in T1 (3.7 Gy) and T2 (10.1 Gy) tumours. VMAT_A delivered the lowest maximum spinal cord dose out of the intensity-modulated methods for T1 (21.3 Gy) and T2 (23 Gy) tumours.

Adapted volume plans (VMAT_A and IMRT_A) significantly improved IPCM doses, with VMAT_A superior to IMRT_A in T1-stage tumours only (35.9 vs 45 Gy, respectively), ($p < 0.05$).

There was mild sparing of contralateral arytenoids and vocal cords from adapted volumes with small but significant differences in mean doses between VMAT_NA and VMAT_A/IMRT_A.

Mean dose to the thyroid glands were significantly lower with VMAT/IMRT techniques compared to 3D-CRT, with further significant sparing of the thyroid gland with adapted volumes compared to VMAT_NA, for both T1 and T2 tumours.

4.4.4 Impact of Swallowing on Dose Delivery

For a dose prescription of 55 Gy in 20 fractions, a mean dose of above 95% of the prescription (> 52.25 Gy) was achieved for VMAT_NA (54.33 Gy, SD 0.81), VMAT_A (53.85 Gy, SD 1.1) and IMRT_A (54.28 Gy, SD 1.34). A single patient with a T2-stage tumour would have received 94.7% of the dose with VMAT_A technique, but all other patients attained a minimum of 95% dose when accounting for swallowing.

4.5 Discussion

4.5.1 Phase 1 – Motion and Toxicity Analyses

The data reported in this chapter show that there is detectable cranio-caudal respiration-related motion of the larynx and hyoid bone and left-right motion of the vocal cords and carotid arteries using cine-MRI. Prior studies of laryngeal motion have utilised a variety of modalities such as videofluoroscopy (5,6), megavoltage/kilovoltage photons (7) and MRI (8,9). Bradley et al analysed the motion of tumours from a range of head and neck subsites, of which only five were glottic cancers (8). The MRI sequences employed by Bradley et al and Gurney-Champion et al had longer acquisition times that required post-processing to extract the motion data, leading to potential issues of missing minute fluctuations in motion and image registration errors (9).

Bruijnen et al have previously utilised cine-MRI to explore swallowing and resting motion in a variety of head and neck subsites, including 29 laryngeal cancers, and show that the mean resting cranio-caudal motion of the larynx is as much as 3.8 mm (10). Osman et al utilised 4D-CT to focus on vocal-cord motion as part of their work-up towards single vocal-cord irradiation (SVCI) and demonstrated limited vocal-cord motion at rest (11). Although other institutions have demonstrated the utility of cine-MRI based motion assessments on the MR-Linac for abdominal tumours (12,13), there are no published data on MR-Linac assessment of laryngeal motion. The data in this study are consistent with the reported literature, with similar magnitudes of motion recorded. The strength of this study lies in the homogenous group of patients compared to other MRI-based studies.

In addition, this project explored the patterns of change in swallowing and motion over the course of radiotherapy. It was hypothesised that progressively worsening toxicities such as mucositis, odynophagia and dysphagia would result in reduction in swallowing frequency and magnitude. The data presented here show a trend for decreasing frequency of swallow but not statistically significant owing to the lower

number of patients who managed all three planned scans. It was originally projected that 35 patients would be required to detect significant differences in motion, but more recruitment time would have been required to reach this target.

Large variations in motion between patients resulted in insignificant differences seen in degrees of motion of all laryngeal structures and the hyoid bone. This may be explained by the anatomical differences between subjects in terms of gender and height. The ipsilateral and contralateral carotid arteries were the only structures that demonstrated significant differences in motion between the beginning and end of radiotherapy, which may be a result of reduced dependence on patient height. van Asselen et al show that frequency of swallow is highest in the first five fractions of radiotherapy, after which frequency decreases until mid-treatment, before increasing in the last week of treatment, although still not as frequent as in the first week (7). Bahig et al report no differences in magnitudes of whole-larynx motion between the beginning and middle of treatment, but it is not described what anatomical part of the larynx was used to measure swallow (14).

Motion measurement techniques vary between institutions. In the respiratory cycle, it is known that exhalation is a longer event compared to inspiration with a relative ratio of 2-3:1 (15). Therefore, it would be expected that the larynx is located in the inferior most position for the majority of the rest period. However, measurements in this study were performed in the manner described in Figure 4-4 to increase consistency of readings as it was difficult to consistently establish the point of near-maximal exhalation. An assumption was therefore made that swallowing would start from a position that is mid-point between full expiration and inspiration. For this reason, resting motion data are reported as maximal motion of the structures at rest, whereas swallowing data are recorded as maximal motion from the point of maximal exhalation, subtracting half the respiration motion from the final value. Therefore, all motion data were interpreted and reported in the cranial direction only.

The progressively decreasing frequency of swallow and static durations of swallow throughout treatment deemed it unnecessary to account for swallow-related motion

within the ITV. Designation of the resting motion in the cranial direction only may have led to bias in the ITV margins by overestimating the resting motion in this direction. However, the resultant target definition and dosimetry from the planning studies would ultimately provide a more conservatively adapted plan.

All planning studies were performed using planning CTs that patients had for their clinically delivered radiotherapy. It is not standard practice at our institute to instruct patients not to swallow or maintain maximal exhalation during CT acquisition, although this approach has been reported to be feasible (9,11,16). Therefore, patients may have had planning CTs acquired in the inspiratory or swallowing phase and do not fully reflect the ideal clinical scenario. Thus, the planning data shown in this study reflect proof-of-principle to demonstrate that adapted-radiotherapy volumes are feasible.

The baseline audit was performed in order to gauge the toxicity profile and average dose statistics for a typical clinically-delivered course of radiotherapy for ESGCs. Grade 3 toxicities only occurred in two patients, with good recovery of toxicities across all patients who received radical radiotherapy. Dosimetric data from an extended population receiving 3D-CRT reflect what were seen in the planning studies. Maximum doses to the carotid arteries, contralateral arytenoid cartilage and vocal cord were above 100% of the prescribed dose, with no sparing of the IPCM. The majority (94.3%) of patients experienced Grade ≥ 1 dysphagia during treatment and a single patient in this group required a nasogastric tube for 15 days.

Detailed toxicity data was not available for all 102 patients and the dysphagia rates could not be compared against all 8 patients who had a feeding tube placed. Seventeen percent of patients had residual dysphagia of at least grade 1 at up to 8 weeks post-radiotherapy, possibly suggesting that although the maximum severity of toxicity from IPCM irradiation may not be as high, the low-grade dysfunction may be more prolonged, but further follow-up is required to investigate this. Peak swallow dysfunctions are reported at around three months post-radiotherapy with variable extents of recovery between different muscles of deglutition at twelve months (17).

The toxicity data was acquired retrospectively and the data set was incomplete due to the lack of clinical information recorded during clinical reviews. However, future work investigating ART for ESGC should prospectively collect patient reported outcome measures and objective toxicity data using a validated grading system such as the “Common Terminology Criteria for Adverse Events.”

4.5.2 Phase 2 – Planning Studies

Motion data revealed large variations in both resting and swallowing motion. Therefore, individualised ITV margins to account for resting motion were used. Motion capture data additionally showed that there was a significant anterior component of motion. The standard RayStation TPS volume-expansion function applies a universally anterior and superior expansion of the entire region of interest, resulting in an overestimated depiction of the ITV. Ideally, the expansions should have occurred in a plane parallel to the vertebrae to reflect the superior and anterior motion in physical space (as the vertebrae were not always parallel to the treatment couch). To avoid inconsistencies between cases, a universal method of superior and anterior expansions from the CTV to ITV was maintained, likely resulting in larger treatment volumes than intended.

The planning studies demonstrate improved dosimetry to OARs, as would be expected, when irradiating a smaller target. Whole-larynx target volumes failed a similar number of dose constraints regardless of whether treated with 3D-CRT or non-adapted VMAT (VMAT_NA) techniques. However, VMAT_NA significantly reduced dose to both carotid arteries whilst maintaining adequate dose to the target.

Adapted volume performances (VMAT_A and IMRT_A) were superior to non-adapted volumes as there were more consistently satisfied dose objectives. Fixed-field IMRT leaves less room for dose conformity in comparison to the VMAT technique and most likely explains the more frequently failing contralateral carotid artery V10 dose constraint. The majority of volumes abutted or overlapped the ipsilateral carotid artery

PRVs and it was not possible to optimally reduce the ipsilateral carotid artery exposure without compromising the PTV coverage.

Plan quality in IMRT can be improved by adding further beams or segments at the major cost of increased fraction delivery time. Estimated mean fraction delivery times with the IMRT_A plans in this study were already longer (167 s, SD 34) compared to VMAT_A (103 s, SD 4.8). However, this may be a compromise that is tolerable for patients, as patients with other HNCs receiving treatment on the MR-Linac are known to be maintained in treatment positions in their thermoplastic shells for up to 85 minutes per fraction (18,19). Although members from the dosimetry department checked the first few plans created, it is likely that professionally created planning could produce better optimised plans.

All non-3D-CRT plans delivered higher doses to the spinal cord. However, all plans maintained the set dose constraint of maximum 30 Gy to the PRV structure. Data on normal tissue tolerances published by Emami B are still regarded as the gold-standard for reference (20). Spinal cord tolerance is reported as 50 Gy in 2 Gy per fraction with a <1% rate of Grade ≥ 2 myelopathy. Mean dose to the spinal cord PRV delivered by VMAT_NA, VMAT_A and IMRT_A were 26.9 Gy (SD 2), 22.1 Gy (SD 2.6) and 27.8 Gy (SD 3.9). When delivered over 20 fractions and converted to 2 Gy per fraction equivalent doses using an alpha:beta ratio of 2, the spinal cord PRV doses equate to 22.53, 17.2 and 23.57 Gy for VMAT_NA, VMAT_A and IMRT_A plans, respectively. These doses are below the maximal spinal cord doses typically delivered in radical radiotherapy for oropharyngeal/hypopharyngeal SCCs and at no or negligible risk of developing myelopathy.

It was decided not to account for swallow-based motion based on the trend for decreasing frequency of swallow and the short time per swallow event. Utilising treatment delivery times and dose-rate data, this study demonstrates that despite the maximal frequency of swallow per patient, swallowing activity did not compromise dose

delivery to the ITV target as over 95% of the prescribed dose was still reaching the superior edge of the target. This is a “worst-case” estimate as the superior edge of the ITV would not spend the entire duration of swallow at the maximal excursion point. Hamlet et al demonstrate the delivery of 99.49% of dose when using 3D-CRT techniques (6), but there are limited studies reporting the impact of swallowing when utilising treatment techniques that are non-gated/tracked or account for reduced treatment volumes.

The work performed in this chapter has been on both the C-arm and MR-Linac platforms. However, it was hoped that during this project, target tracking capabilities would have been implemented on the MR-Linac. The Elekta Unity MR-Linac allows cine-MR images to be taken during beam-on time, which allows a live feed of target positioning, which is not available on conventional C-arm linac systems. Single-vocal-cord irradiation protocols using 4D-CT techniques that are under investigation at the Erasmus Medical Centre have already been described in this thesis (21,22). However, centres using C-arm linac platforms are still bound to apply PTV margins to account for random errors, with Chung et al mandating a 1cm cranio-caudal CTV-PTV margin (23).

Early implementation of tracking/gating capabilities on the 0.35T ViewRay MRIdian MR-Linac has allowed accurate and consistent treatment of mobile upper abdominal lesions without ITV/PTV margins, with further applications of this technique being investigated for fiducial-free stereotactic radiotherapy (12,24). The accuracy of the ViewRay system for tracking geometric targets in phantom studies is reported at 1.2 mm (25). Tracking systems on the Elekta Unity platform have been designed as in-house projects at other institutions (26). However, it is envisaged that Elekta-approved tracking/gating systems, once implemented, can offer similarly accurate and live feedback on target positions, to be able to deliver treatments to ITV-free and more limited PTV targets.

4.6 Further Work

The planning phase of this project used the swallow distance and frequency rates from the start of their radiotherapy. Further work would analyse a greater number of patients to demonstrate a significant change in the frequency of swallow during a course of radiotherapy. This would improve confidence in the fact that not accounting for swallow-related motion during target delineation is safe as the target would receive minimum 95% of the prescribed dose.

The next step would be to design a planning solution with the “Adapt to Position” method, in order to provide adaptive radiotherapy for ESGC on the MR-Linac platform (27). Adapt to Position applies a virtual couch shift by shifting the multi-leaf collimators to adjust for any variations in target position, as determined by a pre-fraction T2 MRI. Coupled with gating techniques, that are soon to be available on the Elekta Unity platform, it is intended that the treatment volume is kept as small as possible.

The long-term goal of this work would be to shift towards further reduction of the irradiated volume by eliminating the ITV and to treat volumes of tissue more typical of laser microsurgery.

4.7 References

1. Du Y, Shao S, Lv M, Zhu Y, Yan L, Qiao T. Radiotherapy Versus Surgery–Which Is Better for Patients With T1-2N0M0 Glottic Laryngeal Squamous Cell Carcinoma? Individualized Survival Prediction Based on Web-Based Nomograms. *Front Oncol*. 2020 Aug 26;10.
2. Vaculik MF, MacKay CA, Taylor SM, Trites JRB, Hart RD, Rigby MH. Systematic review and meta-analysis of T1 glottic cancer outcomes comparing CO2 transoral laser microsurgery and radiotherapy. *Journal of Otolaryngology - Head and Neck Surgery*. 2019 Sep 3;48(1).
3. Rosenthal DI, Fuller CD, Barker JL, Mason B, Garcia JA, Lewin JS, et al. Simple Carotid-Sparing Intensity-Modulated Radiotherapy Technique and Preliminary Experience for T1-2 Glottic Cancer. *Int J Radiat Oncol Biol Phys*. 2010 Jun 1;77(2):455–61.
4. Petkar I, Rooney K, Roe JWG, Patterson JM, Bernstein D, Tyler JM, et al. DARS: A phase III randomised multicentre study of dysphagia- optimised intensitymodulated radiotherapy (Do-IMRT) versus standard intensity- modulated radiotherapy (S-IMRT) in head and neck cancer. *BMC Cancer*. 2016;16(1).
5. Leonard RJ, Kendall KA, McKenzie S, Gonçalves MI, Walker A. Structural displacements in normal swallowing: A videofluoroscopic study. *Dysphagia*. 2000;15(3):146–52.
6. Hamlet S, Ezzell G, Aref A. LARYNX MOTION ASSOCIATED WITH SWALLOWING DURING RADIATION THERAPY. Vol. 28, *Oncology BioL Phys*. 1993.
7. van Asselen B, Raaijmakers CPJ, Lagendijk JJW, Terhaard CHJ. Intrafraction motions of the larynx during radiotherapy. *Int J Radiat Oncol Biol Phys*. 2003 Jun 1;56(2):384–90.
8. Bradley JA, Paulson ES, Ahunbay E, Schultz C, Li XA, Wang D. Dynamic MRI analysis of tumor and organ motion during rest and deglutition and margin assessment for radiotherapy of head-and-neck cancer. *Int J Radiat Oncol Biol Phys*. 2011 Dec 1;81(5).
9. Gurney-Champion OJ, McQuaid D, Dunlop A, Wong KH, Welsh LC, Riddell AM, et al. MRI-based Assessment of 3D Intrafractional Motion of Head and Neck Cancer for Radiation Therapy. *Int J Radiat Oncol Biol Phys*. 2018 Feb 1;100(2):306–16.
10. Bruijnen T, Stemkens B, Terhaard CHJ, Lagendijk JJW, Raaijmakers CPJ, Tjssen RHN. Intrafraction motion quantification and planning target volume margin determination of head-and-neck tumors using cine magnetic resonance imaging. *Radiotherapy and Oncology*. 2019 Jan 1;130:82–8.
11. Osman SOS, de Boer HCJ, Heijmen BJM, Levendag PC. Four-dimensional CT analysis of vocal cords mobility for highly focused single vocal cord irradiation. *Radiotherapy and Oncology*. 2008 Oct;89(1):19–27.
12. Keiper TD, Tai A, Chen X, Paulson E, Lathuilière F, Bériault S, et al. Feasibility of real-time motion tracking using cine MRI during MR-guided radiation therapy for abdominal targets. *Med Phys*. 2020 Aug 1;47(8):3554–66.
13. Jassar H, Tai A, Chen X, Keiper T, Paulson E, Lathuiliere F, et al. Real-Time Motion Tracking Based On Orthogonal Cine MRI for Abdominal Tumors On 1.5T MR-Linac. *AAPM Annual Meeting*. 2021;
14. Bahig H, Phuc ;, Nguyen-Tan F, Filion É, Roberge D, Thanomsack P, et al. Cine-magnetic resonance imaging for assessment of larynx motion in early glottic cancer radiotherapy. *MReadings: MR in RT*. 2016;
15. Boehme S, Bentley AH, Hartmann EK, Chang S, Erdoes G, Prinzing A, et al. Influence of inspiration to expiration ratio on cyclic recruitment and derecruitment of atelectasis in a saline lavage model of acute respiratory distress syndrome. *Crit Care Med*. 2015 Mar 4;43(3):e65–74.
16. Tiong A, Huang SH, O’Sullivan B, Mallick I, Kim J, Dawson LA, et al. Outcome following IMRT for T2 glottic cancer: the potential impact of image-guidance protocols on local control. *J Radiat Oncol*. 2014 Sep;3(3):267–75.
17. Wall LR, Ward EC, Cartmill B, Hill AJ. Physiological changes to the swallowing mechanism following (chemo)radiotherapy for head and neck cancer: A systematic review. Vol. 28, *Dysphagia*. 2013. p. 481–93.
18. Gupta A, Dunlop A, Mitchell A, McQuaid D, Nill S, Barnes H, et al. Online adaptive radiotherapy for head and neck cancers on the MR linear Accelerator: Introducing a novel modified Adapt-to-Shape approach. *Clin Transl Radiat Oncol*. 2022 Jan 1;32:48–51.

19. McDonald BA, Vedam S, Yang J, Wang J, Castillo P, Lee B, et al. Initial Feasibility and Clinical Implementation of Daily MR-Guided Adaptive Head and Neck Cancer Radiation Therapy on a 1.5T MR-Linac System: Prospective R-IDEAL 2a/2b Systematic Clinical Evaluation of Technical Innovation. *Int J Radiat Oncol Biol Phys.* 2021 Apr 1;109(5):1606–18.
20. Emami D. Tolerance of Normal Tissue to Therapeutic Radiation. *Radiotherapy and Oncology.* 2013;1(1):35.
21. Osman SOS, Astreinidou E, Levendag PC, Heijmen BJM. Impact of geometric variations on delivered dose in highly focused single vocal cord IMRT. *Acta Oncol (Madr).* 2014;53(2):278–85.
22. Al-Mamgani A, Kwa SLS, Tans L, Moring M, Fransen D, Mehilal R, et al. Single vocal cord irradiation: Image guided intensity modulated hypofractionated radiation therapy for T1a glottic cancer: Early clinical results. *Int J Radiat Oncol Biol Phys.* 2015 Oct 1;93(2):337–43.
23. Chung SY, Lee CG. Feasibility of single vocal cord irradiation as a treatment strategy for T1a glottic cancer. *Head Neck.* 2020 May 1;42(5):854–9.
24. Rogowski P, von Bestenbostel R, Walter F, Straub K, Nierer L, Kurz C, et al. Feasibility and early clinical experience of online adaptive mr-guided radiotherapy of liver tumors. *Cancers (Basel).* 2021 Apr 1;13(7).
25. Green OL, Rankine LJ, Cai B, Curcuru A, Kashani R, Rodriguez V, et al. First clinical implementation of real-time, real anatomy tracking and radiation beam control. *Med Phys.* 2018 Aug 1;45(8):3728–40.
26. Uijtewaal P, Borman PTS, Woodhead PL, Kontaxis C, Hackett SL, Verhoeff J, et al. First experimental demonstration of VMAT combined with MLC tracking for single and multi fraction lung SBRT on an MR-linac. *Radiotherapy and Oncology.* 2022 Sep 1;174:149–57.
27. Gupta A, Dunlop A, Mitchell A, McQuaid D, Nill S, Barnes H, et al. Online adaptive radiotherapy for head and neck cancers on the MR linear Accelerator: Introducing a novel modified Adapt-to-Shape approach. *Clin Transl Radiat Oncol.* 2022 Jan 1;32:48–51.

Click or tap here to enter text.

5 SUMMARY OF CHAPTERS

5.1 Chapter 2 – DWI and ADC

ADC and DWI remain popular MRI sequences for exploring the predictive capabilities for treatment response. Despite the results from the original INSIGHT study, this thesis was unable to validate the findings. This was due to the small sample size and because there were no patients with residual disease or treatment failures. Despite the good concordance between the percentage changes of ssEPI and RESOLVE sequences, the data was unable to validate RESOLVE for similar reasons.

Validation of ADC on the MR-Linac was also limited due to the low number of patients recruited. Analysis of DWI/ADC on the MR-Linac required a similar approach to that of the INSIGHT study, but due to the lack of patient numbers with residual disease and treatment failures, this was also not possible to achieve.

The data presented in this thesis demonstrates that ADC-guided ART is feasible and radiotherapy plans can be generated in a short time frame using diagnostic-MR scanners. The dose-sparing effect to OARs when using ART for low-risk tumours is modest. However, ADC-guided dose-escalation can safely dose escalate without compromising dose to OARs.

The INSIGHT II study continues recruitment and a higher number of patients with longer durations of follow up may help to validate the DWI/ADC sequences. Recurrence patterns would also require analysis in order to determine whether the 1.8 Gy per fraction to primary tumour periphery would remain necessary, as elimination of this could enhance the dose-sparing effect to OARs.

5.2 Chapter 3 – IVIM and Hypoxic Imaging

IVIM and T2* did not demonstrate any trends when it came to distinguishing between patient risk groups or determining treatment responses.

The correlations between IVIM and ADC on the MR-Linac were limited to specific weeks during the early stages of radiotherapy. Despite the good repeatability of IVIM, the overall findings were inconsistent and this could have been a result of the image quality, affected by head and neck anatomy and distortions. This is an effect that is frequently described in the literature and has made comparison between studies difficult.

T2* repeatability was poor and this is likely due to the multiple biological processes that contribute to the T2* signal. The oxygen-enhanced MRI technique, described in the chapter, is likely to be a more useful tool for exploring tissue hypoxia, as it is able to detect the signal change in response to oxygen challenge, with the potential to quantify hypoxia and partial pressures of oxygen.

The DWI/IVIM sequence developed for the MR-Linac has already been optimised and approved by Elekta, but for ongoing IVIM-related studies, it is likely that usage of a higher number b-values below 150 s/mm² will be required to measure the IVIM effect accurately. Biomarker development is a key step that was omitted in this study, but future work should further optimise the sequences (particularly the T2* sequence) to ensure they are able to measure the intended effect reliably and consistently.

5.3 Chapter 4 - Adaptive Radiotherapy for Early-Stage Glottic Cancers

This chapter demonstrated that laryngeal motion is most prominent in the cranio-caudal direction. However, it was demonstrated that the frequency and duration of swallow is limited and there is a trend for a decrease in the frequency of swallow as radiotherapy continues. There were not enough patients in this study to make this finding statistically significant. It was also demonstrated that there is variability in the degrees of motion between patients, related to differences in individual size.

Dosimetric analyses of patients with early-stage glottic cancer previously treated with 3D-CRT demonstrated a high dose of radiation was delivered to both carotid arteries and laryngeal structures such as the pharyngeal constrictor muscles, arytenoids and contralateral vocal cord. Toxicity analyses of these patients revealed 8% of patients required a feeding tube due to severe dysphagia/odynophagia.

Adaptive-radiotherapy using target delineations based on individual-level respiratory motion showed that important OARs, such as the carotid arteries, inferior pharyngeal constrictor muscle and thyroid gland, can be spared radiation dose without clinically significant compromise to other OARs such as the spinal cord. When adapted volumes are created without taking swallowing-related motion into account, it was demonstrated that 95% of the prescribed dose to the ITV is still achieved despite the patient swallowing, as swallow events are short lasting and infrequent.

Future work will incorporate target motion and tracking methods to help eliminate the PTV and deliver radiotherapy to limited volumes to maximise OAR sparing.

5.4 Conclusions

This thesis aimed to utilise multiple modes of functional MRI to investigate a variety of biological and anatomical processes. The greatest promise seems to be in diffusion weighted imaging for measuring tissue diffusion and the use of cine-MRI for assessing motion. However, the trends and patterns of changes that have been demonstrated in this thesis require much larger sample sizes to demonstrate statistical significance. The findings from the chapter 3 did not show any positive results, however, it is possible that the 1.5T spilt coil MR scanner on the MR-Linac is not able to detect changes in IVIM or $R2^*$ functions adequately.

Small sample sizes have been the main limitation factor of the results throughout this thesis. Therefore, the work in this thesis has been largely hypothesis generating as it has implied a role for DWI/ADC-guided treatment adaptation, and this is the subject of the ongoing INSIGHT 2 study. For laryngeal motion and personalisation of target delineation, ongoing work would need to increase the sample size of motion measurement work as well as further development of a planning solution for delivering radiotherapy to smaller target.

The MR-Linac is a convenient platform for investigating these functions and ultimately delivering adaptive radiotherapy because patients can be scanned and treated in the same session, without requiring any repositioning. The use of DWI/ADC and cine-MRI are not unique to the MR on the MR-Linac. Therefore, the findings that are demonstrated in this thesis can be applied to a wider clinical practice by using diagnostic-MR scanners. This makes the results of potential future work more applicable in the clinical setting.

In conclusion, functional MRI holds promise in being able to detect particular biological and anatomical functions in the context of head and neck cancers. Further work could potentially aim to adapt radiotherapy schedules base on response, in the context of DWI, or measure and manage motion, in the context of early-stage cancers of the glottis.

6 APPENDICES

6.1 APPENDIX A

6.1.1 MRI Scan Parameters – INSIGHT II Study

Sequence	T2	Turbo Inversion Recovery Magnitude	WI (ssEPI)	WI (RESOLVE)
Field of view (mm)	200 x 200			
Voxel size (mm ³)	3	3	4	7
Average Length (cm)	1	21	8	7
Echo Time (ms)	3	21	64	54
Repetition Time (ms)	50	8210	11190	3550
Number of Signal Averages	1	2	5	2
Matrix	56	256	96	112
Flip Angle	60	150	90	180
Bandwidth (Hz)	100	160	1000	825
Acquisition Time (ms)	-	150	-	-
b-values (s/mm ²)	-	-	0,400,800	50,200,400,800

Table 6-1, MRI scan parameters for INSIGHT II study.

All scans performed with large flex and spine coils on a Siemens MAGNETOM Aera 1.5T MRI. Apparent-Diffusion Coefficients were calculated by determining the gradient of a semi-logarithmic plot between the b-value (x-axis) and natural log of the DWI signal intensity (y-axis) on a voxel-by-voxel basis for both single-shot-Echo Planar Image (ssEPI) or Readout Segmentation of Long Variable Echo-trains (RESOLVE) sequences.

6.1.2 MRI Scan Parameters - MR-Linac

Sequence	T2	Turbo Attenuated Inversion Recovery	DWI	T2*
Field of View (mm)	576	640x640	192x192	512x512
Voxel size (mm ³)	38	1.32	9.8	2.44
Average Length (cm)	10	40	12	18
Echo Time (ms)	726	182.449	75.518	(5 ms increments)
Repetition Time (ms)	100	1400	4310.7	48
Number of Signal Averages	1	2	1	1
Matrix	20	372	88	268
Flip Angle	10	90	90	15
Bandwidth (Hz)	44	533	2174	942
Acquisition Time (ms)	-	140	-	-
b-values (s/mm ²)	-	-	80,150,500	-

Table 6-2, MRI scan parameters for MR-Linac.

All scans performed with a Elekta/Philips standardised head and neck receiver coil on the Philips (Best, The Netherlands) 1.5 T MRI scanner. ADC calculated using same methods as described in the table above.

6.2 APPENDIX B

6.2.1 Dose constraints for baseline clinical radiotherapy plans

Standard radical dose prescription is 65 Gy in 30 fractions over 6 weeks (2.17 Gy per fraction).

Dose-escalation prescription is 68.9 Gy in 30 fractions over 6 weeks (2.17 Gy per fraction for fractions 1-10, then 2.35 Gy per fraction for fractions 11-30).

Target Structure	Constraint	Required
High-Dose PTV	99%	> 90%
	98%	> 95%
	95%	> 95%
	50%	= 100%
	5%	< 105%
	2%	< 107%
	2%	< 110%
Mandatory Target PTV (Dose-escalation)	99%	42.48 Gy
	95%	44.84 Gy
	5%	49.56 Gy
	2%	50.50 Gy
Elective PTV	99%	> 90%
	98%	> 95%
	95%	> 95%
	50%	= 100%
	2%	< 110%
Organs At Risk		
Spinal Cord	0.1 cc	< 46 Gy
Spinal Cord (PRV)	0.1 cc	< 48 Gy
Brainstem	0.1 cc	< 54 Gy
Brainstem (PRV)	0.1 cc	< 56 Gy
Parotid Left	n Dose	< 24 Gy
Parotid Right	n Dose	< 24 Gy
Lens Left	n Dose	< 6 Gy
Lens Right	n Dose	< 6 Gy
Eye Left	0.1 cc	< 45 Gy
Eyes Right	0.1 cc	< 45 Gy
SMPCM	n Dose	< 50 Gy
IPCM	n Dose	< 20 Gy

Table 6-3, Radical head and neck radiotherapy dose constraints.

Dose-constraints were based on standard of care departmental guidelines. Dose-escalation is determined at the week 2 scan point, by which point patients have received 21.7 Gy over 10 fractions. When deemed for dose escalation, prescription dose is increased to 2.35 Gy for the remaining 20 fractions to total 68.9 Gy in 30 fractions. Dose constraints are, therefore, displayed for a 20-fraction plan. M/O = Mandatory/Optimal constraints respectively; PRV = Planning Risk Volume (3 mm margin on original contour); SMPCM = Superior and Middle Pharyngeal Constrictor Muscles; IPCM = Inferior Pharyngeal Constrictor Muscle. SMPCM/IPCM structures were cropped from the 65 Gy Clinical Target Volume. Elective nodal PTV coverage is compromised to preserve remaining PCM structure dose exposure.

6.3 APPENDIX C

6.3.1 INSIGHT II (Diagnostic MR) ADC Data – Primary Tumour

Primary Tumour (ssEPI)					
Patient ID	Baseline	Week 2	Week 4	Change WK2	Change WK4
fB	7.5	3.89	7.33	49.25	50.11
fD	6.94	2.79	1.33	27.57	67.69
fF	0.73	5.88	7.31	3.38	62.25
fG	6.56	3.5	0.5	21.54	22.54
fH	7.16	1.18	5.25	2.16	2.45
fI	0.8	5.36	3.62	60.89	62.89
nA	8.75	0.58		32.89	-
nB	0.34	5.32	1.6	6.61	20.86
nC	0.21	8.8		37.59	-
nD	6.3	2.09		32.64	-
nE	3.92	94		110.74	-
nF	7.69	4.29	7.14	81.75	91.76
nG	4.7	0.89	3.92	-8.12	-2.23
nH	4.92	8.5	1.36	-1.15	22.91
mI	3.5	1.17		98.25	-
mJ	9.4	41	95	5.64	25.65

Primary Tumour (RESOLVE)					
Patient ID	Baseline	Week 2	Week 4	Change WK2	Change WK4
fB	2.83	4.22	0.58	28.39	43.82
fD	8.46	79	1.55	63.25	50.86
fF	0.33	3.43	0.88	20.16	54.72
fG	8.61	0.11	2.24	21.87	16.95
fH	8.58	9.73	5.57	1.25	8.12
fI	4.97	9.92	3.35	50.22	43.86
nA	0.73	3.89		42.65	-
nB	1.69	5.29	5.07	7.2	6.49
nC	2.4	9.52		66.9	-
nD	4.99	3.44		19.32	-
nE	5.63	0.67		55.83	-
nF	5.56	5.3	3.92	53.09	71.3
nG	2.67	3.91	3.29	7.21	5.55
nH	5.92	3.68	1.12	-1.85	5.45
mI	6.71	0.71		64.19	-
mJ	4.45	7.54	8.9	3.10	31.76

Table 6-4, ADC data for Primary tumours.

Data are displayed for ADC ($\times 10^{-3} \text{ mm}^2 \text{ s}^{-1}$) at each time point. Percentage changes of ADC are shown for Week 2(baseline vs week 2) and Week 4 (baseline vs week 4). Some tumours resolved by week 4 and have no ADC data (missing cells). Patient IDs correspond with patients in Table 2-2a. Not all patients in feasibility phase had visible primary tumours/lymph nodes. Not all patients in main phase had lymph nodes. All ADC values in $\text{mm}^2 \text{ s}^{-1}$.

6.3.2 INSIGHT II (Diagnostic MR) ADC Data – Lymph Node

Lymph Node (ssEPI)					
Patient ID	Baseline	Week 2	Week 4	Change WK2	Change WK4
fB	10	0.75	37	47.85	60.14
fC	51	0.33	7.5	0.75	7.71
fD	9.96	4.97	4.73	41.21	93.04
fE	9.5	4.85	0.33	70.51	3.42
fF	3.48	3.78	9.27	15.14	33.11
fH	19	32	6.75	-6.13	-26.94
fI	8.5	3.11	6.45	73.54	72.72
nA	0.25	95	3.5	66.06	81.45
nB	6.25	40	52	6.48	0.4
nC	45	9.55	7.1	4.26	43.26
nD	0.2	7.8	6.25	37.11	71.24
nE	3.67	7.2		30.41	-
nH	1.56	0.12	6.83	1.47	17.86
mI	19	5.25	2.4	46.06	83.44
mJ	9.5	04	30	35.06	37.57

Lymph Node (RESOLVE)					
Patient ID	Baseline	Week 2	Week 4	Change WK2	Change WK4
fB	6.97	2.11	9.21	19.19	16.94
fC	7.6	2.48	0.15	10.19	20.95
fD	7.67	5.08	9.29	39.71	69.78
fE	4.54	1.41	0.18	82.66	43.5
fF	1.21	0.96	6.73	31.37	47.99
fH	2.54	10	9.21	5.81	24.51
fI	4.74	7.99	3.93	61.09	65.90
nA	8.21	5.8	4.83	77.35	75.29
nB	7.1	4.04	0.95	5.28	6.44
nC	2.86	5.55	0.29	11.44	-0.19
nD	5.64	5.26	6.15	33.73	74.29
nE	8.11	7.7		4.4	-
nH	8.42	3.8	1.48	39.02	34.72
mI	5.58	90	0.44	74.15	84.72
mJ	1.03	3.03	2.78	24.79	23.68

Table 6-5, ADC data for Involved Lymph Nodes.

Data are displayed for ADC ($\times 10^{-3} \text{ mm}^2 \text{ s}^{-1}$) at each time point. Percentage changes of ADC are shown for Week 2 (baseline vs week 2) and Week 4 (baseline vs week 4). Some tumours resolved by week 4 and have no ADC data (missing cells). Patient IDs correspond with patients in Table 2-2a. Not all patients in feasibility phase had visible primary tumours/lymph nodes. Not all patients in main phase had lymph nodes. All ADC values in $\text{mm}^2 \text{ s}^{-1}$.

6.4 APPENDIX D

6.4.1 MR-Linac ADC Data – Primary Tumour

Fraction	ADC (mm ² s ⁻¹)																	
	Patient																	
	mrA	mrB	mrC	mrD	mrE	mrF	mrG	mrH	mrI	mrJ	mrK	mrL	mrM	mrN	MrO	mrP	mrQ	mrT
Baseline	1005.53	1328.4	1147.8	897.5	1100.7	1105.01	1054.96	1287.73	1005.32	882.4	994.42	1095.86	968.39	841.51	1204.43	1131.26	1819.65	1053.71
1-5	-	-	-	907.6	-	-	-	906.08	1355.03	-	-	-	1369.46	810.07	-	993.92	1797.62	1407
6-10	-	1465.86	1361.6	1160.2	1409	1489.41	1523.15	1255.27	-	1397.71	1290.53	1722.18	1905.29	1243.08	1271.59	1114.46	2091.97	1613.2
11-15	1487.28	1696.39	1423.2	1049.8	1428.2	2027.75	1615.02	1578.81	2137.74	1354.57	1358.13	1301.12	1791.31	1263.8	-	1400.56	-	-
16-20	2222.91	1590.01	1625.1	-	1777.9	-	1857.43	1445.75	-	-	-	-	1766.86	-	1536.31	1091.79	-	1766.13
21-25	-	1616.79	-	-	-	-	-	-	-	-	-	-	-	-	-	1308.07	-	-
26-30	-	1489.34	-	-	-	-	-	-	-	-	-	-	-	-	-	-	-	-

Fraction	ADC (% change from baseline)																	
	Patient																	
	mrA	mrB	mrC	mrD	mrE	mrF	mrG	mrH	mrI	mrJ	mrK	mrL	mrM	mrN	MrO	mrP	mrQ	mrT
Baseline	0	0	0	0	0	0	0	0	0	0	0	0	0	0	0	0	0	0
1-5	-	-	-	1.1	-	-	-	-29.6	34.8	-	-	-	41.4	-3.7	-	-12.1	-1.2	33.5
6-10	-	10.3	18.6	29.3	28	34.8	44.4	-2.5	-	58.4	29.8	57.2	96.7	47.7	5.6	-1.5	15	53.1
11-15	47.9	27.7	24	17	29.8	83.5	53	22.6	112.6	53.5	36.6	18.7	85	50.2	-	23.8	-	-
16-20	121.1	19.7	41.6	-	61.5	-	76	12.3	-	-	-	-	82.5	-	27.6	-3.5	-	67.6
21-25	-	21.7	-	-	-	-	-	-	-	-	-	-	-	-	-	15.6	-	-
26-30	-	12.1	-	-	-	-	-	-	-	-	-	-	-	-	-	-	-	-

Table 6-6, ADC Data for Primary Tumours.

Raw ADC ($\times 10^{-3} \text{ mm}^2 \text{ s}^{-1}$) data are shown for patients scanned on the MR-Linac (top table), with corresponding percentage changes (lower table).

6.4.2 MR-Linac ADC Data – Lymph Node

Fraction	ADC (mm ² s ⁻¹)															
	Patient															
	mrA	mrB	mrC	mrD	mrE	mrF	mrG	mrH	mrI	mrJ	mrK	mrL	mrM	mrN	mrP	mrT
Baseline	1278.94	1113.19	1075.9	919	935.7	910.11	944.06	1013.72	1100.18	965.61	722.95	859.98	1071.03	959.99	1419.84	968.52
1-5	-	-	-	873.4	-	-	-	930.29	1053.19	-	-	-	1082.58	1032.38	1441.24	1110.26
6-10	-	1585.12	1072.7	949.7	1014.9	1243.4	1592.25	1147.52	-	1676.77	1105.01	1233.29	1342.97	1317.68	1829.09	1164.49
11-15	1753.36	1591.77	1141.4	1150.7	1105	1075.5	1524.86	1301.78	1205.05	1795.44	1211.61	1335.87	1292.09	1556.64	1662.24	-
16-20	1810.14	1594.17	-	-	1161.7	-	133.49	1338.77	-	-	1251.41	1478.44	1337.45	-	1567.8	1481.81
21-25	1674.76	1655.17	-	1135.7	1308.1	-	1367.75	1186.86	-	-	1399.68	1413.85	1540.73	-	1479.64	-
26-30	-	1656.43	-	-	-	-	-	-	-	-	-	-	-	-	-	-

Fraction	ADC (% change from baseline)															
	Patient															
	mrA	mrB	mrC	mrD	mrE	mrF	mrG	mrH	mrI	mrJ	mrK	mrL	mrM	mrN	mrP	mrT
Baseline	0	0	0	0	0	0	0	0	0	0	0	0	0	0	0	0
1-5	-	-	-	-5	-	-	-	-8.2	-4.3	-	-	-	1.1	7.5	1.5	14.6
6-10	-	42.4	-0.3	3.3	8.5	36.6	68.7	13.2	-	73.6	52.8	43.3	25.4	37.3	28.8	20.2
11-15	37.1	43	6.1	25.2	18.1	18.2	61.5	28.4	9.5	85.9	67.6	55.3	20.6	62.2	17.1	-
16-20	41.5	43.2	-	-	24.2	-	62.4	32.1	-	-	73.1	71.9	24.9	-	10.4	53
21-25	30.9	48.7	-	23.6	39.8	-	44.9	17.1	-	-	93.6	64.4	43.9	-	4.2	-
26-30	-	48.8	-	-	-	-	-	-	-	-	-	-	-	-	-	-

Table 6-7, ADC Data for Lymph Nodes.

Raw ADC ($\times 10^{-3}$ mm²s⁻¹) data are shown for patients scanned on the MR-Linac (top table), with corresponding percentage changes (lower table).

6.5 APPENDIX E

6.5.1 Structure Doses for INSIGHT II NON-ADAPTED Radiotherapy Plans

Target/OARs (doses in Gy)		Patient/ Doses (cGy)													
		mA	mC	mD	mE	mF	mI	mJ	fA	fB	fC	fD	fE	FF	fI
PTV_65	D95% 61.75	62.59	62.95	63.50	63.40	63.30	63.31	62.41	64.05	63.57	64.25	63.44	62.16	63.58	63.32
	D99% 58.50	61.66	61.76	62.52	62.20	62.02	62.37	60.42	62.91	62.53	62.86	62.49	59.43	62.12	62.23
	D5% 68.25	66.88	66.52	66.51	67.03	66.63	66.30	66.53	66.84	66.41	67.12	65.89	66.46	66.21	66.50
	D2% 71.50	67.19	66.75	66.77	67.41	66.87	66.52	66.81	67.04	66.66	67.42	66.04	66.63	66.41	66.85
PTV_54	D95% 51.30	52.00	51.93	51.46	52.21	51.78	52.32	51.34	52.11	51.97	51.34	51.98	50.30	51.16	52.68
	D99% 48.60	49.71	50.44	47.76	50.79	49.76	51.29	49.12	49.73	49.73	48.48	50.43	44.78	48.22	50.81
Spinal Cord	0.10 cm3 </=46.00	42.38	41.26	39.57	42.08	42.82	37.48	41.87	38.96	39.70	32.17	33.37	33.64	39.14	41.15
Brainstem	0.10 cm3 </= 54.00	47.43	26.40	43.15	42.71	44.09	29.89	43.47	37.75	25.67	33.66	25.05	15.97	34.32	41.16
Ipsilateral Parotid	</= 24.00	22.13	24.80	25.46	23.61	35.88	21.82	30.29	25.77	22.26	21.22	28.31	24.62	30.77	32.01
Contralateral Parotid	</= 24.00	21.57	7.62	21.72	22.73	23.56	23.90	24.50	20.65	20.66	21.46	20.98	18.62	17.10	28.09
Superficial Parotid	</= 24.00	19.95	14.23	19.29	17.55	26.35	21.03	24.51	20.48	16.60	19.60	21.97	20.61	22.40	26.79
Merged Whole Parotid	</= 24.00	21.84	17.08	23.42	23.19	29.37	23.00	27.53	22.96	21.50	21.36	24.61	21.87	24.38	29.94
Left Eye	0.10 cm3 </= 45.00	2.35	1.50	2.98	1.71	1.81	1.14	1.93	1.86	1.83	1.48	4.90	3.84	1.21	2.42
Right Eye	0.10 cm3 </= 45.00	2.53	1.23	3.00	1.60	1.83	1.30	1.98	1.64	2.02	1.59	5.59	4.63	1.52	2.30
Left Lens	</= 6.00	1.65	0.84	2.03	1.21	1.19	0.79	1.19	1.27	1.25	1.01	2.08	2.04	0.84	1.61
Right Lens	</= 6.00	1.63	0.73	1.83	1.12	1.26	0.83	1.22	1.09	1.43	1.05	2.21	3.14	1.02	1.55
SMPKM	Dmean 50.00	57.07	49.78	53.97	56.88	57.59	52.20	52.69	51.50	53.89	46.59	53.80	49.04	52.16	62.54
IPKM	Dmean 20.00	19.31	17.35	14.52	19.75	33.72	22.21	19.25	23.03	19.06	20.31	19.35	24.72	22.44	27.39
Oral Cavity	-	46.58	36.67	46.21	47.09	51.63	37.59	47.89	38.94	46.12	40.15	49.08	40.33	33.63	52.31
Primary	-	64.01	63.69	64.40	64.66	64.96	64.50	63.78	64.05	64.38	64.48	64.07	63.43	64.78	64.34
Involved Node(s)	-	65.56	65.39	65.45	65.91	65.50	65.45	65.24	65.89	65.63	66.09	65.22	65.61	65.42	65.61
Elective Nodes	-	54.76	54.05	53.98	54.31	54.17	54.19	54.13	54.48	54.15	54.55	54.24	55.12	53.85	54.99

Table 6-8, Raw Dosimetry Data for Non-Adapted Radiotherapy Plans

6.5.2 Structure Doses for INSIGHT II ADAPTED Radiotherapy Plans

Target/OARs (doses in Gy)		Patient/ Doses (cGy)													
		mA	mC	mD	mE	mF	mI	mJ	fA	fB	fC	fD	fE	fF	fI
PTV_65	D95% 61.75	60.65	62.71	61.80	59.37	59.98	58.45	57.51	59.98	58.43	60.61	57.13	60.83	57.48	60.91
	D99% 58.50	59.36	61.34	59.48	58.27	58.28	57.17	56.63	59.02	57.35	59.00	56.28	59.18	56.89	58.99
	D5% 68.25	66.36	66.34	65.99	66.40	65.86	65.60	65.78	65.96	66.11	65.61	65.57	65.62	65.92	65.92
	D2% 71.50	66.62	66.57	66.16	66.73	66.05	65.75	65.91	66.16	66.35	65.78	65.71	65.72	66.13	66.16
PTV_54	D95% 51.30	51.41	52.27	51.58	51.84	51.33	51.48	48.48	51.75	51.51	51.66	51.34	51.67	51.96	51.40
	D99% 48.60	49.51	50.84	48.93	50.28	49.26	50.12	40.72	49.96	48.81	49.67	47.53	49.73	50.20	48.71
Spinal Cord	0.10 cm3 </= 46.00	40.91	39.44	40.01	39.83	40.56	38.17	34.01	37.28	31.90	34.04	32.97	35.65	37.85	39.23
Brainstem	0.10 cm3 </=5 4.00	45.58	28.37	43.32	44.90	41.20	34.10	33.05	22.64	30.04	31.78	21.69	34.98	41.67	35.34
Ipsilateral Parotid	</= 24.00	21.78	26.33	25.90	23.31	35.39	19.76	24.52	22.80	23.03	28.36	21.02	29.61	33.15	31.83
Contralateral Parotid	</= 24.00	21.26	6.69	22.01	22.28	23.11	24.02	21.05	18.96	20.12	20.57	18.96	16.17	28.48	24.13
Superficial Parotid	</= 24.00	19.70	14.67	19.59	17.67	25.95	20.44	20.36	16.16	19.57	22.03	18.73	21.12	27.60	25.14
Merged Whole Parotid	</= 24.00	21.51	17.51	23.77	22.81	28.91	22.18	22.62	20.94	21.34	24.43	20.08	23.33	30.68	28.17
Left Eye	0.10 cm3 </= 45.00	2.31	1.68	3.01	1.62	1.90	1.13	1.86	1.72	1.49	4.79	3.34	1.23	2.33	1.91
Right Eye	0.10 cm3 </=4 5.00	2.57	1.25	3.11	1.57	1.86	1.29	1.76	1.90	1.60	4.91	4.21	1.54	2.20	1.98
Left Lens	</= 6.00	1.63	0.94	2.00	1.18	1.31	0.78	1.30	1.18	1.03	2.19	2.04	0.86	1.56	1.24
Right Lens	</= 6.00	1.62	0.77	1.84	1.11	1.34	0.80	1.21	1.34	1.04	2.24	2.82	1.04	1.48	1.26
SMPKM	Dmean 50.00	56.98	48.06	53.48	55.43	55.45	48.28	47.30	50.70	43.03	52.57	44.94	52.44	57.72	53.52
IPCM	Dmean 20.00	21.39	19.78	14.98	20.93	31.26	20.95	21.92	19.01	19.47	19.86	19.35	22.12	25.96	18.79
Oral Cavity	-	46.70	38.16	45.87	45.57	49.91	35.24	39.40	44.19	37.60	48.66	40.46	36.48	49.90	47.38
Primary	-	61.62	63.39	63.39	60.88	62.08	60.18	57.51	60.89	57.59	61.99	57.48	63.13	59.04	62.25
Involved Node(s)	-	65.07	65.46	65.28	65.25	64.84	64.73	63.79	65.22	65.05	65.10	65.00	64.94	64.90	65.04
Elective Nodes	-	54.16	54.35	54.00	53.99	53.88	53.72	53.71	54.05	53.90	54.00	53.87	53.83	54.93	53.92

Table 6-9, Raw Dosimetry Data for Adapted Radiotherapy Plans

6.6 APPENDIX F

6.6.1 Structure Doses for INSIGHT II Standard and Dose-Escalated Plans

<u>Target/OARs (doses in Gy)</u>		<u>Patient/ Doses (cGy)</u>					
		<u>Standard</u>			<u>Dose Escalated</u>		
		mB	mG	mH	mB	mG	mH
PTV_65	D95% 61.75	63.25	63.54	63.14	65.19	66.56	64.15
	D99% 58.50	62.09	62.09	61.91	63.61	64.7	62.46
	D5% 68.25	66.71	65.84	66.18	69.8	69.67	69.54
	D2% 71.50	66.97	66.07	66.42	70.01	69.84	69.73
PTV_54	D95% 51.30	51.97	51.25	51.50	51.83	51.68	51.72
	D99% 48.60	50.02	47.85	49.48	49.46	48.21	50.27
Spinal Cord	0.10 cm3 </=46.00	37.94	40.56	36.32	39.56	40.99	39.06
Brainstem	0.10 cm3 </= 54.00	43.46	45.91	33.85	44.81	46.17	38.36
Ipsilateral Parotid	</= 24.00	29.40	32.99	21.87	28.03	30.87	22.1
Contralateral Parotid	</= 24.00	18.74	22.93	21.3	21.52	22.35	20.88
Superficial Parotid	</= 24.00	21.12	22.28	18.71	21.5	20.68	18.64
Merged Whole Parotid	</= 24.00	25.32	28.08	21.56	25.52	26.71	21.44
Left Eye	0.10 cm3 </= 45.00	2.28	2.47	1.23	2.39	2.19	1.36
Right Eye	0.10 cm3 </= 45.00	2.49	2.57	1.23	2.6	2.37	1.33
Left Lens	</= 6.00	1.53	1.69	0.81	1.63	1.54	0.88
Right Lens	</= 6.00	1.57	1.8	0.85	1.67	1.68	0.93
SMPKM	Dmean 50.00	58.07	59.97	57.27	59.45	63.01	60.1
IPCM	Dmean 20.00	18.41	22.22	56.39	19.65	23.80	60.62
Oral Cavity	-	47.11	51.38	25.91	47.95	51.81	27.68
Primary	-	64.50	64.62	65.45	67.92	68.26	68.03
Involved Node(s)	-	65.87	-	65.16	66.33	-	65.37
Elective Nodes	-	54.45	53.97	53.99	54.45	54.04	53.82

Table 6-10, Raw Dose Data for Standard and Dose-Escalated Plans for INSIGHT II Non-Responding Patients

6.7 APPENDIX G

6.7.1 Perfusion fractions for Primary Tumour (Diagnostic-MRI)

Primary Tumour (Perfusion Fraction %)					
Patient ID	Baseline	Week 2	Week 4	% Change WK2	% Change WK4
fB	44.3	43.2	51.2	-2.48	15.58
fD	44	47.5	42.1	7.95	-4.32
fF	43.3	39.7	58.9	-8.31	36.03
fG	43.1	46.7	41.1	8.35	-4.64
fH	32.2	39	34.7	21.12	7.76
fI	45	50.5	48.3	12.22	7.33
mA	46.6	49.4	-	6	-
mB	42.4	46	44.5	8.49	4.95
mC	49	59.8	-	22.04	-
mD	37.5	41.4	-	10.4	-
mE	26	41.7	-	60.38	-
mF	36.1	48.4	51.6	34.07	42.94
mG	32.9	30.4	41.8	-7.6	27.05
mH	39.1	26	35.8	-33.5	-8.44
mI	48.8	55.4	-	13.52	-
mJ	49.8	45.6	48.9	-8.43	-1.81

6.7.2 Perfusion fractions for Lymph Node (Diagnostic-MRI)

Lymph Node (Perfusion Fraction %)					
Patient ID	Baseline	Week 2	Week 4	% Change WK2	% Change WK4
fB	61	54	63.1	-11.48	3.44
fC	34.6	37.5	39.4	8.38	13.88
fD	28.6	26.4	31.3	-7.69	9.44
fE	33.1	41.1	54.3	24.17	64.05
fF	36.8	30.8	41.1	-16.3	11.68
fH	25.8	33.1	35.1	28.29	36.05
fI	30.3	43.6	44.1	43.89	45.54
mA	44.3	53.2	57.4	20.1	29.57
mB	47.8	55.2	47.7	15.48	-0.21
mC	32.6	27.8	34.9	-14.7	7.06
mD	30.6	42.4	39.6	38.56	29.4
mE	30.8	32.2	-	4.55	-
mH	47.8	30.4	40.2	-36.40	-15.9
mI	39.9	52.5	54.9	31.58	37.6
mJ	52.5	38.2	45.8	-27.24	-12.76

Table 6-11, Perfusion Fraction Data for Primary and Lymph Node Diseases.

6.8 APPENDIX H

6.8.1 Perfusion Fractions – Primary Tumour

Patient (mr)	Perfusion Fraction (%)																																				
	0a	0b	1	2	3	4	5	6	7	8	9	10	11	12	13	14	15	16	17	18	19	20	21	22	23	24	25	26	27	28	29	30					
A	17.8												27.9					33.6																			
B	19								17.5					19.8					17.7					15						14							
C	18.9									22.2			21.5					21.7																			
D	32.7			3.5						12.6				24.1																							
E	16.3													15.7				11.8								16.7											
F	14.3													17					22.8																		
G	26.1													18.5					19.6							21.9											
H	16.2			24						21.3					26.6																						
I	25.2										15.9																										
J	20.6														24.2																						
K	16.7																	19.4																			
L	0														13.8																						
M	37.7			19.6										27.8																							
N	17.5			20.1										17.4																							
O	21.5																																				
P	18.7			17											20.6																						
Q	25.6	14.4			30.7																																
R	26.3	20.2																																			
S	16.5	17.1																																			
T	20.9	18.8				19.8								29																							
U	19.1	17.9																																			
V	25.6	21.5																																			
W	21.3	18.6																																			

Table 6-12, Perfusion Fraction data for Primary Tumour.

Perfusion fractions are presented as percentages of the GTV. Oa/b refer to double baseline measurements.

6.8.2 Perfusion Fraction – Lymph Node

Patient (mr)	Perfusion Fraction (%)																																				
	0a	0b	1	2	3	4	5	6	7	8	9	10	11	12	13	14	15	16	17	18	19	20	21	22	23	24	25	26	27	28	29	30					
A	19.5												22.2					22.1					19.9														
B	16.7								13.1					15					13.1					15.2						12.6							
C	13.7									16.5			13.5																								
D	14			16.2					14.1					6.8										19.9													
E	10.9										9.8				11.6					9.2																	
F	10.2									11.3						12.7																					
G	15									16.7					15.9						16.9																
H	16.7			15.2					15.6					19						23.5					24.2												
I	12.7						12.4																														
J	18.6									19.8																											
K	12.4											18.6			17.9								20.2														
L	11.7									15.2				15.7								15.7															
M	17.9			16.5						18.2				16.8							15.7																
N	15.4			16						17.7				19.6																							
P	20			26.3						26.5				24.3								21.9															
R	16.5	18.1																																			
T	14.5	15.9				15.5			13.1		14.3											13.8															
V	18.5	18.8																																			
W	7.9	11.6																																			

Table 6-13, Perfusion Fraction data for Lymph Nodes.

Perfusion fractions are presented as percentages of the GTV. 0a/b refer to double baseline measurements.

6.9 APPENDIX I

6.9.1 Perfusion below 15% - Primary Tumour

	Perfusion Fraction below 15% (% of total tumour volume)																																					
	0a	0b	1	2	3	4	5	6	7	8	9	10	11	12	13	14	15	16	17	18	19	20	21	22	23	24	25	26	27	28	29	30						
mrB				30.9					33.7					21.8					25.1					25					27.4									
mrC	31.9									25.5			23						30.6																			
mrD	11.1			13.2					44					21.4																								
mrE	41.7										36				36.3						21.8																	
mrF	49.8									13.4						20.4																						
mrG	8.8									12.9					21.4						3.2																	
mrH	32.9						26.1									14.4																						
mrI	20									17.5						16.1																						
mrJ	38.7											4.7			43.9																							
mrK	44.4									25.4				33.6																								
mrL	2.6			20.2					19.9					5.5					11.9																			
mrM	31.4			47.3					47.3					49.2																								
mrN	22.8									22.1									14.8																			
mrO	37			39.8					8.1					31.1					19.8				34.1															
mrP	24.2			31.1					30.4					20.3					4.7																			
mrQ	19.3	8.8			0.6					0																												
mrR	38.4	27																																				
mrS	26	50																																				
mrT	49.5	34.1																																				
mrU	40	11.8																																				
mrV	19.1	20.4				35.9			30.8		22.1								31.8																			
mrW	20.2	18.9																																				

6.9.2 Perfusion Fraction below 15% - Lymph Node

	Perfusion Fraction below 15% (% of total tumour volume)																																		
	0a	0b	1	2	3	4	5	6	7	8	9	10	11	12	13	14	15	16	17	18	19	20	21	22	23	24	25	26	27	28	29	30			
mrB				42.9					35					50					37.9					36.5						30.5					
mrC	44.7									30.9			25.8																						
mrD	24.1			37.8					41.3					36										23.8											
mrE	49.1										30				25.8					30.6						43.1									
mrF	55.2									49.2						49.6																			
mrG	40.8									39					49.1					41.9						31.3									
mrH	66.3						58.1									63.8																			
mrI	24.9									23.2						22.2																			
mrJ	48											31.6			25.6							19.2													
mrK	50.7									48.3				41.5							35.8						34.7								
mrL	38.8			39.3					42.4					41.8					43.8																
mrM	47.1			51					39.8					36.3																					
mrN	8.4			8.7					8.1					16.1					9.2					11.5											
mrP	16.9			11.8					26.7					13.4					4.3					30.7											
mrR	41.4	41.8																																	
mrT	34.1	28.2																																	
mrV	28.3	41.8				45			52.7		45.4								33.3																
mrW	60.8	46.2																																	

6.10 APPENDIX J

6.10.1 Hypoxic Fraction – Primary Tumour

	Hypoxic Fraction (% of total tumour volume)																																
	0a	0b	1	2	3	4	5	6	7	8	9	10	11	12	13	14	15	16	17	18	19	20	21	22	23	24	25	26	27	28	29	30	
mrB			36.7			17.4		16.9			2.4		2.4			4.7		8.0			4.4					15.4		62.9			50.0		
mrC	4.2									14.6			33.8																				
mrD	26		3.8					0.6			5.9		18.9			27.8									54.3						46.7		
mrE	4.1										4.4				2.7					0													
mrF	10.2									5.9						4.0																	
mrG	7.3										8.0				62.8					0													
mrH	18.3						9.1									3.0																	
mrI	6.1					0.6		1.2			0.5		17.3			10.5		37.2			7.6												
mrJ	14.6									32.7						21.2																	
mrK	0.6											1.2			2.4																		
mrL	8.9									25.4				25.7							28.2												
mrM	5.2		4.6			1.6		3.0			1.0		0			0.2		1.9			3.3												
mrN	85.2		20.8			21.8		20.5			47.6		46																				
mrO	45										2.2																						
mrP	25.2		25.0			56.1		37.3			28.8		27.3			25.9		13.2			16.4		19.2			21.1							
mrQ	127.5	110.8			97.6						122.2																						
mrR	18.0	18.6																															
mrS	5.9	4.2																															
mrT	5.2	4.3																															
mrU	19.2	9.5																															
mrV	12.1	3.6						2.0		2.1			0.7		2.2																		
mrW	55.6	0																															

6.10.2 Hypoxic Fraction – Lymph Node

	Hypoxic Fraction (% of total tumour volume)																																
	0a	0b	1	2	3	4	5	6	7	8	9	10	11	12	13	14	15	16	17	18	19	20	21	22	23	24	25	26	27	28	29	30	
mrB			9.5			16.9		7.4			2.4		4.2			2.6		5.3			3.0					10.7		11.9			24.1		
mrC	10.7									17.6			39.9																				
mrD	25.6		10.6					10.3			13.0		9.7			12.8									12.8						54.9		
mrE	19.9										16.1				20.9					21.0					25.4								
mrF	1.2									0.9						0.6																	
mrG	1.1										0.5				3.0					1.6					5.9								
mrH	2.2						0.9									0.5																	
mrI	22.9					13.8		24.0			13.4		37.7			40.4		32.7			23.2		15.7										
mrJ	8.0									34.4						24.0																	
mrK	3.2											7.6			5.1							15.4			16.6								
mrL	5.1								3.0				8.2							7.2					24.4								
mrM	1.4		1.2			1.2		0.6			1.0		2.1			1.9		0.9			0.7					1.0					1.1		
mrN	29		42.2			15.7		19.2			62.0		58.8																				
mrP	14.6		10.2			79.6		15.7			49.7		17.6			25.7		9.5			10.8		1.8			11.2							
mrR	25.0	49.3																															
mrT	8.4	5.8																															
mrV	18.4	27.4						3.5	4.2				3.1	1.8																			
mrW	60.1	4.4																															

6.11 APPENDIX K

6.11.1 Mean doses for all radiotherapy plans

Mean Dose (SD, Gy)					
Stage	Structure/ Constraint	Planning Modality			
		3D-CRT	VMAT_NA	VMAT_A	IMRT_A
T1	Ipsilateral Carotid (PRV), V35	55.21 (0.98)	42.34 (4.35)	29.08 (2.85)	33.14 (2.17)
	Ipsilateral Carotid (PRV), V10	55.68 (1.54)	30.97 (3.46)	15.46 (5.84)	16.26 (6.19)
	Contralateral Carotid (PRV), V35	55.15 (0.89)	42.29 (3.72)	19.9 (1.92)	28.43 (2.98)
	Contralateral Carotid (PRV), V10	55.65 (1.35)	31.04 (3.43)	9.76 (3.58)	18.24 (6.19)
	Spinal Cord (PRV, D _{max} to 0.1 cm ³)	3.74 (2.83)	27.22 (1.41)	21.29 (2.69)	27.39 (3.5)
	Inferior Pharyngeal Constrictor Muscle (D _{mean})	54.51 (0.52)	55.17 (0.35)	35.9 (7.03)	44.99 (6.49)
	Contralateral Arytenoid (D _{mean})	55.68 (0.38)	55.47 (0.36)	45.01 (4.34)	53.25 (2.0)
	Contralateral Vocal Cord (D _{mean})	56.0 (0.52)	55.15 (0.32)	52.65 (3.08)	54.68 (0.86)
	Thyroid Gland (PRV, D _{mean})	23.76 (9.46)	19.44 (5.22)	11.97 (6.31)	15.40 (14.07)
T2	Ipsilateral Carotid (PRV), V35	55.09 (1.94)	42.08 (5.06)	34.96 (5.81)	33.98 (5.91)
	Ipsilateral Carotid (PRV), V10	56.0 (1.22)	31.67 (3.93)	23.83 (4.99)	15.81 (4.31)
	Contralateral Carotid (PRV), V35	54.68 (3.04)	43.22 (4.15)	25.37 (7.41)	29.96 (4.2)
	Contralateral Carotid (PRV), V10	55.72 (1.66)	32.12 (3.71)	9.93 (0.48)	21.82 (3.1)
	Spinal Cord (PRV, D _{max} to 0.1 cm ³)	10.14 (7.73)	26.60 (2.59)	22.99 (2.54)	28.23 (4.38)
	Inferior Pharyngeal Constrictor Muscle (D _{mean})	55.0 (0.72)	55.32 (0.52)	44.73 (6.71)	48.88 (4.82)
	Contralateral Arytenoid (D _{mean})	52.86 (7.47)	55.57 (0.53)	51.77 (4.57)	52.14 (3.98)
	Contralateral Vocal Cord (D _{mean})	55.56 (0.71)	55.39 (0.35)	54.68 (0.84)	55.19 (0.61)
	Thyroid Gland (PRV, D _{mean})	25.05 (6.63)	18.88 (5.45)	14.25 (5.77)	14.45 (10.03)

Table 6-14, Mean doses for Structures.

Mean doses are displayed for all structures across all early-stage glottic cancer plans, separated by T-stages